UNIVERSITÀ DEGLI STUDI DI GENOVA

Facoltà di Scienze Matematiche, Fisiche e Naturali

Tesi di dottorato

MULTIQUARK STATES AND EXOTIC SPECTROSCOPY

Candidato:
Alessandro Giachino

Relatore:
Dr. Elena Santopinto

CICLO DI DOTTORATO XXXII

Solo osservando e imparando dalla natura
si possono fare grandi cose.

A mia nonna Teresa,
una donna fatta di fede, volontà, sacrifici
e tanto Amore.

The research activity illustrated in this thesis has been supported in part by the National Institute for Nuclear Physics (INFN).

Contents

Chapter 1

Introduction

The LHCb experiment at CERN is a hotbed of new and outstanding physics results, both from side of the heavy hadrons and from the side of the so-called exotic hadron phenomenology. In the conventional quark model, composite particles can be either mesons formed of quark–antiquark pairs or baryons formed of three quarks. Particles not classified within this scheme are known as exotic hadrons. The pentaquark represents an example of these exotic states. When Murray Gell-Mann and George Zweig proposed the quark model in their 1964 papers, they mentioned the possibility of exotic hadrons such as pentaquarks, but it took 50 years to demonstrate their existence experimentally, when in 2016 the LHCb collaboration reported the first discovery of pentaquark states [1], [2, 3]. Recently, the LHCb Collaboration announced the observation of five narrow Ω_c states in the $\Xi_c^+ K^-$ decay channel [97], Later, Belle observed five resonant states in the $\Xi_c^+ K^-$ invariant mass distribution and unambiguously confirmed four of the states announced by LHCb [98].
The discoveries of new resonances not only enrich the present experimental knowledge of the hadron zoo, but they also provide essential information to explain the fundamental forces that govern nature. As the hadron mass patterns carry information on the way the quarks interact with one another, they provide a means of gaining insight into the fundamental binding mechanism of matter at an elementary level. For this reason the investigation of such new states is fundamental to push forward our understanding of the nature.

This thesis is specifically concerned with the heavy hadrons and the hidden-charm and -bottom pentaquark phenomenology, where the adjective hidden-charm (hidden-bottom) is related to the pentaquark quark content $qqqc\bar{c}$ ($qqqb\bar{b}$) with $q = u, d$ and s. The thesis is divided into two parts corresponding to chapter 2 and chapter 3. Chapter 2 is devoted to the pentaquark states observed by the LHCb collabo-

ration; all the discussions and the results reported in this chapter are published [8], [96], [66] or they have been submitted on the ArXiv [67].

Chapter 2 contains:

1. the calculation of the pentaquark decay widths for all the states predicted within the compact pentaquark approach (see [8]);

2. the investigation of the hidden-charm pentaquarks as $\bar{D}^{(*)}\Lambda_c$ and $\bar{D}^{(*)}\Sigma_c^{(*)}$ molecules coupled to the five-quark states, and the extension of the calculations performed in the charmed sector to the hidden-bottom pentaquark states. The coupling to the five-quark states is described as the short-range potential between the meson and the baryon. We also introduce the long-range force given by the one-pion exchange potential. Predictions for hidden-charmed and hidden-bottom pentaquark mass and decay widths are given by solving the coupled channel Schrödinger equation for hidden-charm and hidden-bottom pentaquark states with $J^P = \frac{1}{2}^-$, $\frac{3}{2}^-$, and $\frac{5}{2}^-$ and isospin $I = \frac{1}{2}$ [96], [66],[67].

Chapter 3 is devoted to the Ω_c states observed by the LHCb and Belle; all the discussions and the results reported in this chapter are published [68].

Specifically, chapter 3 contains:

1. the introduction of a three-dimensional harmonic oscillator hamiltonian (h.o.) plus spin-orbit, isospin and flavour dependent contributions which turned out to be fundamental in describing the heavy-baryon mass pattern [68]; this hamiltonian was the extension of the model introduced by us in Ref. [8] to study the pentaquark states within the compact approach;

2. the study the Ω_c-mass spectra performed by estimating the contributions due to spin-orbit interactions, spin-, isospin- and flavour-dependent interaction from the well-established charmed baryon mass spectrum [68];

3. the computation of the strong decays of ssQ baryons in $sqQ - K$ ($q = u, d$) final states [68] by means of the $^3P_0$ model [114, 115, 116, 117].

The results illustrated in this thesis are summarised below ([8], [68], [96], [66],[67]):

- **1)** In Ref. [96] we predicted the new three pentaquark states observed by LHCb in 2019 [34], $P_c^+(4312)$, $P_c^+(4440)$ and $P_c^+(4457)$, one year and a half before the new analysis performed by LHCb [34]; later, in a further study [67], we predicted the pentaquark masses and decay

widths consistently with the new data by LHCb with the following quantum number assignments [67]: $J^P_{P_c^+(4312)} = 1/2^-$, $J^P_{P_c^+(4440)} = 3/2^-$ and $J^P_{P_c^+(4457)} = 1/2^-$.

- **2)** we studied in details the origin of the mass difference between $P_c^+(4440)$ and $P_c^+(4457)$ by performing the calculations with and without the tensor term of the one-pion exchange potential (OPEP). The new LHCb results, indeed, provide us with the important opportunity of studying the spin-dependent forces between the Σ_c baryon and the $\bar{D}^*$ meson. The experimental determination of the pentaquark spin is very important since for nucleon systems only the spin 1 state (the deuteron) is available, without partners, and so this is the first example where the role of the tensor force can be compared in two partner states, *i.e.* $P_c^+(4440)$ and $P_c^+(4457)$. As a result of our investigation we found that both the short range interaction by the coupling to the 5-quark-core states and the long range interaction by the one-pion exchange potential make contributions to the attraction between Σ_c and $\bar{D}^{(*)}$. The mass difference between $P_c^+(4440)$ and $P_c^+(4457)$ comes mainly from the tensor interaction by the one-pion exchange potential. Because of the importance of the tensor interaction mediated by the pion in the heavy-hadron dynamics, we call it 'chiral tensor dynamics' [67].

- **3)** we showed that in the hidden-bottom sector, the OPEP is strong enough to produce states due to the mixing effect enhanced by the small mass splitting between B and B^*, and $\Sigma_{\rm b}$ and $\Sigma_{\rm b}^*$. Thus, both the OPEP and the $5q$ potential play the important role to produce many states, while the $5q$ potential has the dominant role to yield the states in the hidden-charm sector. Since the attraction from the OPEP is enhanced and the kinetic term is suppressed due to the large hadron masses, the hidden-bottom pentaquarks are more likely to form rather than the hidden-charm pentaquarks [96].

- **4)** by means of the introduction of a three-dimensional harmonic oscillator hamiltonian (h.o.) plus spin-orbit, isospin and flavour dependent contributions, which turned out to be fundamental in describing the heavy-baryon mass pattern [68], we reproduced quantitatively the spectrum of the Ω_c states.

- **5)** we extended our mass and decay width predictions also to the orbitally excited Ω_b states [68] that, at that time, were still to be observed. Very recently, the LHCb Collaboration observed four narrow peaks, $\Omega_b(6316)$,

$\Omega_b(6330), \Omega_b(6340)$ and $\Omega_b(6350)$ in $\Xi_b^0 K^-$ mass spectrum [65]. As reported by the same LHCb collaboration [65], the observed peaks and the $\Xi_b^0 K^-$ decay widths are consistent with our predictions given in Ref. [68].

- **6)** in Ref. [68] we calculated the mass splitting between the ρ- and λ-mode excitations of the $\Omega_{c(b)}$ resonances,and we highlighted that the heavy-light baryons are the most suitable environment to access to inner heavy-light baryon structure, owing to large mass splitting ρ- and λ-mode excitations, that we predict to be greater than 150 MeV. Indeed, if the ρ-excitations in the predicted mass region will not be observed in the future, then the three-quark model effective degrees of freedom for the heavy-light baryons will be ruled out, supporting the Heavy Quark Effective Theory (HQET) picture of the heavy-light baryons described as heavy quark-light diquark systems. If the HQET is valid for the heavy-light baryons, the heavy quark symmetry, predicted by the HQET in the heavy-light meson sector, can be extended to the heavy-quark-light-diquark baryon sector, opening the way to new future theoretical applications.

Chapter 2

Pentaquark states

2.1 Experimental introduction

In 2016 the LHCb collaboration reported the observation of two exotic structures, $P_c^+(4380)$ and $P_c^+(4450)$, in Λ_b decay [1]; these have been further supported by another two articles by the same collaboration [2, 3].

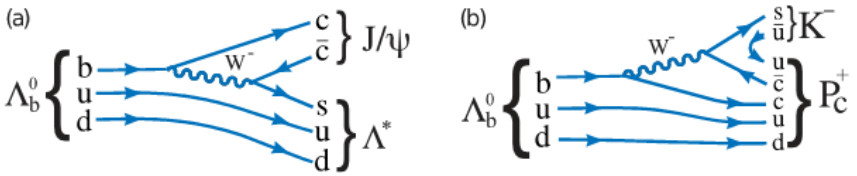

Figure 2.1: *Figure taken from [1] (APS copyright).* Feynman diagrams for (a) $\Lambda_b^0 \to J/\psi + \Lambda^*$ and (b) $\Lambda_b^0 \to P_c^+ + K^-$.

The Λ_b decay can proceed by the diagram shown in 2.1 a, and is expected to be dominated by $\Lambda^* \longrightarrow K^- p$ resonances:

$$\Lambda_b^0 \longrightarrow J/\psi + \Lambda^*, \Lambda^* \longrightarrow K^- + p \tag{2.1}$$

but it also has exotic contributions, as indicated by the diagram in fig. 2.1 b, which result as resonant structures in the $J/\Psi p$ mass spectrum:

$$\Lambda_b^0 \longrightarrow P_c^+ + K^-, P_c^+ \longrightarrow J/\Psi + p \tag{2.2}$$

The resonances decaying strongly into J/Ψ must have a minimal quark content of $c\bar{c}ccuud$. For this reason, these resonance are charmonium pentaquark states. These two pentaquark states are found to have masses of $4380 \pm 8 \pm 28$ MeV and

$4449.8 \pm 1.7 \pm 2.5$ MeV, with corresponding widths of $205 \pm 18 \pm 86$ MeV and $39 \pm 5 \pm 19$ MeV. The spin-parities, J^P, of these states have not yet been determined and the statistical significance of each of these resonances was more than 9 standard deviations. The parities of these states are preferred to be opposite, and one state has $J = 3/2$ and the other $J = 5/2$. $(J^P_{P_c^+(4380)}, J^P_{P_c^+(4450)}) = (3/2^-, 5/2^+)$ gives the best fit solution, but $(3/2^+, 5/2^-)$ and $(5/2^-, 3/2^+)$ are also acceptable. The results by LHCb have motived hundreds of theoretical articles (just to make some examples see [4, 5, 6, 7, 8, 9, 10, 11, 12, 13, 14, 15, 16, 17, 18, 19, 20, 21, 22, 23, 24, 25, 26, 27, 28, 29, 30, 31, 32, 33]).
Recently, a new analysis has been reported [34] using nine times more data from the Large Hadron Collider than the 2016 analysis. The nine-fold increase in the number of $\Lambda \to J\Psi pK$ decays reconstructed with the LHCb detector sheds more light onto the $J\Psi p$ structures found in this final state. The data set was first analyzed in the same way as before and the parameters of the previously reported $P_c^+(4450)$, and $P_c^+(4380)$ structures were consistent with the original results. As well as revealing the new $P_c^+(4312)$ state, the analysis also uncovered a more complex structure of $P_c^+(4450)$, consisting of two narrow nearby separate peaks, $P_c^+(4440)$ and $P_c^+(4457)$, with the two-peak structure hypothesis having a statistical significance of 5.4 sigma with respect to the single-peak structure hypothesis. Regarding the broad state, $P_c^+(4380)$ (width $\sim$ 200MeV), in the new analysis, data can be fitted equally well with and without the Breit-Wigner contribution corresponding to the $P_c^+(4380)$ state, and so, in the case of $P_c^+(4380)$ more experimental and theoretical studies are needed to understand the situation.

In this new analysis [34] the previously reported $P_c(4450)^+$ peak [1] is confirmed and resolved at 5.4σ significance into two narrow states: the $P_c(4440)^+$ and $P_c(4457)^+$ exotic baryons. A narrow companion state, $P_c(4312)^+$, is discovered with 7.3σ significance. The masses and widths of the three narrow penataquark states are as follows [34].

$$\begin{aligned} P_c^+(4312): M &= 4311.9 \pm 0.7^{+6.8}_{-0.6}\ \text{MeV}, \\ \Gamma &= 9.8 \pm 2.7^{+3.7}_{-4.5}\ \text{MeV}; \\ P_c^+(4440): M &= 4440.3 \pm 1.3^{+4.1}_{-4.7}\ \text{MeV}, \\ \Gamma &= 20.6 \pm 4.9^{+8.7}_{-10.1}\ \text{MeV}; \\ P_c^+(4457): M &= 4457.3 \pm 0.6^{+4.1}_{-1.7}\ \text{MeV}, \\ \Gamma &= 6.4 \pm 2.0^{+5.7}_{-1.9}\ \text{MeV}. \end{aligned}$$

As discussed by LHCb [34], $P_c^+(4312)$ is just below the $\Sigma_c \bar{D}$ threshold, while the higher ones $P_c^+(4440)$ and $P_c^+(4457)$ are both below the $\Sigma_c \bar{D}^*$ threshold.

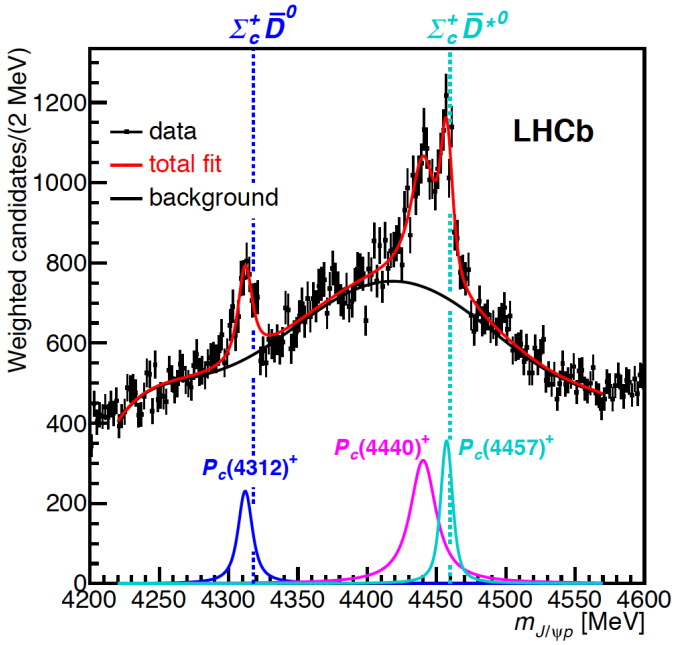

Figure 2.2: *Figure taken from [34] (APS copyright).* The figure shows the $J/\Psi p$ invariant mass spectrum and the three Breit-Wigner amplitudes corresponding to the three resonances, $P_c^+(4312), P_c^+(4440)$ and $P_c^+(4457)$. The mass thresholds for $\Sigma_c^+\bar{D}^0$ and $\Sigma_c^+\bar{D}^{*0}$ are superimposed.

2.2 The hidden-charm pentaquarks in the compact approach

2.2.1 Classification of the $qqqc\bar{c}$ multiplets as based on symmetry properties

In classifying the pentaquark multiplets we made use of symmetry principles without introducing any explicit dynamical models. We used the Young tableaux technique, adopting for each representation the notation $[f]_d = [f_1, \ldots, f_n]_d$, where f_i denotes the number of boxes in the i-th row of the Young tableau, and d is the dimension of the representation.

In agreement with the LHCb hypothesis [1], we think of the charmonium pentaquark wave function as $qqqc\bar{c}$ where $q = u, d, s$ is a light quark and c is the heavy charm quark.
Let us first discuss the possible configurations of qqq quarks in the $qqqc\bar{c}$ sys-

tem. The $c\bar{c}$ pair can be a colour octet or singlet with spin 0 or 1. The colour wave function of the $qqqc\bar{c}$ system must be an $SU_c(3)$ singlet, so the remaining three light quarks are also in a color-singlet, or in a color-octet.
The orbital symmetry of the quark wave function depends on the quantum numbers of the pentaquark state $P_c^+(4380)$. Indeed, the parity P of the pentaquark system is:

$$\mathrm{P} \mid qqqc\bar{c} >= (-1)^{l+1} \mid qqqc\bar{c} > , \tag{2.3}$$

where l is the pentaquark angular momentum. In the hypothesis that $P_c^+(4380)$ has $J^{\mathrm{P}} = \frac{3}{2}^-$, from Eq. 2.3 one can see that its orbital angular momentum can be $l = 0, 2$ or 4. As shown in Ref. [8], the possible $SU_f(3)$ multiplets for the charmonium ground-state pentaquarks ($l = 0$) are the octet and the decuplet.

2.2.2 The extension of the Gürsey-Radicati mass formula and the pentaquark mass spectrum

In order to determine the mass splitting between the octet and the decuplet we used a Gürsey-Radicati (GR)-inspired formula [73]. Until the new analysis performed by LHCb [34], there was experimental evidence of only two charmonium pentaquark states; these were not sufficient to determine all parameters in the GR mass formula. For this reason, we used the values of the parameters determined from the three-quark spectrum (reported in App. B, Tab. B.2), assuming that the coefficients in the GR formula are the same for different quark systems [8]. The simplest GR formula extension which distinguishes the different multiplets of $SU_f(3)$ is [8]:

$$\begin{aligned} M_{GR} &= M_0 + AS(S+1) + DY + \\ &+E\left[I(I+1) - \frac{1}{4}Y^2\right] + GC_2(SU(3)) + FN_C \ , \end{aligned} \tag{2.4}$$

where M_0 is a scale parameter: this means that, for example, in baryons, each quark makes a contribution of roughly $\frac{1}{3}M_0$ to the whole mass; I and Y are the isospin and hypercharge, respectively, while $C_2(SU(3))$ is the eigenvalue of the $SU_f(3)$ Casimir operator. Finally, N_C is a counter of c quarks or $\bar{c}$ antiquarks: this term takes into account the mass difference between a c quark (or a $\bar{c}$ antiquark) and the light quarks (u, d). The description of approach adopted in evaluating the coefficients A, D, E, G, F and the scale parameter M_0 is reported in App. B. As we showed in App. A, the possible $SU_f(3)$ multiplets for the charmonium pentaquark states are an octet and a decuplet

[8]. We hypothesized that the lightest pentaquark state reported by the LHCb collaboration in 2016 [1], $P_c^+(4380)$, belongs to the lowest mass $SU_f(3)$ multiplet [8]. According to the GR formula of Eq. 2.4, the mass splitting between two different $SU_f(3)$ multiplets is due to the different eigenvalues of the Casimir operator $C_2(SU(3))$; this mass splitting is proportional to the coefficient G (reported in App. B, Tab. B.1). Since G is positive ($G = 52,5$ MeV) , the lowest mass multiplet is the one with the lowest eigenvalue of the Casimir operator; thus as can be seen from Tab. 2.1, the charmonium pentaquark ground-state is the $[21]_8$ $SU_f(3)$ octet. For this reason, the lightest pentaquark state reported by the LHCb collaboration in 2016 [1], $P_c^+(4380)$, is expected to belong to a $SU_f(3)$ octet.

Table 2.1: *Table from [8] (APS copyright).* Possible charmonium pentaquark multiplets (see App. A), with their corresponding eigenvalues of the Casimir operator $C_2(SU(3))$.

$SU_f(3)$ multiplet	$C_2(SU(3))$
$[3]_{10}$	6
$[21]_8$	3

In the following, we focus on the octet charmonium pentaquark states, and apply the GR mass formula 2.4, with the values of the parameters reported in Tab. B.1, to each state of the octet, in order to predict the corresponding mass.
The octet pentaquark states are reported in Fig. 2.3, while the predicted masses, with the the corresponding uncertainties, are reported in Tab. 2.2.

Regarding the notation, a pentaquark state is labelled as $P^{ij}(M)$, where $i = 0, 1, 2$ is the number of strange quarks, $j = -, 0, +$ is the pentaquark's electric charge, and M the predicted mass.

The $P_c^+(4380)$ theoretical mass, predicted by means of our GR formula extension, is $M = 4377 \pm 49$ MeV.
Despite the simplicity of the approach that we have used, this result is in agreement with the mass reported by the LHCb collaboration, $M = 4380 \pm 8 \pm 29$ MeV.

Table 2.2: *Table from [8] (APS copyright).* Predicted pentaquark states with their corresponding masses. The notation is the same of that of Fig. 2.3.

predicted pentaquark states	masses (MeV)
$P^{00}(4377), P^{0+}(4377)$	4377 ± 49
$P^{1'0}(4520)$	4520 ± 47
$P^{1-}(4584), P^{10}(4584), P^{1+}(4584)$	4584 ± 50
$P^{2-}(4694), P^{20}(4694)$	4694 ± 47

was

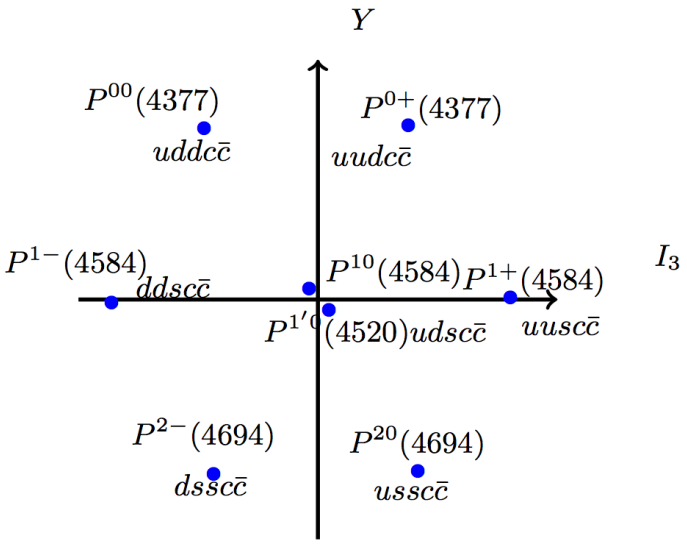

Figure 2.3: *Figure from [8] (APS copyright).* Octet of the ground pentaquark states with $J^P = 3/2^-$.

The compact pentaquark approach predicts that the observed pentaquark, $P_c^+(4380) \equiv P^{0+}(4377)$, is a member of an isospin doublet, with hypercharge $Y = 1$. We observe that, if the compact pentaquark description is correct, the other octet states will also be observed by the LHCb collaboration. By contrast, if the pentaquark is mainly a molecular state, it is not necessary that all the states of that multiplet should exist.

2.2.3 Bottom baryon decay channels involving intermediate pentaquark states and pentaquark decay widths

In this section, we suggest possible bottom baryon decay channels which involve the predicted pentaquark structures as intermediate states. These channels will be described in detail.
The state $P^{0+}(4377)$ is a part of an isospin doublet. A possible decay channel in which we might observe its isospin partner, $P^{00}(4377)$, could be:

$$\Lambda_b^0 \longrightarrow P^{00} + \bar{K}^0, P^{00} \longrightarrow J/\Psi + N \ . \tag{2.5}$$

The corresponding Feynman diagram is reported in Fig. 2.4 .

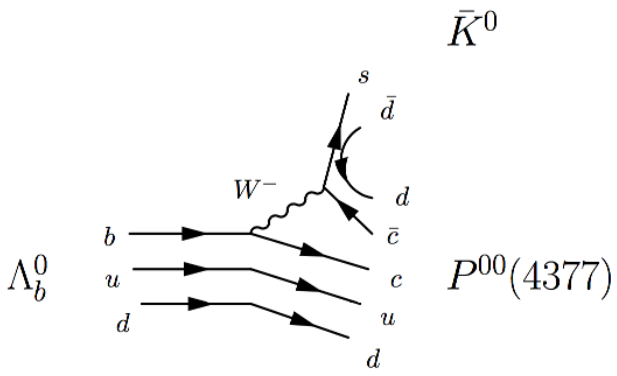

Figure 2.4: Λ_b baryon decay in $P^{00}(4377)$ and $\bar{K}^{00}$, where $P^{00}(4377)$ is the neutral pentaquark state, a member of the isospin doublet with $Y = 1$.

With regards to the other charmonium pentaquark states of the octet, i.e. those with strangeness, we have to focus on the decays of bottom baryons endowed with strange quarks. Let us consider the following Ξ_b^- decay:

$$\Xi_b^- \longrightarrow J/\psi + \Xi^- \ . \tag{2.6}$$

This decay is present in nature and was discovered by the $D0$ collaboration [74]. As in the case of the exotic Λ_b^0 decay shown in Fig. 2.4 , we can expect that an exotic decay may also occur in the case of Ξ_b^- baryon:

$$\Xi_b^- \longrightarrow P^{10}/P^{1'0} + K^-, P^{10}/P^{1'0} \longrightarrow J/\Psi + \Sigma/\Lambda \ . \tag{2.7}$$

In Eq. 2.7, $P^{10}(4584)$ and $P^{1'0}(4520)$ have the same quark content ($usdc\bar{c}$), and belong to the isospin triplet, and to the isosinglet, respectively (see Fig. 2.3). Since they have the same quark content and both are neutral, they can both result from the Ξ_b^- decay.

The charmonium pentaquark state $P^{1-}(4584)$ can be observed in the following decay process:

$$\Xi_b^- \longrightarrow P^{1-} + \bar{K}^0, P^{1-} \longrightarrow J/\Psi + \Sigma^- \ . \tag{2.8}$$

The difference between the two suggested decay modes for the Ξ_b^- baryon (Eq. 2.7, and Eq. 2.8) lies in the final state: in the case of the final state shown in Eq. 2.7, a $u\bar{u}$ pair is created from the vacuum, whereas, in the decay of Eq. 2.8, the $u\bar{u}$ pair is replaced with the $d\bar{d}$ pair. The Ξ_b^- baryon is a member of an isodoublet. The decay of its isospin partner Ξ_b^0

$$\Xi_b^0 \longrightarrow P^{1+} + K^-, P^{1+} \longrightarrow J/\Psi + \Sigma^+, \tag{2.9}$$

is probably the most important one from the experimental point of view, since all the final-state particles are charged and, therefore, easier to detect. In order to obtain a pentaquark candidate with $s = -2$ in the final state, a baryon with two strange quarks in the initial state is needed. The known decay channel of the Ω_b baryon is:

$$\Omega_b^- \longrightarrow J/\psi + \Omega^- \ . \tag{2.10}$$

This decay was discovered by the $D0$ detector at the Fermilab Tevatron collider [75]. Another possible Ω_b^- decay channel may be, in analogy with the exotic Λ_b decay channel shown in Fig. G.8:

$$\Omega_b^- \longrightarrow P^{20} + K^-, P^{20} \longrightarrow J/\Psi + \Xi^0 \ . \tag{2.11}$$

The state $P^{20}(4694)$ of Eq. 2.11 is a part of an isospin doublet (see Fig. 2.3). In order to observe its isospin partner ($P^{2-}(4694)$), it may be possible to use the following decay channel:

$$\Omega_b^- \longrightarrow P^{2-} + \bar{K}^0, P^{2-} \longrightarrow J/\Psi + \Xi^- \ . \tag{2.12}$$

The difference between the Ω_b^- decay of Eq. 2.11 and that of Eq. 2.12 is that, in the former case, a $u\bar{u}$ pair is created from the vacuum, whereas, in the latter case, a $d\bar{d}$ pair is created.

In calculating the decay widths of the pentaquark states we adopted an effective Lagrangian for the PNJ/ψ couplings from Ref. [35] as follows (see

App. C):

$$\mathcal{L}^{3/2^{\pm}}_{PNJ/\psi} = i\overline{P}_{\mu}\left[\frac{g_1}{2M_N}\Gamma^{\pm}_{\nu}N\right]\psi^{\mu\nu} - i\overline{P}_{\mu}\left[\frac{ig_2}{(2M_N)^2}\Gamma^{\pm}\partial_{\nu}N+\frac{ig_3}{(2M_N)^2}\Gamma^{\pm}N\partial_{\nu}\right]\psi^{\mu\nu} + \text{H.c.}, \tag{2.13}$$

where P are the pentaquark fields with spin-parity $J^{\mathrm{P}} = \frac{3}{2}^{\pm}$, N and ψ are the nucleon and the J/Ψ fields, respectively. The Γ matrices are defined as follows:

$$\Gamma^{\pm}_{\nu} = \begin{pmatrix} \gamma_{\nu}\gamma_5 \\ \gamma_{\nu} \end{pmatrix}, \Gamma^{\pm} = \begin{pmatrix} \gamma_5 \\ \mathbf{1} \end{pmatrix}, \tag{2.14}$$

where the first and the second row correspond to $J^{\mathrm{P}} = \frac{3}{2}^{+}$ and $J^{\mathrm{P}} = \frac{3}{2}^{-}$ pentaquark states, respectively. In the following, we calculate the decay widths for the predicted pentaquark states with $J^{\mathrm{P}} = \frac{3}{2}^{-}$. As noticed by Wang [28], the momenta of the final states in the pentaquark decays into $J/\psi p$ are fairly small compared with the nucleon mass. Thus, the higher partial wave terms proportional to $(p/M_N)^2$ and $(p/M_N)^3$ can be neglected; we can therefore consider only the first term in Eq. (2.13). This approximation leads to the following expression for the $P^{0+}(4377)$ partial decay width in the NJ/ψ channel [76]:

$$\Gamma(P^{0+} \to NJ/\psi) = \frac{\bar{g}^2_{NJ/\Psi}}{12\pi}\frac{p_N}{M_{P^{0+}}}(E_N + M_N) \times[2E_N(E_N - M_N) + (M_{P^{0+}} - M_N)^2 + 2M^2_{J/\psi}], \tag{2.15}$$

with

$$\bar{g}_{NJ/\Psi} = \frac{g_1}{2M_N}. \tag{2.16}$$

The kinematic variables E_N and p_N in Eq. (2.15) are defined as $E_N = (M^2_P + M^2_N - M^2_{J/\psi})/(2M_P)$ and $p_N = \sqrt{E^2_N - M^2_N}$.

Unfortunately, as the branching ratio $\mathcal{B}(P^+ \to J/\Psi p)$ is not yet known at present, the coupling constant g_1 of Eq. 2.16 is unknown. However, our pentaquark mass predictions can provide an expression of the partial decay widths for the pentaquark states with open strangeness. For example, the P^{1+} partial decay width in the $\Sigma^+ J/\Psi$ channel is given by:

$$\Gamma(P^{1+} \to \Sigma^+ J/\psi) = \frac{\bar{g}^2_{\Sigma^+ J/\Psi}}{12\pi}\frac{p_{\Sigma^+}}{M_{P^{1\prime}}}(E_{\Sigma^+} + M_{\Sigma^+}) \times[2E_{\Sigma^+}(E_{\Sigma^+} - M_{\Sigma^+}) + (M_{P^{1+}} - M_{\Sigma^+})^2 + 2M^2_{J/\psi}], \tag{2.17}$$

and the coupling constant $\bar{g}_{\Sigma^+ J/\Psi}$ is:

$$\bar{g}_{\Sigma^+ J/\Psi} = \frac{g_1}{2M_{\Sigma^+}} \, . \tag{2.18}$$

The expressions for the partial decay widths of the $\Lambda J/\Psi$, $\Sigma J/\Psi$, and $\Xi J/\Psi$ channels are listed in Tab. 2.3 as from Ref. [8].

initial state	channel	partial width (MeV)
$P^{1'0}$	$\Lambda J/\Psi$	$0.78\ \Gamma_{NJ/\Psi}$
$P^{1-}, P^{10}, P^{1+},$	$\Sigma J/\Psi$	$0.71\ \Gamma_{NJ/\Psi}$
$P^{2-}, P^{20},$	$\Xi J/\Psi$	$0.62\ \Gamma_{NJ/\Psi}$

Table 2.3: *Table from [8] (APS copyright).* Partial decay widths expressions for $\Lambda J/\Psi$, $\Sigma J/\Psi$ and $\Xi J/\Psi$ channels.

Since the pentaquark states have been observed in $J/\Psi p$ channel, it is natural to expect that they can be produced in $J/\Psi p$ photoproduction via the s and u-channel process. Wang et al. [28] calculated the cross-section of the pentaquark states in J/Ψ photoproduction and compared it with the available experimental data ([77], [78], [79]). The coupling between $J/\Psi p$ and the two pentaquark states is extracted by assuming that the decay width of each pentaquark state into $J/\Psi p$ is the 5% of the total width ([28]). As a result, they found that if one assumes that the $J/\Psi p$ channel saturates the total width of the two pentaquark states (that is $\mathcal{B}(P^+ \to J/\Psi p) = 1$) one significantly overestimates the experimental data; In conclusion they found that to be consistent also with the available photoproduction data, the branching ratio for both the pentaquark states needs to be $\mathcal{B}(P^+ \to J/\Psi p) \leq 0.05$.
Thus, if we use the upper branching ratio limit extracted by Wang [28], that is $\mathcal{B}(P^+ \to J/\Psi p) = 0.05$, we obtain that the $P_c(4380)$ partial decay width for the $J/\psi p$ channel is

$$\Gamma_{NJ/\Psi} = \mathcal{B}(P^+ \to J/\Psi p)\Gamma_{tot} = 10.25 \text{ MeV}, \tag{2.19}$$

where Γ_{tot}, as reported by the LHC_b collaboration, is 205 MeV. The numerical results for the other channels are listed in Table 2.4 as from Ref. [8].

initial state	channel	partial width (MeV)
$P^{1'0}$	$\Lambda J/\Psi$	7.94
$P^{1-}, P^{10}, P^{1+},$	$\Sigma J/\Psi$	7.21
$P^{2-}, P^{20},$	$\Xi J/\Psi$	6.35

Table 2.4: *Table from [8] (APS copyright).* Partial decay widths for $\Lambda J/\Psi$, $\Sigma J/\Psi$ and $\Xi J/\Psi$ channels. The partial decay widths are calculated from the constraint that $J/\Psi p$ channel accounts for the 5% of the total pentaquark width, as calculated by Wang in ([28]).

2.2.4 Summary of the section

In this study [8], we focused on describing the lightest resonant state ($J^P = \frac{3}{2}^-$), by means of a compact approach. An extension of the original GR mass formula [73] which correctly describes the charmed baryon sector was performed, and also proved able to give an unexpected prediction for the mass of the lightest pentaquark state $\frac{3}{2}^-$, which is in agreement with the experimental value within one standard deviation.
We found that the lightest pentaquark state $\frac{3}{2}^-$ belonged to the $SU_f(3)$ octet $[21]_8$ [8]. The theoretical mass of the lightest pentaquark state $\frac{3}{2}^-$ predicted by means of the GR formula extension (Eq. 2.4) is $M = 4377$ MeV, in agreement with the experimental mass $M = 4380 \pm 8 \pm 29$ MeV. We also predicted other pentaquark states, which belong to the same $SU_f(3)$ multiplet as the lightest resonance $J^P = \frac{3}{2}^-$, giving their mass, and suggesting possible decay channels in which they can be observed. We have finally computed the partial decay widths for all the suggested octet-pentaquark decay channels.

As the $\Lambda_b \longrightarrow J/\Psi K^- p$ decay is expected to be dominated by $\Lambda^* \longrightarrow K^- p$ resonances [1], we observe that the poor knowledge about the Λ^* excited states can affect the estimation of the parameters of the two pentaquark resonances. Moreover, as was noticed by Wang [28], if the two pentaquark candidates are genuine states, their production in photoproduction should be a natural expectation. For these reasons, on the one hand it is important to increase our knowledge about the missing excited states Λ^* with new experiments in order to improve the analysis and to extract with more precision the two pentaquark masses and widths [8]. On the other hand, a refined measurement of

the J/Ψ photoproduction cross section would provide more information about the nature of the pentaquark states [8].

2.3 The pentaquarks as meson-baryon molecules coupled with five-quark states

2.3.1 Heavy quark symmetry and heavy quark effective theory

The light u, d, and s quarks have masses m_q that are small compared to the scale of Λ_{QCD}. Thus, it is a good approximation to take the massless-quark limit of QCD, $m_Q \to 0$. In this limit the QCD has an $SU_L(3) \times SU_R(3)$ chiral symmetry, which can be used to predict some properties of hadrons containing the light quarks. For quark masses, m_Q, that are large compared with the scale of Λ_{QCD}, it is a good approximation to take the infinite quark-mass limit of QCD, $m_Q \to \infty$. In this limit QCD has spin-flavor heavy quark symmetry, which has important implications for the properties of hadrons containing a single heavy quark. Next sections are devoted to derive the effective Lagrangians which exhibit the heavy quark symmetry and the chiral symmetry.

In quantum field theory the effect of a very heavy particle often become irrelevant at low energies. A familiar example is the Fermi's theory of the weak interactions. For the description of weak decays of hadrons, the weak interactions at low energy ($< M_W \simeq 80$ GeV [51]) can be approximated by point-like four-fermion couplings, governed by a dimensionful coupling constant, $G_F \simeq 1.17\ 10^{-5}$ GeV^{-2} [51]. Only at higher energies one can observe the effects of the intermediate vector bosons, W and Z, on the cross section. Thus the Fermi theory is an effective theory for the weak interaction. In a similar way, the heavy quark effective theory is a good approximation of QCD when the quark mass is much larger than $\Lambda_{QCD} \simeq 200$ MeV.
Consider a single heavy quark with velocity v interacting with external fields.

The starting point in the construction of the low-energy effective theory is the observation that a very heavy quark bound inside a hadron moves more or less with the hadron's velocity, v^μ , and it is almost on-shell [80].

The momentum of an **on-shell** quark is defined by $p_Q^\mu = m_Q v^\mu$. The momentum of an **off-shell** quark can be written as $p_Q^{'\mu} = p_Q^\mu + k^\mu = m_Q v^\mu + k^\mu$, where we defined as k^μ the residual momentum, *i.e.* the hadron momentum which is not carried by the heavy quark and which is, by construction, of the order of

Λ_{QCD} [80]. Note that the four-velocity $v_\mu = (\gamma c, \gamma \vec{v})$, satisfies:

$$v^2 = v_\mu v^\mu = \gamma^2 c^2 - \gamma^2 v^2 = \gamma^2 (c^2 - v^2) = \gamma^2 c^2 \left(1 - \frac{v^2}{c^2}\right) = c^2 = 1 \quad (2.20)$$

in natural units. Observe also that the heavy-quark mass, m_Q, is expected to be nearly equal to the heavy hadron mass, namely $m_Q \simeq m_H$. If one calculates the commutator between the heavy-quark position, x, and velocity, v:

$$[x, v] = \frac{[x, p]}{m_Q} - \frac{[x, k]}{m_Q} = \frac{i\hbar}{m_Q} - \frac{[x, k]}{m_Q} \to 0 \ \text{ if } \ m_Q \to \infty. \quad (2.21)$$

This means that the heavy quark cannot simultaneously have a well-defined position and momentum, but it does have a well-defined position and velocity, which corresponds to the velocity of the hadron.

Let us investigate the consequences of the **off-shell** quark momentum parametrization, [1] $p_Q^\mu = m_Q v^\mu + k^\mu$, on the heavy hadron dynamics. The Feynman fermion propagator is defined in terms of the fermion fields, $\psi(x)$ and $\bar{\psi}$ as [81]:

$$< 0 | T\{\psi(x)\bar{\psi}(x^{'})\} | 0 >, \quad (2.22)$$

where the spinor indices have been suppressed and, for fermion fields, the time-ordered product is defined by:

$$\begin{aligned} T\{\psi(x)\bar{\psi}(x^{'})\} &= \theta(t - t^{'})\psi(x)\bar{\psi}(x^{'}) - \theta(t^{'} - t)\bar{\psi}(x^{'})\psi(x) \\ &= \begin{cases} \psi(x)\bar{\psi}(x^{'}), \ \text{if } t > t^{'} \\ -\bar{\psi}(x^{'})\psi(x), \ \text{if } t^{'} > t \end{cases} \ \text{where } t = x_0 \end{aligned} \quad (2.23)$$

It can be proven that [81]

$$< 0 | T\{\psi(x)\bar{\psi}(x^{'})\} | 0 >= iS_F(x - x^{'}) \quad (2.24)$$

where S_F is defined by [81]:

$$S_F = \left(i\gamma^\mu \frac{\partial}{\partial x^\mu} + m_Q\right) \Delta_F(x). \quad (2.25)$$

[1] To clean up the notation in the following the **off-shell** quark momentum will be denoted simply by p_Q^μ: *i.e.* $p_Q^{'\mu} \equiv p_Q^\mu$.

Here $\Delta_F(x)$ is referred to as the Feynman propagator for the mesons of the Klein-Gordon field, and its explicit expression is given by [81]:

$$\Delta_F(x) = \frac{1}{(2\pi)^4}\int d^4p e^{-ip_\mu x^\mu}\frac{1}{p^2-\mu^2+i\epsilon}. \tag{2.26}$$

By taking the heavy quark propagator in momentum space,

$$S_F = \frac{1}{(2\pi)^4}\int d^4p e^{-ip_\mu x^\mu}\frac{\not{p}+m_Q}{p^2-m_Q^2+i\epsilon}, \tag{2.27}$$

and substituting the parametrization of heavy-quark momentum into Eq. 2.27 we obtain, for $k \sim \Lambda_{QCD} \ll m_Q$:

$$\begin{aligned} i\frac{\not{p}+m_Q}{p^2-m_Q^2+i\epsilon} &= i\frac{m_Q\not{v}+\not{k}+m_Q}{2m_Qvk+k^2+i\epsilon} \simeq i\frac{m_Q\not{v}+m_Q}{2m_Qvk+i\epsilon}+i\frac{\not{k}}{2m_Qvk+i\epsilon} \\ &\simeq i\frac{m_Q\not{v}+m_Q}{2m_Qvk+i\epsilon} = \frac{1+\not{v}}{2}\frac{i}{vk+i\epsilon}+\mathcal{O}\left(\frac{1}{m_Q}\right), \end{aligned} \tag{2.28}$$

where higher order corrections besides the leading term are not shown because they vanish in the limit $m_Q \to \infty$.

We notice that the heavy quark propagator contains a velocity-dependent projector:

$$\hat{P}_+ \equiv \frac{1+\not{v}}{2}, \tag{2.29}$$

that becomes the non-relativistic projector,

$$\hat{P}_+^{\rm NR} = \frac{1+\gamma_0}{2}, \tag{2.30}$$

in the heavy-quark rest frame where $v^\mu = (1,0,0,0)$.

The original heavy quark field in the heavy-quark rest frame, $Q(x)$, can be decomposed into a large component $H_v(x)$, whose energy is of order m_Q and a small component $h_v(x)$, whose energy is much smaller than m_Q, by using the positive and negative energy projection operators, $\hat{P}_+$ and $\hat{P}_-$,

$$Q(x) = \frac{1+\not{v}}{2}Q(x)+\frac{1-\not{v}}{2}Q(x) = \hat{P}_+Q(x)+\hat{P}_-Q(x) \equiv h_v(x)+H_v(x) \tag{2.31}$$

which satisfy:

$$\hat{P}_{\pm}^2 = \hat{P}_{\pm}, \quad \hat{P}_+\hat{P}_- = 0. \tag{2.32}$$

From Eq. 2.28, it follows that the small component of the heavy quark field, $h_v(x)$, is the degree of freedom that remains dynamical in the low-energy theory, whereas the large component, $H_v(x)$, can be integrated out, since it vanishes in the $m_Q \to \infty$ limit, and it will not appear in the EFT.
Then $h_v(x)$ is the field, made of two independent components, that describes in the HQEFT Lagrangian the low-energy modes of the heavy quark. From the definition of the new fields, $h_v(x)$ and $H_v(x)$,

$$\hat{P}_+ h_v(x) = h_v(x) \to \frac{1+\not{v}}{2} h_v(x) = h_v(x) \tag{2.33}$$

$$\hat{P}_- H_v(x) = H_v(x) \to \frac{1-\not{v}}{2} H_v(x) = H_v(x) \tag{2.34}$$

it follows that they satisfy:

$$\not{v}\, h_v(x) = h_v(x) \tag{2.35}$$

$$\not{v}\, H_v(x) = -H_v(x) \tag{2.36}$$

where $h_v(x)$ corresponds to the upper two components of the heavy quark field $Q(x)$, while $H(x)$ corresponds to the lower ones and so

- $h_v(x)$ annihilates a heavy quark with velocity v, but does not create an antiquark;
- $H_v(x)$ creates a heavy antiquark with velocity v but does not annihilate a quark.

One physical consequence of the decoupling between the particle-antiparticle components is that **there is no heavy quark pair production**.

If there is more than one heavy quark flavor, N_h, the effective Lagrangian up to the next to leading order will be (App. D):

$$\begin{aligned} L_{eff} &= L^0_{eff} + L^1_{eff} + \mathcal{O}\left(\frac{1}{m_Q}\right)^2 \\ &= \sum_{j=1}^{N_h} \bar{h}_v^{(j)}(x) iv\cdot D h_v^{(j)}(x) + \frac{1}{2m_Q}\bar{h}_v (iD)^2 h_v + \frac{g}{4m_Q}\bar{h}_v \sigma_{\alpha\beta} G^{\alpha\beta} h_v \end{aligned} \tag{2.37}$$

where the superscript j means that this term is of the order $\left(\frac{1}{m_Q}\right)^j$. The leading order term in Eq. 2.37, $L^0_{eff} = \sum_{j=1}^{N_h} \bar{h}_v^{(j)}(x) iv\cdot D h_v^{(j)}(x)$ is mass independent. Thus, it exhibits explicitly the heavy-flavour symmetry. Moreover, since there are no Dirac matrices in Eq. 2.37, the heavy quark spin is not affected by the interaction of the quarks with gluons and therefore the lagrangian has a SU(2)-spin symmetry. We observe that these symmetries are lost if we keep the next terms in the $\frac{1}{m_Q}$ expansion as it is clear by looking at the first order corrections (see also App. D):

$$L^1_{eff} = \frac{1}{2m_Q}\bar{h}_v (iD)^2 h_v + \frac{g}{4m_Q}\bar{h}_v \sigma_{\alpha\beta} G^{\alpha\beta} h_v \quad . \tag{2.38}$$

Here g is the color charge appearing in the QCD gauge covariant derivative $D_\mu = \partial_\mu + igA^a_\mu T^a$, with A^a_μ the gluon field and T^a the generators of the $SU_c(3)$ group; $\sigma_{\alpha\beta} = \frac{i}{2}\gamma_\alpha\gamma_\beta$ and the gluon field strength tensor is $G^{\alpha\beta} = \frac{1}{ig}[D^\alpha, D^\beta]$ (see App. D for further details).

2.3.2 Effective Lagrangians for light meson-heavy hadrons interactions

As we already mentioned, **from the point of view of the Heavy Quark Effective Field Theory (HQET), it is natural to divide quarks into two classes by comparing their quark masses with** Λ_{QCD}. The u and d quarks belong definitely to the light quark class, $m_u,\ m_d \ll \Lambda_{QCD}$. If we take the limit $m_u,\ m_d,\ m_s \to 0$, the QCD lagrangian for these three quarks possesses a $SU_L(3)\otimes SU_R(3)\otimes U_V(1)$ symmetry which is spontaneously broken down to $SU_V(3)\otimes U_V(1)$. The 8 pseudoscalar mesons of the $SU_f(3)$ octet are then identified with the Goldstone bosons. Due to the explicit symmetry breaking given by the quark mass term in the QCD lagrangian, the 8 pseudoscalar mesons become massive.

Heavy Quark Effective Field Theory (HQET) is based on spontaneously broken $SU_L(3) \otimes SU_R(3)$ chiral symmetry for the light quarks, and spin-flavor symmetry for the heavy quarks.

Now we want to stress the main steps needed to build the chiral Lagrangian that describes the low momentum interactions of the light pseudoscalar and vector mesons with the ground state $s = 1/2$ spin symmetry doublet of heavy mesons, P_a and P_a^*. The Lagrangian for the strong interactions of the pseudoscalar and vector mesons, P_a and P_a^*, with low momentum Goldstone bosons should be the most general one consistent with the chiral and heavy quark symmetries, and it should contain at leading order the minimum number of derivatives and insertions of the light quark mass matrix. We can combine the P_a and P_a^* a fields into a 4×4 matrix [80]:

$$\begin{aligned} h_a &= \frac{1+\not{v}}{2}[P_a^{*\mu} + iP_a\gamma_5], \\ \bar{h}_a &= \gamma_0 h_a^\dagger \gamma_0. \end{aligned} \tag{2.39}$$

Please observe that here $h_v(x)$ corresponds to the upper two components of the heavy quark field Q and that we have called the small-component field [2]:

$$h_v(x) = e^{im_Q vx} P_+ Q(x) = e^{im_Q vx} \frac{1+\not{v}}{2} Q(x); \tag{2.40}$$

v is, as usually, the heavy meson velocity satisfying $v^\mu P_{a\mu}^* = 0$, and $m_H = m_P = m_{P^*}$ in the heavy quark spin-flavor symmetry limit. Moreover $\not{v}h = -h\not{v} = h$, $\bar{h}\not{v} = -\not{v}\bar{h} = \bar{h}$.
$P^{*\mu}$ and P are annihilation operators normalized as follows:

$$\langle 0|P|Q\bar{q}(0^-)\rangle = \sqrt{m_H} \tag{2.41}$$

$$\langle 0|P^{*\mu}|Q\bar{q}(1^-)\rangle = \epsilon^\mu \sqrt{m_H} \quad . \tag{2.42}$$

[2] In order to subtract the quantity $m_Q v$ from the heavy quark momentum, the following definition for the small and the large-component fields is used:

$$h_v(x) = e^{im_Q vx} P_+ Q(x), \quad H_v(x) = e^{im_Q vx} P_- Q(x).$$

From Eq. 2.31 it follows that the heavy quark field $Q(x)$ becomes

$$Q(x) = e^{-im_Q vx}(H_v(x) + h_v(x)).$$

Now, the field h_a defined in Eq. 2.39 under the unbroken $SU_V(3)$ as an antitriplet, in agreement with the chiral symmetry:

$$h_a \to h_b U^\dagger_{ba} \tag{2.43}$$

Moreover, this combination of fields transforms as a doublet, in agreement with the heavy quark symmetry [80]:

$$h_a \to D_Q(R) h_b \tag{2.44}$$

Now, the heavy meson fields, P_a and P^*_a have well-defined transformation rules under the unbroken vector $SU(3)_V$ group. For instance, a heavy meson made up by a heavy quark Q and a light antiquark $\bar{q}_a$ $(a = u, d, s)$, transforms, under a chiral transformation, according to the representation $\bar{3}$ of $SU_V(3)$, that is $(h_a \approx Q\bar{q}_a)$

$$h_a \to h_b U^\dagger_{ba}(x), \tag{2.45}$$

but they do not necessarily form representations of the spontaneously broken $SU_L(3) \otimes SU_R(3)$ chiral symmetry. Thus, in order to construct the chiral Lagrangian, we define an h field that transforms under the full $SU_L(3) \otimes SU_R(3)$ chiral symmetry group in such a way that the transformation reduces to Eq. 2.43 under the unbroken vector subgroup. Here we can not discuss this in details but we just write the solution [3]. The key is to introduce a new field:

$$\xi = e^{\frac{i\mathcal{M}}{2f_\pi}} = \sqrt{\Sigma}. \tag{2.46}$$

Hereafter we are going to use the conventions by Ref. [38], $\xi = e^{\frac{i\mathcal{M}}{2f_\pi}}$, with f_π=92.3 MeV. All the formulas reported below are written according to this convention.

$\Sigma(x)$ is an $SU_f(3)$ matrix which describes the low-momentum strong interactions of the Goldstone bosons:

$$\Sigma(x) = e^{\frac{i\mathcal{M}}{f_\pi}} \tag{2.47}$$

and $\mathcal{M}$ is the traceless 3×3 Hermitian matrix of the Goldstone bosons:

$$\mathcal{M} = \sqrt{2} \begin{pmatrix} \frac{\pi^0}{\sqrt{2}} + \frac{\eta}{\sqrt{6}} & \pi^+ & K^+ \\ \pi^- & -\frac{\pi^0}{\sqrt{2}} + \frac{\eta}{\sqrt{6}} & K^0 \\ K^- & \bar{K}^0 & -\frac{2}{\sqrt{6}}\eta \end{pmatrix} \tag{2.48}$$

[3] The interested reader can see, for example, the review by Manohar and Wise [80].

To the lowest order in the momenta and in the massless quark limit, the most general invariant lagrangian is given by

$$\mathcal{L}_{kin} = \frac{f_\pi^2}{4} Tr\left[\partial^\mu \Sigma \partial_\mu \Sigma^\dagger\right] \tag{2.49}$$

where the constant $f_\pi^2/4$ has been chosen such as to get a canonical kinetic term for the mesonic fields appearing inside the matrix $\mathcal{M}$, moreover, in this notation $f_\pi = 92.3$ MeV (see footnote 4). The transformation properties of $\xi(x)$ under chiral transformations (that is transformations of $SU_L(3) \otimes SU_R(3)$) are

$$\xi(x) \to g_L \xi(x) U^\dagger(x) = U(x) \xi(x) g_R^\dagger \quad . \tag{2.50}$$

The matrix $U(x)$, defined in eq. (2.43), belongs to the $SU_V(3)$ unbroken subgroup and it is defined by the previous equation. As a consequence, $U(x)$ is generally a complicated non-linear function of the field $\xi(x)$ itself, and, as such, space-time dependent. In view of the locality properties of the transformation $U(x)$, one needs covariant derivatives or gauge fields, in order to be able to construct invariant derivative couplings. This is provided by the vector current

$$V_\mu = \frac{1}{2}\left(\xi^\dagger \partial_\mu \xi + \xi \partial_\mu \xi^\dagger\right) \tag{2.51}$$

transforming under the chiral transformation of eq. (2.50) as

$$V_\mu \to U V_\mu U^\dagger + U \partial_\mu U^\dagger \quad . \tag{2.52}$$

It is also possible to introduce an axial current, transforming as the adjoint representation of $SU_V(3)$

$$A_\mu = \frac{i}{2}\left(\xi^\dagger \partial_\mu \xi - \xi \partial_\mu \xi^\dagger\right) \tag{2.53}$$

with

$$A_\mu \to U A_\mu U^\dagger \quad . \tag{2.54}$$

The effective lagrangian for the strong interactions of heavy mesons with light pseudoscalars must satisfy Lorentz and C, P, T invariance. Furthermore, at the leading order in the $1/m_Q$ expansion, and in the massless quark limit, we shall require flavour and spin symmetry in the heavy meson sector, and chiral $SU_L(3) \otimes SU_R(3)$ invariance in the light one. The most general lagrangian

which describes the coupling between the light pseudoscalar mesons and the heavy mesons (pseudoscalar and vector) is [37] [4] :

$$\mathcal{L}_{psHH} = iTr(h_b v^\mu D_{\mu ba}\bar{h}_a) + ig_\pi Tr(h_b\gamma_\mu\gamma_5 A^{\mu_{ba}}\bar{h}_a) + \\ + \frac{f_\pi^2}{4}\partial^\mu\Sigma_{ab}\partial_\mu\Sigma^\dagger_{ba} \tag{2.55}$$

where the sum over the μ index is understood, the first term in the Lagrangian contains the kinetic term for the heavy mesons, $D_\mu = \partial_\mu + V_\mu$ (V_μ is the vector current introduced in Eq. 2.51) is the covariant derivative, and the third term contains the kinetic term for the Goldstone bosons. The Lagrangian describing the interactions of heavy mesons with low momentum vector resonances, respecting chiral and heavy quark symmetries is given by ([37], Eq. 62):

$$\begin{aligned}\mathcal{L}_{vHH} &= \frac{1}{2g_V^2}Tr(F_{\mu\nu}(\rho)F^{\mu\nu}(\rho)) - f_\pi^2\left[Tr(A_\mu^2) + aTr((V_\mu-\rho_\mu)^2)\right] \\ &+ i\beta Tr(h_b v^\mu\left(V_\mu-\rho_\mu\right)_{ba}\bar{h}_a) + i\lambda Tr(h_b\sigma^{\mu\nu}F_{\mu\nu}(\rho)_{ba}\bar{h}_a) \quad , \end{aligned}\tag{2.56}$$

where $F_{\mu\nu}(\rho) = \partial_\mu\rho_\nu - \partial_\nu\rho_\mu + [\rho_\mu,\rho_\nu]$, and $\rho_\mu = i\frac{g_V}{\sqrt{2}}\hat{\rho}_\mu$, with $\hat{\rho}_\mu$ the analogous of $\mathcal{M}$ for the vector meson fields:

$$\hat{\rho}_\mu = \sqrt{2}\begin{pmatrix} \frac{\rho^0}{\sqrt{2}} + \frac{\omega}{\sqrt{2}} & \rho^+ & K^{*+} \\ \rho^- & -\frac{\rho^0}{\sqrt{2}} + \frac{\omega}{\sqrt{2}} & K^{*0} \\ K^{*-} & \bar{K}^{*0} & \phi \end{pmatrix}_\mu \quad . \tag{2.57}$$

Finally, the Lagrangian describing the interactions of heavy mesons and scalar meson σ is given by

$$\mathcal{L}_{\sigma HH} = g_s \mathrm{Tr}\left[h_a\sigma\bar{h}_a\right] \quad . \tag{2.58}$$

The heavy quark and chiral symmetries can also be applied to derive the effective Lagrangian which describes the interactions between the goldstone bosons and the heavy baryons. The heavy baryon Lagrangian are [38]:

$$\mathcal{L}_{\mathcal{B}} = \mathcal{L}_{B_{\bar{3}}} + \mathcal{L}_S + \mathcal{L}_{int}, \tag{2.59}$$

$$\mathcal{L}_{B_{\bar{3}}} = \frac{1}{2}\mathrm{tr}[\bar{B}_{\bar{3}}(iv\cdot D)B_{\bar{3}}] + h.c. \tag{2.60}$$

$$\mathcal{L}_S = -\mathrm{tr}[\bar{S}^\alpha(iv\cdot D - \Delta_B)S_\alpha] \tag{2.61}$$

$$\begin{aligned}\mathcal{L}_{int} &= g_4\mathrm{tr}[\bar{S}^\mu A_\mu B_{\bar{3}}] + i\lambda_I\epsilon^{\mu\nu\lambda\kappa}v_\mu\mathrm{tr}[\bar{S}_\nu F_{\lambda\kappa}B_{\bar{3}}] \\ &+ i\beta_B\mathrm{tr}[\bar{B}_{\bar{3}}v^\mu(A_\mu-\rho_\mu)B_{\bar{3}}] + \ell_B\mathrm{tr}[\bar{B}_{\bar{3}}\sigma B_{\bar{3}}] + \frac{3}{2}g_1(iv_\kappa)\epsilon^{\mu\nu\lambda\kappa}\mathrm{tr}[\bar{S}_\mu A_\nu S_\lambda] \\ &+ i\beta_S\mathrm{tr}[\bar{S}_\mu v_\alpha(A^\alpha-\rho^\alpha)S^\mu] + \lambda_S\mathrm{tr}[\bar{S}_\mu F^{\mu\nu}S_\nu] + \ell_S\mathrm{tr}[\bar{S}_\mu\sigma S^\mu] + h.c., \end{aligned}\tag{2.62}$$

[4] In [37] $f_\pi = 130$ MeV while here we are using $f_\pi = 92.3$ MeV. The two definitions are related by a factor $\sqrt{2}$.

where $\Delta_B = M_6 - M_{\bar{3}}$ is the mass difference between the sextet and the antitriplet, and σ is the scalar singlet meson. Note that B_6 ($\frac{1}{2}^+$) and B_6^* ($\frac{3}{2}^+$) are degenerate because of the heavy quark spin symmetry in this effective theory. Other definitions are given below.

$$B_{\bar{3}} = \begin{pmatrix} 0 & \Lambda_c^+ & \Xi_c^+ \\ -\Lambda_c^+ & 0 & \Xi_c^0 \\ -\Xi_c^+ & -\Xi_c^0 & 0 \end{pmatrix}, \quad B_6 = \begin{pmatrix} \Sigma_c^{++} & \frac{1}{\sqrt{2}}\Sigma_c^+ & \frac{1}{\sqrt{2}}\Xi_c'^+ \\ \frac{1}{\sqrt{2}}\Sigma_c^+ & \Sigma_c^0 & \frac{1}{\sqrt{2}}\Xi_c'^0 \\ \frac{1}{\sqrt{2}}\Xi_c'^+ & \frac{1}{\sqrt{2}}\Xi_c'^0 & \Omega_c^0 \end{pmatrix}, \tag{2.63}$$

$$B_6^* = \begin{pmatrix} \Sigma_c^{*++} & \frac{1}{\sqrt{2}}\Sigma_c^{*+} & \frac{1}{\sqrt{2}}\Xi_c^{*+} \\ \frac{1}{\sqrt{2}}\Sigma_c^{*+} & \Sigma_c^{*0} & \frac{1}{\sqrt{2}}\Xi_c^{*0} \\ \frac{1}{\sqrt{2}}\Xi_c^{*+} & \frac{1}{\sqrt{2}}\Xi_c^{*0} & \Omega_c^{*0} \end{pmatrix}, \tag{2.64}$$

$$\xi = e^{\frac{i\mathcal{M}}{2f_\pi}}, \tag{2.65}$$

$$F_{\mu\nu} = \partial_\mu \rho_\nu - \partial_\nu \rho_\mu + [\rho_\mu, \rho_\nu], \tag{2.66}$$

$$D_\mu B_{\bar{3}} = \partial_\mu B_{\bar{3}} + V_\mu B_{\bar{3}} + B_{\bar{3}} V_\mu^T, \quad D_\mu S_\nu = \partial_\mu S_\nu + V_\mu S_\nu + S_\nu V_\mu^T. \tag{2.67}$$

Please observe that the definitions of the $B_{\bar{3}}, B_6$ and B_6^* matrices in the bottom sector can be obtained by Eqs. 2.63 and 2.64 after the substitution $c \to b$, for example the $B_{\bar{3}}$ matrix in the bottom sector is:

$$B_{\bar{3}} = \begin{pmatrix} 0 & \Lambda_b^0 & \Xi_b^0 \\ -\Lambda_b^0 & 0 & \Xi_b^- \\ -\Xi_b^0 & -\Xi_b^- & 0 \end{pmatrix}. \tag{2.68}$$

.

The field of the B_6^* baryon is given by the Rarita-Schwinger field [39, 38] and the superfield S_μ is represented by

$$\begin{aligned} S_\mu &= B_{6\mu}^* + \frac{\delta}{\sqrt{3}}(\gamma_\mu + v_\mu)\gamma_5 B_6\,, \\ \bar{S}_\mu &= \gamma_0 S_\mu^\dagger \gamma_0 = \gamma_0 [B_{6\mu}^* + \frac{\delta}{\sqrt{3}}(\gamma_\mu + v_\mu)\gamma_5 B_6]^\dagger \gamma_0, \\ &= \bar{B}_{6\mu}^* + \gamma_0 B_6^\dagger \gamma_5^\dagger (\gamma_\mu + v_\mu)^\dagger \frac{\delta^*}{\sqrt{3}}\gamma_0 = \bar{B}_{6\mu}^* + \gamma_0 B_6^\dagger \gamma_5^\dagger (\gamma_0\gamma_\mu\gamma_0 + v_\mu)\frac{\delta^*}{\sqrt{3}}\gamma_0 \\ &= \bar{B}_{6\mu}^* - B_6^\dagger \gamma_5 (\gamma_0\gamma_0\gamma_\mu + \gamma_0 v_\mu \gamma_0)\frac{\delta^*}{\sqrt{3}} = \bar{B}_{6\mu}^* - \frac{\delta^*}{\sqrt{3}} B_6^\dagger \gamma_5 (\gamma_\mu + v_\mu)\,. \end{aligned} \tag{2.69}$$

2.3.3 The model: coupled channel between the meson-baryon states and a compact five-quark core

In general, if more than one state is allowed for a given set of quantum numbers, the hadronic resonant states are unavoidably mixtures of these states. Therefore, an important issue is to clarify how these components are mixed in the physical hadrons. A long-standing and well-known example is $\Lambda(1405)$, which is considered to be a molecule of $\bar{K}N$ and $\pi\Sigma$ coupled channels (see [44] for a recent review). In the heavy quark sector, $X(3872)$ is well explained as a charmonium state plus higher Fock components due to the coupling to the meson-meson continuum [94], Now, the P_c^+ pentaquarks have been found just below the $\bar{D}\Sigma_c^*$ and $\bar{D}^*\Sigma_c$ thresholds. Thus, the $\bar{D}\Sigma_c^*$ and $\bar{D}^*\Sigma_c$ molecular components are expected to be play a role in the formation of these states [9, 10, 11, 12, 13, 14, 15, 16, 17, 18, 19, 29, 20, 21]. We investigate the hidden-charm pentaquarks as $\bar{D}^{(*)}\Lambda_c$ and $\bar{D}^{(*)}\Sigma_c^{(*)}$ molecules coupled to the five-quark states [96]. The idea to couple the five-quark core with the meson-baryon channels is inspired by recent work of Ref. [94] in which the authors highlighted that continuum coupling effects in hadron spectroscopy may be important when a hadron is close to some baryon-meson decay thresholds, which in the case of hidden-charm pentaquarks are the $\bar{D}^{(*)}\Lambda_c$ and $\bar{D}^{(*)}\Sigma_c^{(*)}$ thresholds. Moreover, we extend our calculations to the hidden-bottom sector by providing predictions for hidden-bottom pentaquarks as $B^{(*)}\Lambda_b$ and $B^{(*)}\Sigma_b^{(*)}$ molecules coupled to the five-quark states [96]. Here, $\bar{D}^{(*)}$ ($\Sigma_c^{(*)}$) stands for $\bar{D}$ and $\bar{D}^*$ (Σ_c and Σ_c^*), while $B^{(*)}$ ($\Sigma_b^{(*)}$) stands for B and B^* (Σ_b and Σ_b^*). Coupling to the five-quark states is described as the short-range potential between the meson and the baryon. We also introduce the long-range force given by the one-pion exchange potential. By solving the coupled channel Schrödinger equation, we study the bound and resonant hidden-charm and hidden-bottom pentaquark states for $J^P = \frac{1}{2}^-$, $\frac{3}{2}^-$, and $\frac{5}{2}^-$ with isospin $I = \frac{1}{2}$ [96].
In Section 2.3.4, the meson-baryon and the five-quark channels are introduced, while in Sections 2.3.5 and 2.3.6, respectively, the OPEP as the long-range force, and the five-quark state as the short-range force are presented. The model parameters, the numerical methods, and the results for the hidden-charm and the hidden-bottom sectors are discussed in Sections 2.3.7, 2.3.8, 2.3.9, and 2.3.11, respectively, while in Section 2.3.10, we compare, for the hidden-charm sector, our numerical results with those of the quark cluster model by Takeuchi [7], and we find that for a value of the coupling constant equal to $f/f_0 = 25$ (Fig. 2.12), our results are similar to the ones reported in Ref. [7]. In Section 2.3.11, we discuss the idea that in the hidden-bottom sector, we expect to provide reliable predictions for the hidden-bottom pen-

taquark masses and widths, which will be useful for future experiments. We also discuss that the hidden-bottom pentaquarks are more likely to form than their hidden-charm counterparts; for this reason, we suggest that the experimentalists should look for these states. Finally, Section 2.3.12 summarizes the work as a whole.

2.3.4 Meson-baryon and $5q$ channels

So far many studies for exotic states have been performed by using various models such as hadronic molecules, compact multi-quark states, hybrids with gluons and so on. Strictly in QCD, definitions of these model states are not trivial, while the physical exotic states appear as resonances in scatterings of hadrons. Therefore, the issue is related to the question of the compositeness of resonances, which has been discussed for a long time [40, 41, 82], and recently in the context of hadron resonances (see for instance [42, 43] and references therein). In nuclear physics a similar issue has been discussed in the context of clustering phenomena of nuclei [45]. In the end, it comes down to the question of efficiency in solving the complex many-body systems.

In the current problem of pentaquark P_c, there are two competing sets of channels: the meson-baryon (MB) channels and the five-quark ($5q$) channels[a]. The meson-baryon channels describe the dynamics at long distances, while the $5q$ part describes the dynamics at short distances, which we consider to be in the order of 1 fm or less.

[a] Various combinations of hadrons and quark configurations which may form the pentaquark P_c are called channels.

The base states may be formed by open-charm hadrons, such as $\bar{D}^*\Sigma_c$, and hidden ones, such as $J/\psi N$. Considering the mass of the observed P_c, which is much closer to the open-charm channels than to the hidden ones, we may neglect the hidden-charm channels at the first attempt. However, the hidden-charm channels become important when discussing decays of possible pentaquark states, such as the $J/\psi N$ observed in the LHCb experiment. For the hidden-bottom sector, however, the thresholds between the open-bottom meson-baryon channel and the $\Upsilon(1S)N$ are rather different, of the order of 500 MeV. Therefore, the $\Upsilon(1S)N$ component seems to be suppressed in the hidden-bottom pentaquarks. On the other hand, the threshold of $\Upsilon(2S)N$ is close to the open-bottom thresholds. Experimentally, the measurement in the open-bottom meson-baryon and $\Upsilon(2S)N$ decays is preferred rather than that

in the $\Upsilon(1S)N$ decay. Our model space for open charm hadrons are summarized in Table 2.5 as from Ref. [96]. For the interaction between them, we employ the one-pion exchange potential, which is the best established interaction due to chiral symmetry and its spontaneous breaking. Explicit forms of the potential are given in Appendix F.

The $5q$ part describes the dynamics at short distances, which we consider to be in the order of 1 fm or less. The $5q$ compact states is formed by color-octet light quarks ($3q$) and color octet $c\bar{c}$ (the color singlet light quarks-color singlet $c\bar{c}$ channel is not attractive as it was shown in Ref. [7]). The relevant channels are summarized in Table 2.6 as from Ref. [96]. Notations are $[q^3 D_C, S_{3q}]S_{c\bar{c}}$ where $D_C = 8$ indicates that qqq form the color octet, S_{3q} is the spin of the light quarks $qqq = uud$, and $S_{c\bar{c}}$ the spin of $c\bar{c}$.

Channels	$\bar{D}\Lambda_c$	$\bar{D}^*\Lambda_c$	$\bar{D}\Sigma_c$	$\bar{D}\Sigma_c^*$	$\bar{D}^*\Sigma_c$	$\bar{D}^*\Sigma_c^*$
J^P						
$1/2^-$	${}^2S$	${}^2S,\ {}^4D$	${}^2S$	${}^4D$	${}^2S,\ {}^4D$	${}^2S,\ {}^4D,\ {}^6D$
$3/2^-$	${}^2D$	${}^4S,\ {}^2D,\ {}^4D$	${}^2D$	${}^4S,\ {}^4D$	${}^4S,\ {}^2D,\ {}^4D$	${}^4S,\ {}^2D,\ {}^4D,\ {}^6D,\ {}^6G$
$5/2^-$	${}^2D$	${}^2D,\ {}^4D,\ {}^4G$	${}^2D$	${}^4D,\ {}^4G$	${}^2D,\ {}^4D,{}^4G$	${}^6S,\ {}^2D,\ {}^4D,{}^6D,\ {}^4G,\ {}^6G$

Table 2.5: *Table from [96] (APS copyright).* Various channels of open-charm meson-baryons of total spin parity J^P with ${}^{2S+1}L$.

Table 2.6: *Table from [96]* (APS copyright). Channels of $5q$'s with color octet qqq and $c\bar{c}$ with possible total spin J. For notations, see text.

Channel	$[q^3 8, \frac{1}{2}]0$	$[q^3 8, \frac{1}{2}]1$	$[q^3 8, \frac{3}{2}]0$	$[q^3 8, \frac{3}{2}]1$
J	1/2	1/2, 3/2	3/2	1/2, 3/2, 5/2

Thus, our model Hamiltonian, expanded by the open-charm MB and $5q$ channels, is written as

$$H = \begin{pmatrix} H^{MB} & V \\ V^\dagger & H^{5q} \end{pmatrix} \tag{2.70}$$

where the MB part H^{MB} contains K_i; the kinetic energy of each MB channel i and V_{ij}^{π}; the OPEP potential, and H^{5q} stands for the $5q$ channels. For simplicity, we consider that H^{5q} is diagonalized by the $5q$ channels (denoted by α) of Table 2.6 and its eigenvalue is expressed by M_α. The off-diagonal part in (2.70), V, represents the transition between the MB and $5q$ channels. In the quark cluster model, such interactions are modeled by quark exchanges accompanied by gluon exchanges. In the present paper, we shall make a simple assumption that ratios of transitions between various channels $i \sim MB$ and $\alpha \sim 5q$ are dominated by the spectroscopic factors, overlaps $\langle i|\alpha\rangle$. The absolute strengths are then assumed to be determined by a single parameter. The various components of the Hamiltonian are then written as

$$\left(H_{ij}^{MB}\right) = \begin{pmatrix} K_1 + V_{11}^{\pi} & V_{12}^{\pi} & \cdots \\ V_{21}^{\pi} & K_2 + V_{22}^{\pi} & \cdots \\ \cdots & \cdots & \cdots \end{pmatrix}, \quad \left(H_{\alpha\beta}^{5q}\right) = \begin{pmatrix} M_1 & 0 & \cdots \\ 0 & M_2 & \cdots \\ \cdots & \cdots & \cdots \end{pmatrix} \tag{2.71}$$

and

$$(V_{i\alpha}) = (\langle i|\alpha\rangle) = \begin{pmatrix} V_{11} & V_{12} & \cdots \\ V_{21} & V_{22} & \cdots \\ \cdots & \cdots & \cdots \end{pmatrix}. \tag{2.72}$$

Now let us consider the coupled equation for the MB and $5q$ channels, $H\psi = E\psi$, where $\psi = (\psi^{MB}, \psi^{5q})$,

$$\begin{aligned} H^{MB}\psi^{MB} + V\psi^{5q} &= E\psi^{MB}, \\ V^{\dagger}\psi^{MB} + H^{5q}\psi^{5q} &= E\psi^{5q}. \end{aligned}$$

Solving the second equation for ψ^{5q}, $\psi^{5q} = (E - H^{5q})^{-1}V^{\dagger}\psi^{MB}$ and substituting for the first equation, we find the equation for ψ^{MB},

$$\left(K^{MB} + V^{\pi} + V\frac{1}{E - H^{5q}}V^{\dagger}\right)\psi^{MB} = E\psi^{MB}. \tag{2.73}$$

The last term on the left-hand side is due to the elimination of the $5q$ channels, and is regarded as an effective interaction for the MB channels. Thus, the total interaction for the MB channels is defined by

$$U = V^{\pi} + V\frac{1}{E - H^{5q}}V^{\dagger}. \tag{2.74}$$

We then insert the assumed $5q$ eigenstates into the second term of (2.74),

$$U_{ij} = V_{ij}^{\pi} + \sum_{\alpha} \langle i \,|\, V \,|\, \alpha \rangle \frac{1}{E - E_{\alpha}^{5q}} \langle \alpha \,|\, V^{\dagger} \,|\, j \rangle \tag{2.75}$$

where E_{α}^{5q} is the eigenenergy of a $5q$ channel. In this equation, we have indicated the meson-baryon channel by i, j, and the $5q$ channels by α. In this way, the effects of the $5q$ channels are included in the form of effective short range interaction. A visual representation of Eq. 2.75 is displayed in Fig. 2.5. The computations for the OPEP and the short range interactions are discussed in the next sections.

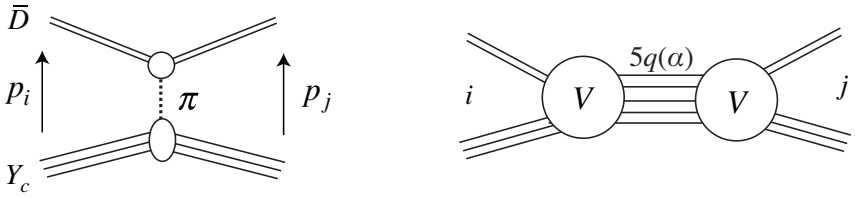

Figure 2.5: *Figure from [96]* (APS copyright). One pion exchange potential (left) and the effective interaction due to the coupling to the $5q$ channel (right). The meson-baryon channels are generally represented by $\bar{D}$ and Y_c, respectively, and i is for the initial and j the final channels. A $5q$ channel is denoted by α.

2.3.5 One pion exchange potential

In this subsection, we derive the one pion exchange potential (OPEP) between $\bar{D}^{(*)}$ and Y_c, V_{ij}^{π}, which corresponds to the first term of Eq. (2.75). Hereafter, we use the notation $\bar{D}^{(*)}$ to stand for a $\bar{D}$ meson, or a $\bar{D}^*$ meson, and Y_c to stand for Λ_c, Σ_c, or Σ_c^*.

The OPEP is obtained by the effective Lagrangians for heavy mesons (baryons) and the Nambu-Goldstone boson, satisfying the heavy quark and chiral symmetries. For a short introduction on heavy quark and chiral symmetries please read see sections 2.3.1, 2.3.2 and appendix D, D.2. The interested reader can also find some examples of applications in App. D.3. All the necessary equations are written in Sections 2.3.1, 2.3.2, however, for the sake of clarity, here we write again the most important equations. The Lagrangians for heavy mesons and the Nambu-Goldstone bosons are given by [46, 47, 48, 49, 37, 50]

$$\mathcal{L}_{\pi HH} = g_{\pi} \mathrm{Tr} \left[h_b \gamma_{\mu} \gamma_5 A_{ba}^{\mu} \bar{h}_a \right] . \tag{2.76}$$

The trace $\mathrm{Tr}\left[\cdots\right]$ is taken over the gamma matrix. The heavy meson fields h and $\bar{h}$ are represented by

$$h_a = \frac{1+\not{v}}{2}\left[\bar{P}^*_{a\mu}\gamma^\mu - \bar{P}_a\gamma_5\right], \tag{2.77}$$

$$\bar{h}_a = \gamma_0 h_a^\dagger \gamma_0, \tag{2.78}$$

where the fields are constructed by the heavy pseudoscalar meson $\bar{P}$ and the vector meson $\bar{P}^*$ belonging to the heavy quark spin (HQS) doublet. v_μ is a four-velocity of a heavy quark, and satisfies $v^\mu v_\mu = 1$ and $v^0 > 0$. The subscripts a, b are for the light flavor u, d. The axial vector current for the pion, A_μ, is given by

$$A_\mu = \frac{i}{2}\left[\xi^\dagger(\partial_\mu\xi) + (\partial_\mu\xi)\xi^\dagger\right], \tag{2.79}$$

where $\xi = \exp\left(\frac{i\hat{\pi}}{2f_\pi}\right)$ with the pion decay constant $f_\pi = 92.3$ MeV. The pion field $\hat{\pi}$ is given by

$$\hat{\pi} = \sqrt{2}\begin{pmatrix} \frac{\pi^0}{\sqrt{2}} & \pi^+ \\ \pi^- & -\frac{\pi^0}{\sqrt{2}} \end{pmatrix}. \tag{2.80}$$

The coupling constant g_π is determined by the strong decay of $D^* \to D\pi$ as $g_\pi = 0.59$ [37, 50, 51].

The Lagrangians for heavy baryons and Nambu-Goldstone bosons are given by [48, 38]

$$\mathcal{L}_{\pi BB} = \frac{3}{2}g_1(iv_\kappa)\varepsilon^{\mu\nu\lambda\kappa}\mathrm{tr}\left[\bar{S}_\mu A_\nu S_\lambda\right] + g_4\mathrm{tr}\left[\bar{S}^\mu A_\mu B_{\bar{3}}\right] + \mathrm{H.c.} \tag{2.81}$$

The trace $\mathrm{tr}\left[\cdots\right]$ is for the flavor space. The superfields S_μ and $\bar{S}_\mu$ are represented by

$$\begin{aligned} S_\mu &= B^*_{6\mu} + \frac{\delta}{\sqrt{3}}\left(\gamma_\mu + v_\mu\right)\gamma_5 B_6\,, \\ \bar{S}_\mu &= \bar{B}^*_{6\mu} - \frac{\delta^*}{\sqrt{3}}B_6^\dagger\gamma_5\left(\gamma_\mu + v_\mu\right). \end{aligned} \tag{2.82}$$

The phase factor δ is set at $\delta = -1$, as discussed in Ref. [38], and the heavy baryon fields, $B_6, B^*_{6\mu}$ and $B_{\bar{3}}$ are defined in Sec. 2.3.2. The coupling constants g_1 and g_4, satisfying $g_1 = (\sqrt{8}/3)g_4 = 1$, are obtained by the quark model

estimation discussed in Ref. [38]. For the coupling g_4, this value can also be fixed by the $\Sigma_c^{(*)} \to \Lambda_c \pi$ decay, and agrees with the one obtained by the quark model [38].

For the hidden-bottom sector, these effective Lagrangians are also applied by replacing the charmed hadron fields by the bottom hadron fields, while the same coupling constants are used.

In order to parametrize the internal structure of hadrons, we introduce the dipole form factor at each vertex:

$$F(\Lambda, \vec{q}) = \frac{\Lambda^2 - m_\pi^2}{\Lambda^2 + \vec{q}^{\,2}}, \tag{2.83}$$

with the pion mass m_π and the three-momentum $\vec{q}$ of an incoming pion. As discussed in Refs. [52, 53, 54], the cutoffs of heavy hadrons are fixed by the ratio between the sizes of the heavy hadron and nucleon, $\Lambda_N/\Lambda_H = r_H/r_N$ with the cutoff and size of the heavy hadron being Λ_H and r_H, respectively. The nucleon cutoff is determined to reproduce the deuteron-binding energy by the OPEP as $\Lambda_N = 837$ MeV [52, 53, 54]. The ratios are computed by the means of constituent quark model with the harmonic oscillator potential [55], where the frequency is evaluated by the hadron charge radii in Refs. [56, 57]. For the heavy meson [52], we obtain $\Lambda_{\bar{D}} = 1.35\Lambda_N$ and $\Lambda_B = 1.29\Lambda_N$ for the $\bar{D}^{(*)}$ meson and the B meson, respectively. For the heavy baryon [55], we obtain $\Lambda_{\Lambda_c} \sim \Lambda_{\Sigma_c} \sim \Lambda_N$ for the charmed baryon, and $\Lambda_{\Lambda_b} \sim \Lambda_{\Sigma_b} \sim \Lambda_N$ for the bottom baryon. We note that values of these cutoffs are smaller than those used in other studies, e.g. $\Lambda = 2.35$ GeV and $\Lambda = 1.77$ GeV in Ref. [13].

From these Lagrangians (2.76) and (2.81), and the form factor (2.83), we obtain the OPEP as the Born term of the scattering amplitude. The explicit form of the OPEP is summarized in Appendix F. The OPEP is also used for the hidden-bottom sector, $B^{(*)}Y_b$, by employing the cutoff parameters Λ_B, Λ_{Λ_b}, and Λ_{Σ_b}, where $B^{(*)}$ stands for B or B^*, and Y_b stands for Λ_b, Σ_b or Σ_b^*. Let us remark about the contact term of the OPEP. In this study, it is neglected as shown in Eq. (F.15) as is in the conventional nuclear physics. We assume that the OPEP appears only in the long range hadronic region. As discussed above, the cutoff parameters of the OPEP are determined from the ratio of sizes of the relevant hadron and nucleon. The cutoff of the nucleon is determined so as to reproduce the deuteron binding energy without the contact term [52].

2.3.6 Couplings to $5q$ states

In this subsection, we derive the effective short-range interaction, the 2nd term of (2.75). To do so, we need to know the matrix elements $\langle i \,|\, V \,|\, \alpha \rangle$

and the eigenenergies, E_α^{5q}. As discussed in the previous section 2.3.4, the matrix elements are assumed to be proportional to the spectroscopic factor, the overlap $\langle i \,|\, \alpha \rangle$,

$$\langle i \,|\, V \,|\, \alpha \rangle = f \,\langle i \,|\, \alpha \rangle \,, \tag{2.84}$$

where f is the only free parameter of the model [96], and it determines the overall strength of the matrix elements. As we will discuss later, the approximation (2.84) turns out to be rather good in comparison with the quark cluster model calculations [7].

For the computation of the spectroscopic factor, let us construct the MB and $5q$ wave functions explicitly. We employ the standard non-relativistic quark model with a harmonic oscillator confining potential. The wave functions are written as the products of color, spin, flavor and orbital wave functions. Let us introduce the notation $\left|\bar{D}Y_c(\vec{p}_i)\right\rangle$ for the open-charm meson-baryon channel i of relative momentum $\vec{p}_i$. Thus, we can write the wave function for $\left|\bar{D}Y_c(\vec{p}_i)\right\rangle$ as [58]

$$\left\langle \vec{\rho}, \vec{\lambda}, \vec{r}, \vec{x} \,\middle|\, \bar{D}Y_c(\vec{p}_i) \right\rangle = \psi_{\bar{D}}^{int}(\vec{r})\psi_{Y_c}^{int}(\vec{\rho}, \vec{\lambda}) e^{i\vec{p}_i \cdot \vec{x}} \times \phi_{\bar{D}Y_c}(CSF). \tag{2.85}$$

In (2.85), we indicate only the spatial coordinates explicitly, while the other coordinates for the color, spin and flavor are summarized in $\phi_{\bar{D}Y_c}(CSF)$. These coordinates are shown in Fig. 2.6. The spatial wave functions $\psi_{\bar{D}}^{int}(\vec{r})\psi_{\Lambda_c}^{int}(\vec{\rho}, \vec{\lambda})$ are then written by those of harmonic oscillator.

For the five-quark state, we assume that the quarks move independently in a single confined region, and hence the $\vec{x}$ motion is also confined. Therefore, by introducing $|5q\,(\alpha)\rangle$, we have

$$\left\langle \vec{\rho}, \vec{\lambda}, \vec{r}, \vec{x} \,\middle|\, 5q\,(\alpha) \right\rangle = \psi_{5q}^{int}(\vec{\rho}, \vec{\lambda}, \vec{r}) \left(\frac{2A}{\pi}\right)^{3/4} e^{-A^2 x^2} \times \phi_{5q}(CSF), \tag{2.86}$$

where the index α is for the $5q$ configurations, as shown in Table 2.6 for a given spin. The parameter A represents the inverse of the spatial separation of $\vec{x}$-motion, corresponding to the qqc and $q\bar{c}$ clusters, which is in the order of 1 fm, or less. Again, the color, spin and flavor part is summarized in $\phi_{5q}(CSF)$.

Now the spectroscopic factor is the overlap of (2.85) and (2.86). Assuming that the spatial wave functions $\psi_{\bar{D}}^{int}(\vec{r})\psi_{\Lambda_c}^{int}(\vec{\rho}, \vec{\lambda})$ and $\psi_{5q}^{int}(\vec{\rho}, \vec{\lambda}, \vec{r})$ are the same, the overlap is given by the color, spin and flavor parts, as labeled by CSF

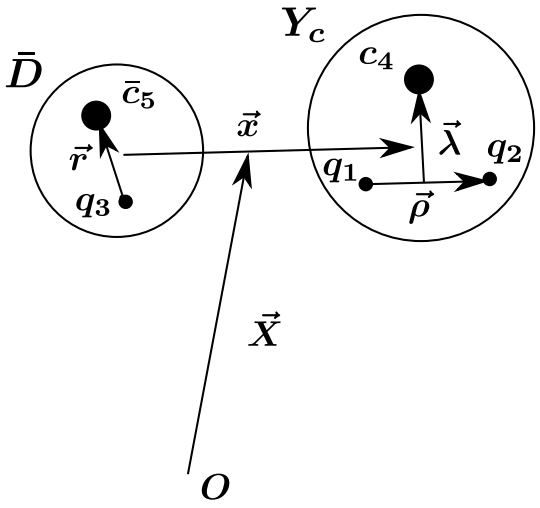

Figure 2.6: *Figure from [96]* (APS copyright). Jacobi coordinates of "$\bar{D}$ meson" and "Y_c baryon" in the $5q$ configuration. q_i $(i = 1, 2, 3)$ stands for the light quark, and c_4 $(\bar{c}_5)$ stands for the (anti)charm quark. The coordinate $\vec{\rho}$ is the relative coordinate of q_1q_2, $\vec{\lambda}$ the relative coordinate between the center of mass of q_1q_2 and c_4, $\vec{r}$ the relative coordinate of $q_3\bar{c}_5$, and $\vec{x}$ the relative coordinate between the centers of mass of $q_1q_2c_4$ and $\bar{c}_5q_3$. Though we do not use the total center-of-mass coordinate $\vec{X}$ in the present paper explicitly, it is also shown in the figure.

below, and by the Fourier transform of the Gaussian function,

$$\begin{aligned}\left\langle \bar{D}Y_c(\vec{p}_i) \,\middle|\, 5q\,(\alpha) \right\rangle &= \langle \phi_{\bar{D}Y_c}(CSF) \,|\, \phi_{5q}(CSF) \rangle \int d^3x \left(\frac{2A}{\pi}\right)^{3/4} e^{-Ax^2} e^{i\vec{p}_i\cdot\vec{x}} \\ &= \langle \phi_{\bar{D}Y_c}(CSF) \,|\, \phi_{5q}(CSF) \rangle \left(\frac{2\pi}{A}\right)^{3/4} e^{-p_i^2/4A} \equiv S_i^\alpha g(\vec{p}_i),\end{aligned} \tag{2.87}$$

where S_i^α is the spectroscopic factor, reported in Table 2.7, for the color, flavor and spin parts of the wave function, and $g(\vec{p}_i)$ the form factor for the transition $\bar{D}Y_c(\vec{p}_i) \to 5q(\alpha)$. The explicit calculations of S_i^α are presented in Appendix G.

The wave functions should reflect the antisymmetric nature (a quark exchange effect) under the permutation among all light quarks especially in different clusters $\bar{D}Y_c$. This is neglected in $\left|\bar{D}Y_c(\vec{p}_i)\right\rangle$. The effect, however, is introduced in the present model at least partially by considering the above overlap, because the $\psi_{5q}^{int}\phi_{5q}$ is totally antisymmetric over the three light quarks. Such quark exchange effect is suppressed, as the two color-singlet clusters $\bar{D}Y_c$ are

Table 2.7: *Table from [96]* (APS copyright). Spectroscopic factor of the $5q$ potential. J is the total angular momentum of the system, $S_{c\bar{c}}$ is the total spin of $c\bar{c}$, and S_{3q} is the total spin of the three light quarks.

J	$S_{c\bar{c}}$	S_{3q}	$\bar{D}\Lambda_c$	$\bar{D}^*\Lambda_c$	$\bar{D}\Sigma_c$	$\bar{D}\Sigma_c^*$	$\bar{D}^*\Sigma_c$	$\bar{D}^*\Sigma_c^*$
$\frac{1}{2}$	0	$\frac{1}{2}$	0.35	0.61	−0.35	—	0.20	−0.58
	1	$\frac{1}{2}$	0.61	−0.35	0.20	—	−0.59	−0.33
	1	$\frac{3}{2}$	0.00	0.00	−0.82	—	−0.47	0.33
$\frac{3}{2}$	0	$\frac{3}{2}$	—	0.00	—	−0.50	0.58	−0.65
	1	$\frac{1}{2}$	—	0.71	—	0.41	−0.24	−0.53
	1	$\frac{3}{2}$	—	0.00	—	−0.65	−0.75	−0.17
$\frac{5}{2}$	1	$\frac{3}{2}$	—	—	—	—	—	−1.00

further apart for larger x and therefore the above overlap is suppressed.

Finally, the transition amplitude from i to j of $\bar{D}Y_c$ channels is expressed by

$$T_{ij} = f' \sum_\alpha S_i^\alpha S_j^\alpha g(\vec{p}_i) g(\vec{p}_j) \frac{1}{E - E_\alpha^{5q}}. \tag{2.88}$$

The overall strength f' of this amplitude is not determined, and is treated as a parameter, while the relative strengths of various channels i, j are determined by the factors S_i^α and S_j^α.

The transition amplitude T_{ij} in (2.88) has been given in a separable form. To use it in the Schrödinger equation, it is convenient to express it in the form of local potential, which is a function of the momentum transfer $\vec{q} = \vec{p}_i - \vec{p}_f$. We attempt to set

$$g(\vec{p}_i) g(\vec{p}_j) = e^{-(p_i^2 + p_j^2)/4\alpha} \sim e^{-\beta q^2}. \tag{2.89}$$

On ignoring the angle-dependent term of $q^2 = (\vec{p}_i - \vec{p}_f)^2 =$
$= p_i^2 + p_j^2 - 2\vec{p}_i \cdot \vec{p}_j$, it is reasonable to set $\beta = \frac{1}{4}A$.
Therefore, the transition amplitude is parametrized as

$$T_{ij} \sim \sum_\alpha S_i^\alpha S_j^\alpha e^{-q^2/4A} \frac{1}{E - E_{5q}^\alpha}. \tag{2.90}$$

This gives an energy dependent local potential

$$V_{ij}^{5q}(E;r) \sim \sum_{\alpha} S_i^{\alpha} S_j^{\alpha} e^{-Ar^2} \frac{1}{E - E_{5q}^{\alpha}}, \tag{2.91}$$

with the relative coordinate r between the heavy meson and baryon.

Now, if we further expect that the compact five-quark configuration $|5q\,(\alpha)\rangle$ is located sufficiently above the energy region in which we are interested, namely $E_{5q}^{\alpha} \gg m_{\bar{D}} + m_{Y_c}$, then we may further approximate

$$V_{ij}^{5q}(r) = -f \sum_{\alpha} S_i^{\alpha} S_j^{\alpha} e^{-Ar^2}, \tag{2.92}$$

where f is a positive overall coupling strength. As shown in Table 2.8, in a simple quark model estimation, the $qqqc\bar{c}$ five-quark masses with the color-octet three light quarks are about 400 MeV larger than the threshold energies of $\bar{D}Y_c$ in the present study. The masses of hidden-bottom five-quarks are similarly higher than the $\bar{B}Y_b$ thresholds. This makes the potential (2.92) attractive for both of the hidden-charm and hidden-bottom sectors. As we will discuss later in this paper, especially this attraction turns out to be the driving force to produce the P_c states.

Table 2.8: *Table from [96]* (APS copyright). Masses of the hidden-charm five-quark states with the color-octet three light quarks, E_{5q}^{α}, calculated by using parameters in Ref. [7]. All the entries are listed in MeV. J stands for the total spin of the five-quarks, $[q^3 8s]S$ stands for the five-quark state, which consists of the uud quarks with a spin of s and the $c\bar{c}$ pair with a spin of S.

J	$[q^3 8\frac{1}{2}]0$	$[q^3 8\frac{1}{2}]1$	$[q^3 8\frac{3}{2}]0$	$[q^3 8\frac{3}{2}]1$
$\frac{1}{2}$	4816.2	4759.1	-	4772.2
$\frac{3}{2}$	-	4822.3	4892.5	4835.4
$\frac{5}{2}$	-	-	-	4940.7

2.3.7 Numerical results

Model parameters

To start with, let us discuss the two parameters, f and A, in the $5q$ potential (2.92). The Gaussian range $A = \mu\omega/2$ originates the frequency of the

harmonic oscillator potential $V(x) = \frac{1}{2}\mu\omega^2 x^2$ of a "meson" and a "baryon" in the $5q$ state, as shown in Fig. 2.6. Hence, A is expressed by the relative distance $\langle x^2\rangle \equiv \langle\psi\,|\,x^2\,|\,\psi\rangle$ of the "meson" and "baryon" as

$$A = \frac{3}{4\,\langle x^2\rangle}, \tag{2.93}$$

with the harmonic oscillator wave function

$$\psi(x) = \left(\frac{2A}{\pi}\right)^{3/4} e^{-Ax^2}\,. \tag{2.94}$$

In this study, we assume that $\sqrt{\langle x^2\rangle}$ is less than 1 fm, namely $A \geq \frac{3}{4}$ fm^{-2}, and employ $A = 1$ fm^{-2}.

The overall strength f is a free parameter and so our numerical results are reported as a function of f. It is then convenient to set a reference value f_0. Here we use the $\bar{D}^*\Sigma_c$ diagonal term of the OPEP,

$$f_0 = \left|C^{\pi}_{\bar{D}^*\Sigma_c}(r=0)\right| \sim 6 \text{ MeV}, \tag{2.95}$$

where $C^{\pi}_{\bar{D}^*\Sigma_c}(r) \equiv -\frac{gg_1}{3f_\pi^2}C(r)$ is the central force of $V^{\pi}_{\bar{D}^*\Sigma_c-\bar{D}^*\Sigma_c}(r)$ without the spin-dependent operator $\vec{S}\cdot\vec{\sigma}$, as shown in Eq. (F.11).

When $f_0 = 6$ MeV and $A = 1$ fm^{-2} are used, the short range interaction is not as strong as what we expect from the NN force. To see this point, we compare the volume integrals of the potentials [5]

$$\left|\int d^3r f_0 e^{-Ar^2}\right| = 4.3\times10^{-6}\ \text{MeV}^{-2}, \tag{2.96}$$

$$\left|\int d^3r C^{\pi}_{\bar{D}^*\Sigma_c}(r)\right| = 1.8\times10^{-5}\ \text{MeV}^{-2}, \tag{2.97}$$

$$\left|\int d^3r V^{\pi}_{NN}(r)\right| = 6.3\times10^{-5}\ \text{MeV}^{-2}, \tag{2.98}$$

$$\left|\int d^3r V^{\sigma}_{NN}(r)\right| = 3.8\times10^{-3}\ \text{MeV}^{-2}, \tag{2.99}$$

with the central force of the OPEP and the σ exchange, V^{π}_{NN} and V^{σ}_{NN}, in the Bonn potential [59]. From Eqs. (2.96)-(2.99), we obtain

$$\left|\int d^3r f_0 e^{-Ar^2}(r)\right| \sim \frac{1}{4}\left|\int d^3r C^{\pi}_{\bar{D}^*\Sigma_c}(r)\right| \sim \frac{1}{15}\left|\int d^3r V^{\pi}_{NN}(r)\right| \sim \frac{1}{880}\left|\int d^3r V^{\sigma}_{NN}(r)\right|. \tag{2.100}$$

[5] The volume integral corresponds to the potential in the momentum space at zero momentum. Therefore, it makes an important contribution to the amplitude in the low-energy scattering.

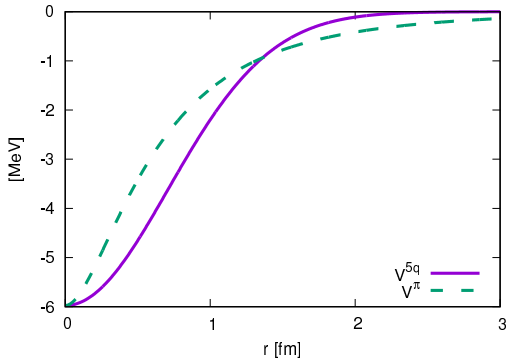

Figure 2.7: *Figure from [96]* (APS copyright). The plot of the $5q$ potential, V^{5q}, (solid line) and the central force of the OPEP in the diagonal $\bar{D}^*\Sigma_c - \bar{D}^*\Sigma_c$ term, V^{π}, (dashed line).

We find that the volume integral of the $5q$ potential with $f = f_0$ (2.96) is smaller than that of the NN potentials (2.98) and (2.99). In particular, the volume integral in Eq. (2.96) is much smaller than in Eq. (2.99) for the σ exchange potential in the NN interaction. In Section 2.3.7, we will see that the non-trivial bound and resonant states are produced for $f > 25f_0$. In Fig. 2.7, we show the $5q$ potential with the fixed parameters f_0 and A, where the obtained $5q$ potential is compared with $C^{\pi}_{\bar{D}^*\Sigma_c}(r)$.

2.3.8 Numerical methods

The bound and resonant states are obtained by solving the coupled-channel Schrödinger equation with the OPEP, $V^{\pi}(r)$, and $5q$ potential, $V^{5q}(r)$,

$$\left(K + V^{\pi}(r) + V^{5q}(r)\right)\Psi(r) = E\Psi(r), \tag{2.101}$$

with the kinetic term K. The OPEP and kinetic terms are summarized in Appendix F.

The Schrödinger equation (2.101) is solved by using the variational method. The trial function $\Psi_{JM,IM_I}(\vec{r})$ with the total angular momentum J, total isospin I, and their z-components M and M_I is expressed by the Gaussian

expansion method [60] as

$$\Psi_{JM,IM_I}(\vec{r}) = \sum_{i=1}^{i_{max}} \sum_{L,S} C_{iLS} \left[\psi_{iLM_L}(\vec{r}) \otimes \left[\chi_{s_1 m_{s_1}} \chi_{s_2 m_{s_2}} \right]_{SM_S} \right]_{JM} \left[\eta_{I_1 m_{I_1}} \eta_{I_2 m_{I_2}} \right]_{IM_I}, \tag{2.102}$$

$$\psi_{iLM_L}(\vec{r}) = \sqrt{\frac{2}{\Gamma(L+3/2) b_i^3}} \left(\frac{r}{b_i} \right)^L \exp\left(-\frac{r^2}{2b_i^2} \right) Y_{LM_L}(\hat{r}). \tag{2.103}$$

In the Gaussian expansion method, the wave function is expanded in terms of Gaussian basis functions, as shown in Eq. (2.103). The coefficients C_{iLS} are determined by diagonalizing the Hamiltonian, and $\psi_{iLM_L}(\vec{r})$ are the radial wave function of the meson-baryon with the orbital angular momentum L and the z-component M_L. The (iso)spin wave functions $\chi_{s_k m_{s_k}}$ ($\eta_{I_k m_{I_k}}$) with $k = 1, 2$ are for the (iso)spin s_k (I_k) of the hadron k, with the z-component m_{s_k} (m_{I_k}). The total (iso)spin is given by S (I) with the z-component M_S (M_I). The angular part of the wave function is represented by the spherical harmonics $Y_{LM_L}(\hat{r})$. The Gaussian ranges b_i are given by the form of geometric series as

$$b_i = b_1 a^{i-1} \quad (i = 1, \cdots, i_{max}), \tag{2.104}$$

with the variational parameters b_1 and $b_{i_{max}}$, and $a = (b_{i_{max}}/b_1)^{1/(i_{max}-1)}$.

In order to find not only bound states, but also resonances, the complex scaling method [69, 70, 71, 72] is employed. By diagonalizing the complex scaled Hamiltonian with $r \to re^{i\theta}$ and $p \to pe^{-i\theta}$, binding energies and resonance energies with decay widths are obtained as eigenenergies of the complex scaled Schrödinger equation.

2.3.9 Numerical results for the hidden-charm sector

Let us show the numerical results of the hidden-charm meson-baryon molecules. The coupling strength f dependence of the energy spectrum is summarized in Figs. 2.8-2.9 and Tables 2.9-2.10 for $J^P = 1/2^-$, in Figs. 2.10-2.11 and Tables 2.11-2.12 for $J^P = 3/2^-$, and in Fig. 2.12 and Table 2.13 for $J^P = 5/2^-$.

Figure 2.8 shows the strength f dependence of the obtained energy spectra for $J^P = 1/2^-$ by employing the OPEP and one of the three $5q$ potentials derived from the configurations (i) $(S_{c\bar{c}}, S_{3q}) = (0, 1/2)$, (ii) $(1, 1/2)$, or (iii) $(1, 3/2)$. We obtain no state only with the OPEP, corresponding to the result at $f/f_0 = 0$, while the bound and resonant states appear by increasing the strength f of the $5q$ potential. The filled circle in figures shows the starting

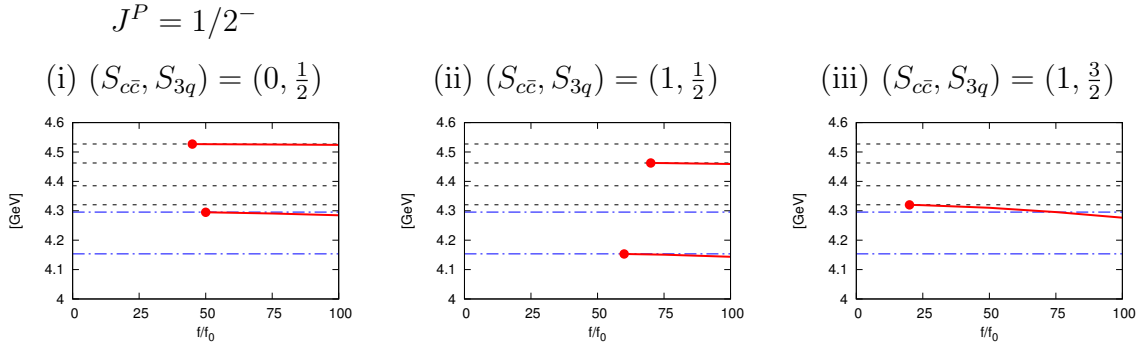

Figure 2.8: *Figure from [96]* (APS copyright). Bound and resonant state energies of the $J^P = 1/2^-$ hidden-charm molecules (solid lines) as a function of the coupling constant f/f_0 for the three possible spin configurations,(i) $(S_{c\bar{c}}, S_{3q}) = (0, 1/2)$, (ii) $(1, 1/2)$, or (iii) $(1, 3/2)$. The horizontal axis shows the ratio f/f_0, where f_0 is the reference value defined in Sec. 2.3.7. Filled circle is the starting point where the states appear. Dashed lines are the $\bar{D}\Sigma_c$, $\bar{D}\Sigma_c^*$, $\bar{D}^*\Sigma_c$, and $\bar{D}^*\Sigma_c^*$ thresholds. Dot-dashed lines are the $\bar{D}\Lambda_c$ and $\bar{D}^*\Lambda_c$ thresholds.

point where the state is found. In Fig. 2.8 (i), two resonances appear below $\bar{D}^*\Lambda_c$ and $\bar{D}^*\Sigma_c^*$ thresholds for f larger than $f/f_0 = 50$ and 45, respectively. In Fig. 2.8 (ii), the bound state and resonance are obtained below $\bar{D}\Lambda_c$ and $\bar{D}^*\Sigma_c$ thresholds for f larger than $f/f_0 = 60$ and 70, respectively. In Fig. 2.8 (iii), the resonance below the $\bar{D}\Sigma_c$ threshold appears at and above $f/f_0 = 20$ which is smaller than the strength in other channels. Thus, the $5q$ potential from the configuration with $S_{3q} = 3/2$ produces the strong attraction rather than the potential from the configuration with $S_{3q} = 1/2$, corresponding to the results in Figs. 2.8 (i) and (ii).

As shown in Fig. 2.8, the energy spectra appear just below the meson-baryon thresholds. The obtained spectrum structure can be explained by the spectroscopic factor (S-factor) of the $5q$ potential in Table 2.7. Since the S-factor gives the relative strength of the $5q$ potential among $\bar{D}^{(*)}\Lambda_c$ and $\bar{D}^{(*)}\Sigma_c^{(*)}$ channels, the channels with a large S-factor play an important role to produce bound and resonant states. For (i) $(S_{c\bar{c}}, S_{3q}) = (0, 1/2)$, the large S-factors are obtained for the $\bar{D}^*\Lambda_c$ and $\bar{D}^*\Sigma_c^*$ channels and indeed, the resonances are obtained below the $\bar{D}^*\Lambda_c$ and $\bar{D}^*\Sigma_c^*$ thresholds. In (ii) $(S_{c\bar{c}}, S_{3q}) = (1, 1/2)$, the bound and resonant states below $\bar{D}\Lambda_c$ and $\bar{D}^*\Sigma_c$ are obtained, where the large S-factors are obtained in the $\bar{D}\Lambda_c$ and $\bar{D}^*\Sigma_c$ channels. In (iii) $(S_{c\bar{c}}, S_{3q}) = (1, 3/2)$, one resonance below the $\bar{D}\Sigma_c$ threshold is found, where the large

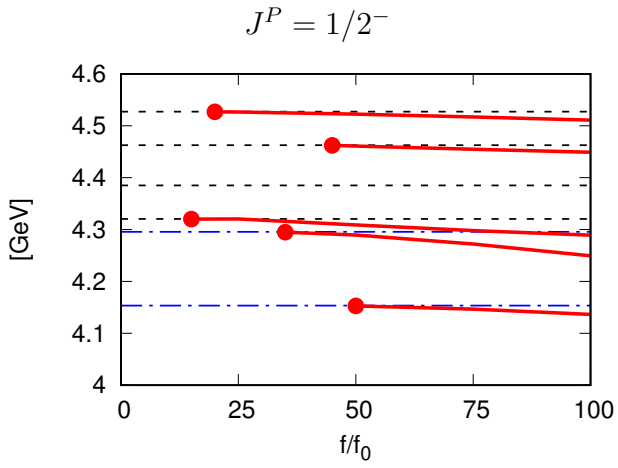

Figure 2.9: *Figure from [96]* (APS copyright). The same as Fig. 2.8 for the bound and resonant states of the hidden-charm molecules for $J^P = 1/2^-$ using the OPEP and the sum of the three $5q$ potentials.

S-factor is obtained in the $\bar{D}\Sigma_c$ channel.

In Fig. 2.9, we show the energy spectra with the full potential including OPEP and the sum of the three $5q$ potentials with the same weight. As expected, the result is a combination of the three results in Fig. 2.8 with some more attraction. As f/f_0 is increased, the resonance appear even for $f/f_0 = 15$, which would corresponds to the state found in Fig. 2.8 (iii). We see that the $5q$ potential produces many states when the strength f/f_0 is increased.

The states are also obtained in $J^P = 3/2^-$ and $5/2^-$ as well as $1/2^-$, where the structure of the energy spectra is explained by the S-factor. In Figs. 2.10 and 2.11, the strength f dependence of the energies for $J^P = 3/2^-$ is shown. We also obtain no state only with the OPEP, corresponding to the results at $f/f_0 = 0$, but the states appear when the strength of the $5q$ potential is increased as seen in $J^P = 1/2^-$. There are three $5q$ potentials derived from the quark configurations (i) $(S_{c\bar{c}}, S_{3q}) = (0, 3/2)$, (ii) $(1, 1/2)$, and (iii) $(1, 3/2)$. In Fig. 2.10 (i), two resonances are obtained near the $\bar{D}\Sigma_c^*$ and $\bar{D}^*\Sigma_c$ thresholds, where the large S-factors are obtained in the $\bar{D}\Sigma_c^*$, $\bar{D}^*\Sigma_c$, and $\bar{D}^*\Sigma_c^*$ components. In Fig. 2.10 (ii), one resonance is found near the $\bar{D}^*\Lambda_c$ threshold for $f/f_0 \geq 35$, where the S-factor of the $\bar{D}^*\Lambda_c$ is also large. In Fig. 2.10 (iii), the two resonances are found near the $\bar{D}\Sigma_c^*$ and $\bar{D}^*\Sigma_c$ thresholds, and the large S-factors are also obtained in the $\bar{D}\Sigma_c^*$ and $\bar{D}^*\Sigma_c$ channels. In Fig. 2.11, the results with the summation of the three $5q$ potentials are shown. The four resonances appear below the $\bar{D}\Lambda_c^*$ threshold for $f/f_0 \geq 35$, below the $\bar{D}\Sigma_c^*$

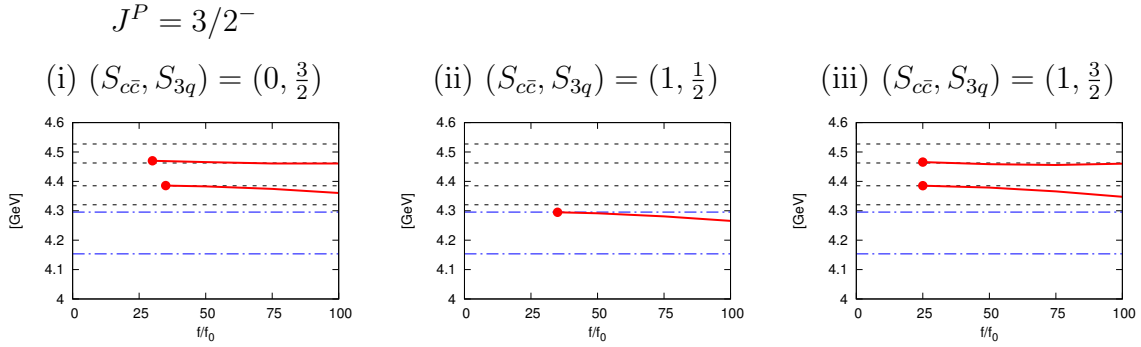

Figure 2.10: (Color online) The same as Fig. 2.8 for the resonant states of the hidden-charm molecules for $J^P = 3/2^-$ using the OPEP and one of the three $5q$ potentials derived from the configuration (i) $(S_{c\bar{c}}, S_{3q}) = (0, 3/2)$, (ii) $(1, 1/2)$, or (iii) $(1, 3/2)$.

threshold for $f/f_0 \geq 20$, below the $\bar{D}^*\Sigma_c$ threshold for $f/f_0 \geq 20$, and below the $\bar{D}^*\Sigma_c^*$ threshold for $f/f_0 \geq 30$, respectively.

The obtained energy spectra for $J^P = 5/2-$ are shown in Fig. 2.12. There is only one $5q$ potential from the quark configuration $(S_{c\bar{c}}, S_{3q}) = (1, 3/2)$, which appears only in the $\bar{D}^*\Sigma_c^*$ channel. No state is found only by employing the OPEP, while one resonance below the $\bar{D}^*\Sigma_c^*$ threshold is obtained for $f/f_0 \geq 25$.

2.3.10 Comparison with the Quark Cluster Model

It is interesting to compare our results with those of the quark model [7]. Because of the color confinement, the quark degrees of freedom become relevant only when the hadrons come close to each other. Investigating $q^4\overline{q}\ (0s)^5$ states will give a clue to the short-range part of the hadron interaction arising quark degrees of freedom.

The number of allowed states $q^4\overline{q}\ (0s)^5$ is smaller than that of the meson-baryon states. As shown in Table 2.6, the configuration of the isospin-1/2 three light quarks is either color-singlet spin-1/2, color-octet spin-1/2, or color-octet spin-3/2. Together with the spin-0 or -1 $c\bar{c}$ pair, there exist five spin-1/2, four spin-3/2, and one spin-5/2 $q^4\overline{q}\ (0s)^5$ states. The number of S-wave meson-baryon states is seven for $J = 1/2$, five for $J = 3/2$, and one for $J = 5/2$.

So, there are two [one] forbidden states for the $J = 1/2$ [3/2] system, where

Table 2.9: *Table from [96]* (APS copyright). Energy spectra of the hidden-charm molecules for $J^P = 1/2^-$ using the OPEP and one of the $5q$ potentials from the configuration (i) $(S_{c\bar{c}}, S_{3q}) = (0, 1/2)$, (ii) $(1, 1/2)$, or (iii) $(1, 3/2)$. The energy E and half decay width $\Gamma/2$ in the various coupling constants f/f_0 are shown. The third column is for the point, where the state appears. The fourth, fifth, sixth and seventh rows show the obtained values with $f = 25f_0$, $50f_0$, $75f_0$, and $100f_0$, respectively. The values are given in units of MeV. The lowest threshold $\bar{D}\Lambda_c$ is at 4153.46 MeV, and the state whose energy is lower than the threshold is a bound state (see Ref. [96]).

(i) $(0, 1/2)$	f/f_0	45	25	50	75	100
	E [MeV]	4527	—	4527	4526	4524
	$\Gamma/2$ [MeV]	0.87	—	0.98	1.77	2.53
	f/f_0	50	25	50	75	100
	E [MeV]	4295	—	4295	4291	4285
	$\Gamma/2$ [MeV]	0.22	—	0.22	1.42	4.33
(ii) $(1, 1/2)$	f/f_0	70	25	50	75	100
	E [MeV]	4463	—	—	4462	4459
	$\Gamma/2$ [MeV]	1.44	—	—	1.66	2.37
	f/f_0	60	—	—	75	100
	E [MeV]	4153	—	—	4151	4144
	$\Gamma/2$ [MeV]	—	—	—	—	—
(iii) $(1, 3/2)$	f/f_0	20	25	50	75	100
	E [MeV]	4320	4319	4310	4295	4276
	$\Gamma/2$ [MeV]	0.33	0.35	0.15	3.90×10^{-3}	8.21×10^{-2}

Table 2.10: *Table from [96]* (APS copyright). The same as Table 2.9 for the energy spectra of the hidden-charm molecules for $J^P = 1/2^-$ using the OPEP and the sum of the three $5q$ potentials.

SUM	f/f_0	20	25	50	75	100
	E [MeV]	4527	4526	4523	4517	4511
	$\Gamma/2$ [MeV]	0.63	0.85	2.00	2.79	3.33
	f/f_0	45	25	50	75	100
	E [MeV]	4462	—	4461	4455	4449
	$\Gamma/2$ [MeV]	3.27	—	3.93	6.54	8.66
	f/f_0	15	25	50	75	100
	E [MeV]	4320	4320	4309	4298	4289
	$\Gamma/2$ [MeV]	0.45	1.70	3.40	2.34	2.57×10^{-2}
	f/f_0	35	25	50	75	100
	E [MeV]	4295	—	4290	4272	4249
	$\Gamma/2$ [MeV]	2.01×10^{-2}	—	6.17×10^{-2}	9.23×10^{-2}	7.93×10^{-2}
	f/f_0	50	25	50	75	100
	E [MeV]	4153	—	4153	4147	4136
	$\Gamma/2$ [MeV]	—	—	—	—	—

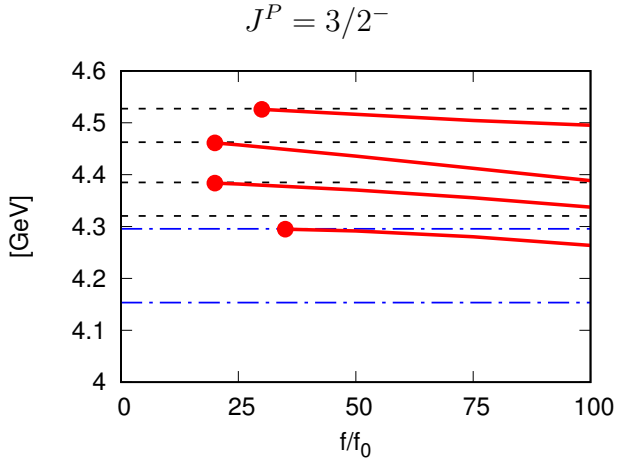

Figure 2.11: *Figure from [96]* (APS copyright). The same as Fig. 2.8 for the resonant states of the hidden-charm molecules for $J^P = 3/2^-$ using the OPEP and the sum of the three $5q$ potentials.

a certain combination of the meson-baryon states is forbidden to exist as a $(0s)^5$ configuration. The normalization of such states reduces to zero. This leads to a strong repulsion to that particular combination of the meson-baryon states. On the other hand, there are channels where the normalization is larger than 1, which brings the system an attraction. The five quark states listed in Table 2.8 have a normalization of 4/3.

Moreover, the color magnetic interaction (CMI) between quarks can contribute to the hadron interaction. In Ref. [7], the CMI, especially, in the color-octet spin-3/2 configuration of three light quarks brings to an attraction between $\bar{D}Y_c$.

It was reported in Ref. [7] that the quark cluster model gives a very shallow bound state for $J = 5/2$ (4519.9 MeV), a cusp and a resonance for 3/2 (4379.3, 4457.8 MeV), and a resonance for $J = 1/2$ channels (4317.0 MeV), which have a very similar mass to the recently observed $P_c(4312)$. This result is impressive as at the time in which we made these predictions the $P_c(4312)$ was still to be observed. The lightest observed pentaquark $P_c(4312)$ was also investigate by Ramirez et al. in Ref. [36], but they did not find support for a bound molecule. Based on a systematic analysis of the reaction amplitudes, they conclude instead that the interpretation of the $P^c(4312)$ peak as a virtual (unbound) state is more likely.

The bound state appears which appear in the $J^P = 5/2^-$ channel when the

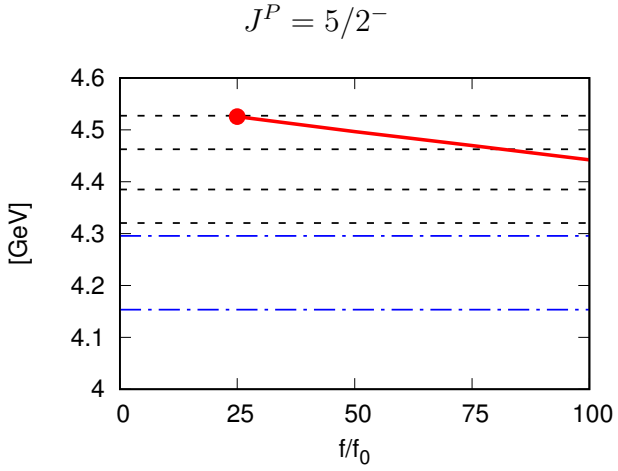

Figure 2.12: *Figure from [96]* (APS copyright). The same as Fig. 2.8 for the resonant states of the hidden-charm molecules for $J^P = 5/2^-$ using the OPEP and the $5q$ potential from the configuration $(S_{c\bar{c}}, S_{3q}) = (1, \frac{3}{2})$.

strength of the short-range interaction is about $f/f_0 = 25$ (Fig. 2.12) has a mass compatible with the shallow bound state for $J = 5/2$ (4519.9 MeV) found in Ref. [7] so we may consider that this strength roughly corresponds to that of the quark cluster model because there is a shallow bound state in the channel. Suppose the strength determined in the $J^P = 5/2^-$ channel can also apply to the other channels, then there are two resonances in the $J^P = 3/2^-$ channels at around the same energies as those of the quark cluster model (Fig. 2.11). In the $J^P = 1/2^-$ channel, there are two resonances at $f/f_0 = 25$; one of them corresponds to the quark model results, but additional resonance appears at around $\bar{D}^*\Sigma_c^*$ threshold (Fig. 2.9). With this exception, the results of the present work are similar to the quark model one. In the present approach, coupling to the five-quark states gives an attraction to the meson-baryon channel, which plays the same role as the ones from the above mentioned attraction in the quark model.

Table 2.11: *Table from [96]* (APS copyright). The same as Table 2.9 for the energy spectra of the hidden-charm molecules for $J^P = 3/2^-$ using the OPEP and one of the three $5q$ potentials from the configuration (i) $(S_{c\bar{c}}, S_{3q}) = (0, 3/2)$, (ii) $(1, 1/2)$, or (iii) $(1, 3/2)$.

(i) $(0, 3/2)$	f/f_0	30	25	50	75	100
	E [MeV]	4470	—	4466	4461	4461
	$\Gamma/2$ [MeV]	10.49	—	17.16	26.61	38.75
	f/f_0	35	25	50	75	100
	E [MeV]	4386	—	4383	4374	4360
	$\Gamma/2$ [MeV]	2.21	—	3.33	4.08	3.66
(ii) $(1, 1/2)$	f/f_0	35	25	50	75	100
	E [MeV]	4295	—	4292	4281	4265
	$\Gamma/2$ [MeV]	2.64×10^{-2}	—	4.47×10^{-2}	8.92×10^{-4}	0.109
(iii) $(1, 3/2)$	f/f_0	25	25	50	75	100
	E [MeV]	4466	4466	4459	4456	4460
	$\Gamma/2$ [MeV]	9.96	9.96	16.51	23.50	28.94
	f/f_0	25	25	50	75	100
	E [MeV]	4385	4385	4379	4366	4348
	$\Gamma/2$ [MeV]	1.85	1.85	2.96	2.45	1.57

Table 2.12: *Table from [96]* (APS copyright). The same as Table 2.9 for the energy spectra of the hidden-charm molecules for $J^P = 3/2^-$ using the OPEP and the sum of the three $5q$ potentials.

SUM	f/f_0	30	25	50	75	100
	E [MeV]	4526	—	4516	4505	4495
	$\Gamma/2$ [MeV]	9.58	—	13.52	17.60	22.34
	f/f_0	20	25	50	75	100
	E [MeV]	4461	4457	4436	4412	4389
	$\Gamma/2$ [MeV]	11.61	12.83	14.70	13.17	10.56
	f/f_0	20	25	50	75	100
	E [MeV]	4384	4382	4370	4355	4338
	$\Gamma/2$ [MeV]	3.11	3.62	4.69	4.86	4.59
	f/f_0	35	25	50	75	100
	E [MeV]	4295	—	4291	4280	4264
	$\Gamma/2$ [MeV]	1.41×10^{-2}	—	5.09×10^{-2}	7.71×10^{-2}	8.15×10^{-2}

Table 2.13: *Table from [96]* (APS copyright). The same as Table 2.9 for the energy spectra of the hidden-charm molecules for $J^P = 5/2^-$ using the OPEP and the $5q$ potential from the configuration $(S_{c\bar{c}}, S_{3q}) = (1, 3/2)$.

$(1, 3/2)$	f/f_0	25	25	50	75	100
	E [MeV]	4526	4526	4496	4470	4442
	$\Gamma/2$ [MeV]	28.04	28.04	27.15	22.61	17.54

Table 2.14: Energy spectra of the hidden-bottom molecules only with the OPEP. The energy E and the half decay width $\Gamma/2$ are given in units of MeV. The lowest threshold $B\Lambda_b$ is at 10898.51 MeV.

$J^P = 1/2^-$	E [MeV]	10898	10943	11151
	$\Gamma/2$ [MeV]	—	1.80×10^{-2}	2.01
$J^P = 3/2^-$	E [MeV]	10942		
	$\Gamma/2$ [MeV]	3.08×10^{-2}		

2.3.11 Numerical results for the hidden-bottom sector

We discuss the hidden-bottom meson-baryon molecules in this section. The basic features of the potentials are unchanged from those of the hidden-charm, except that the cutoff parameters of the OPEP are different as summarized in Sec. 2.3.5. However, the hadron masses in the bottom sector are larger than those in the charm sector, and the mass splittings of the HQS multiplet (B and B^*, and Σ_b and Σ_b^*) are small. Because of these facts, more states are expected for the bottom sector. As a matter of fact, we find that only the OPEP provides sufficiently strong attraction to generate several bound and resonant states. The obtained energies only with the OPEP are summarized in Table. 2.14. Since the OPEP yields the strong attraction, we will see that both the OPEP and the $5q$ potentials have an important role to produce the energy spectra, while the S-factor of the $5q$ potential designs the spectra in the hidden-charm sector.

In Fig. 2.13 and Tables 2.15-2.17, the strength f dependence of the energy spectra obtained for $J^P = 1/2^-$ by using the OPEP and one of the three $5q$ potentials is shown. The three $5q$ potentials are from the configurations (i) $(S_{b\bar{b}}, S_{3q}) = (0, 1/2)$, (ii) $(1, 1/2)$, and (iii) $(1, 3/2)$ which are the same as discussed in the hidden-charm sector. In Fig. 2.13 (i), we find three states appearing for $f/f_0 \geq 0$ below the three thresholds of $B\Lambda_b$, $B^*\Lambda_b$, and $B^*\Sigma_b^*$. These states originate in those obtained only by using the OPEP in Table 2.14. As f is increased, and reaches around $f/f_0 \sim 100$, another state appears below the $B\Sigma_b^*$ threshold. Here, we find that the S-factor of the $5q$ potential is zero in the $B\Sigma_b^*$ component, while the large S-factor is obtained in the $B^*\Lambda_b$ and $B^*\Sigma_b^*$ components. In producing the state, not only the $5q$ potential, but also the OPEP have the important role.

In Figs. 2.13 (ii) and (iii), and Tables 2.16 and 2.17, we show the energy spectra for using the $5q$ potentials from the other quark configurations (ii) and

(iii). These energy spectra also show the three states for $f/f_0 \geq 0$ originating in those produced only by the OPEP. In Fig. 2.13 (ii) , one resonance appears below the $B\Sigma_b^*$, as f is increased. In Fig. 2.13 (iii), two resonances appear below the $B\Sigma_b$ threshold, where the large S-factor of the $5q$ potential is obtained in the $B\Sigma_b$ component.

In Fig. 2.14 and Table 2.18, the results are shown with the full potential including OPEP and the sum of the three $5q$ potentials for $J^P = 1/2^-$. The three states appearing below the $B\Lambda_b$, $B^*\Lambda_b$ and $B^*\Sigma_b$ thresholds for $f/f_0 \geq 0$ originate those obtained only by using the OPEP. Moreover, we obtain three resonances as f is increased.

The states are also found in $J^P = 3/2^-$. Fig. 2.15 and Tables 2.19-2.21 show the results with the OPEP and one of the $5q$ potentials derived from the quark configurations (i) $(S_{b\bar{b}}, S_{3q}) = (0, 3/2)$, (ii) $(1, 1/2)$, and (iii) $(1, 3/2)$. In Figs. 2.15 (i), (ii), and (iii), one state appears below the $B^*\Lambda_b$ threshold for $f/f_0 \geq 0$, which originates in the state obtained only by using the OPEP in Table 2.14. In addition, we obtain the states as f is increased. In Fig. 2.15 (i), two resonances appear below the $B\Sigma_b^*$ and $B^*\Sigma_b$ thresholds, where the large S-factors of the $5q$ potential are obtained in the $B\Sigma_b^*$, $B^*\Sigma_b$, and $B^*\Sigma_b^*$ components. In Fig. 2.15 (ii), two resonances appear below the $B^*\Lambda_b$ and $B^*\Sigma_b$ thresholds, where the large S-factor is obtained in the $B^*\Lambda_b$ component. In Fig. 2.15 (ii), three resonances appear near the $B\Sigma_b^*$, $B^*\Sigma_b$, and $B^*\Sigma_b^*$ thresholds, where the large S-factors are obtained in the $B\Sigma_b^*$ and $B^*\Lambda_b$ components. In the results obtained for $J^P = 3/2^-$, several spectra can be explained by the large S-factors of the $5q$ potential, while both the OPEP and $5q$ potential are important in producing the other states. The energy spectra with the full potential including the OPEP and the sum of the three $5q$ potentials for $J^P = 3/2^-$ are displayed in Fig. 2.16 and Tables 2.22-2.23. The state below the $B^*\Lambda_b$ threshold for $f/f_0 \geq 0$ originates the state obtained only by using the OPEP. Moreover, many states appear, when the $5q$ potential is switched on.

Figure 2.17 and Table 2.24 give the strength f dependence of the energy spectra for $J^P = 5/2^-$ with the OPEP and the $5q$ potential from the quark configuration $(S_{b\bar{b}}, S_{3q}) = (1, 3/2)$. For $J^P = 5/2^-$, we do not obtain any state when only the OPEP is employed. The three resonances are obtained, as f of the $5q$ potential is increased. Two resonances appear near the $B^*\Sigma_b$ threshold. The state obtained for $20 \leq f/f_0 \leq 50$ disappears as f is increased, whose width becomes large. Moreover, one resonance appears above the $B^*\Lambda_b$ threshold for $f/f_0 \geq 50$.

In the hidden-bottom sector, the OPEP is strong enough to produce states due to the mixing effect enhanced by the small mass splitting between B and B^*, and Σ_b and Σ_b^*. Thus, both the OPEP and the $5q$ potential play the

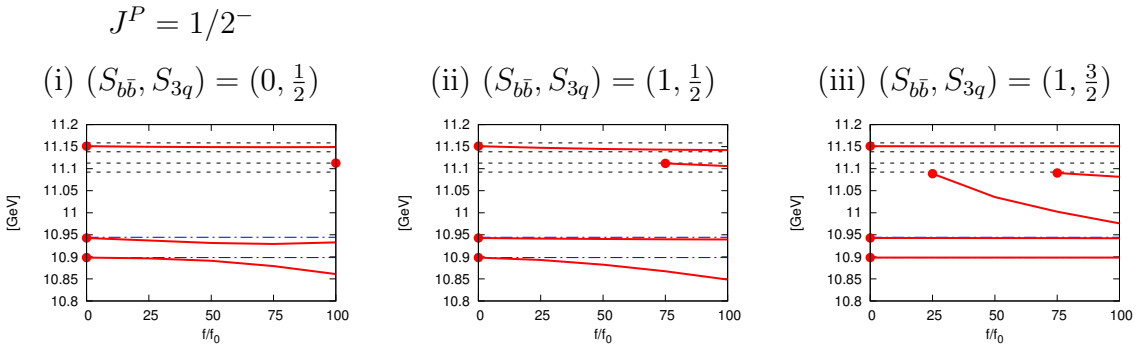

Figure 2.13: *Figure from [96]* (APS copyright). Bound and resonant states of the hidden-bottom molecules with various coupling constants f for $J^P = 1/2^-$, using the OPEP and one of the three $5q$ potentials derived from the configuration (i) $(S_{b\bar{b}}, S_{3q}) = (0, 1/2)$, (ii) $(1, 1/2)$, or (iii) $(1, 3/2)$. The horizontal axis shows the ratio f/f_0, where f_0 is the reference value defined in Sec. 2.3.7. Solid line shows the obtained state. Filled circle is the starting point where the states appear. Dashed lines are the $B\Sigma_b$, $B\Sigma_b^*$, $B^*\Sigma_b$, and $B^*\Sigma_b^*$ thresholds. Dot-dashed lines are the $B\Lambda_b$ and $B^*\Lambda_b$ thresholds.

important role to produce many states, while the $5q$ potential has the dominant role to yield the states in the hidden-charm sector. Since the attraction from the OPEP is enhanced and the kinetic term is suppressed due to the large hadron masses, the hidden-bottom pentaquarks are more likely to form rather than the hidden-charm pentaquarks.

2.3.12 Summary of the section

We have studied hidden-charm and hidden-bottom pentaquark states. Since the observed P_c's are in the open-charm threshold region, we have performed a coupled channel analyses with various meson-baryon states which may generate bound and resonant states. In such an analysis, the hadronic interaction is the most important input. At long distances, we employ the one-pion exchange potential which is best known among various hadron interactions. As discussed and emphasized in many works, the OPEP provides attraction when the tensor force is at work through the SD coupled channels. This is crucially important for the formation of the exotic pentaquark states.

Contrary, for short range interaction which is far less known, we inferred from a recent quark cluster model analysis pointing out the importance of the colorful $5q$ configurations. We have included these $5q$ configurations in the

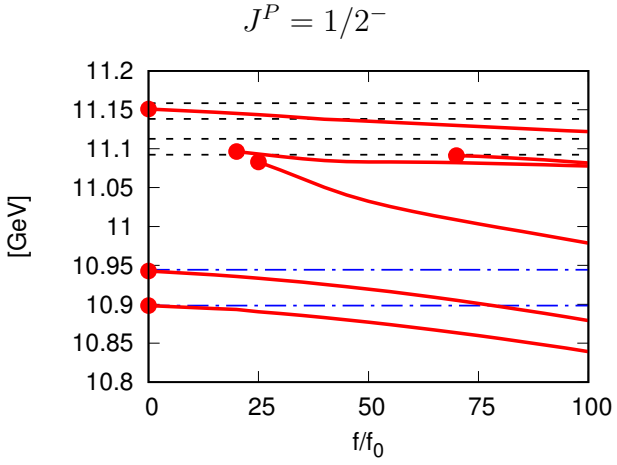

Figure 2.14: *Figure from [96]* (APS copyright). The same as Fig. 2.13 for the bound and resonant states of the hidden-bottom molecules for $J^P = 1/2^-$ using the OPEP and the sum of the three $5q$ potentials.

coupled channel problems as one-particle states. By eliminating them we have derived an effective interaction at short distances. Since all the expected $5q$ states locate above the meson-baryon threshold region, the resulting effective interaction is attractive, which can be another driving force for the generation of the pentaquark states. The coupling of this interaction to various meson-baryon channels is estimated by the spectroscopic factor. Therefore, our model contains essentially only one parameter which is the overall strength of the short range interaction f. Then results are shown for various f up to the maximum strength which we expect from our current knowledge of the hadron interaction.

For the charm sector, when the $5q$ interaction is turned on, bound and resonant states are generated for various spins, $1/2^-$, $3/2^-$, and $5/2^-$. Among them, $3/2^-$ state with mass around 4460 MeV and width around 25 MeV (see Table 2.11) is a candidate of the observed P_c, though the spin parity identification is not the suggested one. Therefore, in this paper, we have further concentrated on the mechanism how the pentaquark states are generated.

For the bottom sector, due to the suppression of the kinetic energy, we have seen pentaquark states even only by the OPEP. These are the rather robust predictions of our analysis. Therefore, with possible further attractions from the short range interaction, we indeed expect many exotic pentaquark states. In this way, we suggest experimental analysis to search for further states in the bottom region.

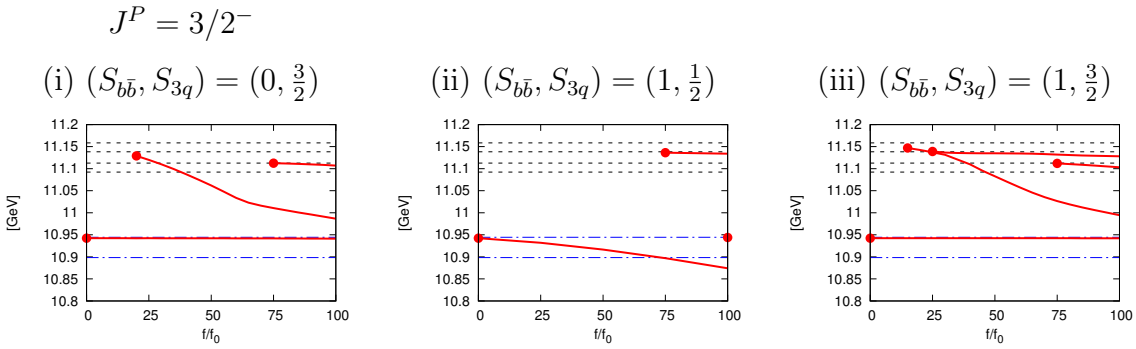

Figure 2.15: *Figure from [96]* (APS copyright). The same as Fig. 2.13 for the bound and resonant states of the hidden-bottom molecules for $J^P = 3/2^-$ using the OPEP and one of the three $5q$ potentials derived from the configuration (i) $(S_{b\bar{b}}, S_{3q}) = (0, 3/2)$, (ii) $(1, 1/2)$, or (iii) $(1, 3/2)$.

We have also compared our present analysis with the previous quark cluster model one. We have found similarities between them, and therefore, our approach provides a good method to make physical interpretations for the results of the quark cluster model.

In the present analysis we have studied negative parity states dominated by the S-wave configurations of open charm channels. For more complete analysis, it is needed to include hidden-charm channels such as $J/\psi p$. In the case of the $Z_c(3900)$, the importance of the mixing of $\bar{D}D^* - J/\psi\pi$ has been indicated by a lattice QCD simulation [61]. It is also interesting to study positive parity states. For this, we need P-wave excitations for both meson-baryon and for 5q states. Moreover, couplings to such as $\bar{D}\Lambda_c(2595)$ channel can be important because of their very close threshold to the $\bar{D}\Lambda_c(2595)$ threshold, and to the reported $P_c(4450)$ state [19]. As discussed in Ref. [62], such a coupling may show up a unique feature of the universal phenomena caused by the almost on-shell pion decaying from the $\Lambda_c(2595)$. All these issues may be studied as interesting future investigations.

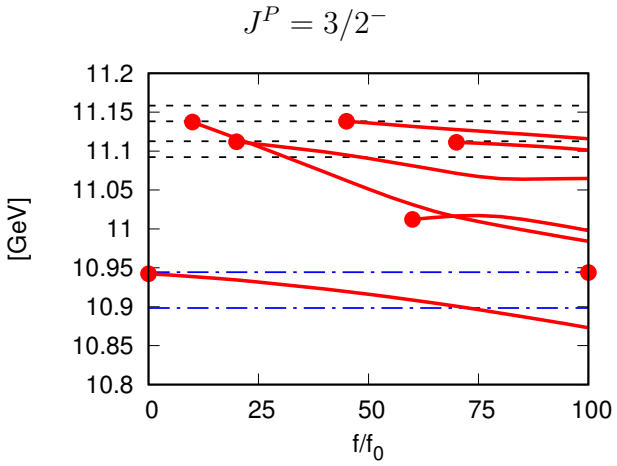

Figure 2.16: *Figure from [96]* (APS copyright). The same as Fig. 2.13 for the bound and resonant states of the hidden-bottom molecules for $J^P = 3/2^-$ using the OPEP and the sum of the three $5q$ potentials.

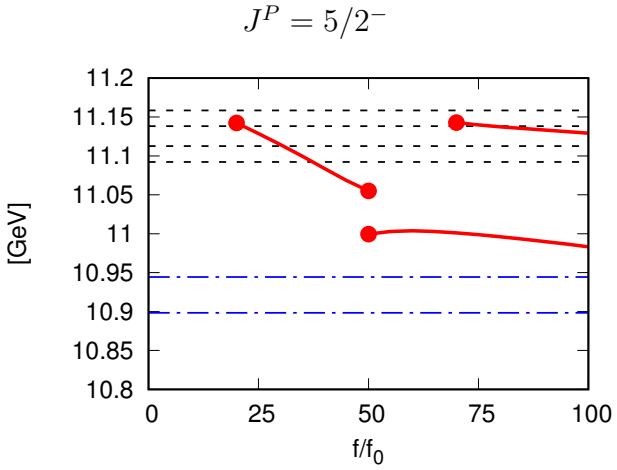

Figure 2.17: *Figure from [96]* (APS copyright). The same as Fig. 2.13 for the resonant states of the hidden-bottom molecules for $J^P = 5/2^-$ using the OPEP and the $5q$ potential from the configuration $(S_{b\bar{b}}, S_{3q}) = (1, \frac{3}{2})$.

Table 2.15: *Table from [96]* (APS copyright). Energy spectra of the hidden-bottom molecules for $J^P = 1/2^-$ using the OPEP and the $5q$ potential from the configuration (i) $(S_{b\bar{b}}, S_{3q}) = (0, 1/2)$. The energy E and half decay width $\Gamma/2$ in the various coupling constants f/f_0 are shown. The third row is for the point, where the state appears. The fourth, fifth, sixth and seventh rows show the obtained values with $f = 25f_0$, $50f_0$, $75f_0$, and $100f_0$, respectively. The values are given in units of MeV. The lowest threshold $B\Lambda_b$ is at 10898.51 MeV, and the state whose energy is lower than the threshold is a bound state.

(i) $(0, 1/2)$	f/f_0	0	25	50	75	100
	E [MeV]	11151	11150	11149	11149	11149
	$\Gamma/2$ [MeV]	2.01	3.05	4.25	5.32	6.08
	f/f_0	100	25	50	75	100
	E [MeV]	11113	—	—	—	11113
	$\Gamma/2$ [MeV]	6.43	—	—	—	6.43
	f/f_0	0	25	50	75	100
	E [MeV]	10943	10937	10932	10929	10933
	$\Gamma/2$ [MeV]	1.80×10^{-2}	0.55	2.92	7.13	7.89
	f/f_0	0	25	50	75	100
	E [MeV]	10898	10897	10891	10879	10861
	$\Gamma/2$ [MeV]	—	—	—	—	—

Table 2.16: *Table from [96]* (APS copyright). The same as Table 2.15 for the energy spectra of the hidden-bottom molecules for $J^P = 1/2^-$ using the OPEP and the $5q$ potential from the configuration (ii) $(S_{b\bar{b}}, S_{3q}) = (1, 1/2)$.

(ii) $(1, 1/2)$	f/f_0	0	25	50	75	100
	E [MeV]	11151	11147	11145	11143	11142
	$\Gamma/2$ [MeV]	2.01	1.75	2.76	4.22	5.52
	f/f_0	75	25	50	75	100
	E [MeV]	11112	—	—	11112	11106
	$\Gamma/2$ [MeV]	7.68	—	—	7.68	5.25
	f/f_0	0	25	50	75	100
	E [MeV]	10943	10941	10941	10940	10939
	$\Gamma/2$ [MeV]	1.80×10^{-2}	0.19	0.31	0.33	0.22
	f/f_0	0	25	50	75	100
	E [MeV]	10898	10893	10882	10867	10848
	$\Gamma/2$ [MeV]	—	—	—	—	—

Table 2.17: *Table from [96]* (APS copyright). The same as Table 2.15 for the energy spectra of the hidden-bottom molecules for $J^P = 1/2^-$ using the OPEP and the $5q$ potential from the configuration (iii) $(S_{b\bar{b}}, S_{3q}) = (1, 3/2)$.

(iii) $(1, 3/2)$	f/f_0	0	25	50	75	100
	E [MeV]	11151	11151	11151	11151	11151
	$\Gamma/2$ [MeV]	2.01	2.63	2.89	2.92	2.91
	f/f_0	75	25	50	75	100
	E [MeV]	11090	—	—	11090	11082
	$\Gamma/2$ [MeV]	0.37	—	—	0.37	0.30
	f/f_0	25	25	50	75	100
	E [MeV]	11089	11089	11036	11002	10976
	$\Gamma/2$ [MeV]	29.54	29.54	26.93	12.38	4.35
	f/f_0	0	25	50	75	100
	E [MeV]	10943	10943	10943	10943	10942
	$\Gamma/2$ [MeV]	1.80×10^{-2}	0.13	0.13	0.13	0.17
	f/f_0	0	25	50	75	100
	E [MeV]	10898	10898	10898	10898	10898
	$\Gamma/2$ [MeV]	—	—	—	—	—

Table 2.18: *Table from [96]* (APS copyright). The same as Table 2.15 for the energy spectra of the hidden-bottom molecules for $J^P = 1/2^-$ using the OPEP and the sum of the three $5q$ potentials.

SUM	f/f_0	0	25	50	75	100
	E [MeV]	11151	11144	11135	11129	11122
	$\Gamma/2$ [MeV]	2.01	2.67	0.60	0.58	0.60
	f/f_0	70	25	50	75	100
	E [MeV]	11091	—	—	11090	11082
	$\Gamma/2$ [MeV]	0.36	—	—	0.44	0.75
	f/f_0	20	25	50	75	100
	E [MeV]	11096	11093	11083	11081	11078
	$\Gamma/2$ [MeV]	44.69	11.35	14.15	31.45	39.32
	f/f_0	25	25	50	75	100
	E [MeV]	11083	11083	11033	11003	10979
	$\Gamma/2$ [MeV]	78.77	78.77	40.76	14.49	4.03
	f/f_0	0	25	50	75	100
	E [MeV]	10943	10934	10920	10901	10879
	$\Gamma/2$ [MeV]	1.80×10^{-2}	1.91×10^{-2}	5.80×10^{-2}	0.12	—
	f/f_0	0	25	50	75	100
	E [MeV]	10898	10891	10877	10860	10839
	$\Gamma/2$ [MeV]	—	—	—	—	—

Table 2.19: *Table from [96]* (APS copyright). The same as Table 2.15 for the energy spectra of the hidden-bottom molecules for $J^P = 3/2^-$ using the OPEP and the $5q$ potential from the configuration (i) $(S_{b\bar{b}}, S_{3q}) = (0, 3/2)$.

(i) $(0, 3/2)$	f/f_0	75	25	50	75	100
	E [MeV]	11112	—	—	11112	11107
	$\Gamma/2$ [MeV]	1.13	—	—	1.13	1.13
	f/f_0	20	25	50	75	100
	E [MeV]	11129	11120	11062	11011	10987
	$\Gamma/2$ [MeV]	57.15	59.69	64.94	34.53	16.76
	f/f_0	0	25	50	75	100
	E [MeV]	10942	10942	10942	10942	10941
	$\Gamma/2$ [MeV]	3.08×10^{-2}	0.15	0.17	0.16	0.23

Table 2.20: *Table from [96]* (APS copyright). The same as Table 2.15 for the energy spectra of the hidden-bottom molecules for $J^P = 3/2^-$ using the OPEP and the $5q$ potential from the configuration (ii) $(S_{b\bar{b}}, S_{3q}) = (1, 1/2)$.

(ii) $(1, 1/2)$	f/f_0	75	25	50	75	100
	E [MeV]	11136	—	—	11136	11134
	$\Gamma/2$ [MeV]	19.45	—	—	19.45	11.86
	f/f_0	100	25	50	75	100
	E [MeV]	10944	—	—	—	10944
	$\Gamma/2$ [MeV]	0.11	—	—	—	0.11
	f/f_0	0	25	50	75	100
	E [MeV]	10942	10932	10917	10897	10874
	$\Gamma/2$ [MeV]	3.08×10^{-2}	0.13	0.11	—	—

Table 2.21: *Table from [96]* (APS copyright). The same as Table 2.15 for the energy spectra of the hidden-bottom molecules for $J^P = 3/2^-$ using the OPEP and the $5q$ potential from the configuration (iii) $(S_{b\bar{b}}, S_{3q}) = (1, 3/2)$.

(iii) $(1, 3/2)$	f/f_0	25	25	50	75	100
	E [MeV]	11139	11139	11135	11132	11128
	$\Gamma/2$ [MeV]	22.58	22.58	16.00	11.53	12.61
	f/f_0	75	25	50	75	100
	E [MeV]	11112	—	—	11112	11103
	$\Gamma/2$ [MeV]	1.91	—	—	1.91	1.15
	f/f_0	15	25	50	75	100
	E [MeV]	11147	11137	11083	11027	10995
	$\Gamma/2$ [MeV]	47.21	45.51	40.07	28.14	11.19
	f/f_0	0	25	50	75	100
	E [MeV]	10942	10942	10942	10942	10942
	$\Gamma/2$ [MeV]	3.08×10^{-2}	8.92×10^{-3}	1.01×10^{-2}	1.21×10^{-2}	1.68×10^{-2}

Table 2.22: *Table from [96]* (APS copyright). The same as Table 2.15 for the energy spectra of the hidden-bottom molecules for $J^P = 3/2^-$ using the OPEP and the sum of the three $5q$ potentials.

SUM	f/f_0	45	25	50	75	100
	E [MeV]	11138	—	11136	11126	11116
	$\Gamma/2$ [MeV]	5.13	—	5.71	3.78	1.94
	f/f_0	70	25	50	75	100
	E [MeV]	11111	—	—	11110	11101
	$\Gamma/2$ [MeV]	0.27	—	—	0.35	0.70
	f/f_0	20	25	50	75	100
	E [MeV]	11112	11109	11091	11067	11065
	$\Gamma/2$ [MeV]	4.40	5.57	11.82	28.88	51.60
	f/f_0	60	25	50	75	100
	E [MeV]	11012	—	—	11017	10998
	$\Gamma/2$ [MeV]	53.76	—	—	37.95	10.85

Table 2.23: *Table from [96]* (APS copyright). Continued from Table 2.22.

SUM	f/f_0	10	25	50	75	100
	E [MeV]	11137	11106	11051	11010	10984
	$\Gamma/2$ [MeV]	52.77	58.70	54.22	29.71	12.94
	f/f_0	100	25	50	75	100
	E [MeV]	10944	—	—	—	10944
	$\Gamma/2$ [MeV]	4.70×10^{-3}	—	—	—	4.70×10^{-3}
	f/f_0	0	25	50	75	100
	E [MeV]	10942	10932	10916	10896	10873
	$\Gamma/2$ [MeV]	3.08×10^{-2}	7.83×10^{-3}	1.97×10^{-3}	—	—

Table 2.24: *Table from [96]* (APS copyright). The same as Table 2.15 for the energy spectra of the hidden-bottom molecules for $J^P = 5/2^-$ using the OPEP and the $5q$ potential from the configuration $(S_{b\bar{b}}, S_{3q}) = (1, 3/2)$.

$(1, 3/2)$	f/f_0	70	25	50	75	100
	E [MeV]	11142.84	—	—	11139.85	11129.35
	$\Gamma/2$ [MeV]	15.89	—	—	12.66	5.15
	f/f_0	20	25	50	75	100
	E [MeV]	11142.42	11128.79	11055.16	—	—
	$\Gamma/2$ [MeV]	123.11	125.94	153.98	—	—
	f/f_0	50	25	50	75	100
	E [MeV]	10999.46	—	10999.46	10998.89	10983.33
	$\Gamma/2$ [MeV]	71.82	—	71.82	36.75	17.97

2.4 Heavy quark spin symmetry with chiral tensor dynamics in the light of the recent LHCb pentaquarks

2.4.1 The new analysis by LHCb in 2018

The new analysis by LHCb [34] performed using nine times more data from the Large Hadron Collider than the 2015 analysis showed that the parameters of the previously reported $P_c^+(4450)$, and $P_c^+(4380)$ structures were consistent with the original results. As well as revealing the new $P_c^+(4312)$ state, the analysis also uncovered a more complex structure of $P_c^+(4450)$, consisting of two narrow nearby separate peaks, $P_c^+(4440)$ and $P_c^+(4457)$, with the two-peak structure hypothesis having a statistical significance of 5.4 sigma with respect to the single-peak structure hypothesis. As for a broad state $P_c^+(4380)$ (width $\sim$ 200MeV), in the new analysis using higher-order polynomial functions for the background, data can be fitted equally well without the Breit-Wigner contribution corresponding to broad $P_c^+(4380)$ state. The masses and widths of the three narrow pentaquark states are as follows [34].

$$\begin{aligned} P_c^+(4312): M &= 4311.9 \pm 0.7^{+6.8}_{-0.6}\ \text{MeV}\,, \\ \Gamma &= 9.8 \pm 2.7^{+3.7}_{-4.5}\ \text{MeV}\,; \\ P_c^+(4440): M &= 4440.3 \pm 1.3^{+4.1}_{-4.7}\ \text{MeV}\,, \\ \Gamma &= 20.6 \pm 4.9^{+8.7}_{-10.1}\ \text{MeV}\,; \\ P_c^+(4457): M &= 4457.3 \pm 0.6^{+4.1}_{-1.7}\ \text{MeV}\,, \\ \Gamma &= 6.4 \pm 2.0^{+5.7}_{-1.9}\ \text{MeV}\,. \end{aligned}$$

As discussed by LHCb [34], $P_c^+(4312)$ is just below the $\Sigma_c\bar{D}$ threshold, while the higher ones $P_c^+(4440)$ and $P_c^+(4457)$ are both below the $\Sigma_c\bar{D}^*$ threshold. This change of the experimental observation motivated new theoretical investigations [86, 87, 88, 89, 90, 91, 92, 93, 95].

In Ref. [96] we studied the hidden-charm pentaquarks by coupling the $\bar{D}^{(*)}\Lambda_c$ and $\bar{D}^{(*)}\Sigma_c^{(*)}$ meson-baryon channels to a $uudc\bar{c}$ compact core with a meson-baryon binding interaction satisfying the heavy quark and chiral symmetries. In that work we expressed the hidden-charm pentaquark masses and decay widths as functions of one free parameter, which is proportional to the coupling strength between the meson-baryon and 5-quark-core states. Here we show that once the parameter is determined, we can predict the masses and widths of various pentaquark states and discuss the underlying dynamics.

Interestingly enough, our model has predicted two years before the new LHCb analysis [34] the masses and decay widths consistently with the new data [34] with the following quantum number assignments: $\mathbf{J^P_{P_c^+(4312)} = 1/2^-}$, $\mathbf{J^P_{P_c^+(4440)} = 3/2^-}$ and $\mathbf{J^P_{P_c^+(4457)} = 1/2^-}$ [96],[67].

In this section, following Ref. [67], we study the origin of the mass difference between $P_c^+(4440)$ and $P_c^+(4457)$ by performing the calculations with and without the tensor term of the one-pion exchange potential (OPEP). The importance of the tensor force is emphasized as "chiral tensor dynamics".

2.4.2 Results and summary of the section

All the ingredients of our model of Ref. [96] are reported in chapter 2.3. In Fig. 2.18, experimental data and our predictions are compared. The center of the bars are located at the central values of pentaquark masses whiles their lengths correspond to the pentaquark widths with the exception of the $P_c(4380)$ width, which is too large and does not fit into the shown energy region. The boxed numbers are the masses of the recently observed states [34], and the corresponding predictions in our model [96]. The dashed lines are for threshold values. Our predicted masses and the decay widths are obtained by setting the free parameter introduced in Ref. [96], f/f_0, at $f/f_0 = 45$ [67], which corresponds to the minimum value necessary to have all the three new LHCb states [34]. Here, f_0 is the strength of the one-pion exchange diagonal term for the $\Sigma_c\bar{D}^*$ meson-baryon channel, $f_0 = \left|C^{\pi}_{\bar{D}^*\Sigma_c}(r=0)\right| \sim 6$ MeV (see Ref. [96]). We observe that not only the masses of all the three new states but also their small widths are reproduced within the experimental errors. We find as expected that the dominant components of these states are nearby threshold channels and with the quantum numbers as follows; $\Sigma_c\bar{D}$ with $J^P = 1/2^-$ ($P_c^+(4312)$), $\Sigma_c\bar{D}^*$ with $J^P = 3/2^-$ ($P_c^+(4440)$) and with $J^P = 1/2^-$ ($P_c^+(4457)$) meson-baryon molecular states. In Tab. 2.25, our predicted experimental mass spectra and decay widths [67] are compared with our predictions and the ones reported in Ref. [87] and scenario A of Ref. [88]. The mass difference between $P_c(4440)$ and $P_c(4457)$ is not reproduced in [87] and the assignments of the quantum numbers for these states are different from ours.

Since these two states are located near $\Sigma_c\bar{D}^*$ threshold and both states have the narrow widths, it is natural to consider them to form the spin doublet of 1/2 and 3/2 in S-wave.

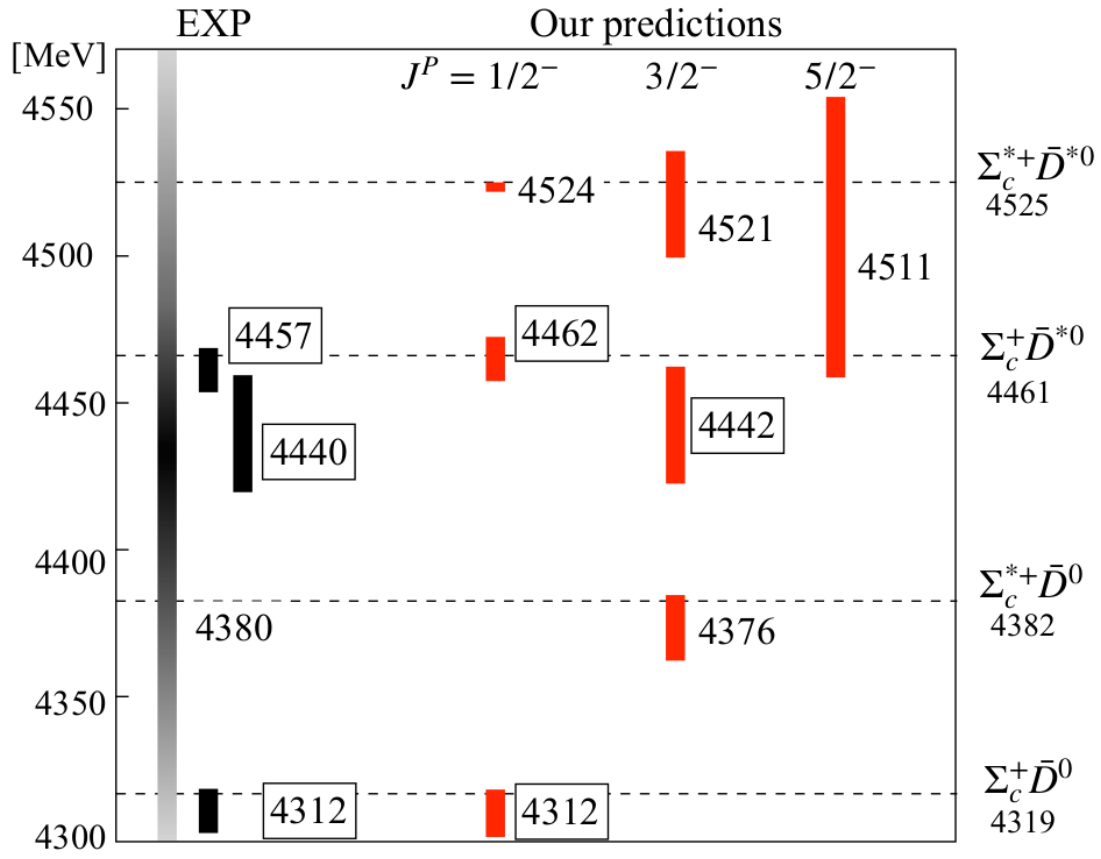

Figure 2.18: Experimental data (EXP) and our predictions for various P_c states as from Ref. [67].

State	$M^{exp.}$	$\Gamma^{exp.}$	(M,J^P,Γ) [87]	(M,J^P) [88]	(M,J^P,Γ)
$P_c(4312)$	$4311.9 \pm 0.7^{+6.8}_{-0.6}$	$9.8 \pm 2.7^{+3.7}_{-4.5}$	(4306.4, $\frac{1}{2}^-$,15.2)	(4306,$\frac{1}{2}^-$)	(4312, $\frac{1}{2}^-$, 5)
$P_c(4380)$	$4380 \pm 8 \pm 29$	$205 \pm 18 \pm 86$	(4374, $\frac{3}{2}^-$,13.7)	(4371, $\frac{3}{2}^-$)	(4376, $\frac{3}{2}^-$,8)
$P_c(4440)$	$4440.3 \pm 1.3^{+4.1}_{-4.7}$	$20.6 \pm 4.9^{+8.7}_{-10.1}$	(4453.0, $\frac{1}{2}^-$,23.4)	(4440*, $\frac{3}{2}^-$)	(4442, $\frac{3}{2}^-$,26)
$P_c(4457)$	$4457.3 \pm 0.6^{+4.1}_{-1.7}$	$6.4 \pm 2.0^{+5.7}_{-1.9}$	(4452.5, $\frac{3}{2}^-$,3.0)	(4457*, $\frac{1}{2}^-$)	(4462, $\frac{1}{2}^-$,6.6)
			(4520.5, $\frac{1}{2}^-$, 22.2)	(4523, $\frac{1}{2}^-$)	(4524, $\frac{1}{2}^-$,1.5)
			(4519.0, $\frac{3}{2}^-$, 13.7)	(4516, $\frac{3}{2}^-$)	(4521 $\frac{3}{2}^-$,23)
				(4500 $\frac{5}{2}^-$)	(4511 $\frac{5}{2}^-$,55)

Table 2.25: Comparison between the experimental mass spectra and decay widths [34] with our predictions [67] and the ones reported in Ref. [87] and scenario A of Ref. [88]. Numbers with asterisk are used as inputs. All values except J^P are in units of MeV.

In Ref. [67] we emphasized for the first time that the new LHCb results give us an opportunity to study the spin-dependent forces between the Σ_c and D^* meson since the two pentaquark states, $P_c(4440)$ and $P_c(4457)$ are the first example where the role of the tensor force can be compared in two partner states. For nucleon systems only spin 1 state (deuteron) is available without partners.

To take into account the important role of the tensor force, coupled channel analysis with states of different angular momenta by 2 units must be properly performed. It is important to determine which of the above spin 1/2 and 3/2 states is more deeply bound. There are two sources for the spin-dependent force in our model:

- One is the short range interaction by the coupling to the 5- quark-core states.
- The other is the long range interaction by the OPEP, especially the tensor term.

To examine the effects of the tensor interaction of the OPEP, we have investigated the energy of the two resonant P_c states below the $\Sigma_c D^*$ threshold,

with spin 1/2 and 3/2, with and without the OPEP tensor term. In the case in which the OPE interaction is turned off the attractive force is not enough strong to produce bound or resonant states for any values of $\frac{f}{f_0} > 0$. Then we turned on the OPEP and we have computed resonance energies for several values $\frac{f}{f_0} > 0$.

As a result, we found that $\frac{f}{f_0} = 45$ is minimum value necessary to have all the three new LHCb states. With this value of the coupling all the masses and the decay widths of the three states are also reproduced.

For $f/f_0 = 45$ we have found that the tensor interaction gives about 4 MeV attraction for the $J^P = 1/2^-$ $\Sigma_c\bar{D}^*$ state, and 16 MeV for $J^P = 3/2^-$ states so the mass the tensor interaction is responsible of a mass difference of 12 MeV. The mass difference between the two experimental states $P_c(4440)$ and $P_c(4457)$ is 17 MeV so the missing 5 MeV are provided by the spin-dependent force of the 5-quark-core states. So to summarize:

- the $P_c(4440)$-$P_c(4457)$ mass difference, 17 MeV, is mainly due to the tensor interaction; in particular the tensor interaction gives about 4 MeV attraction for the $J^P = 1/2^-$ $\Sigma_c\bar{D}^*$ state, and 16 MeV for $J^P = 3/2^-$ states so the mass the tensor interaction is responsible of a mass difference of 12 MeV. More attraction is in the $J^P = 3/2^-$ state than in the $J^P = 1/2^-$ state.

- the missing 5 MeV are provided by the spin-dependent force of the 5-quark-core states.

The reason that more attraction is in the $J^P = 3/2^-$ state than in the $J^P = 1/2^-$ state is that the $J^P = 3/2^-$ state consists of ${}^4S, {}^2D, {}^4D$ channels, while the $J^P = 1/2^-$ state consists of ${}^2S, {}^4D$. The tensor interaction provides attraction through channel couplings such as S-D and D-D. For the $J^P = 3/2^-$ state there are three combinations of such channel couplings, while for $1/2^-$ state there is only one. Considering the strengths of these couplings, the $J^P = 3/2^-$ state receives more attraction than the $1/2^-$ state.

Although we have obtained the $J^P = 3/2^-$ state at 4376 MeV, we do not consider that this meson-baryon molecular state corresponds to the LHCb's $P_c^+(4380)$ state. The observed $P_c^+(4380)$ has a width of about 200 MeV while that of the state at 4376 MeV that we obtained is of order 10 MeV. In the new LHCb analysis [34], using higher-order polynomials for the background,

data could be fitted without the broad $P_c^+(4380)$ Breit-Wigner resonance contribution. Therefore, further theoretical as well as experimental studies are necessary for the $P_c^+(4380)$ state.

Besides the three states observed in the LHCb, we obtained four additional narrow molecular states as shown in Fig. 2.18 and Tab. 2.25. If we exclude the $P_c^+(4380)$ as $\Sigma_c^*\bar{D}$ molecular state, we see that all the three pentaquarks observed lie below $\Sigma_c\bar{D}^{(*)}$ threshold and the molecular states that contain Σ_c^* are not seen.

In addition to these seven states, we obtained two more narrow resonance states below $\Lambda_c\bar{D}^*$ threshold [96]. Since Λ_c is isoscalar, and no diagonal terms of the OPEP contribute to the $\Lambda_c\bar{D}^*$ channel, we do not discuss them here. We only point out that these states are also not observed experimentally.

In order to clarify why those states cannot be observed in the LHCb experiment, the study of the non-leptonic weak decay process $\Lambda_b^0 \to P_c^+K^-$ is desired as well as the higher statistics observations and full amplitude analysis.

In conclusion, by coupling the open charm meson-baryon channels to a compact $uudc\bar{c}$ core with an interaction satisfying the heavy quark and chiral symmetries, we predict the masses and decay widths of the three new pentaquark states reported in [34]. Both the masses and widths of these three hidden-charm pentaquark states we have obtained are in good agreement with the experimental results. We point out that the three pentaquark states have quantum numbers $J^P_{P_c^+(4312)} = 1/2^-$, $J^P_{P_c^+(4440)} = 3/2^-$, and $J^P_{P_c^+(4457)^+} = 1/2^-$ and the dominant molecular component of $P_c^+(4312)$ is the $\Sigma_c\bar{D}$ and that of $P_c^+(4440)$ and $P_c^+(4457)$ is $\Sigma_c\bar{D}^*$. We find that both the short range interaction by the coupling to the 5-quark-core states and the long range interaction by the one-pion exchange potential make contributions to the attraction between Σ_c and $\bar{D}^{(*)}$. The mass difference between $P_c^+(4440)$ and $P_c^+(4457)$ comes mainly from the tensor interaction by the one-pion exchange potential. Because of the importance of the tensor interaction mediated by the pion in the heavy-hadron dynamics, we call it "chiral tensor dynamics" [67].

Chapter 3

The Ω_c puzzle and the heavy baryon spectroscopy

3.1 Experimental introduction

The discovery of new resonances always enriches the present experimental knowledge of the hadron zoo, it also provides essential information to explain the fundamental forces that govern nature. As the hadron mass patterns carry information on the way the quarks interact one another, they provide a means of gaining insight into the fundamental binding mechanism of matter at an elementary level.

In 2017, the LHCb Collaboration announced the observation of five narrow Ω_c states in the $\Xi_c^+ K^-$ decay channel [97]: $\Omega_c(3000)$, $\Omega_c(3050)$, $\Omega_c(3066)$, $\Omega_c(3090)$ and $\Omega_c(3119)$. They also reported the observation of another structure around 3188 MeV, the so-called $\Omega_c(3188)$, though they did not have enough statistical significance to interpret it as a genuine resonance [97]. The $\Xi_c K$ invariant mass distribution for the combined data sets is shown in Fig. 3.1 where the five narrow structures can be observed.

Later, Belle observed five resonant states in the $\Xi_c^+ K^-$ invariant mass distribution, reported in Fig. 3.2, and unambiguously confirmed four of the states announced by LHCb, $\Omega_c(3000)$, $\Omega_c(3050)$, $\Omega_c(3066)$, and $\Omega_c(3090)$, but no signal was found for the $\Omega_c(3119)$ [98]. Belle also measured a signal excess at 3188 MeV, corresponding to the $\Omega_c(3188)$ state reported by LHCb [98].

A comparison between the results reported by the two collaborations is displayed in Table 3.1.

Here, it is shown that the $\Omega_c(3188)$, even if not yet confirmed, was seen both by LHCb and Belle, while, on the contrary, the $\Omega_c(3119)$ was not observed

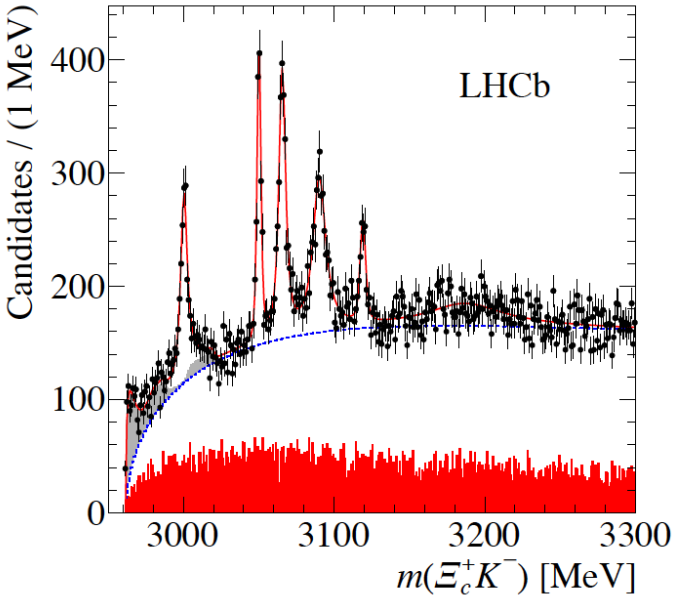

Figure 3.1: *Figure from Ref. [97], APS copyright.* $\Xi_c K$ invariant mass distribution as reported by LHCb [97]; the solid red curve shows the result of the fit, while the dashed blue line indicates the fitted background.

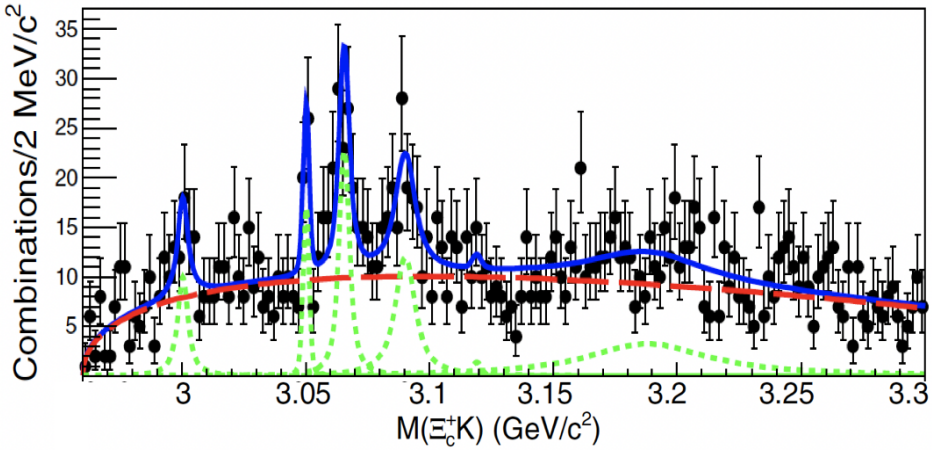

Figure 3.2: *Figure from Ref. [98], APS copyright.* $\Xi_c K$ invariant mass distribution as reported by Belle [98]; The fit shown by the solid line is the sum of a threshold function (dashed line) and six Voigtian (Breit-Wigner convolved with Gaussian resolution) functions, with fixed masses, intrinsic widths and resolutions (dotted lines).

Table 3.1: Measured masses (in MeV) of the six resonances observed in $\Xi_c^+ K^-$ decay channel (see text) according to the LHCb [97] and the Belle [98] collaborations in pp and e^+e^- collisions, respectively.

Ω_c excited state	Mass (LHCb [97])	Mass (Belle [98])
$\Omega_c(3000)$	$3000.4 \pm 0.2 \pm 0.1$	$3000.7 \pm 1.0 \pm 0.2$
$\Omega_c(3050)$	$3050.2 \pm 0.1 \pm 0.1$	$3050.2 \pm 0.4 \pm 0.2$
$\Omega_c(3066)$	$3065.6 \pm 0.1 \pm 0.3$	$3064.9 \pm 0.6 \pm 0.2$
$\Omega_c(3090)$	$3090.2 \pm 0.3 \pm 0.5$	$3089.3 \pm 1.2 \pm 0.2$
$\Omega_c(3119)$	$3119 \pm 0.3 \pm 0.9$	-
$\Omega_c(3188)$	$3188 \pm 5 \pm 13$	$3199 \pm 9 \pm 4$

by Belle. It is also worth to mention that the LHCb collaboration has just announced the observation of a new bottom baryon, $\Xi_b(6227)^-$, in both $\Lambda_b^0 K^-$ and $\Xi_b^0 \pi$ decay modes [99], and of two bottom resonances, $\Sigma_b(6097)^\pm$, in the $\Lambda_b^0 \pi^\pm$ channels [100].

However, neither LHCb nor Belle were able to measure the Ω_c angular momenta and parities. For this reason, several authors tried to provide different quantum number assignments for these states. The current Ω_c puzzle consists in the discrepancy between the experimental results, reported by LHCb [97] and Belle [98], and the existing theoretical predictions [101, 102, 103, 104, 105]. Indeed, for a given Ω_c experimental state, more than one quantum number assignment was suggested [101]. In particular, the $\Omega_c(3119)$ was allocated to possibly be a $J^P = \frac{1}{2}^+$ or a $J^P = \frac{3}{2}^+$ state [103], while the authors in Ref. [104] proposed a $J^P = \frac{5}{2}^-$ assignment.

In this thesis, we first study the Ω_c-mass spectra by estimating the contributions due to spin-orbit interactions, spin-, isospin- and flavour-dependent interaction from the well-established charmed baryon mass spectrum [68].

We reproduce quantitatively the spectrum of the Ω_c states within a harmonic oscillator hamiltonian plus spin-orbit, isospin and flavour dependent contributions [68]. Based on our results, we describe these five states as P-wave λ-excitations of the ssc system; we also calculate their $\Xi_c^+ K^-$ decay widths. Similarly to Refs. [106, 107, 108], we suggest a molecular interpretation of the $\Omega_c(3119)$ state, which was not observed by Belle. Later, we extend our mass and decay width predictions to the Ω_b sector, which will be useful for future experimental searches. Finally, we calculate the mass splitting between the ρ- and λ-mode excitations of $\Omega_{c(b)}$ resonances (see Fig. 3.3 upper-pannel). This calculation is fundamental to access to inner heavy-light baryon structure, as the presence or absence of ρ-mode excitations in the experimental spectrum will be the key to discriminate between the three-quark (see Fig. 3.3 upper-pannel) and the quark-diquark structures (see Fig. 3.3 lower-pannel) [68], as it will be discussed the following.

Very recently, the LHCb Collaboration observed four narrow peaks, $\Omega_b(6316), \Omega_b(6330), \Omega_b(6340)$ and $\Omega_b(6350)$ in $\Xi_b^0 K^-$ mass spectrum [65]. As reported by the same LHCb collaboration [65], the observed peaks and the $\Xi_b^0 K^-$ decay widths are consistent with our predictions given in Ref. [68].

3.1.1 S- and P-wave ssQ states.

The three-quark system (ssQ) Hamiltonian can be written in terms of two coordinates [109], ρ and λ, which encode the system spatial degrees of freedom (see Fig. 3.3). For simplicity, we use the compact notation ssQ to denote them ($Q = c$ or b). Let $m_\rho = m_s$ and $m_\lambda = \frac{3m_s m_Q}{2m_s+m_Q}$ be the ssQ system reduced masses; then, the ρ- and λ-mode frequencies are $\omega_{\rho,\lambda} = \sqrt{\frac{3K_Q}{m_{\rho,\lambda}}}$, where K_Q is the spring constant, which implies that in three equal-mass-quark baryons, in which $m_\rho = m_\lambda$, the λ- and ρ- orbital excitation modes are completely mixed together. By contrast, in heavy-light baryons, in which $m_\rho \ll m_\lambda$, the two excitation modes can be decoupled from each other as long as the light-heavy quark mass difference increases.

First of all, we construct the ssc and ssb ground and excited states to establish the quantum numbers of the five confirmed Ω_c states. A single quark is described by its spin, flavor and color. As a fermion, its spin is $S = \frac{1}{2}$, its flavor, spin-flavor and color representations are $\mathbf{3}_{\rm f}$, $\mathbf{6}_{\rm sf}$, and $\mathbf{3}_{\rm c}$, respectively. An ssQ state, $|ssQ, S_\rho, S_{\rm tot}, l_\rho, l_\lambda, J\rangle$, is characterized by total angular momentum $\mathbf{J} = \mathbf{l}_\rho + \mathbf{l}_\lambda + \mathbf{S}_{\rm tot}$, where $\mathbf{S}_{\rm tot} = \mathbf{S}_\rho + \mathbf{\frac{1}{2}}$. In order to construct an ssQ color singlet state, the light quarks must transform under ${\rm SU_c}(3)$ as the anti-symmetric $\bar{\mathbf{3}}_{\rm c}$ representation. The Pauli principle postulates that the wave function of identical fermions must be anti-symmetric for particle exchange. Thus, the ss spin-flavor and orbital wave functions have the same permutation symmetry: symmetric spin-flavor in S-wave, or antisymmetric spin-flavor in antisymmetric P-wave. Two equal flavour quarks are necessarily in the $\mathbf{6}_{\rm f}$ flavor-symmetric state. Thus, they are in an S-wave symmetric spin-triplet state, $S_\rho = 1$, or in a P-wave antisymmetric spin-singlet state, $S_\rho = 0$.

If $l_\rho = l_\lambda = 0$, then $S_\rho = 1$, and we find the two ground states, Ω_Q and Ω_Q^*: $|ssQ, 1, S_{\rm tot}, 0_\rho, 0_\lambda, J\rangle$ with $J = S_{\rm tot} = \frac{1}{2}$ and $\frac{3}{2}$, respectively. If $l_\rho = 0$ and $l_\lambda = 1$, then $S_\rho = 1$ and, by coupling the spin and orbital angular momentum, we find five excited states: $|ssQ, 1, S_{\rm tot}, 0_\rho, 1_\lambda, J\rangle$ with $J = \frac{1}{2}$, $\frac{3}{2}$ for $S_{\rm tot} = \frac{1}{2}$, and $J = \frac{1}{2}$, $\frac{3}{2}$, $\frac{5}{2}$ for $S_{\rm tot} = \frac{3}{2}$, which we interpret as λ-mode excitations of the ssQ system. On the other hand, if $l_\rho = 1$ and $l_\lambda = 0$, then $S_\rho = 0$, and we find two excited states $\left|ssQ, 0, \frac{1}{2}, 1_\rho, 0_\lambda, J\right\rangle$ with $J = \frac{1}{2}$, $\frac{3}{2}$ which we interpret as ρ-mode excitations of the ssQ system [1].

[1] A similar analysis is done in Ref. [110] where the authors considered $l_\rho = 0$ and $L = l_\lambda$ in a JJ coupling scheme.

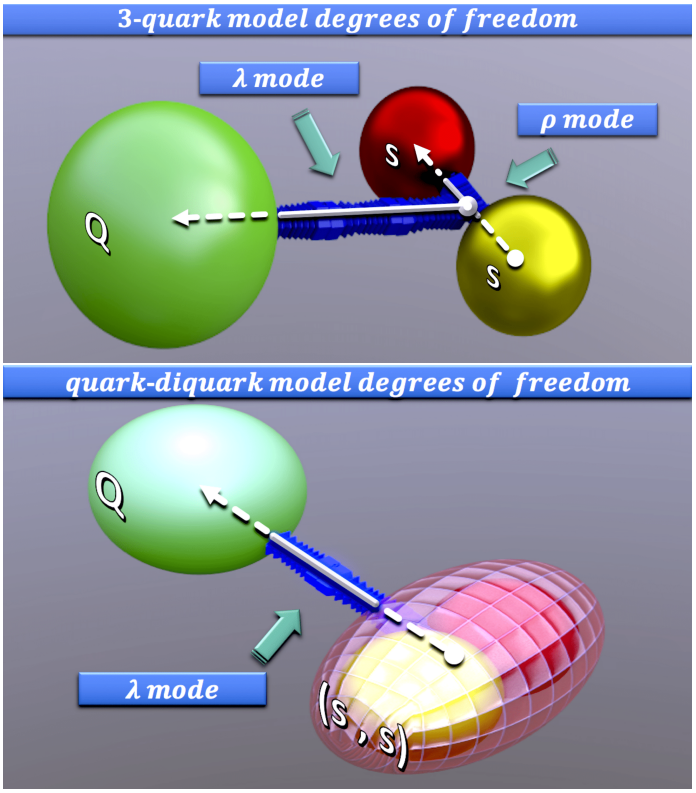

Figure 3.3: *Figure from Ref. [68], EPJ copyright.*.Comparison between three-quark and quark-diquark baryon effective degrees of freedom. Upper panel: three-quark picture with two excitation modes. Lower panel: quark-diquark picture with one relative excitation mode.

3.2 Mass spectra of Ω_Q states

We introduce a three-dimensional harmonic oscillator hamiltonian (h.o.) plus corrections given by spin-orbit, isospin and flavour dependent contributions:

$$H = \bar{H}_{\text{h.o.}} + A\,\mathbf{S}^2 + B\,\mathbf{S}\cdot\mathbf{L} + E\,\boldsymbol{I}^2 + G\,\mathbf{C_2}(\text{SU(3)}_\text{f}); \tag{3.1}$$

here $\mathbf{S}$, $\boldsymbol{I}$ and $\mathbf{C_2}(\text{SU(3)}_\text{f})$ are the spin, the isospin and the $\mathbf{C_2}(\text{SU(3)}_\text{f})$ Casimir operators, and (see App. H.0.2 Eq. H.8)

$$\bar{H}_{\text{h.o.}} = \sum_{i=1}^{3} m_i + \frac{\mathbf{p}_\rho^2}{2m_\rho} + \frac{\mathbf{p}_\lambda^2}{2m_\lambda} + \frac{1}{2}m_\rho\omega_\rho^2\boldsymbol{\rho}^2 + \frac{1}{2}m_\lambda\omega_\lambda^2\boldsymbol{\lambda}^2 \tag{3.2}$$

is the three-dimensional harmonic oscillator Hamiltonian without the centre of mass part (see App. H.0.2 Eq. H.8) written in terms of Jacobi coordinates, $\boldsymbol{\rho}$ and $\boldsymbol{\lambda}$, and conjugated momenta, $\mathbf{p}_\rho$ and $\mathbf{p}_\lambda$, whose eigenvalues are $\sum_{i=1}^{3} m_i + \omega_\rho\, n_\rho + \omega_\lambda n_\lambda$, where $\omega_{\rho(\lambda)} = \sqrt{\frac{3K_Q}{m_{\rho(\lambda)}}}$, $n_{\rho(\lambda)} = 2k_{\rho(\lambda)} + l_{\rho(\lambda)}$, $k_{\rho(\lambda)} = 0, 1, ...,$ and $l_{\rho(\lambda)} = 0, 1, ...$

We set the quark masses to reproduce the $\Omega_c(2695)$, $\Omega_c^*(2765)$, $\Xi_{cc}(3621)$ and $\Sigma_b(5814)$ ground state masses [111]: $m_q = 295$ MeV, $m_s = 450$ MeV, $m_c = 1605$ MeV and $m_b = 4920$ MeV; the spring constant K_c is set to reproduce the mass difference between $\Xi_c(2790)$, with $J^P = \frac{1}{2}^-$, and the $\Xi_c(2469)$ ground state: $K_c = 0.0328$ GeV^3, while K_b is set to reproduce the mass difference between $\Lambda_b(5919)$, with $J^P = \frac{1}{2}^-$, and the $\Lambda_b(5619)$ ground state: $K_b = 0.0235$ GeV^3 [68]. In order to calculate the mass difference between the ρ and λ orbital excitations of ssQ states, we scale the h.o. frequency by the ρ and λ oscillator masses. From the definition of m_ρ and m_λ, one finds $m_\rho = m_s = 450$ MeV and $m_\lambda = \frac{3m_s m_c}{2m_s+m_c} \simeq 865$ MeV for Ω_c states, and $m_\lambda = \frac{3m_s m_b}{2m_s+m_b} \simeq 1141$ MeV for Ω_b states; the ρ- and λ-mode frequencies are $\omega_{\rho,\lambda} = \sqrt{\frac{3K_Q}{m_{\rho,\lambda}}}$. Finally, the mass splitting parameters, A, B, E and G, calculated in the following, are reported in Table B.1.

Table 3.2: *Table from Ref. [68], EPJ copyright.*. Values of the parameter reported in Eq. (3.1) with the corresponding uncertainties expressed in MeV.

Sector	A	B
charm	21.54 ± 0.37	23.91 ± 0.31
bottom	6.73 ± 1.63	5.15 ± 0.33

Sector	E	G
charm	30.34 ± 0.23	54.37 ± 0.58
bottom	26.00 ± 1.80	70.91 ± 0.49

We estimate the mass splittings due to the spin-orbit, spin-, isospin- and flavor-dependent interactions from the well established charmed (bottom) baryon mass spectra, which are reported in App. B. The spin-orbit interaction, which is mysteriously small in light baryons [112, 113], turns out to be fundamental to describe the heavy-light baryon mass patterns, as it is clear from those of the recently observed Ω_c states. The spin-, isospin-, and flavour-dependent interactions are necessary to reproduce the masses of charmed baryon ground states, as observed in Ref. [8]. By means of these estimates, we predict in a parameter-free procedure the spectrum of the ssQ excited states constructed in the previous section . The predicted masses of the λ- and ρ-orbital excitations of the Ω_c and Ω_b baryons are reported in Tab. 3.2 and Tab. 3.4, respectively.

In particular, Tab. 3.2 shows that we are able to reproduce quantitatively the mass spectra of the Ω_c states observed both by LHCb and Belle; the latter are reported in Table 3.1.

We estimate the energy splitting due to the spin-spin interaction from the (isospin-averaged) mass difference between $\Sigma_c^*(2520)$ and $\Sigma_c(2453)$. This value (65 ± 8 MeV) agrees with the mass difference between Ω_c (2695) and Ω_c^* (2770), a value close to 71 MeV. As a consequence, the spin-spin mass splitting between two orbitally excited states characterized by the same flavor configuration but different spins, specifically $S_{\rm tot} = \frac{1}{2}$ and $S_{\rm tot} = \frac{3}{2}$, is around 65 MeV plus corrections due the spin-orbit contribution which can be calculated, for example,

State	$M^{pred.}$	$M^{exp.}$	$\Gamma^{pred.}_{o.f.}$	$\Gamma^{exp.}_{tot}$
$\left\|ssc,1,\frac{1}{2},0_\rho,0_\lambda,\frac{1}{2}\right\rangle \equiv \Omega_c(2695)^\dagger$	2702 ± 12	2695 ± 2	††	$< 10^{-7}$
$\left\|ssc,1,\frac{3}{2},0_\rho,0_\lambda,\frac{3}{2}\right\rangle \equiv \Omega_c^*(2770)^\dagger$	2767 ± 13	2766 ± 2	††	
$\left\|ssc,1,\frac{1}{2},0_\rho,1_\lambda,\frac{1}{2}\right\rangle \equiv \Omega_c(3000)$	3016 ± 9	$3000.4 \pm 0.2 \pm 0.1 \pm 0.3$	0.48	$4.6 \pm 0.6 \pm 0.3$
$\left\|ssc,1,\frac{3}{2},0_\rho,1_\lambda,\frac{1}{2}\right\rangle \equiv \Omega_c(3050)$	3045 ± 13	$3050.2 \pm 0.1 \pm 0.1 \pm 0.3$	1.0	$0.8 \pm 0.2 \pm 0.1$
$\left\|ssc,1,\frac{1}{2},0_\rho,1_\lambda,\frac{3}{2}\right\rangle \equiv \Omega_c(3066)$	3052 ± 15	$3065.6 \pm 0.1 \pm 0.3 \pm 0.3$	3.5	$3.5 \pm 0.4 \pm 0.2$
$\left\|ssc,1,\frac{3}{2},0_\rho,1_\lambda,\frac{3}{2}\right\rangle \equiv \Omega_c(3090)$	3080 ± 13	$3090.2 \pm 0.3 \pm 0.5 \pm 0.3$	1.09	$8.7 \pm 1.0 \pm 0.8$
$\left\|ssc,1,\frac{3}{2},0_\rho,1_\lambda,\frac{5}{2}\right\rangle \equiv \Omega_c(3188)$	3140 ± 14	$3188 \pm 5 \pm 13$	9.87	60 ± 26
$\left\|ssc,0,\frac{1}{2},1_\rho,0_\lambda,\frac{1}{2}\right\rangle$	3146 ± 12		†††	
$\left\|ssc,0,\frac{1}{2},1_\rho,0_\lambda,\frac{3}{2}\right\rangle$	3182 ± 12		†††	

Table 3.3: *Table from Ref. [68], EPJ copyright.* Our ssc state quantum number assignments (first column), predicted masses (second column) and open-flavor strong decay widths into $\Xi_c^+ K^-$ and $\Xi_c'^+ K^-$ channels, $\Gamma^{pred.}_{o.f.}$ (fourth column), are compared with the experimental masses (third column) and total decay widths (fifth column) [97, 111]. An ssc state, $|ssc, S_\rho, S_{tot}, l_\rho, l_\lambda, J\rangle$, is characterized by total angular momentum $\mathbf{J} = \mathbf{l}_\rho + \mathbf{l}_\lambda + \mathbf{S}_{tot}$, where $\mathbf{S}_{tot} = \mathbf{S}_\rho + \frac{1}{2}$. Our results are compatible with the experimental data, the predicted partial decay widths being lower than the total measured decay widths. Masses of states denoted with † are used as inputs while all the others are predictions; partial decay widths denoted with †† and with ††† are zero for phase space and for selection rules, respectively. All the values are in MeV.

from the $\Lambda_c(2595)$-$\Lambda_c(2625)$ mass difference. According to the quark model, $\Lambda_c(2595)$ and $\Lambda_c(2625)$ are the charmed counterparts of $\Lambda(1405)$ and $\Lambda(1520)$, respectively; their spin-parities are $\frac{1}{2}^-$ and $\frac{3}{2}^-$, and their mass difference, about 36 MeV, is due to spin-orbit effects.

In conclusion, by taking into account the spin-spin and spin-orbit contributions, the mass difference between the lowest Ω_c excitation, $\left|ssc,1,\frac{1}{2},0_\rho,1_\lambda,\frac{1}{2}\right\rangle \equiv \Omega_c(3000)$ and $\left|ssc,1,\frac{3}{2},0_\rho,1_\lambda,\frac{1}{2}\right\rangle$, is about $65 - 36 \simeq 30$ MeV. So, we identify the $\left|ssc,1,\frac{3}{2},0_\rho,1_\lambda,\frac{1}{2}\right\rangle$ with the observed $\Omega_c(3050)$ (see Fig. 3.4 and Tab. 3.2). In the bottom sector, the energy splitting due to the spin-spin interaction through the (isospin-averaged) mass difference between Σ_b^* and Σ_b is 20 ± 7 MeV. In such a way, we expect a mass difference between the two S-wave ground states, Ω_b^* and Ω_b, close to 20 ± 7 MeV. Hence, we suggest the experimentalists to look for a Ω_b^* resonance with a mass of about 6082 MeV, as we can see in Figure 3.5 and Table 3.4.

We estimate that the mass of $\left|ssc, 1, \frac{1}{2}, 0_\rho, 1_\lambda, \frac{3}{2}\right\rangle$ is related to the previous spin-orbit splitting. We obtain a value of 3052 ± 15 MeV, which is compatible with the mass of the $\Omega_c(3066)$ within the experimental error. Thus, we identify the $\left|ssc, 1, \frac{1}{2}, 0_\rho, 1_\lambda, \frac{3}{2}\right\rangle$ state with the $\Omega_c(3066)$ resonance. Through the estimation of orbital, spin-spin and spin-orbit interactions, we estimate the $\left|ssc, 1, \frac{3}{2}, 0_\rho, 1_\lambda, \frac{3}{2}\right\rangle$ and $\left|ssc, 1, \frac{3}{2}, 0_\rho, 1_\lambda, \frac{5}{2}\right\rangle$ mass values as 3080 $\pm$13 MeV and 3140 $\pm$14, respectively. Thence, we propose the following assignments: $\left|ssc, 1, \frac{3}{2}, 0_\rho, 1_\lambda, \frac{3}{2}\right\rangle \rightarrow \Omega_c(3090)$ and $\left|ssc, 1, \frac{3}{2}, 0_\rho, 1_\lambda, \ \frac{5}{2}\right\rangle \rightarrow \Omega_c(3188)$.

In the bottom sector, the mass splitting due to the spin-orbit interaction between $\Lambda_b(5912)$ and $\Lambda_b(5920)$ is 8 MeV and we estimated previously that the spin-spin splitting is 20 ± 7 MeV. Thus, we interpret the predicted $\Omega_b(6305)$, $\Omega_b(6313)$, $\Omega_b(6317)$, $\Omega_b(6325)$ and $\Omega_b(6338)$ states, reported in Table 3.4, as the bottom counterparts of the $\Omega_c(3000)$, $\Omega_c(3066)$, $\Omega_c(3050)$, $\Omega_c(3090)$ and $\Omega_c(3188)$, respectively. We observe that, unlike the charm sector, in the bottom sector the state $\left|ssb, 1, \frac{3}{2}, 0_\rho, 1_\lambda, \frac{1}{2}\right\rangle$ is heavier than the state $|ssb, \ 1, \frac{1}{2}, 0_\rho, 1_\lambda, \frac{3}{2}\rangle$: this is due to the fact that in the charm sector the spin-orbit contribution is lesser than the spin-spin one, while in the bottom sector the situation is the opposite (see Table B.1).

In the charm sector, the mass splitting due to the flavor-dependent interaction can be estimated from the mass difference between Ξ_c and $\Xi_c^{'}$, whose isospin-averaged masses are 2469.37 MeV and 2578.1 MeV, respectively; this leads to a value of 109 MeV, approximately. The bottom partner of Ξ_c and $\Xi_c^{'}$ are Ξ_b and $\Xi_b^{'}$, with masses 5793.2 MeV and 5935.02 MeV, respectively. Therefore, in the bottom sector the flavor-dependent interaction gives a contribution of about 142 MeV, which is more than 30% larger than in the charm sector. The mass difference between the lightest charmed ground states, Σ_c and Λ_c, is related to the different isospin and flavor structures of the light quark multiplets: Λ_c is an isospin-singlet state belonging to an $SU(3)_f$ flavor anti-triplet, while Σ_c is an isospin-triplet state belonging to an $SU(3)_f$ flavor sextet. In the bottom sector, the isospin-flavor contribution to the baryon masses can be calculated from the mass difference between Σ_b and Λ_b. We summarize all our proposed quantum number assignments for both Ω_c and Ω_b states in Figs. 3.4 and 3.5, respectively. In the charm sector, we find a good agreement between the mass pattern predicted for the spectrum and the experimental data: in particular, with the exception of the lightest and the heaviest resonant states, $\Omega_c(3000)$ and $\Omega_c(3188)$, respectively, also the absolute mass predictions are in agreement within the experimental error, which is very small (< 1 MeV).

Figure 3.4: *Figure from Ref. [68], EPJ copyright.* Ω_c mass spectra and tentative quantum number assignments. The theoretical predictions (red dots) are compared with the experimental results by LHCb [97] (blue line), Belle [98] (violet line) and Particle Data Group (black lines) [111]. Except the $\Omega_c(3188)$ case, the experimental error for the other states is too small to be appreciated in this energy scale. The spin-$\frac{1}{2}$ and -$\frac{3}{2}$ ground-state masses, $\Omega_c(2695)$ and $\Omega_c^*(2770)$ are indicated with † because are inputs while all the others are predictions.

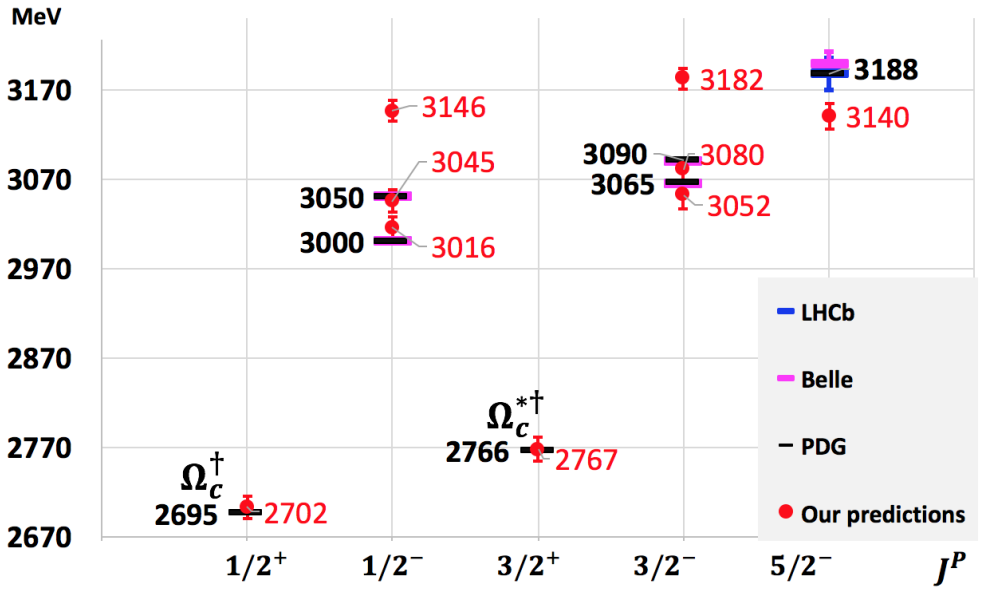

Figure 3.5: *Figure from Ref. [68], EPJ copyright.* Ω_b mass spectrum predictions (red dots) and Ω_b ground-state experimental mass (black line) [111]. The experimental error on the $\Omega_b(6046)$ state, 2 MeV, is too small to be appreciated in this energy scale.

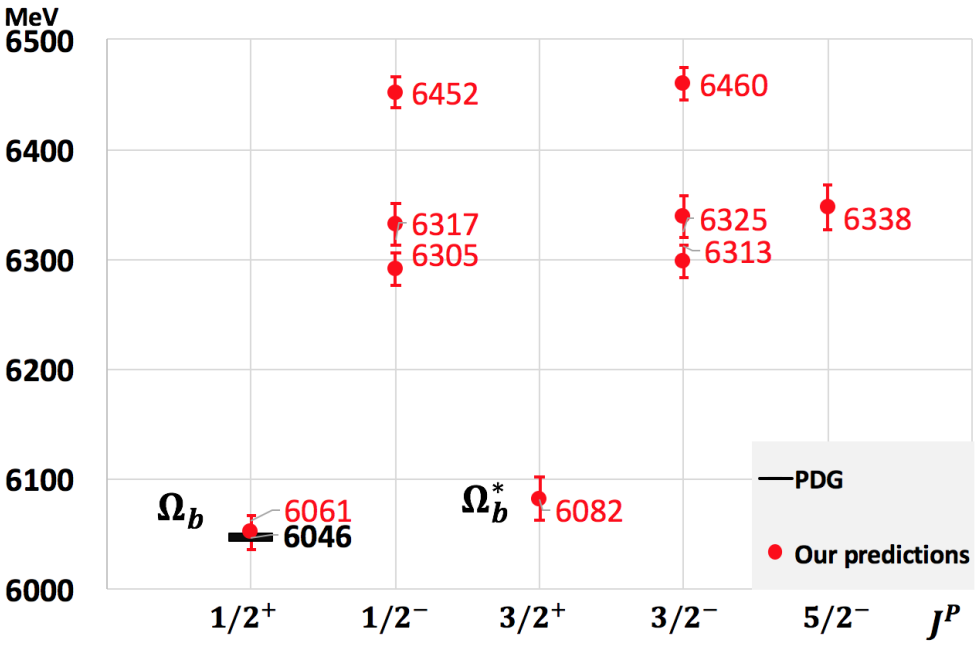

Table 3.4: *Table from Ref. [68], EPJ copyright.* Our ssb state quantum number assignments (first column), predicted masses (second column) and open-flavor strong decay widths (fourth column) are compared with the experimental masses (third column) and total decay widths (fifth column) [111]. An ssb state, $|ssb, S_\rho, S_{\rm tot}, l_\rho, l_\lambda, J\rangle$, is characterized by total angular momentum $\mathbf{J} = \mathbf{l}_\rho + \mathbf{l}_\lambda + \mathbf{S}_{\rm tot}$, where $\mathbf{S}_{\rm tot} = \mathbf{S}_\rho + \frac{1}{2}$. Partial decay widths denoted with †† and with ††† are zero for phase space and for selection rules, respectively.

State	$M^{\rm pred.}$	$M^{\rm exp.}$	$\Gamma^{\rm pred.}_{\Xi_b K}$	$\Gamma^{\rm exp.}_{\rm tot}$
$\left\|ssb, 1, \frac{1}{2}, 0_\rho, 0_\lambda, \frac{1}{2}\right\rangle \equiv \Omega_b$	6061 ± 15	6046 ± 2	††	$< 10^{-9}$
$\left\|ssb, 1, \frac{3}{2}, 0_\rho, 0_\lambda, \frac{3}{2}\right\rangle$	6082 ± 20		††	
$\left\|ssb, 1, \frac{1}{2}, 0_\rho, 1_\lambda, \frac{1}{2}\right\rangle$	6305 ± 15		1.14	
$\left\|ssb, 1, \frac{3}{2}, 0_\rho, 1_\lambda, \frac{1}{2}\right\rangle$	6317 ± 19		2.79	
$\left\|ssb, 1, \frac{1}{2}, 0_\rho, 1_\lambda, \frac{3}{2}\right\rangle$	6313 ± 15		1.49	
$\left\|ssb, 1, \frac{3}{2}, 0_\rho, 1_\lambda, \frac{3}{2}\right\rangle$	6325 ± 19		0.62	
$\left\|ssb, 1, \frac{3}{2}, 0_\rho, 1_\lambda, \frac{5}{2}\right\rangle$	6338 ± 20		4.28	
$\left\|ssb, 0, \frac{1}{2}, 1_\rho, 0_\lambda, \frac{1}{2}\right\rangle$	6452 ± 15		†††	
$\left\|ssb, 0, \frac{1}{2}, 1_\rho, 0_\lambda, \frac{3}{2}\right\rangle$	6460 ± 15		†††	

3.3 Decay widths of ssQ states

In the following, we compute the strong decays of ssQ baryons in $sqQ - K$ ($q = u, d$) final states by means of the $^3P_0$ model [114, 115, 116, 117] (see App. I).

In the $^3P_0$ model, the parameters depend on the harmonic oscillator frequency of the initial and final states. For charmed baryons, we expect the parameters α_ρ and α_λ to lie in the range $0.4 - 0.7$ GeV. In principle, the values of the α_ρ and α_λ h.o. parameters of lower- and higher-lying resonances should be different; see e.g. Ref. [118]. However, as widely discussed in the literature, it is customary to use constant values for α_ρ and α_λ. We also prefer not to take α_ρ and α_λ as free parameters, but to express them in terms of the baryon ρ- and λ-mode frequencies, $\omega_{\rho,\lambda} = \sqrt{3K_Q/m_{\rho,\lambda}}$, using the relation $\alpha^2_{\rho,\lambda} = \omega_{\rho,\lambda} m_{\rho,\lambda}$ for both initial- and final-state baryon resonances; see App. I.1. In light of this, the only free parameter is the pair creation strength, $\gamma_0 = 9.2$, which is fitted to the reproduction of the $\Omega_c(3066)$ width. The frequency of K meson is set to be $\omega_c = 0.46$ GeV [119].

Tab. 3.2 and Tab. 3.4 report our $\Omega_c \to \Xi_c^+ K^-, \Xi_c'^+ K^-$ and $\Omega_b \to \Xi_b^0 K^-$ predicted decay widths. The $\Xi_c^+ K^-$ decay channel is where the Ω_c states were observed by LHCb and Belle; we also consider the $\Xi_c'^+ K^-$ channel, which contributes to the $\Omega_c(3090)$ and $\Omega_c(3188)$ open-flavor decay widths. Both the $\Xi_c^+ K^-$ branching ratios and the quantum numbers of the Ω_c's are unknown; we only have experimental informations on their total widths, $\Gamma_{\rm tot}$. Thus, our predictions have to satisfy the constraint: $\Gamma(\Omega_c \to \Xi_c^+ K^-) \leq \Gamma_{\rm tot}$. In light of this, we state that our strong decay width results, based both on our mass estimates and quantum number assignments, are compatible with the present experimental data. In particular, the λ-mode decay widths of the Ω_c states are in the order 1 MeV, while $\Xi_c^+ K^-$ decay of the two ρ-excitations, $\left|ssc, 0, \frac{1}{2}, 1_\rho, 0_\lambda, \frac{1}{2}\right\rangle$ and $\left|ssc, 0, \frac{1}{2}, 1_\rho, 0_\lambda, \frac{3}{2}\right\rangle$, is forbidden by spin conservation. Similar considerations can be applied to the decay widths of ρ-mode Ω_b states. The presence of inconsistencies between our predictions for the mass spectrum and the open-flavor strong decay widths of Tab. 3.2 can have two possible explanations: I) We used a single set of values for the α_ρ and α_λ h.o. parameters. Those values were extracted from a fit to the spectrum and not fitted to the reproduction of the Ω_c's decay widths; II) There is not a single model which is capable of providing a completely satisfactory description of baryon open-flavor strong decay widths [120].

In conclusion, in addition to our mass estimates, also the $^3P_0$ model results suggest that the five Ω_c resonances, $\Omega_c(3000)$, $\Omega_c(3050)$, $\Omega_c(3066)$, $\Omega_c(3090)$, and $\Omega_c(3188)$, could be interpreted as ssc ground-state P-wave λ-excitations. In principle, both the $\Omega_c(3090)$ and $\Omega_c(3119)$ resonances observed by LHCb are

Figure 3.6: *Adapted from Fig. 2 of Ref. [97], APS copyright.*
Proposed spin- and parity-assignments for the $\Omega_c = css$ excited states reported by the LHCb Collaboration and later confirmed by Belle: $\Omega_c(3000)$, $\Omega_c(3050)$, $\Omega_c(3066)$, $\Omega_c(3090)$, and $\Omega_c(3188)$. We interpret $\Omega_c(3119)$ as a $\Xi_c^* K$ molecule.

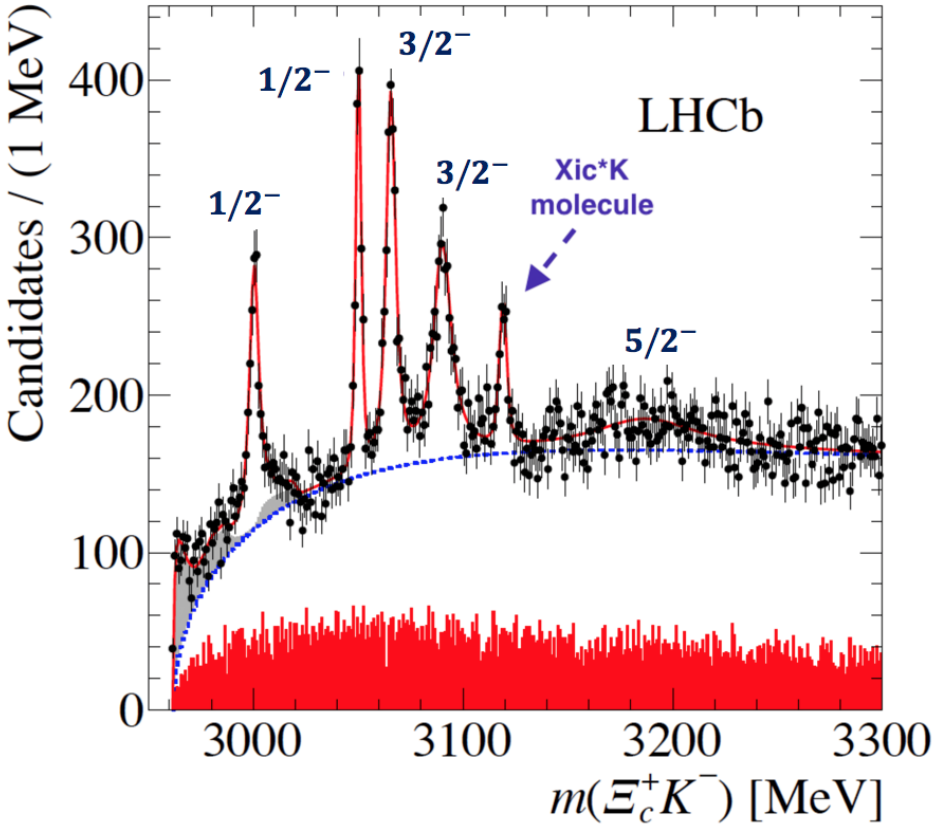

compatible with the properties (mass and decay width) of the $\left|ssc, \frac{3}{2}, 1_\lambda, \frac{3}{2}\right\rangle$ theoretical state. As Belle could neither confirm nor deny the existence of the $\Omega_c(3119)$, given the low significance of its results for the previous state (0.4σ), we prefer to: 1) Assign $\left|ssc, \frac{3}{2}, 1_\lambda, \frac{3}{2}\right\rangle$ to the $\Omega_c(3090)$; 2) Interpret the $\Omega_c(3119)$ as a $\Xi_c^* K$ bound state [106, 108, 107], the $\Omega_c(3119)$ lying 22 MeV below the $\Xi_c^* K$ threshold. See Fig. 3.6. Additionally, in Table 3.5 [2] , we present a comparison of different quantum number assignments for the Ω_c states.

3.4 Comparison between three-quark and quark-diquark structures

In the light sector, the quark model reproduces successfully the baryon spectrum by assuming that the constituent u, d and s quarks have roughly the same mass. This implies that the two oscillators, ρ and λ, have approximately the same frequency, $\omega_\rho \simeq \omega_\lambda$; therefore, the ρ- and λ-excitations are degenerate. By contrast, in the case of heavy-light baryons $m_\rho \ll m_\lambda$; thus, the two excitation modes are decoupled from one another; specifically $\omega_\rho - \omega_\lambda \simeq 130$ MeV for Ω_c states and $\omega_\rho - \omega_\lambda \simeq 150$ MeV for Ω_b states. Thus, the heavy-light baryon sector is the most suitable environment to test what are the correct effective spatial degrees of freedom for reproducing the mass spectra, as the presence or absence of ρ-mode excitations in the spectrum will be the key to discriminate between the three-quark and the quark-diquark structures (see Fig. 3.3). Specifically, if the predicted four ρ-excitations, $\Omega_c(3146)$, $\Omega_c(3182)$, $\Omega_b(6452)$, and $\Omega_b(6460)$, are not be observed, then the other Ω_c states will be characterized by a quark-diquark structure.

Finally, we observe that in the case of a quark-diquark-picture experimental confirmation, the model Hamiltonian introduced in Eq. 3.1 still holds because the quark-diquark h.o. Hamiltonian is the limit of the three-quark h.o. Hamiltonian, Eq. H.5, when we freeze the ρ coordinate (see App. H.0.1):

$$H_{\text{h.o.}} = m_D + m_Q + \frac{\mathbf{p}_\lambda^2}{2m_\lambda} + \frac{1}{2} m_\lambda \omega_\lambda^2 \boldsymbol{\lambda}^2. \tag{3.3}$$

Here $m_D = 2m_s$ is the diquark mass. Indeed, the mass spectrum predicted with this definition of $H_{\text{h.o.}}$ is the same as that reported in Figs. 3.4 and 3.5, but without the frozen ρ excitations. We observe also that, if the quark-diquark scenario turns out to be the correct one, the suppression of the spin-spin interaction that we found going from the charmed to the bottom sector is

[2] In Ref. [110] a different classification scheme, called jj scheme, was used; a detailed comparison between the LS coupling and the jj coupling scheme is reported in App. J

consistent with the heavy quark symmetry, this suppression being an indication that heavy quark effective theory, HQET, still holds also in the heavy-light baryon sector.

Table 3.5: *Figure from Ref. [68], EPJ copyright.* J^P quantum number assignments of Ω_c resonances from previous studies. * Ref. [101] provided two different sets of J^P assignments.

State	Ours	Ref. [101]	Ref. [101]*	Ref [110]
$\Omega_c(3000)$	$1/2^-$	$1/2^-$	$3/2^-$	$1/2^-$
$\Omega_c(3050)$	$3/2^-$	$1/2^-$	$3/2^-$	$3/2^-$
$\Omega_c(3066)$	$1/2^-$	$3/2^-$	$5/2^-$	$3/2^-$
$\Omega_c(3090)$	$3/2^-$	$3/2^-$	$1/2^+$	$1/2^+$
$\Omega_c(3119)$	Molecule	$5/2^-$	$3/2^+$	$5/2^-$
$\Omega_c(3188)$	$5/2^-$	$\cdots$	$\cdots$	$1/2^-(3/2^-)$

3.5 Discussion and summary of the section

We calculated the $\Omega_{c(b)}$'s masses and $\Xi^+_{c(b)}K^-$ strong decay amplitudes. By means of these mass and decay width predictions, we proposed an univocal assignment to the five Ω_c states observed both by LHCb [97] and Belle [98]:

$$|ssc, 1, \tfrac{1}{2}, 0_\rho, 1_\lambda, \tfrac{1}{2}\rangle \to \Omega_c(3000)\,, \tag{3.4}$$
$$|ssc, 1, \tfrac{3}{2}, 0_\rho, 1_\lambda, \tfrac{1}{2}\rangle \to \Omega_c(3050)\,, \tag{3.5}$$
$$|ssc, 1, \tfrac{1}{2}, 0_\rho, 1_\lambda, \tfrac{3}{2}\rangle \to \Omega_c(3066)\,, \tag{3.6}$$
$$|ssc, 1, \tfrac{3}{2}, 0_\rho, 1_\lambda, \tfrac{3}{2}\rangle \to \Omega_c(3090)\,, \tag{3.7}$$
$$|ssc, 1, \tfrac{3}{2}, 0_\rho, 1_\lambda, \tfrac{5}{2}\rangle \to \Omega_c(3188)\,. \tag{3.8}$$

The latter was completely ignored in other studies [101, 102, 103, 104, 105]. In principle, both the $\Omega_c(3119)$ and $\Omega_c(3090)$ could be assigned to the $|ssc, 1, \frac{3}{2}, 0_\rho, 1_\lambda, \frac{3}{2}\rangle$ state. However, as Belle could neither confirm nor deny the existence of the $\Omega_c(3119)$, we prefer the $\Omega_c(3119)$ interpretation as a $\Xi_c^* K$ meson-baryon molecule and assign the $\Omega_c(3090)$ to the $\left|ssc, 1, \frac{3}{2},\ 0_\rho, 1_\lambda, \frac{3}{2}\right\rangle \to \Omega_c(3090)$ state, providing a consistent solution to the Ω_c puzzle.
We calculate the mass splitting between the ρ- and λ-mode excitations of the $\Omega_{c(b)}$ resonances. This large mass splitting, that we predict to be greater

than 150 MeV, is fundamental to access to inner heavy-light baryon structure. If the ρ-excitations in the predicted mass region will not be observed in the future, then the three-quark model effective degrees of freedom for the heavy-light baryons will be ruled out, supporting the Heavy Quark Effective Theory (HQET) picture of the heavy-light baryons described as heavy quark-light diquark systems. If the ρ-excitations in the predicted mass region will not be observed in the future, then the three-quark model effective degrees of freedom for the heavy-light baryons will be ruled out, supporting the Heavy Quark Effective Theory (HQET) picture of the heavy-light baryons described as heavy quark-light diquark systems.

In conclusion we calculated the $\Omega_{c(b)}$'s masses and $\Xi^+_{c(b)}K^-$ strong decay amplitudes. by means of a three-dimensional harmonic oscillator hamiltonian (h.o.) plus spin-orbit, isospin and flavour dependent contributions which turned out to be fundamental in describing the heavy-baryon mass pattern [68]; this hamiltonian was the extension of the model introduced by us in Ref. [8] to study the pentaquark states within the compact approach. By means of these mass and decay width predictions, we proposed an univocal assignment to the five Ω_c states observed both by LHCb [97] and Belle [98]. Finally we calculated the mass splitting between the ρ- and λ-mode excitations of the $\Omega_{c(b)}$ resonanceswe highlighted for the first time that the heavy-light baryon sector is the most suitable environment to test what are the correct effective spatial degrees of freedom for reproducing the mass spectra, as the presence or absence of ρ-mode excitations in the spectrum will be the key to discriminate between the three-quark and the quark-diquark structures. Specifically, if the predicted four ρ-excitations, $\Omega_c(3146)$, $\Omega_c(3182)$, $\Omega_b(6452)$, and $\Omega_b(6460)$, are not be observed, then the other Ω_c states will be characterized by a quark-diquark structure. As a consequence, the three-quark model effective degrees of freedom for the heavy-light baryons will be ruled out, supporting the Heavy Quark Effective Theory (HQET) picture of the heavy-light baryons described as heavy quark-light diquark systems.

Chapter 4

Conclusions

This thesis addressed some aspects of the heavy hadrons and the hidden-charm and -bottom pentaquark phenomenology; specifically ([8], [68], [96], [66],[67]):

- **1)** we predicted the new three pentaquark states observed by LHCb in 2019 [34], $P_c^+(4312)$, $P_c^+(4440)$ and $P_c^+(4457)$, one year and a half before the new analysis performed by LHCb [34]; later, in a further study [67], we predicted the pentaquark masses and decay widths consistently with the new data by LHCb with the following quantum number assignments [67]: $J^P_{P_c^+(4312)} = 1/2^-$, $J^P_{P_c^+(4440)} = 3/2^-$ and $J^P_{P_c^+(4457)} = 1/2^-$.

- **2)** we studied in details the origin of the mass difference between $P_c^+(4440)$ and $P_c^+(4457)$ by performing the calculations with and without the tensor term of the one-pion exchange potential (OPEP). The new LHCb results, indeed, provide us with the important opportunity of studying the spin-dependent forces between the Σ_c baryon and the $\bar{D}^*$ meson. The experimental determination of the pentaquark spin is very important since for nucleon systems only the spin 1 state (the deuteron) is available, without partners, and so this is the first example where the role of the tensor force can be compared in two partner states, *i.e.* $P_c^+(4440)$ and $P_c^+(4457)$. As a result of our investigation we found that both the short range interaction by the coupling to the 5-quark-core states and the long range interaction by the one-pion exchange potential make contributions to the attraction between Σ_c and $\bar{D}^{(*)}$. The mass difference between $P_c^+(4440)$ and $P_c^+(4457)$ comes mainly from the tensor interaction by the one-pion exchange potential. Because of the importance of the tensor interaction mediated by the pion in the heavy-hadron dynamics, we call it 'chiral tensor dynamics' [67].

- **3)** we showed that in the hidden-bottom sector, the OPEP is strong enough to produce states due to the mixing effect enhanced by the small mass splitting between B and B^*, and Σ_b and Σ_b^*. Thus, both the OPEP and the $5q$ potential play the important role to produce many states, while the $5q$ potential has the dominant role to yield the states in the hidden-charm sector. Since the attraction from the OPEP is enhanced and the kinetic term is suppressed due to the large hadron masses, the hidden-bottom pentaquarks are more likely to form rather than the hidden-charm pentaquarks [96].

- **4)** by means of the introduction of a three-dimensional harmonic oscillator hamiltonian (h.o.) plus spin-orbit, isospin and flavour dependent contributions, which turned out to be fundamental in describing the heavy-baryon mass pattern [68], we reproduced quantitatively the spectrum of the Ω_c states.

- **5)** we extended our mass and decay width predictions also to the orbitally excited Ω_b states [68] that, at that time, were still to be observed. Very recently, the LHCb Collaboration observed four narrow peaks, $\Omega_b(6316)$, $\Omega_b(6330), \Omega_b(6340)$ and $\Omega_b(6350)$ in $\Xi_b^0 K^-$ mass spectrum [65]. As reported by the same LHCb collaboration [65], the observed peaks and the $\Xi_b^0 K^-$ decay widths are consistent with our predictions given in Ref. [68].

- **6)** in Ref. [68] we calculated the mass splitting between the ρ- and λ-mode excitations of the $\Omega_{c(b)}$ resonances,and we highlighted that the heavy-light baryons are the most suitable environment to access to inner heavy-light baryon structure, owing to large mass splitting ρ- and λ-mode excitations, that we predict to be greater than 150 MeV. Indeed, if the ρ-excitations in the predicted mass region will not be observed in the future, then the three-quark model effective degrees of freedom for the heavy-light baryons will be ruled out, supporting the Heavy Quark Effective Theory (HQET) picture of the heavy-light baryons described as heavy quark-light diquark systems. If the HQET is valid for the heavy-light baryons, the heavy quark symmetry, predicted by the HQET in the heavy-light meson sector, can be extended to the heavy-quark-light-diquark baryon sector, opening the way to new future theoretical applications.

Appendix A

Construction of the pentaquark states

In principle, the spin-flavour part of the three-light-quark belong to the multiplets on the right side of

$$[1]_6 \otimes [1]_6 \otimes [1]_6 = [3]_{56} \oplus [21]_{70} \oplus [21]_{70} \oplus [111]_{20} \tag{A.1}$$

The wave function of the pentaquark state is the direct product between the $3q$ wave function and that of the $c\bar{c}$ pair. In order to study the internal degrees of freedom of the pentaquark systems it is useful to observe that q^3 and the $c\bar{c}$ pair wave functions can be decomposed in terms of the colour and the spin-flavour degrees of freedom. The three-light-quark wave function must satisfy the Pauli principle, so the spin-flavour part and the color part of the three light quarks are conjugated. For this reason the three light quarks can only be in a spin-flavour symmetric state in color singlet, or in a spin-flavour mixed symmetry state in color octet, while the $[111]_{20}$ spin-flavour multiplet is not allowed. As a consequence the allowed $SU_{sf}(6)$ spin-flavour pentaquark configurations are a 56-plet, which corresponds to the three quarks in a color singlet, and a 70-plet, which corresponds to the three light quarks in a color octet. Tab. G.12 reports the analysis of the flavor and spin content of the spin-flavor 56-plet and of the 70-plet , i.e. their decomposition into the representations of $SU_f(3) \otimes SU_s(2)$. The $SU_{sf}(6)$ 56-plet contains a $SU_f(3)$ flavor octet $[21]_8$ and a decuplet $[3]_{10}$, while the 70-plet contains a $SU_f(3)$ flavor singlet $[111]_1$, two octets $[21]_8$ and a decuplet $[3]_{10}$. Therefore, the allowed $SU_f(3)$ flavor representations to which the charmonium pentaquark states can belong are:

$$[111]_1 \ , \quad [21]_8 \ , \quad [3]_{10} \ . \tag{A.2}$$

In the case of 3 flavors (u, d, s), the hypercharge Y is defined as:

$$Y = B + \mathbf{S} \ , \tag{A.3}$$

Table A.1: Spin-flavor decomposition of the two allowed $SU_{sf}(6)$ spin-flavor pentaquark configurations: the 56-plet and the 70-plet.

$SU_{\rm sf}(6)$	$\supset$	$SU_{\rm f}(3)$	$\otimes$	$SU_{\rm s}(2)$
$[3]_{56}$		$[3]_{10}$	$\otimes$	$[3]_4$
		$[21]_8$	$\otimes$	$[21]_2$
$[21]_{70}$		$[3]_{10}$	$\otimes$	$[21]_2$
		$[21]_8$	$\otimes$	$[3]_4$
		$[21]_8$	$\otimes$	$[21]_2$
		$[111]_1$	$\otimes$	$[21]_2$

where B is the baryonic number, and $\mathbf{S}$ is the strangeness. Since the charmonium pentaquark state $P_c^+(4380)$, as reported by LHCb, has a quark content $uudc\bar{c}$, it does not have strange quarks; thus $\mathbf{S} = C = 0$, the baryonic number is $B = 1$, and Y must be equal to 1.
The singlet $[111]_1$ does not have any submultiplets with hypercharge $Y = 1$, and so it must be excluded. For this reason, the remaining possible $SU_f(3)$ multiplets for the charmonium pentaquark states are the octet and the decuplet:

$$[21]_8 \ , \quad [3]_{10} \ . \tag{A.4}$$

Appendix B

The Gürsey-Radicati mass formula extension

The approach adopted in evaluating the coefficients A, D, E, G, F and the scale parameter M_0 is to fit them at the same time, in order to obtain the best reproduction of the spectrum of all the ground-state charmed baryons, the ground-state hyperons, and the ground-state non-strange baryons (here ground state baryon means that the three constituent quarks of the baryon are in the $S-$ wave). The mass spectrum of these baryons is reported in Tab. B.2, while their quantum number assignments are reported in Tab. B.3. The fitted parameters and their corresponding uncertainties are reported in Tab. B.1.

Table B.1: *Table taken from [1] (APS copyright).* Values of the parameters in the GR mass formula extension (Eq. 2.4) with the corresponding uncertainties.

	M_0	A	D	E	F	G
values (MeV)	940,0	23,0	-158,3	32,0	1354.6	52,5
uncertainties (MeV)	1.5	1.2	1.3	1.3	18.2	1.3

Table B.2: Mass spectrum (MeV) of all the ground-state charmed baryons, the ground-state hyperons, and the ground-state non-strange baryons, as from Particle Data Group [51] (here ground state baryon means that the three constituent quarks of the baryon are in the $S-$ wave).

Baryons	exp. mass	exp. error
$N(940)$	939.565413	10^{-6}
$\Lambda^0(1116)$	1115.683	0.006
$\Sigma^0(1193)$	1192.642	0.024
$\Xi^0(1315)$	1314.86	0.20
$\Delta^0(1232)$	1232	2
$\Sigma^{*0}(1385)$	1383.7	1.0
$\Xi^{*0}(1530)$	1531.80	0.32
$\Omega^-(1672)$	1672.45	0.29
$\Lambda_c^+(2286)$	2286.46	0.14
$\Sigma_c^0(2455)$	2453.75	0.14
$\Xi_c^0(2471)$	2470.85	$^{+0.28}_{-0.40}$
$\Xi_c^{\prime 0}(2576)$	2577.9	2.9
$\Omega_c^0(2695)$	2695.2	1.7
$\Omega_c^{*0}(2770)$	2765.9	2.0
$\Sigma_c^{*0}(2520)$	2518.48	0.2
$\Xi_c^{*0}(2645)$	2649.9	0.5

Table B.3: Quantum number assignment for the baryons reported in Tab. B.2; the notation is the same of that used in Eq. 2.4.

baryons	$SU_f(3)$ multiplet	$C_2(SU(3))$	S	Y	I	N_c
$N(940)$	$[21]_8$	3	$\frac{1}{2}$	1	$\frac{1}{2}$	0
$\Lambda^0(1116)$	$[21]_8$	3	$\frac{1}{2}$	0	0	0
$\Sigma^0(1193)$	$[21]_8$	3	$\frac{1}{2}$	0	1	0
$\Xi^0(1315)$	$[21]_8$	3	$\frac{1}{2}$	-1	$\frac{1}{2}$	0
$\Delta^0(1232)$	$[3]_{10}$	6	$\frac{3}{2}$	1	$\frac{3}{2}$	0
$\Sigma^{*0}(1385)$	$[3]_{10}$	6	$\frac{3}{2}$	0	1	0
$\Xi^{*0}(1530)$	$[3]_{10}$	6	$\frac{3}{2}$	-1	$\frac{3}{2}$	0
$\Omega^-(1672)$	$[3]_{10}$	6	$\frac{3}{2}$	-2	0	0
$\Lambda_c^+(2286)$	$[11]_3$	$\frac{4}{3}$	$\frac{1}{2}$	$\frac{2}{3}$	0	1
$\Sigma_c^0(2455)$	$[2]_6$	$\frac{10}{3}$	$\frac{1}{2}$	$\frac{2}{3}$	1	1
$\Xi_c^0(2471)$	$[11]_3$	$\frac{4}{3}$	$\frac{1}{2}$	$-\frac{1}{3}$	$\frac{1}{2}$	1
$\Xi_c^{0'}(2576)$	$[2]_6$	$\frac{10}{3}$	$\frac{1}{2}$	$-\frac{1}{3}$	$\frac{1}{2}$	1
$\Omega_c^0(2695)$	$[2]_6$	$\frac{10}{3}$	$\frac{1}{2}$	$-\frac{4}{3}$	0	1
$\Omega_c^{*0}(2770)$	$[2]_6$	$\frac{10}{3}$	$\frac{3}{2}$	$-\frac{4}{3}$	0	1
$\Sigma_c^{*0}(2520)$	$[2]_6$	$\frac{10}{3}$	$\frac{3}{2}$	$\frac{2}{3}$	1	1
$\Xi_c^{*0}(2645)$	$[2]_6$	$\frac{10}{3}$	$\frac{3}{2}$	$-\frac{1}{3}$	$\frac{1}{2}$	1

Table B.4: Mass spectrum of all the ground-state and first orbitally-excited state well-established (*** and ****) charmed baryons, as from Particle Data Group [126] (here ground state baryon means that the three constituent quarks of the baryon are in the $S-$ wave). The quantum numbers of the states with † have not been measured yet.

State	S	L_λ	L_ρ	J^P	$SU(3)$ multiplet (C_2)	$\bar{M}$ (MeV)	$\Delta\bar{M}$ (MeV)
$\Lambda_c(2286)$	1/2	0	0	$1/2^+$	$[11]_{\bar{3}}$ (4/3)	2286.46	0.14
$\Lambda_c(2595)$	1/2	1	0	$1/2^-$	$[11]_{\bar{3}}$ (4/3)	2592.25	0.28
$\Lambda_c(2625)$	1/2	1	0	$3/2^-$	$[11]_{\bar{3}}$ (4/3)	2628.11	0.19
$\Sigma_c(2455)$	1/2	0	0	$1/2^+$	$[2]_6$ (10/3)	2453.54	0.23
$\Sigma_c^*(2520)$	3/2	0	0	$3/2^+$	$[2]_6$ (10/3)	2518.13	0.90
$\Xi_c(2471)$	1/2	0	0	$1/2^+$	$[11]_{\bar{3}}$ (4/3)	2469.37	0.31
$\Xi_c'(2576)$	1/2	0	0	$1/2^+$	$[2]_6$ (10/3)	2578.10	0.85
$\Xi_c^{*0}(2645)$	3/2	0	0	$3/2^+$	$[2]_6$ (10/3)	2645.90	0.50
$\Xi_c(2790)$	1/2	1	0	$1/2^-$	$[11]_{\bar{3}}$ (4/3)	2792.40	0.85
$\Xi_c(2815)$	1/2	1	0	$3/2^-$	$[11]_{\bar{3}}$ (4/3)	2818.45	0.32
$\Omega_c(2695)$	1/2	0	0	$1/2^+$	$[2]_6$ (10/3)	2695.20	1.70
$\Omega_c^*(2770)$	3/2	0	0	$3/2^+$	$[2]_6$ (10/3)	2765.90	2.00

Table B.5: Mass spectrum of all the ground-state and first orbitally-excited state well-established (*** and ****) bottom baryons, as from Particle Data Group [126] (here ground state baryon means that the three constituent quarks of the baryon are in the $S-$ wave). The quantum numbers of the states with † have not been measured yet.

State	S	L_λ	L_ρ	J^P	$SU(3)$ multiplet (C_2)	$\bar{M}$ (MeV)	$\Delta\bar{M}$ (MeV)
$\Lambda_b(5620)$	1/2	0	0	$1/2^+$	$[11]_{\bar{3}}$ (4/3)	5916.6	0.17
$\Lambda_b(5912)$	1/2	1	0	$1/2^-$	$[11]_{\bar{3}}$ (4/3)	5912.20	0.30
$\Lambda_b(5920)$	1/2	1	0	$3/2^-$	$[11]_{\bar{3}}$ (4/3)	5919.92	0.19
$\Sigma_b(5813)$	1/2	0	0	$1/2^+$	$[2]_6$ (10/3)	5813.10	0.26
$\Sigma_b^*(5832)$	3/2	0	0	$3/2^+$	$[2]_6$ (10/3)	5832.53	0.29
$\Sigma_b(6097)$ †						6096.90	2.15
$\Xi_b(5794)$	1/2	0	0	$1/2^+$	$[11]_{\bar{3}}$ (4/3)	5794.45	0.70
$\Xi_b'(5935)$	1/2	0	0	$1/2^+$	$[2]_6$ (10/3)	5935.02	0.07
$\Xi_b^*(5954)$	3/2	0	0	$3/2^+$	$[2]_6$ (10/3)	5953.82	0.54
$\Xi_b(6227)$ †						6226.9	2.4
$\Omega_b(6046)$	1/2	0	0	$1/2^+$	$[2]_6$ (10/3)	6046.1	1.7

Appendix C

Calculation of the decay widths

In principle, the excitation of pentaquark candidate $P_c^+(4380)$ in J/ψ photoproduction can occur via both s and u channels, as displayed in Fig. C.1. The

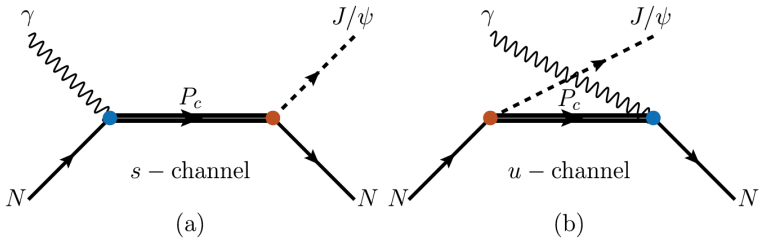

Figure C.1: Photoproduction of pentaquark states through the s and u channels. Fig. taken from [28], APS copyright.

contribution of the s and u channels are proportional to:

$$\mathcal{M}_s \propto \frac{1}{s - M_{P_c}^2} \tag{C.1}$$

and

$$\mathcal{M}_u \propto \frac{1}{u - M_{P_c}^2}, \tag{C.2}$$

respectively. Let us define p_1,p_2 as the momenta of the the income particles:

$$p_\gamma = p_1,\ p_N = p_2, \tag{C.3}$$

and p_3, p_4 as the momenta of the the outgoing particles:

$$p_{J/Psi} = p_3,\ p_{N'} = p_4. \tag{C.4}$$

In the the centre of mass reference system the four-momenta of the particles in the initial state, p_1, p_2 and of the particles in the final state are:

$$p_1 = (E, 0, 0, p),\ p_2 = (E, 0, 0, -p) \tag{C.5}$$

$$p_3 = (E, 0, p\sin\theta, p\cos\theta),\ p_4 = (E, 0, -p\sin\theta, -p\cos\theta), \tag{C.6}$$

where θ is the scattering angle. Thus:

$$s = (p_1 + p_2)^2 = 4E^2 \tag{C.7}$$

and

$$u = (p_1 - p_4)^2 = -2p^2(1 + \cos\theta) \tag{C.8}$$

Now we see that, once replaced s and u, evaluated in the centre of mass reference system, in the expression of the pentaquark propagators:

$$|\mathcal{M}_s| \propto \left|\frac{1}{s - M_{P_c}^2}\right| = \left|\frac{1}{4E^2 - M_{P_c}^2}\right| \gg |\mathcal{M}_u| \propto \left|\frac{1}{-2p^2(1+\cos\theta) - M_{P_c}^2}\right| \tag{C.9}$$

when the centre of mass energy E is close to the pentaquark mass M_{P_c}. As the $\gamma p \to J\Psi p$ cross section was measured in the energy region $4.4 - 5.8$ GeV ([77], [78], [79]), which is very close to the pentaquark mass, $M_{P_c} \simeq 4.380$ GeV, from the previous discussion it follows that in order to reproduce the experimental cross section one can neglect the u-channel contribution.
Since the LHCb analysis suggests that $P_c^+(4380)$ and $P_c^+(4450)$ favor spin $3/2$ and $5/2$, respectively, but with opposite signs, we then investigate the spin parity assignment of $3/2^-$ for the lightest pentaquark state. We adopt an effective Lagrangians from Ref. [35] for the $\gamma N P_c^+$ couplings with the pentaquark states :

$$\mathcal{L}^{3/2^-}_{\gamma N P_c} = \frac{ieh_1}{2M_N}\bar{N}\gamma_\nu F^{\mu\nu} P_{c\mu} - \frac{eh_2}{(2M_N)^2}\partial_\nu \bar{N} F^{\mu\nu} P_{c\mu} + H.c. \tag{C.10}$$

where P_c is the pentaquark fields with spin-parity $J^P = 3/2^-$ and N is the nucleon field. As we will discuss later, the coupling constants in Eq. (C.10) will be related to the couplings for $P_c N J/\psi$ interaction via vector meson dominance (VMD). We also adopt an effective Lagrangians for $P_c N J/\psi$ couplings from Ref. [35]:

$$\mathcal{L}^{3/2^-}_{P_c N\psi} = -\frac{ig_1}{2M_N}\bar{N}\gamma_\nu \psi^{\mu\nu} P_{c\mu} - \frac{g_2}{(2M_N)^2}\partial_\nu \bar{N}\psi^{\mu\nu} P_{c\mu}$$
$$+ \frac{g_3}{(2M_N)^2}\bar{N}\partial_\nu \psi^{\mu\nu} P_{c\mu} + H.c. \quad , \tag{C.11}$$

(C.12)

The higher partial wave states they can have different coupling structures which will make it difficult to determine their values. However, we notice that in $P_c^+(4380)$ decays into $J/\psi p$, the momentum of the final states are small in comparison with the nucleon mass. Thus, the higher partial wave terms, which are proportional to $(p/M_N)^2$ and $(p/M_N)^3$ in Eqs. (C.10) to (C.12) can be neglected. Then, the leading order transition matrix elements can be written as [28]:

$$\mathcal{M}^{3/2^-} = \frac{1}{s - M_{P_c}^2} \frac{e h_1 g_1}{(2M_N)2} \epsilon^*_{\psi\nu} \bar{u}_N \gamma_\sigma \Delta_{\beta\alpha}(P_c, k+p) \gamma_\delta \times (k^\alpha g^{\mu\delta} - k^\delta g^{\alpha\mu}) u_N \epsilon_{\gamma\mu} \tag{C.13}$$

where $\epsilon_{\gamma\mu}$ and $\epsilon^*_{\psi\nu}$ are the polarization vectors for the initial state photon and the final state J/ψ, respectively; $\Delta_{\beta\alpha}(P_c, k+p)$ is the spin 3/2 Rarita-Schwinger spin projection for the pentaquark intermediate state [35]:

$$\Delta_{\beta\alpha}(P_c, p) = (\not{p} + M_{P_c}) \left[-g_{\beta\alpha} + \frac{1}{3}\gamma_\beta\gamma_\alpha + \frac{1}{3M_{P_c}} (\gamma_\beta p_\alpha - \gamma_\alpha p_\beta) + \frac{2}{3M_{P_c}^2} p_\beta p_\alpha \right], \tag{C.14}$$

where M_{P_c} and p denote the mass and momentum of pentaquark P_c. Now, Eq. C.13 contains two unknown coupling constant, one for the $\gamma N P_c$ vertex, h_1, and another one for the $J/\Psi N P_c$ vertex, g_1. The hypothesis proposed by Wang in Ref. [28] was to assume that the coupling between the pentaquark and the photon occur through the J/ψ meson, as displayed in Fig. C.2. As we will see, this assumption make it possible to relate the two coupling constants h_1 and g_1 together. The coupling between the photon and the J/ψ meson is provided by the Vector Meson Dominance model VMD. In the VMD the physical photon is thought as a superposition of a bare photon state and a hadronic component, which is responsible of the hadronic interactions. Obviously, the hadronic component is restricted to particles that have the same quantum numbers of the photon, *i.e* $J^{PC} = 1^{--}$ and $Q = B = S = 0$. The copious photoproduction of these vector mesons qualitatively support this assumption. The leading order coupling between a vector meson and photon in the VMD is given by:

$$\mathcal{L}_{V\gamma} = \sum_V \frac{e}{f_V} \frac{M_V^2}{q^2 - M_V^2} V_\mu A^\mu \ , \tag{C.15}$$

where the coupling constant e/f_V can be determined by the vector meson leptonic decay $V \to e^+e^-$,

$$\frac{e}{f_V} = \left[\frac{3\Gamma_{V\to e^+e^-}}{2\alpha_e |p_e|} \right]^{1/2} \ , \tag{C.16}$$

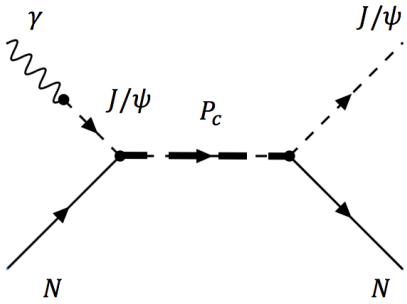

Figure C.2: Photoproduction of pentaquark states in the hypothesis that the coupling between the pentaquark and the photon occur through the J/ψ meson [28].

where $|p_e|$ is the electron three-vector-moment in the vector meson rest frame, and $\alpha_e = 1/137$ is the EM fine-structure constant. For the $\gamma - J/\psi$ coupling, we have $e/f_{J/\psi} = 0.027$ [28]. The explicit relation between the h_1 and g_1 can be found by a comparison of the photocoupling vertexes in the Feynman diagrams of Fig. C.1 a and Fig. C.2, which are obtained from the effective Lagrangians for the $P_cN\psi$ coupling C.12, for the $\gamma N\psi$ coupling C.15 and for the γP_cN coupling C.10:

$$\frac{e}{f_{J/\Psi}} \frac{M_{J/\Psi}^2}{q^2 - M_{J/\Psi}^2} \left(-\frac{ig_1}{2M_N} \right) = \frac{ieh_1}{2M_N}, \tag{C.17}$$

which after inserted the momentum condition for a real photon, $q^2 = 0$, becomes:

$$\frac{e}{f_{J/\Psi}} \left(\frac{ig_1}{2M_N} \right) = \frac{ieh_1}{2M_N}, \tag{C.18}$$

$$\rightarrow \frac{eg_1}{f_{J/\Psi}} = eh_1. \tag{C.19}$$

As a result, we can write the leading order transition matrix elements of Eq. C.13 as a function of the strong coupling constant g_1:

$$\mathcal{M}^{3/2^-} = \frac{1}{s - M_{P_c}^2} \frac{eg_1^2}{2f_{J/\Psi}(2M_N)} \epsilon_{\psi\nu}^* \bar{u}_N \gamma_\sigma \Delta_{\beta\alpha}(P_c, k+p) \gamma_\delta$$
$$\times (k^\alpha g^{\mu\delta} - k^\delta g^{\alpha\mu}) u_N \epsilon_{\gamma\mu} \tag{C.20}$$

The value of g_1 can now be extract from available photoproduction data ([77], [78], [79]), $g_1 = 1.40$, which will give an upper limit for the pentaquark production cross sections in photoproduction.

Appendix D

Derivation of the Heavy Quark Lagrangian from the QCD Lagrangian

QCD describes the dynamics of quarks, and has a non-perturbative scale $\Lambda_{QCD} \simeq 200$ MeV. A single heavy quark, with mass $m_Q > \Lambda_{QCD}$ interacting with light particles can be described by an effective field theory known as Heavy Quark Effective Theory (HQET). In this appendix we derive explicitly the HQET Lagrangian from the QCD Lagrangian. Consider a heavy quark Q interacting with light degrees of freedom, such as light quarks and gluons. The QCD Lagrangian contains a part which describes the heavy quark field, $\mathcal{L}_{heavy}$, and another one which describes the light degrees of freedoms:

$$\mathcal{L}_{QCD} = \mathcal{L}_{heavy} + \mathcal{L}_{light} = \bar{Q}(i\not{D} - m_Q)Q + \mathcal{L}_{light} \tag{D.1}$$

where m_Q is the heavy quark mass, the covariant derivative is given by $D_\mu = \partial_\mu + igA^a_\mu T^a$, A^a_μ is the gluon field and T^a are the generators of the $SU_c(3)$ group. $\mathcal{L}_{light}$ is the Lagrangian for the light quarks and gluons. Inserting the

heavy quark field in the QCD Lagrangian density one obtains [1]:

$$\begin{aligned}
&\bar{Q}(x)(i\not{D} - m_Q)Q(x) = \\
&[\bar{H}_v(x) + \bar{h}_v(x)]e^{im_Q vx}(i\not{D} - m_Q)e^{-im_Q vx}[H_v(x) + h_v(x)] = \\
&[\bar{H}_v(x) + \bar{h}_v(x)]e^{im_Q vx}(i\not{D})e^{-im_Q vx}[H_v(x) + h_v(x)] \\
&- [\bar{H}_v(x) + \bar{h}_v(x)]m_Q[H_v(x) + h_v(x)] \\
&= [\bar{H}_v(x) + \bar{h}_v(x)](i\not{D} + m_Q\not{v})[H_v(x) + h_v(x)] \\
&- [\bar{H}_v(x) + \bar{h}_v(x)]m_Q[H_v(x) + h_v(x)]
\end{aligned} \tag{D.2}$$

which, by using Eq. 2.35, becomes:

$$\begin{aligned}
&[\bar{H}_v(x) + \bar{h}_v(x)](i\not{D})[H_v(x) + h_v(x)] + [\bar{H}_v(x) + \bar{h}_v(x)]m_Q[-H_v(x) + h_v(x)] \\
&- [\bar{H}_v(x) + \bar{h}_v(x)]m_Q[H_v(x) + h_v(x)] = \\
&= [\bar{H}_v(x) + \bar{h}_v(x)]\left\{(i\not{D})[H_v(x) + h_v(x)] + m_Q[-H_v(x) + h_v(x)]\right. \\
&\left.-m_Q[H_v(x) + h_v(x)]\right\} = \\
&[\bar{H}_v(x) + \bar{h}_v(x)]\left\{i\not{D}H_v(x) + i\not{D}h_v(x) - 2m_Q H_v(x)\right\} = \\
&[\bar{H}_v(x) + \bar{h}_v(x)]\left\{i\not{D}h_v(x) + [i\not{D} - 2m_Q]H_v(x)\right\}.
\end{aligned} \tag{D.3}$$

By expanding the product and by using the field equations, reported in Eq. 2.35, and the properties of the projector operators, reported in Eq. 2.32, one finds:

$$\begin{aligned}
&\mathcal{L}_{heavy} = \bar{h}_v(x)i\not{D}h_v(x) + \bar{h}_v(x)i\not{D}H_v(x) + \bar{H}_v(x)i\not{D}h_v(x) \\
&+ \bar{H}_v(x)i\not{D}H_v(x) - 2m_Q\bar{h}_v(x)H_v(x) - 2m_Q\bar{H}_v(x)H_v(x) = \\
&\bar{h}_v(x)\hat{P}_+i\not{D}\hat{P}_+h_v(x) + \bar{h}_v(x)\hat{P}_+i\not{D}\hat{P}_-H_v(x) + \bar{H}_v(x)\hat{P}_-i\not{D}\hat{P}_+h_v(x) \\
&+ \bar{H}_v(x)\hat{P}_-i\not{D}\hat{P}_-H_v(x) - 2m_Q\bar{h}_v(x)\hat{P}_+\hat{P}_-H_v(x) - 2m_Q\bar{H}_v(x)H_v(x)
\end{aligned} \tag{D.4}$$

[1] In order to subtract the quantity $m_Q v$ from the heavy quark momentum, the following definition for the small and the large-component fields is used:

$$h_v(x) = e^{im_Q vx}P_+Q(x), \quad H_v(x) = e^{im_Q vx}P_-Q(x).$$

From Eq. 2.31 it follows that the heavy quark field $Q(x)$ becomes

$$Q(x) = e^{-im_Q vx}(H_v(x) + h_v(x))$$

The Lagrangian density of Eq. D.4 can be simplified if one uses the following relations:

$$\begin{aligned}\hat{P}_+\gamma_\mu\hat{P}_+ = \frac{1+\not{v}}{2}\gamma_\mu\frac{1+\not{v}}{2} = \frac{1+\gamma_\alpha v^\alpha}{2}\gamma_\mu\frac{1+\not{v}}{2} = \\ \frac{\gamma_\mu - \gamma_\mu\gamma_\alpha v^\alpha + 2g_{\mu\alpha}v^\alpha}{2}\frac{1+\not{v}}{2} = \left(\gamma_\mu\frac{1-\not{v}}{2} + v_\mu\right)\frac{1+\not{v}}{2} = \\ \gamma_\mu\frac{1-\not{v}}{2}\frac{1+\not{v}}{2} + v_\mu\frac{1+\not{v}}{2} = v_\mu\frac{1+\not{v}}{2} = v_\mu\hat{P}_+ \\ \rightarrow \hat{P}_+\gamma_\mu\hat{P}_+ = v_\mu\hat{P}_+ \end{aligned} \tag{D.5}$$

By multiplying the last equation times $\hat{P}_+$ we finally obtain:

$$\begin{aligned}\hat{P}_+\hat{P}_+\gamma_\mu\hat{P}_+ = \hat{P}_+v_\mu\hat{P}_+, \\ \rightarrow \hat{P}_+\gamma_\mu\hat{P}_+ = \hat{P}_+v_\mu\hat{P}_+. \end{aligned} \tag{D.6}$$

In the same way one can show that:

$$\hat{P}_-\gamma_\mu\hat{P}_- = -\hat{P}_-v_\mu\hat{P}_-. \tag{D.7}$$

If we sandwich the covariant derivative with the projector operators

$$\begin{aligned}\hat{P}_+\not{D}\hat{P}_- = \hat{P}_+(\not{D}_\perp + v_\mu v\cdot D)\hat{P}_- = \\ \hat{P}_+\not{D}_\perp\hat{P}_- + \hat{P}_+v_\mu v\cdot D\hat{P}_- = \\ \hat{P}_+\not{D}_\perp\hat{P}_- + v_\mu v\cdot D\hat{P}_+\hat{P}_- = \hat{P}_+\not{D}_\perp\hat{P}_-, \end{aligned} \tag{D.8}$$

where $D_\perp = D_\mu - v_\mu v\cdot D$ is the component of the covariant derivative orthogonal to the velocity, *i.e.* it is defined in such a way that $v\cdot D_\perp = 0$. We observe that In the hadron rest frame, where $v_\mu = (1,0,0,0)$, $D_\perp$ contains just the space components of the covariant derivative: $D_\perp = (0,\vec{D})$. Again, with similar steps we find that:

$$\hat{P}_-\not{D}\hat{P}_+ = \hat{P}_-\not{D}_\perp\hat{P}_+ \tag{D.9}$$

So we proved the following identities:

$$\begin{aligned}\hat{P}_+\gamma_\mu\hat{P}_+ &= \hat{P}_+v_\mu\hat{P}_+ \\ \hat{P}_-\gamma_\mu\hat{P}_- &= -\hat{P}_-v_\mu\hat{P}_- \\ \hat{P}_+\not{D}\hat{P}_- &= \hat{P}_+\not{D}_\perp\hat{P}_- \\ \hat{P}_-\not{D}\hat{P}_+ &= \hat{P}_-\not{D}_\perp\hat{P}_+. \end{aligned} \tag{D.10}$$

With the equations D.10 the heavy-quark Lagrangian density of Eq. D.4 becomes:

$$\begin{aligned}\mathcal{L}_{heavy} &= \bar{h}_v(x) iv\cdot D h_v(x) + \bar{h}_v(x) i\not{D}_\perp H_v(x) + \bar{H}_v(x) i\not{D}_\perp h_v(x) \\ &- \bar{H}_v(x) iv\cdot D H_v(x) - 2m_Q \bar{H}_v(x) H_v(x).\end{aligned} \tag{D.11}$$

As the next step, the heavy quark field $H_v(x)$ is eliminated by using the equation of motion of QCD. The classical Euler-Lagrange equation, obtained by taking functional derivatives of the classical QCD action,

$$\frac{\mathcal{L}_{QCD}}{\partial \bar{Q}} - \partial_\mu \frac{\partial \mathcal{L}_{QCD}}{\partial \partial_\mu \bar{Q}} = 0 \tag{D.12}$$

becomes, from Eq. D.1:

$$\frac{\mathcal{L}_{heavy}}{\partial \bar{Q}} - \partial_\mu \frac{\partial \mathcal{L}_{heavy}}{\partial \partial_\mu \bar{Q}} = 0 \rightarrow (i\not{D} - m_Q) Q(x) = 0 \tag{D.13}$$

The equation of motion of the heavy quark field, in terms of the fields $H_v(x)$ and $h_v(x)$ becomes:

$$\begin{aligned}(i\not{D} - m_Q) Q(x) = (i\not{D} - m_Q) e^{-im_Q vx} [H_v(x) + h_v(x)] &= 0, \\ \rightarrow e^{-im_Q vx} (i\not{D} + m_Q \not{v} - m_Q)[H_v(x) + h_v(x)] &= 0, \\ \rightarrow (i\not{D} - m_Q)[H_v(x) + h_v(x)] + m_Q h_v(x) - m_Q H_v(x) &= 0, \\ \rightarrow i\not{D} H_v(x) + i\not{D} h_v(x) - 2m_Q H &= 0,\end{aligned} \tag{D.14}$$

which can be written as:

$$i\not{D}\hat{P}_- H_v(x) + i\not{D}\hat{P}_+ h_v(x) - 2m_Q \hat{P}_- H = 0 \tag{D.15}$$

Multiplying by $\hat{P}_\pm$, this equation gets projected into two different pieces, one for $\hat{P}_+$:

$$\begin{aligned}\hat{P}_+ i\not{D}\hat{P}_- H_v(x) + \hat{P}_+ i\not{D}\hat{P}_+ h_v(x) - 2m_Q \hat{P}_+\hat{P}_- H &= 0, \\ \rightarrow \hat{P}_+ i\not{D}_\perp \hat{P}_- H_v(x) + \hat{P}_+ iv\cdot D\hat{P}_+ h_v(x) &= 0, \\ \rightarrow i\not{D}_\perp H_v(x) + iv\cdot D h_v(x) &= 0.\end{aligned} \tag{D.16}$$

where we have used the identities of Eq. D.10, and one for $\hat{P}_-$:

$$\begin{aligned}\hat{P}_- i\not{D}\hat{P}_- H_v(x) + \hat{P}_- i\not{D}\hat{P}_+ h_v(x) - 2m_Q \hat{P}_-\hat{P}_- H &= 0, \\ \rightarrow -\hat{P}_- iv\cdot D\hat{P}_- H_v(x) + \hat{P}_+ i\not{D}_\perp \hat{P}_+ h_v(x) - 2m_Q \hat{P}_-\hat{P}_- &= 0, \\ \rightarrow -iv\cdot D H_v(x) + i\not{D}_\perp h_v(x) - 2m_Q &= 0.\end{aligned} \tag{D.17}$$

From Eq. D.16 and Eq. D.17 we obtain:

$$iv \cdot D h_v(x) = -i\not{D}_\perp H_v(x) \tag{D.18}$$
$$(iv \cdot D + 2m_Q) H_v(x) = i\not{D}_\perp h_v(x) \tag{D.19}$$

We observe that Eq. D.19 shows explicitly that $H_v(x) \sim \mathcal{O}(1/m_Q)$:

$$H_v(x) = \frac{1}{iv \cdot D + 2m_Q} i\not{D}_\perp h_v(x), \tag{D.20}$$

Inserting Eq. D.20 back into Eq. D.11, one gets for the heavy quark Lagrangian density:

$$\begin{aligned}
&\mathcal{L}_{heavy} = \bar{h}_v(x) iv \cdot D h_v(x) + \bar{h}_v(x) i\not{D}_\perp H_v(x) + \bar{H}_v(x) i\not{D}_\perp h_v(x) \\
&- \bar{H}_v(x) iv \cdot D H_v(x) - 2m_Q \bar{H}_v(x) H_v(x) = \\
&\bar{h}_v(x) iv \cdot D h_v(x) + \bar{h}_v(x) i\not{D}_\perp \frac{1}{iv \cdot D + 2m_Q} i\not{D}_\perp h_v(x) + \bar{H}_v(x) i\not{D}_\perp h_v(x) \\
&- \bar{H}_v(x) iv \cdot D \frac{1}{iv \cdot D + 2m_Q} i\not{D}_\perp h_v(x) \\
&- 2m_Q \bar{H}_v(x) \frac{1}{iv \cdot D + 2m_Q} i\not{D}_\perp h_v(x) = \\
&\bar{h}_v(x) iv \cdot D h_v(x) + \bar{h}_v(x) i\not{D}_\perp \frac{1}{iv \cdot D + 2m_Q} i\not{D}_\perp h_v(x) \\
&+ \bar{H}_v(x) \left[1 - iv \cdot D \frac{1}{iv \cdot D + 2m_Q} - 2m_Q \frac{1}{iv \cdot D + 2m_Q} \right] i\not{D}_\perp h_v(x) = \\
&\bar{h}_v(x) iv \cdot D h_v(x) + \bar{h}_v(x) i\not{D}_\perp \frac{1}{iv \cdot D + 2m_Q} i\not{D}_\perp h_v(x) \\
&+ \bar{H}_v(x) \left[\frac{iv \cdot D + 2m_Q - iv \cdot D - 2m_Q}{iv \cdot D + 2m_Q} \right] i\not{D}_\perp h_v(x) = \\
&\bar{h}_v(x) iv \cdot D h_v(x) + \bar{h}_v(x) i\not{D}_\perp \frac{1}{iv \cdot D + 2m_Q} i\not{D}_\perp h_v(x).
\end{aligned} \tag{D.21}$$

So we have found the following expression for the heavy quark Lagrangian density:

$$\mathcal{L}_{heavy} = \bar{h}_v(x) iv \cdot D h_v(x) + \bar{h}_v(x) i\not{D}_\perp \frac{1}{iv \cdot D + 2m_Q} i\not{D}_\perp h_v(x) \tag{D.22}$$

The last step consists in the observation that derivatives acting on the field $h_v(x)$ produce powers of the small momentum k_μ. Therefore, the non-local

HQET Lagrangian can be expanded in powers of D/m_Q [2]:

$$\mathcal{L}_{heavy} \simeq \bar{h}_v(x) iv \cdot D h_v(x) + \bar{h}_v(x) i\not{D}_\perp \frac{1}{2m_Q} i\not{D}_\perp h_v(x) \tag{D.23}$$

Let us focus on second term of Eq. D.23:

$$\begin{aligned}
\not{D}_\perp \not{D}_\perp = (\not{D} - \not{v} v \cdot D)(\not{D} - \not{v} v \cdot D) = \\
(\gamma_\mu D^\mu - \gamma_\mu v^\mu v \cdot D)(\gamma_\nu D^\nu - \gamma_\nu v^\nu v \cdot D) = \\
\gamma_\mu D^\mu \gamma_\nu D^\nu - \gamma_\mu D^\mu \gamma_\nu v^\nu v \cdot D - \gamma_\mu v^\mu v \cdot D \gamma_\nu D^\nu + \gamma_\mu v^\mu v \cdot D \gamma_\nu v^\nu v \cdot D = \\
\gamma_\mu \gamma_\nu (D^\mu D^\nu - D^\mu v^\nu v \cdot D - v^\mu v \cdot D D^\nu + v^\mu v \cdot D v^\nu v \cdot D) = \\
(g_{\mu\nu} + \frac{1}{i}\sigma_{\mu\nu})(D^\mu D^\nu - D^\mu v^\nu v \cdot D - v^\mu v \cdot D D^\nu + v^\mu v \cdot D v^\nu v \cdot D)
\end{aligned} \tag{D.24}$$

where in the last step we used:

$$\gamma_\mu \gamma_\nu = \frac{1}{2}\{\gamma_\mu, \gamma_\nu\} + \frac{1}{2}[\gamma_\mu, \gamma_\nu] = g_{\mu\nu} - i\sigma_{\mu\nu} \tag{D.25}$$

with

$$\sigma_{\mu\nu} = \frac{i}{2}[\gamma_\mu, \gamma_\nu]. \tag{D.26}$$

Thus, performing the products and observing that $\sigma_{\mu\nu}$ is an antisymmetric operator Eq. D.24 becomes:

$$\begin{aligned}
\not{D}_\perp \not{D}_\perp &= (D)^2 - (v \cdot D)^2 + \frac{1}{i}\sigma_{\mu\nu} D^\mu D^\nu \\
&= D_\perp^2 + \frac{1}{i}\sigma_{\mu\nu}\frac{1}{2}(D^\mu D^\nu - D^\nu D^\mu) \\
&= D_\perp^2 + \frac{1}{i}\sigma_{\mu\nu}\frac{1}{2}[D^\mu, D^\nu] \\
&= D_\perp^2 + \frac{g}{2}\sigma_{\mu\nu} G^{\mu\nu}
\end{aligned} \tag{D.27}$$

In the last line we used the definition of the gluon field strength tensor in terms of the commutator of two covariant derivatives [3]:

$$G^{\mu\nu} = \frac{1}{ig}[D^\mu, D^\nu] = \partial^\mu A^\nu - \partial^\nu A^\mu - ig[A^\mu, A^\nu]. \tag{D.28}$$

[2] Here we use the Taylor expansion $\frac{1}{1+x} = 1 - x + x^2 - x^3 + ... + (-1)^n x^n + \mathcal{O}(x^n)$ and we cut the series at the lowest order in the heavy quark mass expansion.

[3] The gluon field strength tensor is defined as $\pm\frac{1}{ig}[D^\mu, D^\nu]$. Here we adopted the same sign of Ref. [80]

Replacing Eq. D.27 in Eq. D.23 we obtain the Heavy Quark Lagrangian density up to the $\frac{1}{m_Q}$ order:

$$\mathcal{L}_{heavy} = \mathcal{L}^{(0)}_{heavy} + \mathcal{L}^{(1)}_{heavy} + \mathcal{O}\left(\frac{1}{m_Q}\right) \tag{D.29}$$

where $\mathcal{L}^{(0)}_{heavy}$ is the lowest order Lagrangian and it does not depend on the heavy quark mass and spin:

$$\mathcal{L}^{(0)}_{heavy} = \bar{h}_v(x) iv \cdot D h_v(x), \tag{D.30}$$

and $\mathcal{L}^{(1)}_{heavy}$ is the next to leading order correction and it gives a contribution proportional to the inverse of the heavy quark mass:

$$\begin{aligned} \mathcal{L}^{(1)}_{heavy} &= \bar{h}_v(x) i\not{D}_\perp \frac{1}{2m_Q} i\not{D}_\perp h_v(x) \\ &= -\bar{h}_v(x)\frac{(D_\perp)^2}{2m_Q} h_v(x) - \bar{h}_v(x)\frac{g\sigma_{\mu\nu}G^{\mu\nu}}{4m_Q} h_v(x). \end{aligned} \tag{D.31}$$

The physical meaning of the two $\mathcal{O}(1/m_Q)$ operators is rather transparent in the rest frame of the heavy quark, where $D_\perp = (0, \vec{D})$. [4] From the definition of the orthogonal covariant derivative, $D_\perp$, and the fact that $\sigma_{\mu\nu}$ is an antisymmetric tensor (see Eq. D.26), it follows that

$$\sigma_{\mu\nu}G^{\mu\nu} = \sigma_{\mu\nu}\frac{1}{ig}[D^\mu, D^\nu] = \sigma_{\mu\nu}\frac{1}{ig}[D^\mu_\perp, D^\nu_\perp] = \sigma_{ij}\frac{1}{ig}[D^i_\perp, D^j_\perp], \tag{D.32}$$

where in the last step we have used the fact that, in the rest frame of the heavy quark $D_\perp = (0, \vec{D})$:

$$\sigma_{00}G^{00} = \sigma_{00}\frac{1}{ig}[D^0_\perp, D^0_\perp] = 0. \tag{D.33}$$

Hence in the rest frame of the heavy quark:

$$\sigma_{\mu\nu}G^{\mu\nu} = \sigma_{ij}G^{ij} \tag{D.34}$$

[4] In the rest frame of the heavy quark $v_\mu = (1, 0, 0, 0)$ hence $D_{\perp,0} = D_0 - v_0 v_0 D^0 = 0$ and $D_{\perp,i} = D_i - v_i v_i D^i = D_i$.

which can be written more explicitly as:

$$\sigma_{ij}G^{ij} = \frac{i}{2}[\gamma_i,\gamma_j]G^{ij} = \frac{i}{2}(\gamma_i\gamma_j - \gamma_j\gamma_i)G^{ij} =$$
$$\frac{i}{2}\left[\begin{pmatrix} 0 & \sigma_i \\ -\sigma_i & 0 \end{pmatrix}\begin{pmatrix} 0 & \sigma_j \\ -\sigma_j & 0 \end{pmatrix} - \begin{pmatrix} 0 & \sigma_j \\ -\sigma_j & 0 \end{pmatrix}\begin{pmatrix} 0 & \sigma_i \\ -\sigma_i & 0 \end{pmatrix}\right] G^{ij} =$$
$$\frac{i}{2}\left[\begin{pmatrix} -\sigma_i\sigma_j & 0 \\ 0 & -\sigma_i\sigma_j \end{pmatrix} + \begin{pmatrix} -\sigma_j\sigma_i & 0 \\ 0 & -\sigma_j\sigma_i \end{pmatrix}\right] G^{ij} =$$
$$-\frac{i}{2}\left[\begin{pmatrix} [\sigma_i,\sigma_j] & 0 \\ 0 & [\sigma_i,\sigma_j] \end{pmatrix}\right] G^{ij} = -\frac{i}{2}2i\epsilon_{ijk}\left[\begin{pmatrix} \sigma_k & 0 \\ 0 & \sigma_k \end{pmatrix}\right] G^{ij} =$$
$$\epsilon_{ijk}\begin{pmatrix} \sigma_k & 0 \\ 0 & \sigma_k \end{pmatrix} G^{ij}, \tag{D.35}$$

where in the last step we used:

$$[\sigma_i,\sigma_j] = 2i\epsilon_{ijk}\sigma_k. \tag{D.36}$$

Now we observe that, from the definition of the chromo-magnetic field,

$$B_c^i = -\frac{1}{2}\epsilon^{ijk}G^{jk} \tag{D.37}$$

and from the relation between the Pauli matrices σ_i and the spin operators S_i,

$$\vec{S} \equiv \frac{1}{2}\gamma_5\gamma^0\vec{\gamma} = \frac{1}{2}\begin{pmatrix} \vec{\sigma} & 0 \\ 0 & \vec{\sigma} \end{pmatrix} \tag{D.38}$$

Eq. D.35 can be written in a more simple way as:

$$\sigma_{ij}G^{ij} = -4\vec{S}\cdot\vec{B}_c \tag{D.39}$$

Now the next to leading order Lagrangian of Eq. D.31 in the reference system of the heavy quark is:

$$\begin{aligned} \mathcal{L}^{(1)}_{heavy} &= -\bar{h}_v(x)\frac{(D_\perp)^2}{2m_Q}h_v(x) - \bar{h}_v(x)\frac{g\sigma_{\mu\nu}G^{\mu\nu}}{4m_Q}h_v(x) \\ &= +\bar{h}_v(x)\frac{|\vec{D}|^2}{2m_Q}h_v(x) + \bar{h}_v(x)\frac{g\vec{S}\cdot\vec{B}_c}{m_Q}h_v(x) \end{aligned} \tag{D.40}$$

The first operator is the gauge-covariant extension of the kinetic energy associated with the off-shell residual momentum of the heavy quark. The second operator is the non-abelian analog of the QED Pauli term, which describes the interaction of the heavy-quark spin with the gluon field. Therefore the next to leading order terms, which are proportional to the inverse of heavy quark mass m_Q violate the heavy quark symmetry in the finite heavy quark mass.

To summarise, we performed a non-relativistic reduction of the heavy quark part of QCD Lagrangian and we expressed it as a power series in the inverse of the heavy quark mass. In particular we focused on the physical meaning of the leading order Lagrangian, $\mathcal{L}^{(0)}_{heavy}$, and of the next to leading order terms $\mathcal{L}^{(1)}_{heavy}$. We observed that the leading order contribution,

$$\mathcal{L}^{(0)}_{heavy} = \bar{h}_v(x) iv \cdot D h_v(x), \tag{D.41}$$

does not depend on the spin and on the mass and therefore it explicitly manifests spin and flavor symmetries. The next to leading order correction, which is proportional to the inverse of the heavy quark mass, contains two terms:

$$\mathcal{L}^{(1)}_{heavy} = -\bar{h}_v(x)\frac{(D_\perp)^2}{2m_Q}h_v(x) - \bar{h}_v(x)\frac{g\sigma_{\mu\nu}G^{\mu\nu}}{4m_Q}h_v(x). \tag{D.42}$$

The first term is the heavy quark kinetic energy and then it breaks the flavor symmetry but it does not break the heavy spin symmetry. The second term describes the spin-dependent interaction between the heavy quark and the gluon. Thus, it violates both flavor and spin symmetries. As the complete effective Lagrangian is an expansion of the QCD Lagrangian in powers of the inverse of heavy quark mass, in the infinite mass limit, all the next to leading order contributions are suppressed and the only part which survives is the leading order Lagrangian, which exhibits heavy quark flavor and spin symmetries.

D.1 Spectroscopic implications of the heavy quark symmetries

Let us denote s_l the total spin of the light degrees of freedom in a hadron containing a single heavy quark Q. As we discussed previously, in the $m_Q \to \infty$ limit, the dynamics is independent of the heavy-quark spin. Therefore, we expect to find two degenerate hadronic states with $J = s_l \pm \frac{1}{2}$. For Qq mesons the ground state has negative parity and $s_l = \frac{1}{2}$, giving a doublet of degenerate spin-zero and spin-one mesons. The measured mass spectrum of heavy mesons [51] shows that this is true to a quite good approximation for the charmed mesons:

$$M_{D^*} - M_D \simeq 142 \ \text{MeV}, \to \frac{M_{D^*} - M_D}{M_D} \simeq 8\%, \tag{D.43}$$

and a very good approximation for the bottom mesons:

$$M_{B^*} - M_B \simeq 46 \ \text{MeV}, \to \frac{M_{B^*} - M_B}{M_B} \simeq 0.9\%. \tag{D.44}$$

D.2 The chiral symmetry

As we discussed in the previous section the QCD Lagrangian contains a part which describes the heavy quark field, $\mathcal{L}_{heavy}$, and another one which describes the light degrees of freedoms, $\mathcal{L}_{light}$:

$$\mathcal{L}_{QCD} = \mathcal{L}_{heavy} + \mathcal{L}_{light} = \mathcal{L}_{heavy} + \sum_{f=u,d,s} \bar{q}_f (i\not{D} - m_q) q_f - \frac{1}{4} G^a_{\mu\nu} G^{\mu\nu,a} \tag{D.45}$$

where m_q is the light quark mass, the index f runs on the light flavours, and $G_{\mu\nu}$ is the gluon field tensor:

$$G^a_{\mu\nu} = \partial_\mu A^a_\nu - \partial_\nu A^a_\mu + g f_{abc} A^b_\mu A^c_\nu. \tag{D.46}$$

In order to fully exhibit the global symmetries of the light part of the QCD Lagrangian,

$$\mathcal{L}_{light} = \sum_{f=u,d,s} \bar{q}_f (i\not{D} - m_q) q_f - \frac{1}{4} G^a_{\mu\nu} G^{\mu\nu,a}, \tag{D.47}$$

we consider the chirality matrix $\gamma_5 = \gamma^5 = i\gamma^0\gamma^1\gamma^2\gamma^3 = \gamma_5^\dagger$, $\{\gamma^\mu, \gamma_5\} = 0$, $\gamma_5^2 = 1$, and the projection operators

$$P_R = \frac{1}{2}(1 + \gamma_5) = P_R^\dagger, \quad P_L = \frac{1}{2}(1 - \gamma_5) = P_L^\dagger, \tag{D.48}$$

where the indices R and L refer to right-handed and left-handed, respectively, as defined in appendix D. Under parity, the quark field is transformed into its parity conjugate,

$$P : q(t, \vec{x}) \mapsto \gamma_0 q(t, -\vec{x}),$$

and hence

$$q_R(t, \vec{x}) = P_R q(t, \vec{x}) \mapsto P_R \gamma_0 q(t, -\vec{x}) = \gamma_0 q_L(t, -\vec{x}) \neq \pm q_R(t, -\vec{x}),$$

and similarly for q_L. Our goal is to analyze the symmetry of the QCD Lagrangian with respect to independent global transformations of the left- and right-handed fields. There are 16 independent 4×4 matrices, that can be expressed in terms of the unit matrix, the Dirac matrices γ^μ, the chirality matrix γ_5, the products $\gamma^\mu\gamma_5$, and the six matrices $\sigma^{\mu\nu} = i[\gamma^\mu, \gamma^\nu]/2$. In order to decompose the corresponding 16 quadratic forms into their respective projections to right- and left-handed fields, we make use of

$$\bar{q}\Gamma_i q = \begin{cases} \bar{q}_R \Gamma_1 q_R + \bar{q}_L \Gamma_1 q_L & \text{for} \quad \Gamma_1 \in \{\gamma^\mu, \gamma^\mu\gamma_5\} \\ \bar{q}_R \Gamma_2 q_L + \bar{q}_L \Gamma_2 q_R & \text{for} \quad \Gamma_2 \in \{1, \gamma_5, \sigma^{\mu\nu}\} \end{cases}, \tag{D.49}$$

where $\bar{q}_R = \bar{q}P_L$ and $\bar{q}_L = \bar{q}P_R$. We stress that the validity of Eq. (D.49) is general and does not refer to "massless" quark fields.

We now apply Eq. (D.49) to the term containing the contraction of the covariant derivative with γ^μ. This quadratic quark form decouples into the sum of two terms which connect only left-handed with left-handed and right-handed with right-handed quark fields. Thus, the QCD Lagrangian of Eq. D.47 in the so-called chiral limit, in which $m_u = m_d = m_s \to 0$ can then be written as

$$\mathcal{L}^0_{\text{QCD}} = \sum_{l=u,d,s} (\bar{q}_{R,l} i \not{D}\, q_{R,l} + \bar{q}_{L,l} i \not{D}\, q_{L,l}) - \frac{1}{4} \mathcal{G}_{\mu\nu,a} \mathcal{G}^{\mu\nu}_a. \tag{D.50}$$

As one can see from Eq. D.50, in the chiral limit the QCD Lagrangian possesses an $\text{SU}(3)_L \times \text{SU}(3)_R \times \text{U}(1)_V$ symmetry. For this reason, one would expect that hadrons organize themselves into approximately degenerate multiplets fitting the dimensionalities of irreducible representations of the group $\text{SU}(3)_L \times \text{SU}(3)_R \times \text{U}(1)_V$. The $\text{U}(1)_V$ symmetry results in baryon number conservation and leads to a classification of hadrons into mesons ($B = 0$) and baryons ($B = 1$). The linear combinations $Q^a_V = Q^a_R + Q^a_L$ and $Q^a_A = Q^a_R - Q^a_L$ of the left- and right-handed charge operators commute with H^0_{QCD}, have opposite parity, and thus for any state of positive parity one would expect the existence of a degenerate state of negative parity (parity doubling). However,

the low-energy spectrum of baryons does not contain a degenerate baryon octet of negative parity. The non-existence of degenerate multiplets of opposite parity points to the fact that SU(3) instead of $\mathrm{SU}(3)_L \times \mathrm{SU}(3)_R$ is approximately realized as a symmetry of the hadrons. Furthermore the octet of the pseudoscalar mesons is special in the sense that the masses of its members are small in comparison with the corresponding 1^- vector mesons. They are candidates for the Goldstone bosons of a spontaneous symmetry breaking. In order to understand the origin of the SU(3) symmetry let us consider the vector charges $Q_V^a = Q_R^a + Q_L^a$. It was shown by Vafa and Witten [63] that, in the chiral limit, the ground state is necessarily invariant under $\mathrm{SU}(3)_V \times \mathrm{U}(1)_V$, i.e., the eight vector charges Q_V^a as well as the baryon number operator,[5] $Q_V/3$, annihilate the ground state,

$$Q_V^a|0\rangle = Q_V|0\rangle = 0. \tag{D.51}$$

If the vacuum is invariant under $\mathrm{SU}(3)_V \times \mathrm{U}(1)_V$, then so is the Hamiltonian (but not vice versa) (Coleman's theorem [83]). Moreover, the invariance of the ground state *and* the Hamiltonian implies that the physical states of the spectrum of H^0_{QCD} can be organized according to irreducible representations of $\mathrm{SU}(3)_V \times \mathrm{U}(1)_V$. The index V (for vector) indicates that the generators result from integrals of the zeroth component of vector current operators and thus transform with a positive sign under parity. Since the parity doubling is not observed for the low-lying states, one assumes that the Q_A^a do *not* annihilate the ground state,

$$Q_A^a|0\rangle \neq 0, \tag{D.52}$$

i.e., the ground state of QCD is not invariant under "axial" transformations. In that case the ground state is not invariant under the full symmetry group of the Lagrangian resulting in a spontaneous symmetry breaking. According to Goldstone's theorem, to each axial generator Q_A^a, which does not annihilate the ground state, corresponds a massless Goldstone boson field $\phi^a(x)$ with spin 0, whose symmetry properties are tightly connected to the generator in question. The Goldstone bosons have the same transformation behavior under parity,

$$\phi^a(t,\vec{x}) \overset{P}{\mapsto} -\phi^a(t,-\vec{x}), \tag{D.53}$$

i.e., they are pseudoscalars, and transform under the subgroup $H = \mathrm{SU}(3)_V$, which leaves the vacuum invariant, as an octet. $\mathrm{SU}(3)_V$ has 8 generators and so we expect eight Goldstone bosons. In constructing the most general theory describing the dynamics of the Goldstone bosons associated with the spontaneous symmetry breakdown in QCD we must consider that:

[5] Recall that each quark is assigned a baryon number 1/3.

- In the chiral limit, we want the effective Lagrangian to be invariant under $\mathrm{SU}(3)_L \times \mathrm{SU}(3)_R \times \mathrm{U}(1)_V$.

- It should contain exactly eight pseudoscalar degrees of freedom transforming as an octet under the subgroup $H = \mathrm{SU}(3)_V$.

- Taking account of spontaneous symmetry breaking, the ground state should only be invariant under $\mathrm{SU}(3)_V \times \mathrm{U}(1)_V$.

Following the previous discussion we collect the dynamical variables in the $SU_f(3)$ matrix $\Sigma(x) = e^{\frac{i\mathcal{M}}{f}}$, where $\mathcal{M}$ is the traceless 3×3 Hermitian matrix of the Goldstone bosons defined in Eq. 2.42.

To the lowest order in the momenta and in the massless quark limit, the most the most general, chirally invariant, effective Lagrangian density with the minimal number of derivatives reads

$$\mathcal{L}_{kin} = \frac{f_\pi^2}{4} Tr\left[\partial^\mu \Sigma \partial_\mu \Sigma^\dagger\right] \tag{D.54}$$

where the constant $\frac{f_\pi^2}{4}$ has been chosen such as to get a canonical kinetic term, $\frac{1}{2}\partial_\mu\phi_a\partial^\mu\phi_a$, for the mesonic fields, $\phi_a, a = 1, .., 8$, appearing inside the matrix $\mathcal{M}$. In the following we show that this Lagrangian is invariant under *global* $\mathrm{SU}(3)_L \times \mathrm{SU}(3)_R$ transformations:

$$\begin{aligned}
\Sigma(x) &\mapsto R\Sigma(x)L^\dagger, \\
\partial_\mu\Sigma(x) &\mapsto \partial_\mu(R\Sigma(x)L^\dagger) = \underbrace{\partial_\mu R}_{0}\Sigma(x)L^\dagger + R\partial_\mu\Sigma(x)L^\dagger + R\Sigma(x)\underbrace{\partial_\mu L^\dagger}_{0} = R\partial_\mu\Sigma(x)L^\dagger, \\
\Sigma(x)^\dagger &\mapsto L\Sigma(x)^\dagger R^\dagger, \\
\partial_\mu\Sigma(x)^\dagger &\mapsto L\partial_\mu\Sigma(x)^\dagger R^\dagger,
\end{aligned}$$

because

$$\mathcal{L}_{\text{eff}} \mapsto \frac{f_\pi^2}{4}\mathrm{Tr}\Big(R\partial_\mu\Sigma(x)\underbrace{L^\dagger L}_{1}\partial^\mu\Sigma(x)^\dagger R^\dagger\Big) = \frac{f_\pi^2}{4}\mathrm{Tr}\Big(\underbrace{R^\dagger R}_{1}\partial_\mu\Sigma(x)\partial^\mu\Sigma(x)^\dagger\Big) = \mathcal{L}_{\text{eff}},$$

where we made use of the trace property $\mathrm{Tr}(AB) = \mathrm{Tr}(BA)$. The global $\mathrm{U}(1)_V$ invariance is trivially satisfied, because the Goldstone bosons have baryon number zero, thus transforming as $\phi \mapsto \phi$ under $\mathrm{U}(1)_V$.

D.3 Some examples of application

D.3.1 The heavy mesons-light psedudoscalar meson couplings

As an example to show how to work with the effective Lagrangian we calculate the coupling between the heavy mesons and the light pseudoscalar mesons, with quantum numbers $J^P = 0^{-+}$. We observe that a three pseudoscalar vertex, $0^- - 0^- - 0^-$, does not conserve the parity symmetry and so the possible vertexes are the the $0^- - 1^- - 0^-$ and $1^- - 1^- - 0^-$ represented in Fig. D.1 and D.2.

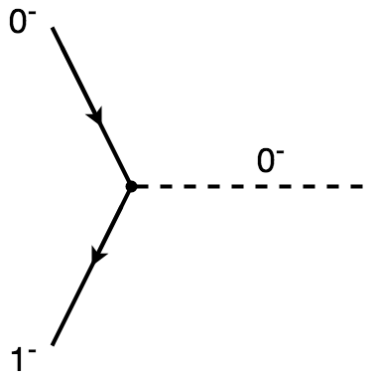

Figure D.1: Feynman diagram for the $0^- - 1^- - 0^-$ vertex. Solid line denotes the heavy mesons, while the dashed line denotes the exchanged light pseudoscalar meson.

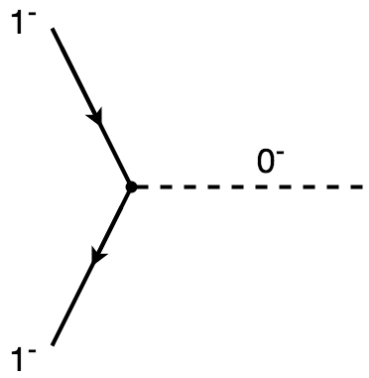

Figure D.2: Feynman diagram for the $1^- - 1^- - 0^-$ vertex. Solid line denotes the heavy mesons, while the dashed line denotes the exchanged light pseudoscalar meson.

From the expression of the heavy meson field, h, given in Eq. 2.39:

$$\bar{h} = \gamma_0 h^\dagger \gamma_0 = \gamma_0 [P^*_\mu \gamma^\mu - P\gamma_5]^\dagger \frac{(1+\not{v})^\dagger}{2}\gamma_0 =$$
$$\gamma_0 [P^{*\dagger}_\mu \gamma_0 \gamma^\mu \gamma_0 - P^\dagger \gamma_5] \frac{(1+\gamma_0\gamma_\alpha\gamma_0 v^\alpha)}{2}\gamma_0 =$$
$$[P^{*\dagger}_\mu \gamma^\mu \gamma_0 - P^\dagger \gamma_0 \gamma_5] \frac{(\gamma_0 + \gamma_0\gamma_\alpha v^\alpha)}{2} =$$
$$[P^{*\dagger}_\mu \gamma^\mu + P^\dagger \gamma_5] \frac{(1+\not{v})}{2}, \tag{D.55}$$

where we have used the properties of the γ matrices (see App. E). The pseudoscalar meson axial current, A_μ, is defined as (Eq. 2.53):

$$A_\mu = \frac{1}{2}\left(\xi^\dagger \partial_\mu \xi - \xi \partial_\mu \xi^\dagger\right) \tag{D.56}$$

with

$$\xi(x) = \sqrt{\Sigma(x)} = e^{\frac{i\mathcal{M}}{2f_\pi}} \tag{D.57}$$

and $\mathcal{M}$ is the traceless 3×3 Hermitian matrix of the Goldstone bosons, defined in Eq. 2.48. On replacing Eq. D.57 into Eq. D.56 we obtain the following expression for the axial current:

$$A_\mu = \frac{1}{2}\left(\xi^\dagger \partial_\mu \xi - \xi \partial_\mu \xi^\dagger\right) = \frac{1}{2}\left(e^{\frac{-i\mathcal{M}^\dagger}{2f_\pi}} \partial_\mu e^{\frac{i\mathcal{M}}{2f_\pi}} - e^{\frac{i\mathcal{M}}{2f_\pi}} \partial_\mu e^{\frac{-i\mathcal{M}^\dagger}{2f_\pi}}\right) =$$
$$\frac{1}{2}\left(e^{\frac{-i\mathcal{M}}{2f_\pi}} \frac{i}{2f_\pi} \partial_\mu \mathcal{M} e^{\frac{i\mathcal{M}}{2f_\pi}} - e^{\frac{i\mathcal{M}}{2f_\pi}} \frac{-i}{2f_\pi} \partial_\mu \mathcal{M}^\dagger e^{\frac{-i\mathcal{M}^\dagger}{2f_\pi}}\right), \tag{D.58}$$

Observe that the matrix of the meson fields $\mathcal{M}$ is hermitian, so the previous expression becomes:

$$A_\mu = \frac{1}{2}\left(e^{\frac{-i\mathcal{M}}{2f_\pi}} \frac{i}{2f_\pi} \partial_\mu \mathcal{M} e^{\frac{i\mathcal{M}}{2f_\pi}} - e^{\frac{i\mathcal{M}}{2f_\pi}} \frac{-i}{2f_\pi} \partial_\mu \mathcal{M} e^{\frac{-i\hat{\pi}}{2f_\pi}}\right) =$$
$$\frac{1}{2}\left(\frac{i}{2f_\pi}\partial_\mu \mathcal{M} + \frac{i}{2f_\pi}\partial_\mu \mathcal{M}\right) = \frac{i}{2f_\pi}\partial_\mu \mathcal{M}. \tag{D.59}$$

From substitution of the expressions of h and $\bar{h}$ fields (Eqs. 2.39, D.55) and of the axial current (Eq. D.59) into the interaction part of Lagrangian of Eq. 2.55 we get:

$$\mathcal{L}_{\text{psHH}} = i g_\pi Tr(h_b \gamma_\mu \gamma_5 A^{\mu_{ba}} \bar{h}_a) =$$
$$i g_\pi Tr\left(\frac{(1+\not{v})}{2}[P^*_{b,\alpha}\gamma^\alpha - P_b\gamma_5]\gamma_\mu\gamma_5 \frac{i}{2f_\pi}\partial^\mu \mathcal{M}_{ba}[P^{*\dagger}_{a,\beta}\gamma^\beta + P^\dagger_a\gamma_5]\frac{(1+\not{v})}{2}\right) =$$
$$i g_\pi Tr\left([P^*_{b,\alpha}\gamma^\alpha - P_b\gamma_5]\gamma_\mu\gamma_5 \frac{i}{2f_\pi}\partial^\mu \mathcal{M}_{ba}[P^{*\dagger}_{a,\beta}\gamma^\beta + P^\dagger_a\gamma_5]\frac{(1+\not{v})}{2}\right). \tag{D.60}$$

In the last step we have used the cyclic property of the trace and the fact that $\frac{1\pm\not{v}}{2}$ is a projection operator and so

$$\left(\frac{1\pm\not{v}}{2}\right)^2 = \frac{1\pm\not{v}}{2}. \tag{D.61}$$

Before proceeding in the calculation of the trace we observe that, in the Feyman diagram of Fig. D.1, only one heavy pseudoscalar meson, $P^\dagger$, and one vector meson, P^*_α, are involved, so by cutting all the fields that do not contribute to the process, we obtain the psPP^* coupling vertex so we write $\mathcal{L}_{\rm psHH} \to \mathcal{L}_{{\rm ps}PP^*}$:

$$\begin{aligned}
&\mathcal{L}_{{\rm ps}PP^*} = -\frac{g_\pi}{2f_\pi} Tr\left((P^*_{b,\alpha}\gamma^\alpha\gamma_\mu\gamma_5\partial^\mu\mathcal{M}_{ba}P^\dagger_a\gamma_5 + \right.\\
&\left.(-P_b\gamma_5\gamma_\mu\gamma_5\partial^\mu\mathcal{M}_{ba}P^{*\dagger}_{a,\beta}\gamma^\beta))\frac{(1+\not{v})}{2}\right) = \\
&-\frac{g_\pi}{2f_\pi} Tr\left((P^*_{b,\alpha}\gamma^\alpha\gamma_\mu\partial^\mu\mathcal{M}_{ba}P^\dagger_a + P_b\gamma_\mu\partial^\mu\mathcal{M}_{ba}P^{*\dagger}_{a,\beta}\gamma^\beta)\frac{(1+\not{v})}{2}\right) = \qquad \text{(D.62)}\\
&-\frac{g_\pi}{2f_\pi} Tr\left((P^*_{b,\alpha}\gamma^\alpha\gamma_\mu\partial^\mu\mathcal{M}_{ba}P^\dagger_a + P_b\gamma_\mu\partial^\mu\mathcal{M}_{ba}P^{*\dagger}_{a,\beta}\gamma^\beta)\frac{1}{2}\right) + \\
&-\frac{g_\pi}{2f_\pi} Tr\left((P^*_{b,\alpha}\gamma^\alpha\gamma_\mu\partial^\mu\mathcal{M}_{ba}P^\dagger_a + P_b\gamma_\mu\partial^\mu\mathcal{M}_{ba}P^{*\dagger}_{a,\beta}\gamma^\beta)\frac{\not{v}}{2}\right) = \\
&-\frac{g_\pi}{2f_\pi} Tr\left((P^*_{b,\alpha}\gamma^\alpha\gamma_\mu\partial^\mu\mathcal{M}_{ba}P^\dagger_a + P_b\gamma_\mu\partial^\mu\mathcal{M}_{ba}P^{*\dagger}_{a,\beta}\gamma^\beta)\frac{1}{2}\right), \qquad \text{(D.63)}
\end{aligned}$$

where we used the fact that the trace of an odd number of γ matrices:

$$< \gamma_\alpha\gamma_\mu\gamma_\beta >= 0, \tag{D.64}$$

Now we replace the trace of two γ matrices

$$Tr\left(\gamma_\alpha\gamma_\mu\right) = 4g_{\alpha\mu}, \tag{D.65}$$

into Eq. D.63:

$$\begin{aligned}
&\mathcal{L}_{{\rm ps}PP^*} = -\frac{g_\pi}{2f_\pi}(P^*_{b,\alpha}\frac{1}{2}4g_{\alpha\mu}\partial^\mu\mathcal{M}_{ba}P^\dagger_a + P_b\partial^\mu\mathcal{M}_{ba}P^{*\dagger}_{a,\beta}\frac{1}{2}4g_{\mu\beta}) = \\
&-\frac{g_\pi}{f_\pi}(P^*_{b,\mu}P^\dagger_a + P_bP^{*\dagger}_{a,\mu})\partial^\mu\mathcal{M}_{ba}. \qquad \text{(D.66)}
\end{aligned}$$

In calculating the vector-vector interaction vertex, corresponding to the Feynman diagram of Fig. D.2, we observe that only the creation and annihilation

operators for the heavy mesons, respectively $P^{*\dagger}$ and P^{*}, give a contribution different from zero:

$$\begin{aligned}
&\mathcal{L}_{\mathrm{ps}P^{*}P^{*}} = ig < [P^{*}_{b,\alpha}\gamma^{\alpha}]\gamma_{\mu}\gamma_{5}\frac{i}{2f_{\pi}}\partial^{\mu}\mathcal{M}_{ba}[P^{*\dagger}_{a,\beta}\gamma^{\beta}]\frac{(1+\gamma_{\delta}v^{\delta})}{2} >= \\
&-\frac{g_{\pi}}{4f_{\pi}} < [P^{*}_{b,\alpha}\gamma^{\alpha}]\gamma_{\mu}\gamma_{5}\partial^{\mu}\mathcal{M}_{ba}[P^{*\dagger}_{a,\beta}\gamma^{\beta}]\gamma_{\delta}v^{\delta}) >= \\
&-\frac{g_{\pi}}{4f_{\pi}}P^{*}_{b,\alpha}\partial^{\mu}\mathcal{M}_{ba}P^{*\dagger}_{a,\beta}v^{\delta}(-4i\epsilon^{\delta\alpha\beta\mu}) >= \\
&\frac{ig_{\pi}}{f_{\pi}}\epsilon^{\delta\alpha\beta\mu}P^{*}_{b,\alpha}P^{*\dagger}_{a,\beta}v^{\delta}\partial^{\mu}\mathcal{M}_{ba},
\end{aligned} \tag{D.67}$$

where we have used:

$$< \gamma_{\alpha}\gamma_{\mu}\gamma_{5}\gamma_{\beta} >= 0, \tag{D.68}$$

$$< \gamma_{\alpha}\gamma_{\mu}\gamma_{5}\gamma_{\beta}\gamma_{\delta} >= -4i\epsilon^{\delta\alpha\beta\mu}. \tag{D.69}$$

The coupling vertices for the heavy mesons, P and P^{*}, with the light pseudoscalar mesons, calculated from the effective Lagrangian of Eq. 2.55, are summarized in Tab. D.1.

Table D.1: Coupling vertexes for the heavy mesons, P and P^{*}, with the light pseudoscalar mesons ps, obtained from the effective Lagrangian of Eq. 2.55. $f_{\pi} = 92.3$ MeV, as according to the convention used in this thesis.

$psPP^{*}$	$-\frac{g_{\pi}}{f_{\pi}}(P^{*}_{b,\mu}P^{\dagger}_{a} + P_{b}P^{*\dagger}_{a,\mu})\partial^{\mu}\mathcal{M}_{ba}$
$psP^{*}P^{*}$	$\frac{ig_{\pi}}{f_{\pi}}\epsilon^{\delta\alpha\beta\mu}v^{\delta}P^{*}_{b,\alpha}P^{*\dagger}_{a,\beta}\partial_{\mu}\mathcal{M}_{ba}$

From the coupling vertices one can easily obtain the transition matrix elements which are necessary, for example, to calculate the decay widths. As an illustrative example, let us calculate the $D^{*+} \to D^{0}\pi^{+}$ decay width. The generic coupling vertex for the heavy mesons, P and P^{*}, with the light pseudoscalar mesons, is (see Tab. D.1), :

$$V_{psPP^{*}} = -\frac{g_{\pi}}{f_{\pi}}(P^{*}_{b,\mu}P^{\dagger}_{a} + P_{b}P^{*\dagger}_{a,\mu})\partial^{\mu}\mathcal{M}_{ba}, \tag{D.70}$$

From Eq. D.70 one finds that the $D^{*+} \to D^0\pi^+$ transition matrix element is

$$\begin{aligned} |M(D^{*+} \to D^0\pi^+)| &= |\langle D^0\pi^+|V_{psPP^*}|D^{*+}\rangle| \\ &= \frac{g_\pi}{f_\pi}\langle D^0\pi^+|(P^*_{b,\mu}P^\dagger_a + P_bP^{*\dagger}_{a,\mu})\partial^\mu\mathcal{M}_{ba}|D^{*+}\rangle, \end{aligned} \tag{D.71}$$

where

$$\mathcal{M} = \sqrt{2}\begin{pmatrix} \frac{\pi^0}{\sqrt{2}} + \frac{\eta}{\sqrt{6}} & \pi^+ & K^+ \\ \pi^- & -\frac{\pi^0}{\sqrt{2}} + \frac{\eta}{\sqrt{6}} & K^0 \\ K^- & \bar{K}^0 & -\frac{2}{\sqrt{6}}\eta \end{pmatrix} \tag{D.72}$$

is the flavour matrix of the Goldstone bosons, and $P^{*\mu}$ and P are annihilation operators satisying

$$\begin{aligned} \langle 0|P|D\rangle &= \sqrt{m_H} \\ \langle 0|P^{*\mu}|D^*\rangle &= \epsilon^\mu\sqrt{m_H} \quad . \end{aligned} \tag{D.73}$$

The initial and final states in Eq. D.71 select the operators which make a non zero contribution to the $D^{*+} \to D^0\pi^+$ transition matrix element. In fact, since $P^{*\mu}$ and P are annihilation operators then $\langle D^0|P_bP^{*\dagger}_{a,\mu}|D^{*+}\rangle = 0$ and so $\langle D^0|(P^*_{b,\mu}P^\dagger_a + P_bP^{*\dagger}_{a,\mu})|D^{*+}\rangle = \langle D^0|P^*_{b,\mu}P^\dagger_a|D^{*+}\rangle$. The expression of $\langle D^0|P^*_{b,\mu}P^\dagger_a|D^{*+}\rangle$ can be evaluated by means of Eq. D.73:

$$\langle D^0|P^*_{b,\mu}P^\dagger_a|D^{*+}\rangle = \epsilon^\mu m_H. \tag{D.74}$$

By substitution of Eq. D.74 into Eq. D.71 one obtains:

$$|M(D^{*+} \to D^0\pi^+)| = \frac{g_\pi}{f_\pi}\epsilon_\mu m_H\partial^\mu\mathcal{M}_{ba} \tag{D.75}$$

where $\partial^\mu\mathcal{M}_{ba} = iq^\mu \times \sqrt{2} = i\sqrt{2}q^\mu$:

$$|M(D^{*+} \to D^0\pi^+)| = \frac{\sqrt{2}g_\pi}{f_\pi}m_H\epsilon_\mu q^\mu \tag{D.76}$$

From Eq. D.75

$$\begin{aligned}\sum_{pol}|M(D^{*+}\to D^0\pi^+)|^2 &= \left(\sqrt{2}\frac{g_\pi}{f_\pi}\epsilon_\mu\right)^2 m_H^2 q^\mu q^\nu \sum_{pol}\epsilon_\mu(v)\epsilon_\nu^*(v)\\ &= 2\frac{g_\pi^2}{f_\pi^2}m_H^2 q^\mu q^\nu\left(g_{\mu\nu}-\frac{v_\mu v_\nu}{v^2}\right)\\ &= 2\frac{g_\pi^2}{f_\pi^2}m_H^2(q^2-(q_\mu v^\mu)^2)\\ &= 2\frac{g_\pi^2}{f_\pi^2}m_H^2(q^2-E_\pi^2) = 2m_H^2\frac{g_\pi^2}{f_\pi^2}|\mathbf{p}_\pi|^2,\end{aligned} \tag{D.77}$$

where the static limit condition, $v_\mu=(1,0,0,0)$, was used. Please observe that, in Eq. D.77, $|\mathbf{p}_\pi|$ is the modulus of the pion 3-momentum in the centre of mass frame, which correspond to the D^* reference frame. The general expression for the two body decay width is given by:

$$\Gamma(D^{*+}\to D^0+\pi^+) = \frac{1}{2m_H}\Phi_2^{LI}\frac{1}{2S_{D^*}+1}\sum_{pol}|M(D^{*+}\to D^0\pi^+)|^2, \tag{D.78}$$

where the matrix element modulus squared is given by Eq. D.77, and the two body Lorentz invariant phase space for the $D^{*+}\to D^0\pi^+$ decay is:

$$\Phi_2^{LI} = \frac{1}{4\pi}\frac{|\mathbf{p}_\pi|}{m_H}, \tag{D.79}$$

After the substitution of Eqs. D.77 and D.79 into Eq. D.78 one obtains the $D^{*+}\to D^0\pi^+$ decay width

$$\Gamma(D^{*+}\to D^0+\pi^+) = \frac{1}{12\pi}\frac{g_\pi^2}{f_\pi^2}|\mathbf{p}_\pi|^3, \tag{D.80}$$

where, as always, $f_\pi = 92.3$ MeV.

Appendix E

Dirac matrices

In mathematical physics, the gamma matrices, $\gamma_0, \gamma_1, \gamma_2, \gamma_3$ also known as the Dirac matrices, are a set of conventional matrices with specific anticommutation relations that ensure they generate a matrix representation of the Clifford algebra. γ^0 is the time-like matrix and the other three are space-like matrices. In the Dirac-Pauli representation, the γ matrices are given by:

$$\gamma^0 = \begin{pmatrix} 1 & 0 \\ 0 & -1 \end{pmatrix}, \gamma^i = \begin{pmatrix} 0 & \sigma_i \\ -\sigma_i & 0 \end{pmatrix}, \tag{E.1}$$

where the Pauli matrices σ_i are defined as:

$$\sigma^1 = \begin{pmatrix} 0 & 1 \\ 1 & 0 \end{pmatrix}, \sigma^2 = \begin{pmatrix} 0 & -i \\ i & 0 \end{pmatrix}, \sigma^3 = \begin{pmatrix} 1 & 0 \\ 0 & -1 \end{pmatrix}, \tag{E.2}$$

The Pauli matrices obey the following commutation and anticommutation relations:

$$\begin{aligned} [\sigma_i, \sigma_j] &= 2\epsilon_{ijk}\sigma_k \\ \{\sigma_i, \sigma_j\} &= 2\delta_{ij}, \end{aligned} \tag{E.3}$$

where ϵ_{ijk} is the Levi-Civita symbol, is the Kronecker delta, and δ_{ij} is the identity matrix. The above two relations are equivalent to:

$$\sigma_i\sigma_j = \delta_{ij}I_2 + i\sum_K \epsilon_{ijk}\sigma_k, \tag{E.4}$$

where I_2 is the identity matrix in two dimensions. Finally, contracting each side of the previous equation with components of two 3-vectors, $\vec{a}$ and $\vec{b}$ (which commutes with the Pauli matrices) one finds a useful relation:

$$(\vec{a}\cdot\vec{\sigma})(\vec{b}\cdot\vec{\sigma}) = (\vec{a}\cdot\vec{b})I_2 + i(\vec{a}\times\vec{b})\cdot\vec{\sigma}. \tag{E.5}$$

The γ matrices defined in Eq. I.1 satisfy the following anticommutation relations:

$$\{\gamma^\mu, \gamma^\nu\} = 2g^{\mu\nu} I_4 \tag{E.6}$$

where $g^{\mu\nu}$ is the Minkowski metric with signature $(+ - --)$ and I_4 is the 4×4 identity matrix. This defining property is more fundamental than the numerical values used in the specific representation of the gamma matrices. Covariant gamma matrices are defined by:

$$\gamma_\nu = g_{\mu\nu}\gamma^\mu \tag{E.7}$$

The Hermitian conjugates and squares of γ matrices are summarized as follows.

$$\begin{aligned} \gamma^{\mu\dagger} &= \gamma^0\gamma^\mu\gamma^0 \\ \gamma^{0\dagger} &= \gamma^0 \\ \gamma^{i\dagger} &= -\gamma^i \\ (\gamma^0)^2 &= I_4 \\ (\gamma^i)^2 &= -I_4 \end{aligned} \tag{E.8}$$

The commutator of γ matrices is often expressed with the tensor $\sigma_{\mu\nu}$ defined as:

$$\sigma_{\mu\nu} = \frac{i}{2}[\gamma_\mu, \gamma_\nu] = i(\gamma_\mu\gamma_\nu - g_{\mu\nu}) \tag{E.9}$$

In Dirac-Pauli representation, γ_5 matrix is written as:

$$\gamma_5 \equiv i\gamma_0\gamma_1\gamma_2\gamma_3 = \begin{pmatrix} 0 & 1 \\ 1 & 0 \end{pmatrix} \tag{E.10}$$

γ^5 has also an alternative form:

$$\gamma_5 = \frac{i}{4!}\epsilon_{\mu\nu\alpha\beta}\gamma^\mu\gamma^\nu\gamma^\alpha\gamma^\beta \tag{E.11}$$

This matrix is useful in discussions of quantum mechanical chirality. For example, a Dirac field can be projected onto its left-handed and right-handed components by:

$$\psi_L = \frac{1-\gamma_5}{2}\psi, \quad \psi_R = \frac{1+\gamma_5}{2}\psi \tag{E.12}$$

It is hermitian:

$$\gamma_5^\dagger = \gamma_5 \tag{E.13}$$

and, in the Dirac-Pauli representation:

$$(\gamma_5)^2 = \begin{pmatrix} 0 & 1 \\ 1 & 0 \end{pmatrix} \begin{pmatrix} 0 & 1 \\ 1 & 0 \end{pmatrix} = \begin{pmatrix} 0 & 1 \\ 1 & 0 \end{pmatrix} = I_4, \tag{E.14}$$

γ_5 anti-commutes with all the γ matrices:

$$\{\gamma_5, \gamma_\mu\} = 0. \tag{E.15}$$

Some traces of γ matrices are given below:

$$\begin{aligned} \text{Tr(odd number of } \gamma\text{'s)} &= 0, \\ \text{Tr}(\gamma_\mu \gamma_\nu) &= 4g_{\mu\nu}, \\ \text{Tr}(\gamma_\mu \gamma_\nu \gamma_\rho \gamma_\sigma)) &= 4(g_{\mu\nu}g_{\rho\sigma} - g_{\mu\rho}g_{\nu\sigma} + g_{\mu\sigma}g_{\nu\rho}) \\ \text{Tr}(\gamma_5) &= 0, \\ \text{Tr}(\gamma_\mu \gamma_\nu \gamma_5) &= 0, \\ \text{Tr}(\gamma_\mu \gamma_\nu \gamma_\rho \gamma_\sigma \gamma_5)) &= -4i\epsilon_{\mu\nu\rho\sigma}. \end{aligned} \tag{E.16}$$

Appendix F

Explicit form of the OPEP

The OPEP is given by the effective Lagrangians in Eqs. (2.76) and (2.81). We use the static approximation where the energy transfer is neglected as compared to the momentum transfer. The OPEP for isospon $I = 1/2$ is obtained by

$$V^{\pi}_{\bar{D}^*\Sigma_c-\bar{D}\Lambda_c}(r) = -\frac{gg_4}{3\sqrt{2}f_\pi^2}\left[\vec{\varepsilon}^{\,\dagger}\cdot\vec{\sigma}C(r) + S_{\varepsilon\sigma}(\hat{r})T(r)\right], \tag{F.1}$$

$$V^{\pi}_{\bar{D}^*\Sigma_c^*-\bar{D}\Lambda_c}(r) = \frac{gg_4}{\sqrt{6}f_\pi^2}\left[\vec{\varepsilon}^{\,\dagger}\cdot\vec{\bar{\Sigma}}C(r) + S_{\varepsilon\bar{\Sigma}}(\hat{r})T(r)\right], \tag{F.2}$$

$$V^{\pi}_{\bar{D}\Sigma_c-\bar{D}^*\Lambda_c}(r) = -\frac{gg_4}{3\sqrt{2}f_\pi^2}\left[\vec{\varepsilon}\cdot\vec{\sigma}C(r) + S_{\varepsilon\sigma}(\hat{r})T(r)\right], \tag{F.3}$$

$$V^{\pi}_{\bar{D}\Sigma_c^*-\bar{D}^*\Lambda_c}(r) = \frac{gg_4}{\sqrt{6}f_\pi^2}\left[\vec{\varepsilon}\cdot\vec{\bar{\Sigma}}C(r) + S_{\varepsilon\bar{\Sigma}}(\hat{r})T(r)\right], \tag{F.4}$$

$$V^{\pi}_{\bar{D}^*\Sigma_c-\bar{D}^*\Lambda_c}(r) = -\frac{gg_4}{3\sqrt{2}f_\pi^2}\left[\vec{S}\cdot\vec{\sigma}C(r) + S_{S\sigma}(\hat{r})T(r)\right], \tag{F.5}$$

$$V^{\pi}_{\bar{D}^*\Sigma_c^*-\bar{D}^*\Lambda_c}(r) = \frac{gg_4}{\sqrt{6}f_\pi^2}\left[\vec{S}\cdot\vec{\bar{\Sigma}}^{\dagger}C(r) + S_{S\bar{\Sigma}}(\hat{r})T(r)\right], \tag{F.6}$$

$$V^{\pi}_{\bar{D}^*\Sigma_c-\bar{D}\Sigma_c}(r) = \frac{gg_1}{3f_\pi^2}\left[\vec{\varepsilon}^{\,\dagger}\cdot\vec{\sigma}C(r) + S_{\varepsilon\sigma}(\hat{r})T(r)\right] \tag{F.7}$$

$$V^{\pi}_{\bar{D}^*\Sigma_c^*-\bar{D}\Sigma_c}(r) = \frac{gg_1}{2\sqrt{3}f_\pi^2}\left[\vec{\varepsilon}^{\,\dagger}\cdot\vec{\bar{\Sigma}}^{\,\dagger}C(r) + S_{\varepsilon\bar{\Sigma}}(\hat{r})T(r)\right], \tag{F.8}$$

$$V^{\pi}_{\bar{D}^*\Sigma_c-\bar{D}\Sigma_c^*}(r) = \frac{gg_1}{2\sqrt{3}f_\pi^2}\left[\vec{\varepsilon}^{\,\dagger}\cdot\vec{\bar{\Sigma}}C(r) + S_{\varepsilon\bar{\Sigma}}(\hat{r})T(r)\right], \tag{F.9}$$

$$V^{\pi}_{\bar{D}^*\Sigma_c^*-\bar{D}\Sigma_c^*}(r) = \frac{gg_1}{3f_\pi^2}\left[\vec{\varepsilon}^{\,\dagger}\cdot\vec{\Sigma}C(r) + S_{\varepsilon\Sigma}(\hat{r})T(r)\right], \tag{F.10}$$

$$V^{\pi}_{\bar{D}^*\Sigma_c-\bar{D}^*\Sigma_c}(r) = -\frac{gg_1}{3f_\pi^2}\left[\vec{S}\cdot\vec{\sigma}C(r) + S_{S\sigma}(\hat{r})T(r)\right], \tag{F.11}$$

$$V^{\pi}_{\bar{D}^*\Sigma_c^*-\bar{D}^*\Sigma_c}(r) = \frac{gg_1}{2\sqrt{3}f_\pi^2}\left[\vec{S}\cdot\vec{\bar{\Sigma}}^{\dagger}C(r) + S_{S\bar{\Sigma}}(\hat{r})T(r)\right], \tag{F.12}$$

$$V^{\pi}_{\bar{D}^*\Sigma_c^*-\bar{D}^*\Sigma_c^*}(r) = \frac{gg_1}{3f_\pi^2}\left[\vec{S}\cdot\vec{\Sigma}C(r) + S_{S\Sigma}(\hat{r})T(r)\right]. \tag{F.13}$$

The tensor operator $S_{\mathcal{O}_{\bar{D}}\mathcal{O}_{Y_c}}(\hat{r})$ is defined by $S_{\mathcal{O}_{\bar{D}}\mathcal{O}_{Y_c}}(\hat{r}) = 3\vec{\mathcal{O}}_{\bar{D}}\cdot\hat{r}\vec{\mathcal{O}}_{Y_c}\cdot\hat{r} - \vec{\mathcal{O}}_{\bar{D}}\cdot\vec{\mathcal{O}}_{Y_c}$ with the spin operators $\mathcal{O}_{\bar{D}} = \varepsilon, S$ for the meson vertex and $\mathcal{O}_{Y_c} = \sigma, \bar{\Sigma}, \Sigma$ for the baryon vertex. The polarization vector is defined by $\vec{\varepsilon}^{\,(\pm)} = (\mp 1/\sqrt{2}, \pm i/\sqrt{2}, 0)$ and $\vec{\varepsilon}^{\,(0)} = (0,0,1)$. The spin-one operator is $\vec{S} = i\vec{\varepsilon}\times\vec{\varepsilon}^{\,\dagger}$, $\vec{\sigma}$ is the Pauli matrices, $\bar{\Sigma}^\mu$ is given by

$$\bar{\Sigma}^\mu = \begin{pmatrix} \vec{\varepsilon}^{\,(+)} & \sqrt{2/3}\vec{\varepsilon}^{\,(0)} & \sqrt{1/3}\vec{\varepsilon}^{\,(-)} & 0 \\ 0 & \sqrt{1/3}\vec{\varepsilon}^{\,(+)} & \sqrt{2/3}\vec{\varepsilon}^{\,(0)} & \vec{\varepsilon}^{\,(-)} \end{pmatrix}^\mu, \tag{F.14}$$

and $\vec{\Sigma}$ is defined by $\vec{\Sigma} = \frac{3}{2}i\vec{\bar{\Sigma}}\times\vec{\bar{\Sigma}}^{\,\dagger}$. The functions $C(r)$ and $T(r)$ are given by

$$C(r) = \int \frac{d^3q}{(2\pi)^3}\frac{m_\pi^2}{\vec{q}^{\,2}+m_\pi^2}e^{i\vec{q}\cdot\vec{r}}F(\Lambda,\vec{q}), \tag{F.15}$$

$$S_{\mathcal{O}}(\hat{r})T(r) = \int \frac{d^3q}{(2\pi)^3}\frac{-\vec{q}^{\,2}}{\vec{q}^{\,2}+m_\pi^2}S_{\mathcal{O}}(\hat{q})e^{i\vec{q}\cdot\vec{r}}F(\Lambda,\vec{q}), \tag{F.16}$$

with the form factor (2.83). We note that the contact term of the central force (F.15) is neglected as discussed in the nucleon-nucleon meson exchange potential [59].

The kinetic terms are give by

$$K_i = -\frac{1}{2\mu_i}\triangle_{L_i} + \Delta m_i, \tag{F.17}$$

of the channel i given in Table 2.5. We define the reduced mass $\mu_i = m_{M_i}m_{B_i}/(m_{M_i}+m_{B_i})$ of the meson $M_i(=\bar{D},\bar{D}^*)$ and baryon $B_i(=\Lambda_c,\Sigma_c,\Sigma_c^*)$, $\triangle_{L_i} = \partial^2/\partial r^2 + (2/r)\partial/\partial r + L_i(L_i+1)/r^2$ with the orbital angular momentum L_i, and $\Delta m_i = (m_{M_i}+m_{B_i}) - (m_{\bar{D}}+m_{\Lambda_c})$.

Appendix G

Computation of spectroscopic factor

The wave function of the hidden-charm five-quark ($5q$) state is written by three light quarks uud and charm and anti-charm quarks $c\bar{c}$ as $|5q\rangle = |u(1)u(2)d(3)c(4)\bar{c}(5)\rangle$ with the particle number assignment. The wave function can also be decomposed into various meson-baron components as

$$|5q\rangle = a\left|(u(1)u(2)c(4))^{\frac{1}{2}}\,(d(3)\bar{c}(5))^{0}\right\rangle + \cdots \equiv a\left|\Sigma_{\rm c}^{++}\bar{D}^{-}\right\rangle + \ldots, \tag{G.1}$$

where a is the definition of the spectroscopic factor [58], and the superscript is the total spin of three quarks or quark-antiquark. Assuming that $\left|(u(1)u(2)c(4))^{\frac{1}{2}}\,(d(3)\bar{c}(5))^{0}\right\rangle$ is exactly the same as the hadronic wave function of $\Sigma_{\rm c}^{++}\bar{D}^{-}$, the spectroscopic factor for the $\Sigma_{\rm c}^{++}\bar{D}^{-}$ channel is obtained by the overlap

$$a = \left\langle \Sigma_{\rm c}^{++}\bar{D}^{-}\,\middle|\,5q\right\rangle. \tag{G.2}$$

In this Appendix, we will focus on the color-flavor-spin wave function of the $5q$ states, in which the uud ($3q$) system and the $c\bar{c}$ system are both in the color octet, and the total color wave function is in the color-singlet[1]. Moreover, the light quarks are assumed to be the $S-$wave state, that is, the orbital wave function is totally symmetric. Since the total wave function of the three light

[1]The case that the uud system and the $c\bar{c}$ system are both in the color singlet corresponds to the $J/\psi p$ system.

quarks must be antisymmetric, it is represented in Young tableaux as

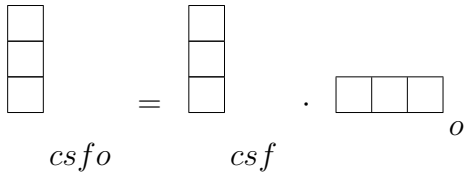

(G.3)

where the subscripts c, s, f, and o denote color, spin, flavor, and orbital wave functions, respectively. The center dot "$\cdot$" denotes the inner product of wave functions in different functional space.

The csf wave function is decomposed into color and spin-flavor parts. In the Young tableaux with the particle number assignment, one obtains (see, e.g., Ref. [64])

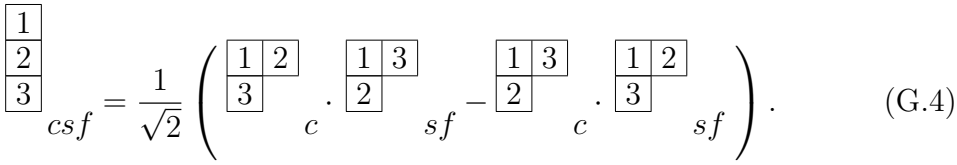

(G.4)

In Eq. (G.4), the color wave functions in the first and second terms have different types of symmetry for exchanges,

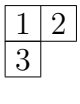

(G.5)

and

(G.6)

where c means that the permutations [21]1 and [21]2 are performed in the color space. The difference between (G.5) and (G.6) lies in the permutation symmetry for exchange: in Eq. (G.5), particles 1 and 2 are symmetric for exchange, while particle 1 and 2 are antisymmetric in Eq. (G.6). The wave function of the $5q$ state is given by the direct product between the $3q$ and $c\bar{c}$ wave functions. For this reason, the color part of the total $5q$ state wave function also contains these two permutation symmetries, the $([21]1)_c$ and the $([21]2)_c$, and so in the calculations of the spectroscopic factors, both permutations will be considered.

Since the spin of the $c\bar{c}$ pair can be $S_{c\bar{c}} = 0$ or 1, there are two $5q$ state wave functions denoted with $|5q, \mathbf{S_{c\bar{c}}} = \mathbf{0}\rangle$ and $|5q, \mathbf{S_{c\bar{c}}} = \mathbf{1}\rangle$. In the case of $S_{c\bar{c}} = 0$, the $c\bar{c}$ wave function $\psi^{s=0}_{c\bar{c}}$ is

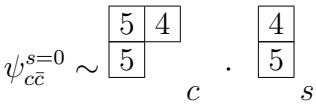

(G.7)

and the $5q$ state wave function $|5q, \mathbf{S_{c\bar{c}}} = \mathbf{0}\rangle$ is given by

$$|5q, \mathbf{S_{c\bar{c}}} = \mathbf{0}\rangle \sim \frac{1}{\sqrt{2}} \left(\begin{array}{|c|c|}\hline 1 & 2 \\ \hline 3 \\ \cline{1-1} \end{array}_{\,c} \cdot \begin{array}{|c|c|}\hline 1 & 3 \\ \hline 2 \\ \cline{1-1} \end{array}_{\,sf} - \begin{array}{|c|c|}\hline 1 & 3 \\ \hline 2 \\ \cline{1-1} \end{array}_{\,c} \cdot \begin{array}{|c|c|}\hline 1 & 2 \\ \hline 3 \\ \cline{1-1} \end{array}_{\,sf} \right) \cdot \left(\begin{array}{|c|c|}\hline 5 & 4 \\ \hline 5 \\ \cline{1-1} \end{array}_{\,c} \cdot \begin{array}{|c|}\hline 4 \\ \hline 5 \\ \cline{1-1} \end{array}_{\,s} \right). \tag{G.8}$$

Similarly, the $c\bar{c}$ wave function with spin-triplet, $\psi_{c\bar{c}}^{s=1}$, and the $5q$ state wave function, $|5q, \mathbf{S_{c\bar{c}}} = \mathbf{1}\rangle$, are written by

$$\psi_{c\bar{c}}^{s=1} \sim \begin{array}{|c|c|}\hline 5 & 4 \\ \hline 5 \\ \cline{1-1} \end{array}_{\,c} \cdot \begin{array}{|c|c|}\hline 4 & 5 \\ \hline \end{array}_{\,s}, \tag{G.9}$$

and

$$|5q, \mathbf{S_{c\bar{c}}} = \mathbf{1}\rangle \sim \frac{1}{\sqrt{2}} \left(\begin{array}{|c|c|}\hline 1 & 2 \\ \hline 3 \\ \cline{1-1} \end{array}_{\,c} \cdot \begin{array}{|c|c|}\hline 1 & 3 \\ \hline 2 \\ \cline{1-1} \end{array}_{\,sf} - \begin{array}{|c|c|}\hline 1 & 3 \\ \hline 2 \\ \cline{1-1} \end{array}_{\,c} \cdot \begin{array}{|c|c|}\hline 1 & 2 \\ \hline 3 \\ \cline{1-1} \end{array}_{\,sf} \right) \otimes \left(\begin{array}{|c|c|}\hline 5 & 4 \\ \hline 5 \\ \cline{1-1} \end{array}_{\,c} \cdot \begin{array}{|c|c|}\hline 4 & 5 \\ \hline \end{array}_{\,s} \right). \tag{G.10}$$

First, let us focus on the term with permutation $([21]1)_c$. The part of the $5q$ state wave function which contains the permutation $([21]1)_c$ is

$$\frac{1}{\sqrt{2}} \left(\begin{array}{|c|c|}\hline 1 & 2 \\ \hline 3 \\ \cline{1-1} \end{array}_{\,c} \cdot \begin{array}{|c|c|}\hline 1 & 3 \\ \hline 2 \\ \cline{1-1} \end{array}_{\,sf} \right) \cdot \left(\begin{array}{|c|c|}\hline 5 & 4 \\ \hline 5 \\ \cline{1-1} \end{array}_{\,c} \cdot (S_{c\bar{c}}) \right), \tag{G.11}$$

where the $c\bar{c}$ spin part $(S_{c\bar{c}})$ is $\begin{array}{|c|}\hline 4 \\ \hline 5 \\ \cline{1-1} \end{array}_{\,s}$ or $\begin{array}{|c|c|}\hline 4 & 5 \\ \hline \end{array}_{\,s}$. The spin-flavor wave function of the three light quark part in Eq. (G.11) can be decomposed into

$$\begin{array}{|c|c|}\hline & \\ \hline \\ \cline{1-1} \end{array}_{\,sf} = \begin{array}{|c|c|c|}\hline & & \\ \hline \end{array}_{\,f} \cdot \begin{array}{|c|c|}\hline & \\ \hline \\ \cline{1-1} \end{array}_{\,s} + \begin{array}{|c|c|}\hline & \\ \hline \\ \cline{1-1} \end{array}_{\,f} \cdot \begin{array}{|c|c|c|}\hline & & \\ \hline \end{array}_{\,s} + \begin{array}{|c|c|}\hline & \\ \hline \\ \cline{1-1} \end{array}_{\,f} \cdot \begin{array}{|c|c|}\hline & \\ \hline \\ \cline{1-1} \end{array}_{\,s} + \begin{array}{|c|}\hline \\ \hline \\ \hline \\ \cline{1-1} \end{array}_{\,f} \cdot \begin{array}{|c|c|}\hline & \\ \hline \\ \cline{1-1} \end{array}_{\,s}. \tag{G.12}$$

Assuming that the $3q$ state belongs to the flavor octet $[21]_8$, there are two possible spin wave functions, $[21]_s$ and $[3]_s$, from Eq. (G.12). In the Young tableaux with particle assignment, Eq. (G.12) can be expressed as

$$\begin{array}{|c|c|}\hline 1&3\\\hline 2\\\cline{1-1}\end{array}_{sf} = -\frac{1}{\sqrt{2}}\left(\begin{array}{|c|c|}\hline 1&2\\\hline 3\\\cline{1-1}\end{array}_{f}\cdot\begin{array}{|c|c|}\hline 1&3\\\hline 2\\\cline{1-1}\end{array}_{s}+\begin{array}{|c|c|}\hline 1&3\\\hline 2\\\cline{1-1}\end{array}_{f}\cdot\begin{array}{|c|c|}\hline 1&2\\\hline 3\\\cline{1-1}\end{array}_{s}\right), \tag{G.13}$$

for the three light quark with spin $\frac{1}{2}$, and

$$\begin{array}{|c|c|}\hline 1&3\\\hline 2\\\cline{1-1}\end{array}_{sf} = \begin{array}{|c|c|}\hline 1&3\\\hline 2\\\cline{1-1}\end{array}_{f}\cdot\begin{array}{|c|c|c|}\hline 1&2&3\\\hline\end{array}_{s}, \tag{G.14}$$

for the three light quark with spin $\frac{3}{2}$.

Finally, the $5q$ state wave function is obtained by combining the $3q$ and $c\bar{c}$ wave functions. Since there are different spin configurations for $3q$ and $c\bar{c}$, namely $S_{3q}=\frac{1}{2}$ or $\frac{3}{2}$, and $S_{c\bar{c}}=0$ or 1, there are several allowed configurations.

1. $(S_{c\bar{c}}, S_{3q}) = (0, \frac{1}{2})$ for $S_{tot}=\frac{1}{2}$

By the substitution of Eq. (G.13) into Eq. (G.11), we get

$$\begin{aligned}|5q\,([21]1,1)\rangle &= \frac{1}{\sqrt{2}}\left[\begin{array}{|c|c|}\hline 1&2\\\hline 3\\\cline{1-1}\end{array}_{c}\cdot\left(-\frac{1}{\sqrt{2}}\left(\begin{array}{|c|c|}\hline 1&2\\\hline 3\\\cline{1-1}\end{array}_{f}\cdot\begin{array}{|c|c|}\hline 1&3\\\hline 2\\\cline{1-1}\end{array}_{s}+\begin{array}{|c|c|}\hline 1&3\\\hline 2\\\cline{1-1}\end{array}_{f}\cdot\begin{array}{|c|c|}\hline 1&2\\\hline 3\\\cline{1-1}\end{array}_{s}\right)\right)\right]\\ &\quad\cdot\left(\begin{array}{|c|c|}\hline 5&4\\\hline 5\\\cline{1-1}\end{array}_{c}\cdot\begin{array}{|c|}\hline 4\\\hline 5\\\cline{1-1}\end{array}_{s}\right)\\ &= -\frac{1}{2}\left[\begin{array}{|c|c|}\hline 1&2\\\hline 3&5\\\hline 4&5\\\cline{1-2}\end{array}_{c}\cdot\left(\begin{array}{|c|c|}\hline 1&2\\\hline 3\\\cline{1-1}\end{array}_{f}\cdot\begin{array}{|c|c|}\hline 1&3\\\hline 2\\\cline{1-1}\end{array}_{s}+\begin{array}{|c|c|}\hline 1&3\\\hline 2\\\cline{1-1}\end{array}_{f}\cdot\begin{array}{|c|c|}\hline 1&2\\\hline 3\\\cline{1-1}\end{array}_{s}\right)\right]\\ &\quad\cdot\left(\begin{array}{|c|}\hline 4\\\hline 5\\\cline{1-1}\end{array}_{s}\right).\end{aligned} \tag{G.15}$$

Herein, S_{tot} is the total spin of the $5q$ state with the quark configuration $(S_{c\bar{c}}, S_{3q})$. We also introduce the notation $|5q\,([21]m,n)\rangle$ to identify the $5q$ state wave function which comes from the color part $m=1,2$ while $n=1,2,3,4$ is the index of the channels, $(S_{c\bar{c}}, S_{3q}) = (0,\frac{1}{2})$, $(0,\frac{3}{2})$, $(1,\frac{1}{2})$ and $(1,\frac{3}{2})$, respectively.

2. $(S_{c\bar{c}}, S_{3q}) = (1, \frac{1}{2})$ for $S_{tot} = \frac{1}{2}$ or $\frac{3}{2}$

In a similar to Eq. (G.15), we get

$$|5q\,(c,[21]1,2)\rangle \;=\; -\frac{1}{2}\left[\begin{array}{|c|c|}\hline 1&2\\\hline 3&5\\\hline 4&5\\\hline\end{array}\;{}_{c}\;\cdot\;\left(\begin{array}{|c|c|}\hline 1&2\\\hline 3\\\cline{1-1}\end{array}\;{}_{f}\;\cdot\;\begin{array}{|c|c|}\hline 1&3\\\hline 2\\\cline{1-1}\end{array}\;{}_{s}+\begin{array}{|c|c|}\hline 1&3\\\hline 2\\\cline{1-1}\end{array}\;{}_{f}\;\cdot\;\begin{array}{|c|c|}\hline 1&2\\\hline 3\\\cline{1-1}\end{array}\;{}_{s}\right)\right]$$
$$\cdot\;\left(\;\begin{array}{|c|c|}\hline 4&5\\\hline\end{array}\;{}_{s}\;\right). \tag{G.16}$$

3. $(S_{c\bar{c}}, S_{3q}) = (0, \frac{3}{2})$ for $S_{tot} = \frac{3}{2}$

By the substitution of Eq. (G.14) into Eq. (G.11), we get

$$|5q\,([21]1,3)\rangle = \frac{1}{\sqrt{2}}\left[\begin{array}{|c|c|}\hline 1&2\\\hline 3&5\\\hline 4&5\\\hline\end{array}\;{}_{c}\;\cdot\;\left(\begin{array}{|c|c|}\hline 1&3\\\hline 2\\\cline{1-1}\end{array}\;{}_{f}\;\cdot\;\begin{array}{|c|c|c|}\hline 1&2&3\\\hline\end{array}\;{}_{s}\right)\right]\;\cdot\;\left(\;\begin{array}{|c|}\hline 4\\\hline 5\\\hline\end{array}\;{}_{s}\;\right). \tag{G.17}$$

4. $(S_{c\bar{c}}, S_{3q}) = (1, \frac{3}{2})$ for $S_{tot} = \frac{1}{2}$, $\frac{3}{2}$, or $\frac{5}{2}$

In a similar way to Eq. (G.17), we get

$$|5q\,([21]1,4)\rangle = \frac{1}{\sqrt{2}}\left[\begin{array}{|c|c|}\hline 1&2\\\hline 3&5\\\hline 4&5\\\hline\end{array}\;{}_{c}\;\cdot\;\left(\begin{array}{|c|c|}\hline 1&3\\\hline 2\\\cline{1-1}\end{array}\;{}_{f}\;\cdot\;\begin{array}{|c|c|c|}\hline 1&2&3\\\hline\end{array}\;{}_{s}\right)\right]\;\cdot\;\left(\;\begin{array}{|c|c|}\hline 4&5\\\hline\end{array}\;{}_{s}\;\right). \tag{G.18}$$

The spin part needs one more step. For instance, in the case number 3 for $|5q\,([21]1,3)\rangle$, the spin wave function has the coupling structure with $S_{123} = S_{3q} = \frac{3}{2}$ and $S_{45} = S_{c\bar{c}} = 0$ as

$$[(S_{13}\otimes S_2)^{S_{123}}\otimes(S_4\otimes S_5)^{S_{45}}]^{S_{tot}} = \left[\left(1\otimes\frac{1}{2}\right)^{\frac{3}{2}}\otimes\left(\frac{1}{2}\otimes\frac{1}{2}\right)^{0}\right]^{\frac{3}{2}}, \tag{G.19}$$

which is recoupled for the channel of the $\Sigma_c^{(*)}$ baryon and the $\bar{D}^{(*)}$ meson by the spin rearrangement

$$\left[\left(1\otimes\frac{1}{2}\right)^{\frac{3}{2}}\otimes\left(\frac{1}{2}\otimes\frac{1}{2}\right)^{0}\right]^{\frac{3}{2}}=\sum_{s_{134},s_{25}}C_{s_{134},s_{25}}\left[\left(1\otimes\frac{1}{2}\right)^{S_{134}}\otimes\left(\frac{1}{2}\otimes\frac{1}{2}\right)^{S_{25}}\right]^{\frac{3}{2}}, \tag{G.20}$$

where

$$C_{\frac{1}{2},1}=-\frac{1}{\sqrt{3}},\qquad C_{\frac{3}{2},0}=\frac{1}{2},\qquad C_{\frac{3}{2},1}=\frac{1}{2}\sqrt{\frac{5}{3}}. \tag{G.21}$$

Here, the coefficients $C_{\frac{1}{2},1}$, $C_{\frac{2}{2},0}$ and $C_{\frac{3}{2},1}$ are the amplitude for the spin components $(S_{134},S_{25})=(\frac{1}{2},1)$, $(\frac{3}{2},0)$, and $(\frac{3}{2},1)$, respectively, which correspond to the $\Sigma_c\bar{D}^*$, $\Sigma_c^*\bar{D}$, and $\Sigma_c^*\bar{D}^*$ baryon-meson channel, respectively. From Eq. (G.17), one finds the amplitude of the each baryon-meson components in $|5q\,([21]1,3)\rangle$,

$$|5q\,([21]1,3)\rangle=-\frac{1}{\sqrt{6}}\left|\Sigma_c\bar{D}^*\right\rangle+\frac{1}{2\sqrt{2}}\left|\Sigma_c^*\bar{D}\right\rangle+\frac{1}{2}\sqrt{\frac{5}{6}}\left|\Sigma_c^*\bar{D}^*\right\rangle+\ldots \tag{G.22}$$

From Eqs. (G.2) and (G.22), the spectroscopic factor is obtained.

In a way similar to the permutation $([21]1)_c$, the wave function for $([21]2)_c$ can be obtained. The part of the $5q$ state wave function which contains the permutation $([21]2)_c$ is

$$-\frac{1}{\sqrt{2}}\left(\begin{array}{|c|c|}\hline 1&3\\\hline 2\\\cline{1-1}\end{array}\;{}_c\;\cdot\;\begin{array}{|c|c|}\hline 1&2\\\hline 3\\\cline{1-1}\end{array}\;{}_{sf}\right)\cdot\left(\begin{array}{|c|c|}\hline 5&4\\\hline 5\\\cline{1-1}\end{array}\;{}_c\;\cdot\;\begin{array}{|c|}\hline 4\\\hline 5\\\cline{1-1}\end{array}\;{}_s\right), \tag{G.23}$$

for the $c\bar{c}$ pair in the singlet state and

$$-\frac{1}{\sqrt{2}}\left(\begin{array}{|c|c|}\hline 1&3\\\hline 2\\\cline{1-1}\end{array}\;{}_c\;\cdot\;\begin{array}{|c|c|}\hline 1&2\\\hline 3\\\cline{1-1}\end{array}\;{}_{sf}\right)\cdot\left(\begin{array}{|c|c|}\hline 5&4\\\hline 5\\\cline{1-1}\end{array}\;{}_c\;\cdot\;\begin{array}{|c|c|}\hline 4&5\\\hline\end{array}\;{}_s\right), \tag{G.24}$$

for the $c\bar{c}$ pair in the triplet state. In the Young tableaux with particle assignment, the spin-flavor decomposition of Eq. (G.12) can be expressed as

$$\begin{array}{|c|c|}\hline 1&2\\\hline 3\\\cline{1-1}\end{array}\;{}_{sf}=\frac{1}{\sqrt{2}}\left(\begin{array}{|c|c|}\hline 1&2\\\hline 3\\\cline{1-1}\end{array}\;{}_f\;\cdot\;\begin{array}{|c|c|}\hline 1&2\\\hline 3\\\cline{1-1}\end{array}\;{}_s-\begin{array}{|c|c|}\hline 1&3\\\hline 2\\\cline{1-1}\end{array}\;{}_f\;\cdot\;\begin{array}{|c|c|}\hline 1&3\\\hline 2\\\cline{1-1}\end{array}\;{}_s\right), \tag{G.25}$$

for the three light quark with spin $\frac{1}{2}$ and

$$\begin{array}{|c|c|}\hline 1&2\\\hline 3\\\cline{1-1}\end{array}\;{}_{sf}=\begin{array}{|c|c|}\hline 1&2\\\hline 3\\\cline{1-1}\end{array}\;{}_f\;\cdot\;\begin{array}{|c|c|c|}\hline 1&2&3\\\hline\end{array}\;{}_s, \tag{G.26}$$

for the three light quark with spin $\frac{3}{2}$. As in the case of the color permutation [21]1, from the combination of the $3q$ and $c\bar{c}$ wave functions, several allowed configurations have to be considered.

1. $(S_{c\bar{c}}, S_{3q}) = (0, \frac{1}{2})$ for $S_{tot} = \frac{1}{2}$

By the substitution of Eq. (G.25) into Eq. (G.23) we get

$$|5q\,([21]2,1)\rangle = -\frac{1}{2}\left[\begin{array}{|c|c|}\hline 1&3\\\hline 2&5\\\hline 4&5\\\hline\end{array}_{\,c}\cdot\left(\begin{array}{|c|c|}\hline 1&2\\\hline 3\\\cline{1-1}\end{array}_{\,f}\cdot\begin{array}{|c|c|}\hline 1&2\\\hline 3\\\cline{1-1}\end{array}_{\,s}-\begin{array}{|c|c|}\hline 1&3\\\hline 2\\\cline{1-1}\end{array}_{\,f}\cdot\begin{array}{|c|c|}\hline 1&3\\\hline 2\\\cline{1-1}\end{array}_{\,s}\right)\right]\cdot\left(\begin{array}{|c|}\hline 4\\\hline 5\\\cline{1-1}\end{array}_{\,s}\right). \tag{G.27}$$

2. $(S_{c\bar{c}}, S_{3q}) = (1, \frac{1}{2})$ for $S_{tot} = \frac{1}{2}$ or $S_{tot} = \frac{3}{2}$

By the substitution of Eq. (G.25) into Eq. (G.24) we get

$$|5q\,([21]2,2)\rangle = -\frac{1}{2}\left[\begin{array}{|c|c|}\hline 1&3\\\hline 2&5\\\hline 4&5\\\hline\end{array}_{\,c}\cdot\left(\begin{array}{|c|c|}\hline 1&2\\\hline 3\\\cline{1-1}\end{array}_{\,f}\cdot\begin{array}{|c|c|}\hline 1&2\\\hline 3\\\cline{1-1}\end{array}_{\,s}-\begin{array}{|c|c|}\hline 1&3\\\hline 2\\\cline{1-1}\end{array}_{\,f}\cdot\begin{array}{|c|c|}\hline 1&3\\\hline 2\\\cline{1-1}\end{array}_{\,s}\right)\right]\cdot\left(\begin{array}{|c|c|}\hline 4&5\\\hline\end{array}_{\,s}\right). \tag{G.28}$$

3. $(S_{c\bar{c}}, S_{3q}) = (0, \frac{3}{2})$ for $S_{tot} = \frac{3}{2}$

By the substitution of Eq. (G.26) into Eq. (G.23) we get

$$|5q\,([21]2,3)\rangle = -\frac{1}{\sqrt{2}}\left[\begin{array}{|c|c|}\hline 1&3\\\hline 2&5\\\hline 4&5\\\hline\end{array}_{\,c}\cdot\left(\begin{array}{|c|c|}\hline 1&2\\\hline 3\\\cline{1-1}\end{array}_{\,f}\cdot\begin{array}{|c|c|c|}\hline 1&2&3\\\hline\end{array}_{\,s}\right)\right]\cdot\left(\begin{array}{|c|}\hline 4\\\hline 5\\\cline{1-1}\end{array}_{\,s}\right). \tag{G.29}$$

4. $(S_{c\bar{c}}, S_{3q}) = (1, \frac{3}{2})$ for $S_{tot} = \frac{1}{2}, \frac{3}{2}$, or $\frac{5}{2}$

By the substitution of Eq. (G.26) into Eq. (G.24) we get

$$|5q\,([21]2,4)\rangle = -\frac{1}{\sqrt{2}}\left[\begin{array}{|c|c|}\hline 1&3\\\hline 2&5\\\hline 4&5\\\hline\end{array}_{\,c}\;\cdot\;\left(\begin{array}{|c|c|}\hline 1&3\\\hline 2\\\cline{1-1}\end{array}_{\,f}\;\cdot\;\begin{array}{|c|c|c|}\hline 1&2&3\\\hline\end{array}_{\,s}\right)\right]\cdot\left(\begin{array}{|c|c|}\hline 4&5\\\hline\end{array}_{\,s}\right). \tag{G.30}$$

Appendix H

Comparison between three-quark and quark-diquark systems

H.0.1 Quark-diquark in the two body formalism

The three-dimensional harmonic oscillator Hamiltonian, $H_{h.o}$, for a quark-diquark system is given by the kinetic energy of the diquark and the heavy quark and by their mutual interaction:

$$H_{h.o.} = m_D + m_Q + \frac{\mathbf{p}_D^2}{2m_D} + \frac{\mathbf{p}_Q^2}{2m_Q} + \frac{1}{2}K|\mathbf{r}_D - \mathbf{r}_Q|^2 \tag{H.1}$$

We can make the transformation from $(\mathbf{r}_D, \mathbf{r}_Q)$ to $(\mathbf{R}_{cm}, \mathbf{r})$ where the centre of mass position $\mathbf{R}_{cm}$ describes the average position of the two particles (i.e. the position of the total system), and $\mathbf{r}$ describes the relative position of one particle with respect to the other:

$$\left\{ \begin{array}{c} \mathbf{R}_{cm} = \frac{m_D\mathbf{r}_D + m_Q\mathbf{r}_Q}{m_Q + m_D} \\ \mathbf{r} = \mathbf{r}_D - \mathbf{r}_Q \end{array} \right. \rightarrow \left\{ \begin{array}{l} \mathbf{r}_D = \mathbf{R}_{cm} + \frac{m_Q}{m_D + m_Q}\mathbf{r} \\ \mathbf{r}_Q = \mathbf{R}_{cm} - \frac{m_D}{m_D + m_Q}\mathbf{r} \end{array} \right. \tag{H.2}$$

Also, we can define the center of mass momentum and relative momentum (and velocity):

$$\left\{ \begin{array}{l} \mathbf{P}_{cm} = \mathbf{p}_D + \mathbf{p}_Q \\ \mathbf{p}_r = \frac{m_Q\mathbf{p}_D - m_D\mathbf{p}_Q}{m_Q + m_D} \end{array} \right. \rightarrow \left\{ \begin{array}{l} \mathbf{p}_D = \frac{m_D}{m_D + m_Q}\mathbf{P}_{cm} + \mathbf{P}_r \\ \mathbf{p}_Q = \frac{m_Q}{m_D + m_Q}\mathbf{P}_{cm} - \mathbf{P}_r \end{array} \right. \tag{H.3}$$

Observe that, in the centre of mass system $\mathbf{P}_{cm}$ and so $|\mathbf{p}_r| = |\mathbf{P}_D| = |\mathbf{P}_Q|$ so $|\mathbf{p}_r|$ is the momentum modulus of the two particles in the center of mass

system. By means of the coordinate transformations H.2 and H.3 the h.o. Hamiltonian becomes:

$$H_{h.o.} = m_D + m_Q + \frac{\mathbf{p}_{cm}^2}{2M} + \frac{\mathbf{p}_r^2}{2\mu} + \frac{1}{2}K|\mathbf{r}|^2 \tag{H.4}$$

where $M = m_D + m_Q$ and $\mu = \frac{m_D m_Q}{m_D + m_Q}$ are the total the reduced mass, respectively.

H.0.2 Quark-diquark as the two-body limit of three-body problem

The three-dimensional harmonic oscillator Hamiltonian, $H_{h.o}$, for a thre-quark system of which quarks 1 and 2 have the same mass, m_s, and quark three has mass m_Q (this is the case of interest for us):

$$H_{\text{h.o.}} = 2m_s + m_Q + \frac{\mathbf{p}_1^2}{2m_s} + \frac{\mathbf{p}_2^2}{2m_s} + \frac{\mathbf{p}_3^2}{2m_Q} + \frac{1}{2}K|\mathbf{r}_1 - \mathbf{r}_2|^2 + \frac{1}{2}K|\mathbf{r}_1 - \mathbf{r}_3|^2 + \frac{1}{2}K|\mathbf{r}_2 - \mathbf{r}_3|^2; \tag{H.5}$$

after defining the Jacobi coordinates

$$\begin{cases} \mathbf{R}_{cm} = \frac{m_s\mathbf{r}_1 + m_s\mathbf{r}_2 + m_Q\mathbf{r}_3}{2m_s + m_Q} \\ \boldsymbol{\rho} = \frac{1}{\sqrt{2}}(\mathbf{r}_1 - \mathbf{r}_2) \\ \boldsymbol{\lambda} = \frac{1}{\sqrt{6}}(\mathbf{r}_1 + \mathbf{r}_2 - 2\mathbf{r}_3) \end{cases} \rightarrow \begin{cases} \boldsymbol{r}_1 = \boldsymbol{R} + \frac{1}{\sqrt{2}}\boldsymbol{\rho} + \frac{\sqrt{3/2}m_Q}{2m_s + m_Q}\boldsymbol{\lambda} \\ \boldsymbol{r}_2 = \boldsymbol{R} - \frac{1}{\sqrt{2}}\boldsymbol{\rho} + \frac{\sqrt{3/2}m_Q}{2m_s + m_Q}\boldsymbol{\lambda} \\ \boldsymbol{r}_3 = \boldsymbol{R} - \frac{\sqrt{6}m}{2m_s + m_Q}\boldsymbol{\lambda} \end{cases} \tag{H.6}$$

and the conjugate momenta:

$$\begin{cases} \mathbf{P}_{cm} = (2m_s + m_Q)\frac{d\mathbf{R}_{cm}}{dt} \\ \mathbf{p}_\rho = m_\rho \frac{d\boldsymbol{\rho}}{dt} \\ \mathbf{p}_\lambda = m_\lambda \frac{d\boldsymbol{\lambda}}{dt} \end{cases} \tag{H.7}$$

with $m_\rho = m_s$ and $m_\lambda = \frac{3m_s m_Q}{2m_s + m_Q}$, the h.o. Hamiltonian of Eq. H.5 becomes:

$$H_{\text{h.o.}} = 2m_s + m_Q + \frac{\mathbf{P}_{cm}^2}{2(2m_s + m_Q)} + \frac{\mathbf{p}_\rho^2}{2m_\rho} + \frac{\mathbf{p}_\lambda^2}{2m_\lambda} + \frac{3}{2}K\boldsymbol{\rho}^2 + \frac{3}{2}K\boldsymbol{\lambda}^2 \tag{H.8}$$

In we freeze now the ρ coordinate, that is we consider the quark-diquark limit of the three-quark structure, Eq. H.8 becomes:

$$H_{h.o.} = m_D + m_Q + \frac{\mathbf{P}_{cm}^2}{2(2m_s + m_Q)} + \frac{\mathbf{p}_\lambda^2}{2m_\lambda} + \frac{3}{2}K\boldsymbol{\lambda}^2 \tag{H.9}$$

In the following we show that the the h.o. of Eq. H.9 and that of H.4 are equal:

$$\frac{\mathbf{p}_r^2}{2\mu} + \frac{1}{2}K|\mathbf{r}|^2 = \frac{\mathbf{p}_\lambda^2}{2m_\lambda} + \frac{3}{2}K\boldsymbol{\lambda}^2 \tag{H.10}$$

When we freeze the ρ coordinate, in fact, we recover the expression of the well known two-body h.o. Hamiltonian in the quark-diquark centre of mass frame, $H_{ho} = 2m_D + m_Q + \frac{p_r^2}{2\mu} + \frac{1}{2}\mu\omega_\lambda^2\mathbf{r}^2$, as $\frac{p_\lambda^2}{2m_\lambda} = \frac{p_r^2}{2\mu}$ and $\frac{1}{2}m_\lambda\omega_\lambda^2\boldsymbol{\lambda}^2 = \frac{1}{2}\mu\omega_\lambda^2\mathbf{r}^2$, where $\mu = \frac{m_D m_Q}{m_D+m_Q}$ is the reduced mass, $\mathbf{p}_r = \frac{m_Q\mathbf{p}_D - m_D\mathbf{p}_Q}{m_D+m_Q}$ whose modulus is the quark and the diquark momentum in the centre of mass frame, in which $\mathbf{p}_{cm} = \mathbf{p}_D + \mathbf{p}_Q = 0$, and $\mathbf{r} = \mathbf{r}_D - \mathbf{r}_Q$ is the quark-diquark relative position vector.

Appendix I

$^3P_0$ Decay model

The $^3P_0$ is an effective model to compute the open-flavor strong decays of hadrons in the quark model formalism [114, 115, 116, 117]. In this model, a hadron decay takes place in its rest frame and proceeds via the creation of an additional $q\bar{q}$ pair with vacuum quantum numbers, i.e. $J^{PC} = 0^{++}$. We label the initial baryon- and final baryon- and meson-states as A, B and C, respectively. The final baryon-meson state BC is characterized by a relative orbital angular momentum ℓ between B and C and a total angular momentum $\mathbf{J} = \mathbf{J}_B + \mathbf{J}_C + \boldsymbol{\ell}$. The decay widths can be calculated as [114, 115, 121]

$$\Gamma = \frac{2\pi\gamma_0^2}{2J_A+1}\,\Phi_{A\to BC}(q_0)\sum_{M_{J_A},M_{J_B}}\left|\mathcal{M}^{M_{J_A},M_{J_B}}\right|^2 .$$

Here, $\mathcal{M}^{M_{J_A},M_{J_B}}$ is the $A \to BC$ amplitude which, for simplicity, is usually expressed in terms of hadron harmonic-oscillator wave functions, γ_0 is the dimensionless pair-creation strength:

$$\begin{aligned}
&\sum_{pol}\mathcal{M} = 3\gamma\sum_{pol} < L_A, M_{L_A}, S_A, M_{S_A}|J_A, M_{J_A} > \\
&< L_B, M_{L_B}, S_B, M_{S_B}|J_B, M_{J_B} >< L_C, M_{L_C}, S_C, M_{S_C}|J_C, M_{J_C} > \\
&< 1, m, 1, -m|0, 0 >< \chi^{124}_{S_B,M_{S_B}}\chi^{35}_{S_C,M_{S_C}}|\chi^{123}_{S_A,M_{S_A}}\chi^{45}_{1,-m} > \\
&< \phi_B^{124}\phi_C^{35}|\phi_A^{123}\phi_0^{45} > I(\vec{q}_0),
\end{aligned} \tag{I.1}$$

where $< \chi^{124}_{S_B,M_{S_B}}\chi^{35}_{S_C,M_{S_C}}|\chi^{123}_{S_A,M_{S_A}}\chi^{45}_{1,-m} >$ and $< \phi_B^{124}\phi_C^{35}|\phi_A^{123}\phi_0^{45} >$ denote the spin and flavor matrix elements, respectively. In our case, in which the final state baryon and meson are in their ground state ($L_B = L_C = 0$) and the

initial state baryon is in P wave ($L_A = 1$), equation I.1 reduces to:

$$\sum_{pol} \mathcal{M} = 3\gamma \sum_{pol} < 1, M_{L_A}, S_A, M_{S_A} | J_A, M_{J_A} >< 1, m, 1, -m | 0, 0 >$$
$$< \chi^{124}_{S_B, M_{S_B}} \chi^{35}_{S_C, M_{S_C}} | \chi^{123}_{S_A, M_{S_A}} \chi^{45}_{1,-m} >< \phi^{124}_B \phi^{35}_C | \phi^{123}_A \phi^{45}_0 > I(\vec{q}_0), \qquad \text{(I.2)}$$

In Eq. I.1 q_0 is the relative momentum between B and C, and the coefficient $\Phi_{A\to BC}(q_0)$ is the relativistic phase space factor [121],

$$\Phi_{A\to BC}(q_0) = 4\pi q_0 \frac{E_B(q_0) E_C(q_0)}{M_A} ,$$
$$\text{with} \quad E_{B,C} = \sqrt{M^2_{B,C} + q_0^2}. \qquad \text{(I.3)}$$

Here, $\mathcal{M}$ is the $A \to BC$ amplitude, calculated in terms of the h.o. wave functions of the three hadrons, and can be written as ([124], Eq. 2.188 p. 102 and [122], Eq. 6 [1]): The decay scheme is shown in Fig. I.1.

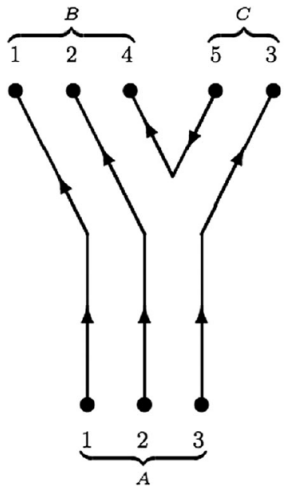

Figure I.1: The initial state Ω_c, $css \equiv 123$, decays into Ξ_c^+, $csu \equiv 124$, and K^-, $\bar{u}s \equiv 53$. (Fig. taken from [123], APS copyright).

[1] In our calculations we use the convections introduced by Le Yaouanc in his book [124]. Chen uses a different normalization than Le Yaouanc. In order to restore the normalization by Le Yaouanc, we have to divide the expression found by Chen in [122], Eq. 6, by the expectation values of the hadron creation operators, defined in Eq. 2 and Eq. 3 in [122], and also multiply by the factor 3, which Le Yaouanc introduces in order to compensate the color spectroscopic factor, which is $\frac{1}{3}$.

I.1 Baryon wave functions

Differently from light baryon phenomenology, where the ρ- and λ-modes of the mixed-symmetry spatial wave function are degenerate in energy, in the heavy-light sector the previous modes decouple; so, they can be distinguished through an analysis of the heavy-light baryon mass spectra. This happens because frequency of the ρ- and λ-modes are different,

$$\omega_\rho = \sqrt{\frac{3K_Q}{m_\rho}} \;\text{ and }\; \omega_\lambda = \sqrt{\frac{3K_Q}{m_\lambda}}, \tag{I.4}$$

where m_ρ and m_λ are defined in Section 3.1.1 . We write the baryon wave functions in terms of ω_ρ and ω_λ by using the relation $\alpha^2_{\rho,\lambda} = \omega_{\rho,\lambda} m_{\rho,\lambda}$.

For the S-wave charmed baryon,

$$\begin{aligned}\psi(0,0,0,0) &= 3^{3/4}\,(\frac{1}{\pi\omega_\rho m_\rho})^{\frac{3}{4}}\,(\frac{1}{\pi\omega_\lambda m_\lambda})^{\frac{3}{4}} \\ &\times \exp\Big[-\frac{\mathbf{p}^2_\rho}{2\omega_\rho m_\rho} - \frac{\mathbf{p}^2_\lambda}{2\omega_\lambda m_\lambda}\Big].\end{aligned} \tag{I.5}$$

For the P-wave charmed baryon,

$$\begin{aligned}\psi(1,m,0,0) &= -i\,3^{3/4}\left(\frac{8}{3\sqrt{\pi}}\right)^{1/2}\left(\frac{1}{\omega_\rho m_\rho}\right)^{5/4}\mathcal{Y}^m_1(\mathbf{p}_\rho) \\ &\times \left(\frac{1}{\pi\omega_\lambda m_\lambda}\right)^{3/4}\exp\Big[-\frac{\mathbf{p}^2_\rho}{2\omega_\rho m_\rho} - \frac{\mathbf{p}^2_\lambda}{2\omega_\lambda m_\lambda}\Big],\end{aligned} \tag{I.6}$$

$$\begin{aligned}\psi(0,0,1,m) &= -i\,3^{3/4}\left(\frac{8}{3\sqrt{\pi}}\right)^{1/2}\left(\frac{1}{\omega_\lambda m_\lambda}\right)^{5/4}\mathcal{Y}^m_1(\mathbf{p}_\lambda) \\ &\times \left(\frac{1}{\pi\omega_\rho m_\rho}\right)^{3/4}\exp\Big[-\frac{\mathbf{p}^2_\rho}{2\omega_\rho m_\rho} - \frac{\mathbf{p}^2_\lambda}{2\omega_\lambda m_\lambda}\Big].\end{aligned} \tag{I.7}$$

I.2 Explicit calculation of the ssc λ-excitation $\Xi_c K$ decay widths within the $^3P0$ model

I.2.1 Classification of the states

The Pauli principle postulates that the wave function of identical fermions must be anti-symmetric for particle exchange. The color part of the ss quarks is the antisymmetric $\bar{3}_c$. Thus, the spin of two light quarks is $\mathbf{S}_\rho = 1$ for 6_F or $\mathbf{S} = 0$ for $\bar{3}_F$. A ssQ (sqQ) state is characterised by total angular momentum $\mathbf{J} = \mathbf{l}_\rho + \mathbf{l}_\lambda + \mathbf{S}_{tot}$, where $\mathbf{S}_{tot} = \mathbf{S}_\rho + \frac{1}{2}$. The $SU(3)$ flavor multiplets of charmed and bottom baryons are reported in Figs. I.2 and I.3.

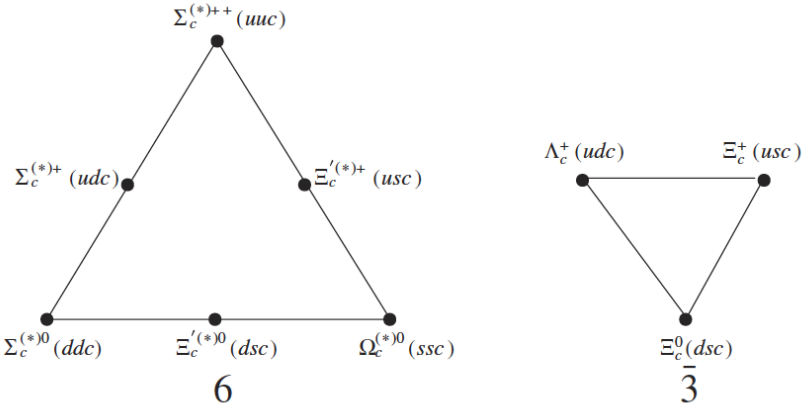

Figure I.2: The $SU(3)$ flavor multiplets of charmed baryons (Fig. taken from [122], APS copyright).

The notation $|ssQ(sqQ), \mathbf{S}_\rho, \mathbf{S}_{tot}, \mathbf{l}_\rho, \mathbf{l}_\lambda, \mathbf{J}\rangle$ will be used in the following to identify the ssQ (sqQ) states (see Tab. I.1).

I.2.2 Spin and flavor matrix elements

As we explained previously owing to the Pauli principle in all the ssc λ excitation the light quark spin, $S_\rho = 1$. Ξ_c^+ belongs to an $\bar{3}$ flavour multiplet and then the the light quark spin is 0 (see Tab. I.1). By keeping this in mind we can calculate the spin matrix elements of Eq. I.2 for the decay process of five ssc λ excitations, reported in Tab. 3.2, into a Ξ_c^+ baryon and a K^- meson. This decay channel is interesting because is the one in which the five Ω_c have been observed by LHCb and Belle. From the definition of Clebsch-Gordan (C.G.)

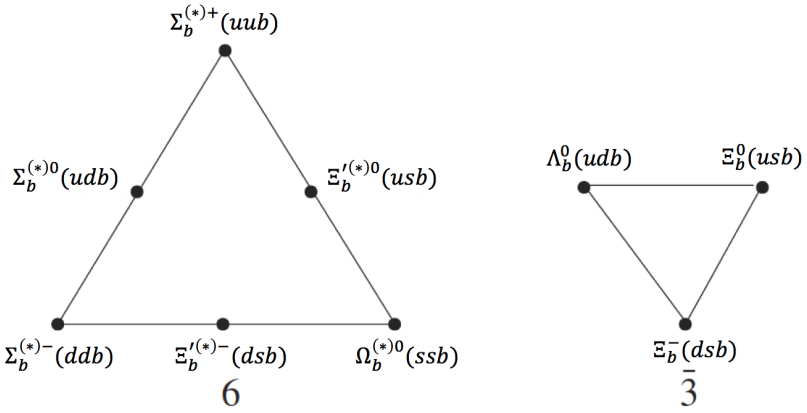

Figure I.3: The $SU(3)$ flavor multiplets of bottom baryons.

Table I.1: ssQ and sqQ ground state classification (see also Fig. I.2) of the states that we will use in the $^3P0$ model. For the notation see text.

$\left\|ssQ, 1, \frac{1}{2}, 0_\rho, 0_\lambda, \frac{1}{2}\right\rangle \equiv$	Ω_Q
$\left\|ssQ, 1, \frac{3}{2}, 0_\rho, 0_\lambda, \frac{3}{2}\right\rangle \equiv$	Ω_Q^*
$\left\|sqQ, 0, \frac{1}{2}, 0_\rho, 0_\lambda, \frac{1}{2}\right\rangle \equiv$	Ξ_Q
$\left\|sqQ, 1, \frac{1}{2}, 0_\rho, 0_\lambda, \frac{1}{2}\right\rangle \equiv$	Ξ_Q'
$\left\|sqQ, 1, \frac{3}{2}, 0_\rho, 0_\lambda, \frac{3}{2}\right\rangle \equiv$	Ξ_Q^*

coefficients, a $|J, M_J>$ function can can be expanded in terms of functions $|j_1, m_1> |j_2, m_2>$ and vice versa (see [125], Eq. 2.7):

$$|J, M_J >= \sum_{m_1,m_2} < j_1, m_1; j_2, m_2|J, M_J > |j_1, m_1 > |j_2, m_2 > \tag{I.8}$$

where the expansion coefficient $< j_1, m_1; j_2, m_2|J, M_J >$ is known as the Clebsch-Gordan (C.G.) coefficient or the vector addition coefficient and it is the unitary transformation coefficient that occurs when one goes from the uncoupled to the coupled representation [125]. It is sometimes useful to write it in terms of Wigner $3j$ symbol, $\begin{pmatrix} j_1 & j_2 & J \\ m_1 & m_2 & M_J \end{pmatrix}$, by inverting the following relation (see [125], Eq. 2.33):

$$\begin{pmatrix} j_1 & j_2 & J \\ m_1 & m_2 & M_J \end{pmatrix} = \frac{1}{\sqrt{2j+1}}(-1)^{j_1-j_2-M_J} < j_1, m_1; j_2, m_2|J, -M_J >$$

$$\rightarrow < j_1, m_1; j_2, m_2|J, M_J >= \sqrt{2j+1}(-1)^{j_2-j_1-M_J} \begin{pmatrix} j_1 & j_2 & J \\ m_1 & m_2 & -M_J \end{pmatrix}. \tag{I.9}$$

In order to calculate the spin matrix elements,

$$< \chi^{124}_{S_B,M_{S_B}} \chi^{35}_{S_C,M_{S_C}} |\chi^{123}_{S_A,M_{S_A}} \chi^{45}_{1,-m} >, \tag{I.10}$$

we have to apply Eq. I.8 and Eq. I.9 several times. For example by using Eq. I.8 we obtain the spin functions of initial state, $\chi^{123}_{S_A,M_{S_A}}$:

$$\chi^{123}_{S_A,M_{S_A}} \equiv |S_A, M_{S_A} >= \sum_{m_{23},m_1} < 1, m_{23}; 1/2, m_1|S_A, M_{S_A} > |1, m_{23} > |1/2, m_1 >, \tag{I.11}$$

of final state pseudoscal meson, $\chi^{35}_{S_C,M_{S_C}}$,

$$\chi^{35}_{S_C,M_{S_C}} \equiv |S_C, M_{S_C} >= \sum_{m_3,m_5} < 1/2, m_3; 1/2, m_5|0, 0 > |1/2, m_3 > |1/2, m_5 >, \tag{I.12}$$

of final state baryon $\chi^{124}_{S_B,M_{S_B}}$:

$$\chi^{124}_{S_B,M_{S_B}} \equiv |S_B, M_{S_B} >= \sum_{m_1} < 0, 0; 1/2, m_1|S_B, M_{S_B} > |0, 0 > |1/2, m_1 >, \tag{I.13}$$

and of vacuum $\chi^{45}_{1,-m}$:

$$\chi^{45}_{1,-m} \equiv |1,-m>= \sum_{m_4,m_5} < 1/2,m_4;1/2,m_5|1,-m > |1/2,m_4 > |1/2,m_5 > . \quad \text{(I.14)}$$

By replacing the spin wave functions into the spin matrix elements we obtain:

$$\begin{aligned} &< \chi^{124}_{S_B,M_{S_B}} \chi^{35}_{S_C,M_{S_C}} | \chi^{123}_{S_A,M_{S_A}} \chi^{45}_{1,-m} >= \sum_{m_1} < 0,0;1/2,m_1|S_B,M_{S_B} > \\ &< 0,0| < 1/2,m_1| \sum_{m_3,m_5} < 1/2,m_3;1/2,m_5|0,0 >< 1/2,m_3| < 1/2,m_5| \\ &\sum_{m_{23},m_1} < 1,m_{23};1/2,m_1|S_A,M_{S_A} > |1,m_{23} > |1/2,m_1 > \\ &\sum_{m_4,m_5} < 1/2,m_4;1/2,m_5|1,-m > |1/2,m_4 > |1/2,m_5 > \end{aligned} \quad \text{(I.15)}$$

which can be written as:

$$\begin{aligned} &< \chi^{124}_{S_B,M_{S_B}} \chi^{35}_{S_C,M_{S_C}} | \chi^{123}_{S_A,M_{S_A}} \chi^{45}_{1,-m} >= \sum_{\substack{m_1,m_3,m_4 \\ m_5,m_{23}}} < 0,0;1/2,m_1|S_B,M_{S_B} > \\ &< 1/2,m_3;1/2,m_5|0,0 >< 1,m_{23};1/2,m_1|S_A,M_{S_A} >< 1/2,m_4;1/2,m_5|1,-m > \\ &< 1/2,m_1||1/2,m_1 >< 1/2,m_5||1/2,m_5 >< 1/2,m_3| < 0,0| \\ &|1,m_{23} > |1/2,m_4 >= \\ &\sum_{\substack{m_1,m_3,m_4 \\ m_5,m_{23}}} < 0,0;1/2,m_1|S_B,M_{S_B} >< 1/2,m_3;1/2,m_5|0,0 > \\ &< 1,m_{23};1/2,m_1|S_A,M_{S_A} >< 1/2,m_4;1/2,m_5|1,-m > \\ &< 1/2,m_3| < 0,0||1,m_{23} > |1/2,m_4 > . \end{aligned} \quad \text{(I.16)}$$

Eq. I.16 can be further developed by observing that:

$$< 0,0| = \sum_{m_2,m_4} < 1/2,m_2;1/2,m_4;0,0 >< 1/2,m_2| < 1/2,m_4| \quad \text{(I.17)}$$

and that:

$$|1,m_{23} >= \sum_{m_2,m_3} < 1/2,m_2;1/2,m_3;1,m_{23} > |1/2,m_2 > |1/2,m_3 > . \quad \text{(I.18)}$$

Then we obtain:

$$
\begin{aligned}
&< \chi^{124}_{S_B,M_{S_B}} \chi^{35}_{S_C,M_{S_C}} | \chi^{123}_{S_A,M_{S_A}} \chi^{45}_{1,-m} >= \sum_{\substack{m_1,m_2,m_3 \\ m_4,m_5,m_{23}}} < 0,0;1/2,m_1|S_B,M_{S_B}> \\
&< 1/2,m_3;1/2,m_5|0,0>< 1,m_{23};1/2,m_1|S_A,M_{S_A}> \\
&< 1/2,m_4;1/2,m_5|1,-m>< 1/2,m_2;1/2,m_4;0,0>< 1/2,m_2;1/2,m_3;1,m_{23}> \\
&< 1/2,m_3||1/2,m_3>< 1/2,m_2||1/2,m_2>< 1/2,m_4||1/2,m_4>= \\
&\sum_{\substack{m_1,m_2,m_3 \\ m_4,m_5,m_{23}}} < 0,0;1/2,m_1|S_B,M_{S_B}>< 1/2,m_3;1/2,m_5|0,0> \\
&< 1,m_{23};1/2,m_1|S_A,M_{S_A}>< 1/2,m_4;1/2,m_5|1,-m> \\
&< 1/2,m_2;1/2,m_4|0,0>< 1/2,m_2;1/2,m_3|1,m_{23}> .
\end{aligned}
\tag{I.19}
$$

Now we use Eq. I.9 to write Eq. I.19 in terms of the $3j$ symbols:

$$
\begin{aligned}
&< \chi^{124}_{S_B,M_{S_B}} \chi^{35}_{S_C,M_{S_C}} | \chi^{123}_{S_A,M_{S_A}} = \sum_{\substack{m_1,m_2,m_3 \\ m_4,m_5,m_{23}}} < 0,0;1/2,m_1|S_B,M_{S_B}> \\
&< 1/2,m_3;1/2,m_5|0,0> \\
&< 1,m_{23};1/2,m_1|S_A,M_{S_A}> \\
&< 1/2,m_4;1/2,m_5|1,-m> \\
&< 1/2,m_2;1/2,m_4|0,0> \\
&< 1/2,m_2;1/2,m_3|1,m_{23}>= \\
&\sum_{\substack{m_1,m_2,m_3 \\ m_4,m_5,m_{23}}} \sqrt{2S_B+1}(-1)^{1/2-0-M_{S_B}} \begin{pmatrix} 0 & 1/2 & S_B \\ 0 & m_1 & -M_{S_B} \end{pmatrix} \\
&\sqrt{1}(-1)^{1/2-1/2-0} \begin{pmatrix} 1/2 & 1/2 & 0 \\ m_3 & m_5 & 0 \end{pmatrix} \sqrt{2S_A+1}(-1)^{1/2-1-M_{S_A}} \begin{pmatrix} 1 & 1/2 & S_A \\ m_{23} & m_1 & -M_{S_A} \end{pmatrix} \\
&\sqrt{2+1}(-1)^{1/2-1/2+m} \begin{pmatrix} 1/2 & 1/2 & 1 \\ m_4 & m_5 & m \end{pmatrix} \sqrt{1}(-1)^{1/2-1/2-0} \begin{pmatrix} 1/2 & 1/2 & 0 \\ m_2 & m_4 & 0 \end{pmatrix} \times
\end{aligned}
\tag{I.20}
$$

$$\times \sqrt{2+1}(-1)^{1/2-1/2-m_{23}} \begin{pmatrix} 1/2 & 1/2 & 1 \\ m_2 & m_3 & -m_{23} \end{pmatrix} =$$
$$3\sqrt{2S_A+1}\sqrt{2S_B+1}(-1)^{m-M_{S_A}-M_{S_B}-m_{23}}$$
$$\begin{pmatrix} 0 & 1/2 & S_B \\ 0 & m_1 & -M_{S_B} \end{pmatrix} \begin{pmatrix} 1/2 & 1/2 & 0 \\ m_3 & m_5 & 0 \end{pmatrix} \begin{pmatrix} 1 & 1/2 & S_A \\ m_{23} & m_1 & -M_{S_A} \end{pmatrix}$$
$$\begin{pmatrix} 1/2 & 1/2 & 1 \\ m_4 & m_5 & m \end{pmatrix} \begin{pmatrix} 1/2 & 1/2 & 0 \\ m_2 & m_4 & 0 \end{pmatrix} \begin{pmatrix} 1/2 & 1/2 & 1 \\ m_2 & m_3 & -m_{23} \end{pmatrix}. \tag{I.21}$$

Now the decay width equation I.2,

$$\sum_{pol} \mathcal{M} = 3\gamma \sum_{pol} < 1, M_{L_A}, S_A, M_{S_A} | J_A, M_{J_A} >< 1, m, 1, -m | 0, 0 >$$
$$< \chi^{124}_{S_B, M_{S_B}} \chi^{35}_{S_C, M_{S_C}} | \chi^{123}_{S_A, M_{S_A}} \chi^{45}_{1,-m} >< \phi^{124}_B \phi^{35}_C | \phi^{123}_A \phi^{45}_0 > I(\vec{q}_0), \tag{I.22}$$

can be written in a way in which the spin spin part is explicit:

$$\sum_{pol} \mathcal{M} = 3\gamma \sum_{pol} \sqrt{2J_A+1}(-1)^{S_A-1-M_{J_A}} \begin{pmatrix} 1 & S_A & J_A \\ M_{L_A} & M_{S_A} & -M_{J_A} \end{pmatrix} \begin{pmatrix} 1 & 1 & 0 \\ m & -m & 0 \end{pmatrix}$$
$$3\sqrt{2S_A+1}\sqrt{2S_B+1}(-1)^{m-M_{S_A}-M_{S_B}-m_{23}}$$
$$\begin{pmatrix} 0 & 1/2 & S_B \\ 0 & m_1 & -M_{S_B} \end{pmatrix} \begin{pmatrix} 1/2 & 1/2 & 0 \\ m_3 & m_5 & 0 \end{pmatrix} \begin{pmatrix} 1 & 1/2 & S_A \\ m_{23} & m_1 & -M_{S_A} \end{pmatrix}$$
$$\begin{pmatrix} 1/2 & 1/2 & 1 \\ m_4 & m_5 & m \end{pmatrix} \begin{pmatrix} 1/2 & 1/2 & 0 \\ m_2 & m_4 & 0 \end{pmatrix} \begin{pmatrix} 1/2 & 1/2 & 1 \\ m_2 & m_3 & -m_{23} \end{pmatrix}$$
$$< \phi^{124}_B \phi^{35}_C | \phi^{123}_A \phi^{45}_0 > I(\vec{q}_0). \tag{I.23}$$

The flavour matrix elements, $< \phi^{124}_B \phi^{35}_C | \phi^{123}_A \phi^{45}_0 >$, can be computed by writing explicitly the flavour wave function of the hadron involved in the decay process. The vacuum wave function is a $SU(3)$ flavour singlet then it can be written as:

$$|\phi^{45}_0 >= \frac{1}{\sqrt{3}}(|u\bar{u} > +|d\bar{d} > +|s\bar{s} >). \tag{I.24}$$

The K^- flavour wave function is ([123], Eq. C1):

$$|K^- > \equiv \phi_C^{35} = |s\bar{u} > \tag{I.25}$$

The Ξ_c^+ baryon belong to an $\bar{3}$ flavour state (see right side of Fig. I.2) and the flavour wave function of two light quarks is anti-symmetric:

$$\Xi_c^+ \equiv \phi_B^{124} = \frac{1}{\sqrt{2}}(|su > -|us >)|c > . \tag{I.26}$$

As we discussed previously the light quarks of five ssc states in λ excitation mode are in symmetric sextet flavour state. Thus:

$$\Omega_c \equiv \phi_A^{123} = |ss > |c > \tag{I.27}$$

After the substitution into the flavour matrix elements we obtain (we omit bracket in the following):

$$\begin{aligned}
&< \phi_B^{124}\phi_C^{35}|\phi_A^{123}\phi_0^{45} >= \\
&\frac{1}{\sqrt{2}}(su - us)c\ s\bar{u}\ (ss)c\frac{1}{\sqrt{3}}(u\bar{u} + d\bar{d} + s\bar{s}) = \\
&\frac{1}{\sqrt{2}}(su - us)\ (ss)\ s\bar{u}\frac{1}{\sqrt{3}}(u\bar{u} + d\bar{d} + s\bar{s}) \\
&\frac{1}{\sqrt{2}}(us - su)\ s\bar{u}\frac{1}{\sqrt{3}}(u\bar{u} + d\bar{d} + s\bar{s}) \\
&\frac{1}{\sqrt{2}}(us - su)\ su\frac{1}{\sqrt{3}} = -\frac{1}{\sqrt{6}}.
\end{aligned} \tag{I.28}$$

I.2.3 Spatial integrals

From Eq. 2.190 of Le Yaouanc textbook [124]:

$$\begin{aligned}
I(\vec{q}_0)^{m,m'} = &\int \Pi_i dp_i \mathcal{Y}_1^m(\vec{p}_4 - \vec{p}_5)\Psi_B(\vec{p}_1, \vec{p}_2, \vec{p}_4)\Psi_C(\vec{p}_3, \vec{p}_5)\Psi_A(\vec{p}_1, \vec{p}_2, \vec{p}_3) \\
&\mathcal{Y}_1^{m'}(\vec{K}_B - \vec{K}_C)\delta(\vec{p}_4 + \vec{p}_5).
\end{aligned} \tag{I.29}$$

where $\vec{p}_i$ are the quark momenta, $\vec{K}_B$ and $\vec{K}_C$ are the final state momenta, and Here $\mathcal{Y}_l^m(\mathbf{p})$ is the solid harmonic polynomial. The the S-wave and P-wave (λ and ρ mode excitations) are reported in App. I.1. The ground state wave function of meson is [122]:

$$\psi_C(\vec{p}_3, \vec{p}_5) = \Big(\frac{1}{\pi\alpha_c^2}\Big)^{3/4} \exp\Big[-\frac{(\mathbf{p}_3 - \mathbf{p}_5)^2}{8\alpha_c^2}\Big]. \tag{I.30}$$

The Jacobi coordinates are defined as follows:

$$\mathbf{p}_\rho = \frac{1}{\sqrt{2}}\left(\mathbf{p}_1 - \mathbf{p}_2\right) \ , \tag{I.31a}$$

$$\mathbf{p}_\lambda = \frac{1}{\sqrt{6}}\left(\mathbf{p}_1 + \mathbf{p}_2 - 2\mathbf{p}_3\right) \ , \tag{I.31b}$$

$$\mathbf{p}_{\rm cm} = \mathbf{p}_1 + \mathbf{p}_2 + \mathbf{p}_3 \ . \tag{I.31c}$$

The final results for angular integrals which correspond to the λ excitation is:

$$I^\lambda(q_0) = I_1^\lambda(\vec{q}_0)\delta(m - M_{L_A}) + I_2^\lambda(\vec{q}_0)\delta(m-0)\delta(M_{L_A}-0) \tag{I.32}$$

where:

$$\begin{aligned} I_1^\lambda(\vec{q}_0) &= c_0(\alpha_\rho,\alpha_\lambda,\alpha_c)e^{-F_0(\alpha_d,\alpha_\rho,\alpha_\lambda,\alpha_c,\vec{q}_0)}\left(\frac{\sqrt{\pi}}{A_{\rho 0}(\alpha_d,\alpha_\rho,\alpha_\lambda,\alpha_c)}\right)^3 \\ &\frac{3}{8}\frac{\sqrt{\pi}}{A_{\lambda 0}(\alpha_d,\alpha_\rho,\alpha_\lambda,\alpha_c)^5}\left(\frac{\sqrt{6}}{3} - \frac{\sqrt{2}a_0(\alpha_d,\alpha_\rho,\alpha_\lambda,\alpha_c)}{A_{\rho 0}(\alpha_d,\alpha_\rho,\alpha_\lambda,\alpha_c)}\right), \end{aligned} \tag{I.33}$$

and

$$\begin{aligned} I_2^\lambda(\vec{q}_0) &= c_0(\alpha_\rho,\alpha_\lambda,\alpha_c)e^{-F_0(\alpha_d,\alpha_\rho,\alpha_\lambda,\alpha_c,\vec{q}_0)}\left(\frac{\sqrt{\pi}}{A_{\rho 0}(\alpha_d,\alpha_\rho,\alpha_\lambda,\alpha_c)}\right)^3 \\ &\times \frac{B_{\lambda 0}(\alpha_d,\alpha_\rho,\alpha_\lambda,\alpha_c)}{A_{\lambda 0}(\alpha_d,\alpha_\rho,\alpha_\lambda,\alpha_c)}\left(\frac{1}{2}\sqrt{\frac{3}{\pi}}\right)^2\left(\frac{\sqrt{\pi}}{A_{\lambda 0}(\alpha_d,\alpha_\rho,\alpha_\lambda,\alpha_c)}\right)^3 \\ &\times \left(\sqrt{2}\left(\frac{b_0(\alpha_d,\alpha_\rho,\alpha_\lambda,\alpha_c)}{A_{\rho 0}(\alpha_d,\alpha_\rho,\alpha_\lambda,\alpha_c)} - a_0(\alpha_d,\alpha_\rho,\alpha_\lambda,\alpha_c)\frac{B_{\lambda 0}(\alpha_d,\alpha_\rho,\alpha_\lambda,\alpha_c)}{A_{\lambda 0}(\alpha_d,\alpha_\rho,\alpha_\lambda,\alpha_c)A_{\rho 0}(\alpha_d,\alpha_\rho,\alpha_\lambda,\alpha_c)}\right) + \right. \\ &\left. + \frac{\sqrt{6}}{3}\frac{B_{\lambda 0}(\alpha_d,\alpha_\rho,\alpha_\lambda,\alpha_c)}{A_{\lambda 0}(\alpha_d,\alpha_\rho,\alpha_\lambda,\alpha_c)} + 2q_0\right) \end{aligned} \tag{I.34}$$

with:

$$\begin{aligned} c_0(\alpha_\rho,\alpha_\lambda,\alpha_c) &= \frac{1}{3\sqrt{3}}(-i)3^{3/4}\frac{8}{3\sqrt{\pi}}^{1/2}\left(\frac{1}{\alpha_\lambda^2}\right)^{5/4}\left(\frac{1}{\pi\alpha_\rho^2}\right)^{3/4} \\ &\times 3^{3/4}\left(\frac{1}{\pi\alpha_\rho^2}\right)^{3/4}\left(\frac{1}{\pi\alpha_\lambda^2}\right)^{3/4}\left(\frac{1}{\pi\alpha_c^2}\right)^{3/4}, \end{aligned} \tag{I.35}$$

$$F_0(\alpha_d,\alpha_\rho,\alpha_\lambda,\alpha_c,\vec{q}_0)=\frac{1}{24}q_0(-6\alpha_d^2)+\frac{1}{24}q_0^2\left(\frac{4}{\alpha_\lambda^2}+\frac{3}{\alpha_c^2}+\frac{4}{\alpha_\rho^2}\right)+$$
$$-\left(\frac{\left(\frac{\alpha_d^2}{4\sqrt{6}}-\frac{q_0}{\sqrt{6}\alpha_\lambda^2}-\frac{q_0}{2\sqrt{6}\alpha_c^2}-\frac{q_0\left(-\frac{2}{\alpha_\lambda^2}-\frac{3}{\alpha_c^2}-\frac{4}{\alpha_\rho^2}\right)}{24\sqrt{6}\alpha_c^2\left(\frac{1}{6\alpha_\lambda^2}+\frac{1}{4\alpha_c^2}+\frac{5}{6\alpha_\rho^2}\right)}\right)^2}{2\sqrt{\frac{1}{12}\left(\frac{12}{\alpha_\lambda^2}+\frac{1}{\alpha_c^2}\right)-\frac{1}{48\alpha_c^2\left(\frac{1}{6\alpha_\lambda^2}+\frac{1}{4\alpha_c^2}+\frac{5}{6\alpha_\rho^2}\right)}}}\right)^2+$$
$$-\frac{\alpha_d^4}{128\left(\frac{1}{6\alpha_\lambda^2}+\frac{1}{4\alpha_c^2}+\frac{5}{6\alpha_\rho^2}\right)}-\frac{q_0\alpha_d^2\left(-\frac{2}{\alpha_\lambda^2}-\frac{3}{\alpha_c^2}-\frac{4}{\alpha_\rho^2}\right)}{96\left(\frac{1}{6\alpha_\lambda^2}+\frac{1}{4\alpha_c^2}+\frac{5}{6\alpha_\rho^2}\right)}-\frac{q_0^2\left(-\frac{2}{\alpha_\lambda^2}-\frac{3}{\alpha_c^2}-\frac{4}{\alpha_\rho^2}\right)^2}{288\left(\frac{1}{6\alpha_\lambda^2}+\frac{1}{4\alpha_c^2}+\frac{5}{6\alpha_\rho^2}\right)}, \tag{I.36}$$

$$a_0(\alpha_d,\alpha_\rho,\alpha_\lambda,\alpha_c)=\frac{\frac{1}{2\sqrt{3}\alpha_c^2}}{2\sqrt{\frac{1}{6\alpha_\lambda^2}+\frac{1}{4\alpha_c^2}+\frac{5}{6\alpha_\rho^2}}}, \tag{I.37}$$

$$A_{\rho 0}(\alpha_d,\alpha_\rho,\alpha_\lambda,\alpha_c)=\sqrt{\frac{1}{6\alpha_\lambda^2}+\frac{1}{4\alpha_c^2}+\frac{5}{6\alpha_\rho^2}} \tag{I.38}$$

$$A_{\lambda 0}(\alpha_d,\alpha_\rho,\alpha_\lambda,\alpha_c)=\sqrt{\frac{1}{12}\left(\frac{12}{\alpha_\lambda^2}+\frac{1}{\alpha_c^2}\right)-\frac{1}{48\alpha_c^2\left(\frac{1}{6\alpha_\lambda^2}+\frac{1}{4\alpha_c^2}+\frac{5}{6\alpha_\rho^2}\right)}} \tag{I.39}$$

$$B_{\lambda 0}(\alpha_d,\alpha_\rho,\alpha_\lambda,\alpha_c)=\frac{\frac{\alpha_d^2}{4\sqrt{6}}-\frac{q_0}{\sqrt{6}\alpha_\lambda^2}-\frac{q_0}{2\sqrt{6}\alpha_c^2}-\frac{q_0\left(-\frac{2}{\alpha_\lambda^2}-\frac{3}{\alpha_c^2}-\frac{4}{\alpha_\rho^2}\right)}{24\sqrt{6}\alpha_c^2\left(\frac{1}{6\alpha_\lambda^2}+\frac{1}{4\alpha_c^2}+\frac{5}{6\alpha_\rho^2}\right)}}{2\sqrt{\frac{1}{12}\left(\frac{12}{\alpha_\lambda^2}+\frac{1}{\alpha_c^2}\right)-\frac{1}{48\alpha_c^2\left(\frac{1}{6\alpha_\lambda^2}+\frac{1}{4\alpha_c^2}+\frac{5}{6\alpha_\rho^2}\right)}}} \tag{I.40}$$

$$b_0(\alpha_d,\alpha_\rho,\alpha_\lambda,\alpha_c)=\frac{\frac{\alpha_d^2}{4\sqrt{2}}-\frac{q_0}{3\sqrt{2}\alpha_\lambda^2}-\frac{q_0}{2\sqrt{2}\alpha_c^2}-\frac{\sqrt{2}q_0}{3\alpha_\rho^2}}{2\sqrt{\frac{1}{6\alpha_\lambda^2}+\frac{1}{4\alpha_c^2}+\frac{5}{6\alpha_\rho^2}}}. \tag{I.41}$$

I.2.4 Example of application: the $\Omega_c(3000) \to \Xi_c^+ K^-$ decay width

As an illustrative example we show the main steps to calculate $\Omega_c(3000) \to \Xi_c^+ K^-$ decay width by means of the $^3P0$ formalism. As a starting point we write explicitly the decay width of Eq. I.1, which for convenience we write again here,

$$\Gamma = \frac{2\pi\gamma_0^2}{2J_A+1}\,\Phi_{A\to BC}(q_0)\sum_{M_{J_A},M_{J_B}}\left|\mathcal{M}^{M_{J_A},M_{J_B}}\right|^2 \tag{I.42}$$

for the case of $\left|ssc,1,\frac{1}{2},0_\rho,1_\lambda,\frac{1}{2}\right\rangle \equiv \Omega_c(3000)$ state decaying into Ξ_c^+ baryon and K^- meson. In Eq. I.42 the explicit expression of the phase space is given by Eq. I.3

$$\Phi_{A\to BC}(q_0) = 4\pi q_0 \frac{E_B(q_0)E_C(q_0)}{M_A}\ ,$$
$$\text{with}\ \ E_{B,C} = \sqrt{M_{B,C}^2+q_0^2}\ \ \text{and}\ \ q_0 = \sqrt{E_B^2-M_B^2} \tag{I.43}$$

where B and C denote the Ξ_c^+ baryon and K^- meson, respectively and A denotes the $\Omega_c(3000)$ state. From Particle Data Group [126] $M_A = M_{\Omega_c} \simeq 3.000$ GeV, $M_B = M_{\Xi_c} \simeq 2.468$ GeV, and $M_C = M_K \simeq 0.494$ GeV. The polarization averaged decay amplitude is given by Eq. I.23

$$\sum_{pol}\mathcal{M} = 3\gamma_0\sum_{pol}\sqrt{2J_A+1}(-1)^{S_A-1-M_{J_A}}\begin{pmatrix}1 & S_A & J_A\\ M_{L_A} & M_{S_A} & -M_{J_A}\end{pmatrix}\begin{pmatrix}1 & 1 & 0\\ m & -m & 0\end{pmatrix}$$
$$3\sqrt{2S_A+1}\sqrt{2S_B+1}(-1)^{m-M_{S_A}-M_{S_B}-m_{23}}$$
$$\begin{pmatrix}0 & 1/2 & S_B\\ 0 & m_1 & -M_{S_B}\end{pmatrix}\begin{pmatrix}1/2 & 1/2 & 0\\ m_3 & m_5 & 0\end{pmatrix}\begin{pmatrix}1 & 1/2 & S_A\\ m_{23} & m_1 & -M_{S_A}\end{pmatrix}$$
$$\begin{pmatrix}1/2 & 1/2 & 1\\ m_4 & m_5 & m\end{pmatrix}\begin{pmatrix}1/2 & 1/2 & 0\\ m_2 & m_4 & 0\end{pmatrix}\begin{pmatrix}1/2 & 1/2 & 1\\ m_2 & m_3 & -m_{23}\end{pmatrix}$$
$$< \phi_B^{124}\phi_C^{35}|\phi_A^{123}\phi_0^{45} > I(\vec{q}_0). \tag{I.44}$$

where $S_A = J_A = \frac{1}{2}$, $S_B = \frac{1}{2}$. the dimensionless pair-creation strength, γ_0 is taken to be 9.2 and the flavor matrix element is given by $-\frac{1}{\sqrt{6}}$. (Eq. I.28). Finally the structure of the spatial integral depends of the type of the ssc excitation, that is ρ or λ. In the case of a λ-excitation, which turns out to be

the case for the $\Omega_c(3000)$ the structure of the spatial integral,$I(\vec{q_0}) \equiv I^\lambda(q_0)$, is (Eq. I.32):

$$I^\lambda(q_0) = I_1^\lambda(\vec{q_0})\delta(m - M_{L_A}) + I_2^\lambda(\vec{q_0})\delta(m-0)\delta(M_{L_A} - 0) \tag{I.45}$$

where the the definitions of $I_1^\lambda(\vec{q_0})$ and $I_2^\lambda(\vec{q_0})$ can be found in Eqs. I.33, I.34, I.35,I.36,I.37,I.38,I.39, I.40 and I.41. By using $\alpha_\rho = \sqrt{\omega_\rho m_\rho} = 0.458$ GeV, $\alpha_\rho = \sqrt{\omega_\rho m_\rho} = 0.540$ GeV and $\omega_c = 0.46$ GeV (see Sec. 3.3) one finds $\Gamma(\Omega_c(3000) \to \Xi_c^+ K^-) = 0.48$ MeV (see Tab. 3.2).

Appendix J

LS-jj change of basis

The basis transformations which link the the Ω_c states expressed in the LS coupling scheme and the Ω_c states expressed in the jj coupling scheme are reported below.

- In the LS coupling scheme, which is the classification scheme that we used to classify the Ω_c states, given ssc state, which is labelled by $|ssc, S_\rho, S_{\rm tot}, l_\rho, l_\lambda, J\rangle$, is characterized by total angular momentum $\mathbf{J} = \mathbf{l}_\rho + \mathbf{l}_\lambda + \mathbf{S}_{\rm tot}$, where $\mathbf{S}_{\rm tot} = \mathbf{S}_\rho + \frac{1}{2}$.

- In the jj coupling scheme, which is the scheme used by B. Chen in [110] to classify the Ω_c states, a given ssc state, which is labelled by $|ssc, S_\rho, l_\lambda, j_l, S_c, J\rangle$, is characterized by total angular momentum $\mathbf{J} = \mathbf{j}_l + \mathbf{S}_c$, where $\mathbf{j}_l = \mathbf{S}_\rho + \mathbf{l}_\lambda$.

We observe that Chen does not consider the ρ excitation because in his model he always takes $l_\rho = 0$ and so his model is equivalent to a quark-diquark model; for this reason we restrict our calculations to the case $l_\rho = 0$ which implies that $L = l_\lambda$. The change of basis between the SS and the jj basis can be written as:

$$[(S_1 \otimes S_2)^{S_{12}} \otimes (S_3 \otimes S_4)^{S_{34}}]^S =$$

$$\sum_{S_{13}} \sum_{S_{24}} C_{S_{13},S_{24}} A_{S_{13},S_{24}} [(S_1 \otimes S_3)^{S_{13}} \otimes (S_2 \otimes S_4)^{S_{24}}]^S \tag{J.1}$$

with

$$A_{S_{13},S_{24}} = \sqrt{(2S_{12}+1)(2S_{34}+1)(2S_{13}+1)(2S_{24}+1)} \tag{J.2}$$

and

$C_{S_{13},S_{24}} = \left\{ \begin{array}{ccc} S_1 & S_2 & S_{12} \\ S_3 & S_4 & S_{34} \\ S_{13} & S_{24} & S \end{array} \right\}$, and the sum is performed over:

$$|S_1 - S_3| \leq S_{13} \leq S_1 + S_3 \rightarrow S_{13} = 0 \text{ or } 1, \tag{J.3}$$

$$|S_2 - S_4| \leq S_{24} \leq S_2 + S_4 \rightarrow S_{24} = 0 \text{ or } 1. \tag{J.4}$$

The change of basis between the $S-L$ coupling and the jj coupling for the λ excitations of Ω_c states is a particular case of Eq. J.1, in which $S_1 = S_\rho, S_2 = S_{24} = S_c, S_{12} = S_{tot}, S_3 = S_{34} = l_\lambda$, $S_{13} = j_l, S_{24} =$ and $S_4 = 0$:

$$[(S_\rho \otimes S_c)^{S_{tot}} \otimes (l_\lambda \otimes 0)^{l_\lambda}]^J =$$

$$\sum_{j_l} \sum_{S_c} C_{j_l,S_c} A_{j_l,S_c} [(S_\rho \otimes l_\lambda)^{j_l} \otimes (S_c \otimes 0)^{S_c}]^J \tag{J.5}$$

with $S_c = \frac{1}{2}$ and S_ρ is always $= 1$ since we are considering only the λ-excitations; C and A are defined some lines above. In Tab. J.1 the explicit coefficients for SL-jj the change of basis are reported. We observe that, as one can see from Tab.J.1, for the two ground states, with $S = J = \frac{1}{2}$ and $S = J = \frac{3}{2}$, and for the state with $S = \frac{3}{2}$ and $J = \frac{5}{2}$ the identification between the states expressed in the LS basis and that expressed in jj basis is straightforward, while for all the other states, which span a 2-dimensional space in the spin space, the change of basis is given by a 2×2 matrix.
Here we give an example of application of Eq. J.5 to the ssc state $\left|ssc, 1, \frac{1}{2}, 1_\lambda, \frac{1}{2}\right\rangle$, while the applications to the other states are reported in App J.0.1. For the ssc state $\left|ssc, 1, \frac{1}{2}, 1_\lambda, \frac{1}{2}\right\rangle$ with $S_\rho = 1, S_c = \frac{1}{2}, S_{tot} = \frac{1}{2}, l_\lambda = 1$ and $J = \frac{1}{2}$, Eq. J.5 becomes:

$$[(1 \otimes 1/2)^{1/2} \otimes (1 \otimes 0)^1]^{1/2} =$$

$$C_{0,1/2} A_{0,1/2} [(1 \otimes 1)^0 \otimes (1/2 \otimes 0)^{1/2}]^{1/2} + C_{1,1/2} A_{1,1/2} [(1 \otimes 1)^1 \otimes (1/2 \otimes 0)^{1/2}]^{1/2},$$

$$\downarrow$$

- $C_{0,1/2} = \left\{ \begin{array}{ccc} 1 & 1/2 & 1/2 \\ 1 & 0 & 1 \\ 0 & 1/2 & 1/2 \end{array} \right\} = \frac{1}{6}$

$$\begin{aligned} A_{0,1/2} &= \sqrt{(2 \cdot 1/2 + 1)(2 \cdot 1 + 1)(2 \cdot 0 + 1)(2 \cdot 1/2 + 1)} \\ &= \sqrt{2 \cdot 3 \cdot 1 \cdot 2} = 2\sqrt{3} \end{aligned} \tag{J.6}$$

quark-diquark states in LS basis $\lvert ssc, S_\rho, S_{\rm tot}, l_\lambda, J\rangle$		quark-diquark states in jj basis $\lvert ssc, S_\rho, l_\lambda, j_l, S_c, J\rangle$
$\left\lvert ssc, 1, \frac{1}{2}, 0_\lambda, \frac{1}{2}\right\rangle$	$\equiv$	$\left\lvert ssc, 1, 0_\lambda, 1, \frac{1}{2}, \frac{1}{2}\right\rangle$
$\left\lvert ssc, 1, \frac{1}{2}, 0_\lambda, \frac{3}{2}\right\rangle$	$\equiv$	$\left\lvert ssc, 1, 0_\lambda, 1, \frac{1}{2}, \frac{3}{2}\right\rangle$
$\left\lvert ssc, 1, \frac{3}{2}, 1_\lambda, \frac{5}{2}\right\rangle$	$\equiv$	$\left\lvert ssc, 1, 1_\lambda, 2, \frac{1}{2}, \frac{5}{2}\right\rangle$
$\begin{pmatrix} \left\lvert ssc, 1, \frac{1}{2}, 1_\lambda, \frac{1}{2}\right\rangle \\ \left\lvert ssc, 1, \frac{3}{2}, 1_\lambda, \frac{1}{2}\right\rangle \end{pmatrix}$	$\equiv$	$\begin{pmatrix} \frac{\sqrt{3}}{3} & \frac{\sqrt{6}}{3} \\ \frac{\sqrt{6}}{3} & -\frac{1}{\sqrt{3}} \end{pmatrix} \begin{pmatrix} \left\lvert ssc, 1, 1, 0, \frac{1}{2}, \frac{1}{2}\right\rangle \\ \left\lvert ssc, 1, 1, 1, \frac{1}{2}, \frac{1}{2}\right\rangle \end{pmatrix}$
$\begin{pmatrix} \left\lvert ssc, 1, \frac{1}{2}, 1_\lambda, \frac{3}{2}\right\rangle \\ \left\lvert ssc, 1, \frac{3}{2}, 1_\lambda, \frac{3}{2}\right\rangle \end{pmatrix}$	$\equiv$	$\begin{pmatrix} \frac{1}{\sqrt{6}} & \sqrt{\frac{5}{6}} \\ \sqrt{\frac{5}{6}} & -\frac{1}{\sqrt{6}} \end{pmatrix} \begin{pmatrix} \left\lvert ssc, 1, 1, 1, \frac{1}{2}, \frac{3}{2}\right\rangle \\ \left\lvert ssc, 1, 1, 2, \frac{1}{2}, \frac{3}{2}\right\rangle \end{pmatrix}$

Table J.1: LS-jj change of basis for the two Ω_c ground states and the five Ω_c λ-excitations.

- $C_{1,1/2} = \left\{ \begin{array}{ccc} 1 & 1/2 & 1/2 \\ 1 & 0 & 1 \\ 1 & 1/2 & 1/2 \end{array} \right\} = \frac{1}{3\sqrt{6}}$

$$\begin{aligned} A_{1,1/2} &= \sqrt{(2\cdot 1/2+1)(2\cdot 1+1)(2\cdot 1+1)(2\cdot 1/2+1)} \\ &= \sqrt{2\cdot 3\cdot 3\cdot 2} = 6 \end{aligned} \tag{J.7}$$

so one finds:

$[(1\otimes 1/2)^{1/2}\otimes(1\otimes 0)^1]^{1/2} =$

$C_{0,1/2}A_{0,1/2}[(1\otimes 1)^0\otimes(1/2\otimes 0)^{1/2}]^{1/2} + C_{1,1/2}A_{1,1/2}[(1\otimes 1)^1\otimes(1/2\otimes 0)^{1/2}]^{1/2} =$

$\frac{1}{6}2\sqrt{3}[(1\otimes 1)^0\otimes(1/2\otimes 0)^{1/2}]^{1/2} + \frac{1}{3\sqrt{6}}6[(1\otimes 1)^1\otimes(1/2\otimes 0)^{1/2}]^{1/2} =$

$\frac{\sqrt{3}}{3}[(1\otimes 1)^0\otimes(1/2\otimes 0)^{1/2}]^{1/2} + \frac{\sqrt{6}}{3}[(1\otimes 1)^1\otimes(1/2\otimes 0)^{1/2}]^{1/2}.$ (J.8)

As a check, we observe that $\left(\frac{\sqrt{3}}{3}\right)^2 + \left(\frac{\sqrt{6}}{3}\right)^2 = \left(\frac{3}{9}\right) + \left(\frac{6}{9}\right) = 1$.

J.0.1 Calculation of the spin coefficients

$[(1\otimes 1/2)^{3/2}\otimes(1\otimes 0)^1]^{1/2} =$

$C_{0,1/2}A_{0,1/2}[(1\otimes 1)^0\otimes(1/2\otimes 0)^{1/2}]^{1/2} + C_{1,1/2}A_{1,1/2}[(1\otimes 1)^1\otimes(1/2\otimes 0)^{1/2}]^{1/2},$

$\downarrow$

- $C_{0,1/2} = \left\{ \begin{array}{ccc} 1 & 1/2 & 3/2 \\ 1 & 0 & 1 \\ 0 & 1/2 & 1/2 \end{array} \right\} = \frac{1}{6}$

$$\begin{aligned} A_{0,1/2} &= \sqrt{(2\cdot 3/2+1)(2\cdot 1+1)(2\cdot 0+1)(2\cdot 1/2+1)} \\ &= \sqrt{4\cdot 3\cdot 1\cdot 2} = 2\sqrt{6} \end{aligned} \tag{J.9}$$

- $C_{1,1/2} = \left\{ \begin{array}{ccc} 1 & 1/2 & 3/2 \\ 1 & 0 & 1 \\ 1 & 1/2 & 1/2 \end{array} \right\} = -\frac{1}{6\sqrt{6}}$

$$\begin{aligned} A_{1,1/2} &= \sqrt{(2\cdot 3/2+1)(2\cdot 1+1)(2\cdot 1+1)(2\cdot 1/2+1)} \\ &= \sqrt{4\cdot 3\cdot 3\cdot 2} = 6\sqrt{2} \end{aligned} \tag{J.10}$$

so one finds:

$$
\begin{aligned}
&[(1\otimes 1/2)^{1/2}\otimes(1\otimes 0)^{1}]^{1/2} = \\
&C_{0,1/2}A_{0,1/2}[(1\otimes 1)^{0}\otimes(1/2\otimes 0)^{1/2}]^{1/2} + C_{1,1/2}A_{1,1/2}[(1\otimes 1)^{1}\otimes(1/2\otimes 0)^{1/2}]^{1/2} = \\
&\frac{1}{6}2\sqrt{6}[(1\otimes 1)^{0}\otimes(1/2\otimes 0)^{1/2}]^{1/2} - \frac{1}{6\sqrt{6}}6\sqrt{2}[(1\otimes 1)^{1}\otimes(1/2\otimes 0)^{1/2}]^{1/2} = \\
&\frac{\sqrt{6}}{3}[(1\otimes 1)^{0}\otimes(1/2\otimes 0)^{1/2}]^{1/2} - \frac{1}{\sqrt{3}}[(1\otimes 1)^{1}\otimes(1/2\otimes 0)^{1/2}]^{1/2}. \qquad \text{(J.11)}
\end{aligned}
$$

Normalization check: $\left(\frac{\sqrt{6}}{3}\right)^2 + \left(\frac{1}{\sqrt{3}}\right)^2 = \frac{6}{9} + \frac{1}{3} = \frac{2}{3} + \frac{1}{3} = 1.$

$$
\begin{aligned}
&[(1\otimes 1/2)^{1/2}\otimes(1\otimes 0)^{1}]^{3/2} = \\
&C_{1,1/2}A_{1,1/2}[(1\otimes 1)^{1}\otimes(1/2\otimes 0)^{1/2}]^{3/2} + C_{2,1/2}A_{2,1/2}[(1\otimes 1)^{2}\otimes(1/2\otimes 0)^{1/2}]^{3/2},
\end{aligned}
$$

$$\downarrow$$

- $C_{1,1/2} = \left\{ \begin{array}{ccc} 1 & 1/2 & 1/2 \\ 1 & 0 & 1 \\ 1 & 1/2 & 3/2 \end{array} \right\} = \frac{1}{6\sqrt{6}}$

$$
\begin{aligned}
A_{1,1/2} &= \sqrt{(2\cdot 1/2+1)(2\cdot 1+1)(2\cdot 1+1)(2\cdot 1/2+1)} \\
&= \sqrt{2\cdot 3\cdot 3\cdot 2} = 6 \qquad \text{(J.12)}
\end{aligned}
$$

- $C_{2,1/2} = \left\{ \begin{array}{ccc} 1 & 1/2 & 1/2 \\ 1 & 0 & 1 \\ 2 & 1/2 & 3/2 \end{array} \right\} = \frac{1}{6\sqrt{2}}$

$$
\begin{aligned}
A_{2,1/2} &= \sqrt{(2\cdot 1/2+1)(2\cdot 1+1)(2\cdot 2+1)(2\cdot 1/2+1)} \\
&= \sqrt{2\cdot 3\cdot 5\cdot 2} = 2\sqrt{15} \qquad \text{(J.13)}
\end{aligned}
$$

so one finds:

$$
\begin{aligned}
&[(1\otimes 1/2)^{1/2}\otimes(1\otimes 0)^{1}]^{3/2} = \\
&C_{1,1/2}A_{1,1/2}[(1\otimes 1)^{1}\otimes(1/2\otimes 0)^{1/2}]^{3/2} + C_{2,1/2}A_{2,1/2}[(1\otimes 1)^{2}\otimes(1/2\otimes 0)^{1/2}]^{3/2} = \\
&\frac{1}{6\sqrt{6}}6[(1\otimes 1)^{1}\otimes(1/2\otimes 0)^{1/2}]^{3/2} + \frac{1}{6\sqrt{2}}2\sqrt{15}[(1\otimes 1)^{2}\otimes(1/2\otimes 0)^{1/2}]^{3/2} = \\
&\frac{1}{\sqrt{6}}[(1\otimes 1)^{0}\otimes(1/2\otimes 0)^{1/2}]^{1/2} + \frac{1}{3}\sqrt{\frac{15}{2}}[(1\otimes 1)^{1}\otimes(1/2\otimes 0)^{1/2}]^{1/2} \\
&\frac{1}{\sqrt{6}}[(1\otimes 1)^{0}\otimes(1/2\otimes 0)^{1/2}]^{1/2} + \sqrt{\frac{5}{6}}[(1\otimes 1)^{1}\otimes(1/2\otimes 0)^{1/2}]^{1/2}. \qquad \text{(J.14)}
\end{aligned}
$$

Normalization check: $\left(\frac{1}{\sqrt{6}}\right)^2 + \left(\sqrt{\frac{5}{6}}\right)^2 = \frac{1}{6} + \frac{5}{6} = 1.$

$$
\begin{aligned}
&[(1\otimes 1/2)^{3/2}\otimes(1\otimes 0)^{1}]^{3/2} = \\
&C_{1,1/2}A_{1,1/2}[(1\otimes 1)^{1}\otimes(1/2\otimes 0)^{1/2}]^{3/2} + C_{2,1/2}A_{2,1/2}[(1\otimes 1)^{2}\otimes(1/2\otimes 0)^{1/2}]^{3/2},
\end{aligned}
$$

$$\downarrow$$

- $C_{1,1/2} = \left\{ \begin{array}{ccc} 1 & 1/2 & 3/2 \\ 1 & 0 & 1 \\ 1 & 1/2 & 3/2 \end{array} \right\} = \frac{1}{12}\sqrt{\frac{5}{3}}$

$$
\begin{aligned}
A_{1,1/2} &= \sqrt{(2\cdot 3/2+1)(2\cdot 1+1)(2\cdot 1+1)(2\cdot 1/2+1)} \\
&= \sqrt{4\cdot 3\cdot 3\cdot 2} = 6\sqrt{2} \qquad \text{(J.15)}
\end{aligned}
$$

- $C_{2,1/2} = \left\{ \begin{array}{ccc} 1 & 1/2 & 3/2 \\ 1 & 0 & 1 \\ 2 & 1/2 & 3/2 \end{array} \right\} = -\frac{1}{12}\sqrt{\frac{1}{5}}$

$$
\begin{aligned}
A_{2,1/2} &= \sqrt{(2\cdot 3/2+1)(2\cdot 1+1)(2\cdot 2+1)(2\cdot 1/2+1)} \\
&= \sqrt{4\cdot 3\cdot 5\cdot 2} = 2\sqrt{30} \qquad \text{(J.16)}
\end{aligned}
$$

so one finds:

$$[(1 \otimes 1/2)^{3/2} \otimes (1 \otimes 0)^1]^{3/2} =$$
$$C_{1,1/2}A_{1,1/2}[(1 \otimes 1)^1 \otimes (1/2 \otimes 0)^{1/2}]^{3/2} + C_{2,1/2}A_{2,1/2}[(1 \otimes 1)^2 \otimes (1/2 \otimes 0)^{1/2}]^{3/2} =$$
$$\frac{1}{12}\sqrt{\frac{5}{3}}6\sqrt{2}[(1 \otimes 1)^1 \otimes (1/2 \otimes 0)^{1/2}]^{3/2} - \frac{1}{12}\sqrt{\frac{1}{5}}2\sqrt{30}[(1 \otimes 1)^2 \otimes (1/2 \otimes 0)^{1/2}]^{3/2} =$$
$$\sqrt{\frac{5}{6}}[(1 \otimes 1)^0 \otimes (1/2 \otimes 0)^{1/2}]^{1/2} - \sqrt{\frac{1}{6}}[(1 \otimes 1)^1 \otimes (1/2 \otimes 0)^{1/2}]^{1/2}. \qquad \text{(J.17)}$$

Normalization check: $\left(\sqrt{\frac{5}{6}}\right)^2 + \left(-\sqrt{\frac{1}{6}}\right)^2 = \frac{5}{6} + \frac{1}{6} = 1.$

Bibliography

[1] R. Aaij *et al.* [LHCb Collaboration], Phys. Rev. Lett. **115**, 072001 (2015) doi:10.1103/PhysRevLett.115.072001 [arXiv:1507.03414 [hep-ex]].

[2] R. Aaij *et al.* [LHCb Collaboration], Phys. Rev. Lett. **117**, no. 8, 082002 (2016) doi:10.1103/PhysRevLett.117.082002 [arXiv:1604.05708 [hep-ex]].

[3] R. Aaij *et al.* [LHCb Collaboration], Phys. Rev. Lett. **117**, no. 8, 082003 (2016) Addendum: [Phys. Rev. Lett. **117**, no. 10, 109902 (2016)] Addendum: [Phys. Rev. Lett. **118**, 119901 (2017)] doi:10.1103/PhysRevLett.118.119901, 10.1103/PhysRevLett.117.082003, 10.1103/PhysRevLett.117.109902 [arXiv:1606.06999 [hep-ex]].

[4] H. X. Chen, W. Chen, X. Liu and S. L. Zhu, Phys. Rept. **639**, 1 (2016) doi:10.1016/j.physrep.2016.05.004 [arXiv:1601.02092 [hep-ph]].

[5] A. Ali, J. S. Lange and S. Stone, Prog. Part. Nucl. Phys. **97**, 123 (2017) doi:10.1016/j.ppnp.2017.08.003 [arXiv:1706.00610 [hep-ph]].

[6] S. G. Yuan, K. W. Wei, J. He, H. S. Xu and B. S. Zou, Eur. Phys. J. A **48**, 61 (2012) doi:10.1140/epja/i2012-12061-2 [arXiv:1201.0807 [nucl-th]].

[7] S. Takeuchi and M. Takizawa, Phys. Lett. B **764**, 254 (2017) doi:10.1016/j.physletb.2016.11.034 [arXiv:1608.05475 [hep-ph]].

[8] E. Santopinto and A. Giachino, Phys. Rev. D **96**, no. 1, 014014 (2017) doi:10.1103/PhysRevD.96.014014 [arXiv:1604.03769 [hep-ph]].

[9] J. J. Wu, R. Molina, E. Oset and B. S. Zou, Phys. Rev. Lett. **105**, 232001 (2010) doi:10.1103/PhysRevLett.105.232001 [arXiv:1007.0573 [nucl-th]].

[10] J. J. Wu, R. Molina, E. Oset and B. S. Zou, Phys. Rev. C **84**, 015202 (2011) doi:10.1103/PhysRevC.84.015202 [arXiv:1011.2399 [nucl-th]].

[11] C. Garcia-Recio, J. Nieves, O. Romanets, L. L. Salcedo and L. Tolos, Phys. Rev. D **87**, 074034 (2013) doi:10.1103/PhysRevD.87.074034 [arXiv:1302.6938 [hep-ph]].

[12] M. Karliner and J. L. Rosner, Phys. Rev. Lett. **115**, no. 12, 122001 (2015) doi:10.1103/PhysRevLett.115.122001 [arXiv:1506.06386 [hep-ph]].

[13] R. Chen, X. Liu, X. Q. Li and S. L. Zhu, Phys. Rev. Lett. **115**, no. 13, 132002 (2015) doi:10.1103/PhysRevLett.115.132002 [arXiv:1507.03704 [hep-ph]].

[14] L. Roca, J. Nieves and E. Oset, Phys. Rev. D **92**, no. 9, 094003 (2015) doi:10.1103/PhysRevD.92.094003 [arXiv:1507.04249 [hep-ph]].

[15] J. He, Phys. Lett. B **753**, 547 (2016) doi:10.1016/j.physletb.2015.12.071 [arXiv:1507.05200 [hep-ph]].

[16] U. G. Meißner and J. A. Oller, Phys. Lett. B **751**, 59 (2015) doi:10.1016/j.physletb.2015.10.015 [arXiv:1507.07478 [hep-ph]].

[17] H. X. Chen, W. Chen, X. Liu, T. G. Steele and S. L. Zhu, Phys. Rev. Lett. **115**, no. 17, 172001 (2015) doi:10.1103/PhysRevLett.115.172001 [arXiv:1507.03717 [hep-ph]].

[18] T. Uchino, W. H. Liang and E. Oset, Eur. Phys. J. A **52**, no. 3, 43 (2016) doi:10.1140/epja/i2016-16043-0 [arXiv:1504.05726 [hep-ph]].

[19] T. J. Burns, Eur. Phys. J. A **51**, no. 11, 152 (2015) doi:10.1140/epja/i2015-15152-6 [arXiv:1509.02460 [hep-ph]].

[20] Y. Yamaguchi and E. Santopinto, Phys. Rev. D **96**, no. 1, 014018 (2017) doi:10.1103/PhysRevD.96.014018 [arXiv:1606.08330 [hep-ph]].

[21] Y. Shimizu and M. Harada, Phys. Rev. D **96**, no. 9, 094012 (2017) doi:10.1103/PhysRevD.96.094012 [arXiv:1708.04743 [hep-ph]].

[22] V. Kubarovsky and M. B. Voloshin, Phys. Rev. D **92**, no. 3, 031502 (2015) doi:10.1103/PhysRevD.92.031502 [arXiv:1508.00888 [hep-ph]].

[23] Y. Huang, J. He, H. F. Zhang and X. R. Chen, J. Phys. G **41**, no. 11, 115004 (2014) doi:10.1088/0954-3899/41/11/115004 [arXiv:1305.4434 [nucl-th]].

[24] Y. Huang, J. J. Xie, J. He, X. Chen and H. F. Zhang, Chin. Phys. C **40**, no. 12, 124104 (2016) doi:10.1088/1674-1137/40/12/124104 [arXiv:1604.05969 [nucl-th]].

[25] E. J. Garzon and J. J. Xie, Phys. Rev. C **92**, no. 3, 035201 (2015) doi:10.1103/PhysRevC.92.035201 [arXiv:1506.06834 [hep-ph]].

[26] X. H. Liu and M. Oka, Nucl. Phys. A **954**, 352 (2016) doi:10.1016/j.nuclphysa.2016.04.040 [arXiv:1602.07069 [hep-ph]].

[27] S. H. Kim, H. C. Kim and A. Hosaka, Phys. Lett. B **763**, 358 (2016) doi:10.1016/j.physletb.2016.10.061 [arXiv:1605.02919 [hep-ph]].

[28] Q. Wang, X. H. Liu and Q. Zhao, Phys. Rev. D **92**, 034022 (2015) doi:10.1103/PhysRevD.92.034022 [arXiv:1508.00339 [hep-ph]].

[29] Y. Shimizu, D. Suenaga and M. Harada, Phys. Rev. D **93**, no. 11, 114003 (2016) doi:10.1103/PhysRevD.93.114003 [arXiv:1603.02376 [hep-ph]].

[30] J. J. Wu and B. S. Zou, Phys. Lett. B **709**, 70 (2012) doi:10.1016/j.physletb.2012.01.068 [arXiv:1011.5743 [hep-ph]].

[31] C. W. Xiao and E. Oset, Eur. Phys. J. A **49**, 139 (2013) doi:10.1140/epja/i2013-13139-y [arXiv:1305.0786 [hep-ph]].

[32] K. Azizi, Y. Sarac and H. Sundu, Phys. Rev. D **96**, no. 9, 094030 (2017) doi:10.1103/PhysRevD.96.094030 [arXiv:1707.01248 [hep-ph]].

[33] C. Cheng and X. Y. Wang, Adv. High Energy Phys. **2017**, 9398732 (2017) doi:10.1155/2017/9398732 [arXiv:1612.08822 [hep-ph]].

[34] R. Aaij *et al.* [LHCb Collaboration], Phys. Rev. Lett. **122**, no. 22, 222001 (2019) doi:10.1103/PhysRevLett.122.222001 [arXiv:1904.03947 [hep-ex]].

[35] S. H. Kim, S. i. Nam, Y. Oh and H. C. Kim, Phys. Rev. D **84**, 114023 (2011) doi:10.1103/PhysRevD.84.114023 [arXiv:1110.6515 [hep-ph]].

[36] C. Fernandez-Ramirez et al., Phys. Rev. Lett. 123, 092001 (2019).

[37] R. Casalbuoni, A. Deandrea, N. Di Bartolomeo, R. Gatto, F. Feruglio and G. Nardulli, Phys. Rept. **281**, 145 (1997) doi:10.1016/S0370-1573(96)00027-0 [hep-ph/9605342].

[38] Y. R. Liu and M. Oka, Phys. Rev. D **85**, 014015 (2012) doi:10.1103/PhysRevD.85.014015 [arXiv:1103.4624 [hep-ph]].

[39] W. Rarita and J. Schwinger, Phys. Rev. **60**, 61 (1941). doi:10.1103/PhysRev.60.61

[40] S. Weinberg, Phys. Rev. **137**, B672 (1965). doi:10.1103/PhysRev.137.B672

[41] S. Weinberg, Phys. Rev. **130**, 776 (1963). doi:10.1103/PhysRev.130.776

[42] H. Nagahiro and A. Hosaka, Phys. Rev. C **88**, no. 5, 055203 (2013) doi:10.1103/PhysRevC.88.055203 [arXiv:1307.2031 [hep-ph]].

[43] H. Nagahiro and A. Hosaka, Phys. Rev. C **90**, no. 6, 065201 (2014) doi:10.1103/PhysRevC.90.065201 [arXiv:1406.3684 [hep-ph]].

[44] T. Hyodo and D. Jido, Prog. Part. Nucl. Phys. **67** (2012) 55 doi:10.1016/j.ppnp.2011.07.002 [arXiv:1104.4474 [nucl-th]].

[45] Y. Funaki, H. Horiuchi, W. von Oertzen, G. Ropke, P. Schuck, A. Tohsaki and T. Yamada, Phys. Rev. C **80**, 064326 (2009)F doi:10.1103/PhysRevC.80.064326 [arXiv:0912.2934 [nucl-th]].

[46] M. B. Wise, Phys. Rev. D **45**, no. 7, R2188 (1992). doi:10.1103/PhysRevD.45.R2188

[47] G. Burdman and J. F. Donoghue, Phys. Lett. B **280**, 287 (1992). doi:10.1016/0370-2693(92)90068-F

[48] T. M. Yan, H. Y. Cheng, C. Y. Cheung, G. L. Lin, Y. C. Lin and H. L. Yu, Phys. Rev. D **46**, 1148 (1992) Erratum: [Phys. Rev. D **55**, 5851 (1997)]. doi:10.1103/PhysRevD.46.1148, 10.1103/PhysRevD.55.5851

[49] A. F. Falk and M. E. Luke, Phys. Lett. B **292**, 119 (1992) doi:10.1016/0370-2693(92)90618-E [hep-ph/9206241].

[50] A. V. Manohar and M. B. Wise, Camb. Monogr. Part. Phys. Nucl. Phys. Cosmol. **10**, 1 (2000).

[51] C. Patrignani *et al.* [Particle Data Group], Chin. Phys. C **40**, no. 10, 100001 (2016). doi:10.1088/1674-1137/40/10/100001

[52] S. Yasui and K. Sudoh, Phys. Rev. D **80**, 034008 (2009) doi:10.1103/PhysRevD.80.034008 [arXiv:0906.1452 [hep-ph]].

[53] Y. Yamaguchi, S. Ohkoda, S. Yasui and A. Hosaka, Phys. Rev. D **84**, 014032 (2011) doi:10.1103/PhysRevD.84.014032 [arXiv:1105.0734 [hep-ph]].

[54] Y. Yamaguchi, S. Ohkoda, S. Yasui and A. Hosaka, Phys. Rev. D **85**, 054003 (2012) doi:10.1103/PhysRevD.85.054003 [arXiv:1111.2691 [hep-ph]].

[55] Y. Oh, C. M. Ko, S. H. Lee and S. Yasui, Phys. Rev. C **79**, 044905 (2009) doi:10.1103/PhysRevC.79.044905 [arXiv:0901.1382 [nucl-th]].

[56] C. W. Hwang, Eur. Phys. J. C **23**, 585 (2002) doi:10.1007/s100520200904 [hep-ph/0112237].

[57] B. Silvestre-Brac, Few Body Syst. **20**, 1 (1996). doi:10.1007/s006010050028

[58] A. Hosaka, M. Oka and T. Shinozaki, Phys. Rev. D **71**, 074021 (2005) doi:10.1103/PhysRevD.71.074021 [hep-ph/0409102].

[59] R. Machleidt, K. Holinde and C. Elster, Phys. Rept. **149**, 1 (1987). doi:10.1016/S0370-1573(87)80002-9

[60] E. Hiyama, Y. Kino and M. Kamimura, Prog. Part. Nucl. Phys. **51**, 223 (2003). doi:10.1016/S0146-6410(03)90015-9

[61] Y. Ikeda *et al.* [HAL QCD Collaboration], Phys. Rev. Lett. **117**, no. 24, 242001 (2016) doi:10.1103/PhysRevLett.117.242001 [arXiv:1602.03465 [hep-lat]].

[62] L. Geng, J. Lu and M. P. Valderrama, Phys. Rev. D **97**, no. 9, 094036 (2018) doi:10.1103/PhysRevD.97.094036 [arXiv:1704.06123 [hep-ph]].

[63] C. Vafa and E. Witten, Nucl. Phys. B **234**, 173 (1984). doi:10.1016/0550-3213(84)90230-X

[64] J. Q. Chen, J. L. Ping and F. Wang, River Edge, USA: World Scientific (2002) 574 p

[65] The LHCb collaboration, R. Aaij et al., arXiv:2001.00851.

[66] Y. Yamaguchi, H. Garcia-Tecocoatzi, A. Giachino, A. Hosaka, E. Santopinto, S. Takeuchi and M. Takizawa, Recent Progress in Few-Body Physics, Chapter NO. 98, Chapter DOI.: 10.1007/978-3-030-32357-8 (2019).

[67] Y. Yamaguchi, H. García-Tecocoatzi, A. Giachino, A. Hosaka, E. Santopinto, S. Takeuchi and M. Takizawa, arXiv:1907.04684 [hep-ph].

[68] E. Santopinto, A. Giachino, J. Ferretti, H. Garcia-Tecocoatzi, M. A. Bedolla, R. Bijker, and E. Ortiz-Pacheco, Eur. Phys. J. C 79, 1012 (2019) doi:10.1140/epjc/s10052-019-7527-4;

[69] J. Aguilar and J. M. Combes, Commun. Math. Phys. **22**, 269 (1971).

[70] E. Balslev and J. M. Combes, Commun. Math. Phys. **22**, 280 (1971).

[71] B. Simon, Commun. Math. Phys. **27**, 1 (1972).

[72] S. Aoyama, T. Myo, K. Katō, and K. Ikeda, Prog. Theor. Phys. **116**, 1 (2006).

[73] F. Gursey and L.A. Radicati , Phys. Rev. Lett. 13, 173 (1964)

[74] V.M. Abazov et al. (D0 collab.), Phys. Rev. Lett. 99, 052001 (2007)

[75] V.M. Abazov et al. (D0 collab.), Phys. Rev. Lett. 101, 232002 (2008)

[76] Y. Oh, J. Korean Phys. Soc. **59**, 3344 (2011).

[77] U. Camerini, J. G. Learned, R. Prepost, C. M. Spencer, D. E. Wiser, W. W. Ash, R. L. Anderson, D. M. Ritson, D. J. Sherden, and C. K. Sinclair, Phys. Rev. Lett. 35, 483 (1975).

[78] R. L. Anderson, Report No. SLAC-PUB-1417.

[79] [26] B. Gittelman, K. M. Hanson, D. Larson, E. Loh, A. Silverman, and G. Theodosiou, Phys. Rev. Lett. 35, 1616 (1975).

[80] A. V. Manohar, M. B. Wise, Camb. Monogr. Part. Phys. Nucl. Phys. Cosmol. 10 (2000) 1-191, (2000).

[81] F. Mandl and G. Shaw, Quantum Field Theory.

[82] D. Lurie and A. J. Macfarlane, Phys. Rev. **136**, B816 (1964).

[83] S. Coleman, J. Math. Phys. **7**, 787 (1966)*

[84] V. Bargmann and E. Wigner: Proc. Nat. Sci. (USA), 34, 211 (1948).

[85] W. Greiner, Relativistic Quantum Mechanics, Wave Equations, edited by Springer.

[86] H. X. Chen, W. Chen and S. L. Zhu, Phys. Rev. D **100** (2019) no.5, 051501 doi:10.1103/PhysRevD.100.051501 [arXiv:1903.11001 [hep-ph]].

[87] C. W. Xiao, J. Nieves and E. Oset, Phys. Rev. D **100** (2019) no.1, 014021 doi:10.1103/PhysRevD.100.014021 [arXiv:1904.01296 [hep-ph]].

[88] M. Z. Liu, Y. W. Pan, F. Z. Peng, M. Sánchez Sánchez, L. S. Geng, A. Hosaka and M. Pavon Valderrama, Phys. Rev. Lett. **122** (2019) no.24, 242001 doi:10.1103/PhysRevLett.122.242001 [arXiv:1903.11560 [hep-ph]].

[89] Y. Shimizu, Y. Yamaguchi and M. Harada, arXiv:1904.00587 [hep-ph].

[90] F. Giannuzzi, Phys. Rev. D **99** (2019) no.9, 094006 doi:10.1103/PhysRevD.99.094006 [arXiv:1903.04430 [hep-ph]].

[91] J. F. Giron, R. F. Lebed and C. T. Peterson, JHEP **1905** (2019) 061 doi:10.1007/JHEP05(2019)061 [arXiv:1903.04551 [hep-ph]].

[92] J. He, Eur. Phys. J. C **79** (2019) no.5, 393 doi:10.1140/epjc/s10052-019-6906-1 [arXiv:1903.11872 [hep-ph]].

[93] A. Ali and A. Y. Parkhomenko, Phys. Lett. B **793** (2019) 365 doi:10.1016/j.physletb.2019.05.002 [arXiv:1904.00446 [hep-ph]].

[94] J. Ferretti, G. Galatà and E. Santopinto, Phys. Rev. C **88** (2013) no.1, 015207 doi:10.1103/PhysRevC.88.015207 [arXiv:1302.6857 [hep-ph]].

[95] Z. H. Guo and J. A. Oller, Phys. Lett. B **793** (2019) 144 doi:10.1016/j.physletb.2019.04.053 [arXiv:1904.00851 [hep-ph]].

[96] Y. Yamaguchi, A. Giachino, A. Hosaka, E. Santopinto, S. Takeuchi and M. Takizawa, Phys. Rev. D **96** (2017) no.11, 114031 doi:10.1103/PhysRevD.96.114031 [arXiv:1709.00819 [hep-ph]].

[97] R. Aaij *et al.* [LHCb Collaboration], Phys. Rev. Lett. **118**, no. 18, 182001 (2017) doi:10.1103/PhysRevLett.118.182001 [arXiv:1703.04639 [hep-ex]].

[98] J. Yelton *et al.* [Belle Collaboration], Phys. Rev. D **97**, no. 5, 051102 (2018) doi:10.1103/PhysRevD.97.051102 [arXiv:1711.07927 [hep-ex]].

[99] R. Aaij *et al.* [LHCb Collaboration], Phys. Rev. Lett. **121**, no. 7, 072002 (2018) doi:10.1103/PhysRevLett.121.072002 [arXiv:1805.09418 [hep-ex]].

[100] R. Aaij *et al.* [LHCb Collaboration], Phys. Rev. Lett. **122**, no. 1, 012001 (2019) doi:10.1103/PhysRevLett.122.012001 [arXiv:1809.07752 [hep-ex]].

[101] M. Karliner and J. L. Rosner, Phys. Rev. D **95**, no. 11, 114012 (2017) doi:10.1103/PhysRevD.95.114012 [arXiv:1703.07774 [hep-ph]].

[102] Z. Zhao, D. D. Ye and A. Zhang, Phys. Rev. D **95**, no. 11, 114024 (2017) doi:10.1103/PhysRevD.95.114024 [arXiv:1704.02688 [hep-ph]].

[103] K. L. Wang, L. Y. Xiao, X. H. Zhong and Q. Zhao, Phys. Rev. D **95**, no. 11, 116010 (2017) doi:10.1103/PhysRevD.95.116010 [arXiv:1703.09130 [hep-ph]].

[104] M. Padmanath and N. Mathur, Phys. Rev. Lett. **119**, no. 4, 042001 (2017) doi:10.1103/PhysRevLett.119.042001 [arXiv:1704.00259 [hep-ph]].

[105] S. S. Agaev, K. Azizi and H. Sundu, Eur. Phys. J. C **77**, no. 6, 395 (2017) doi:10.1140/epjc/s10052-017-4953-z [arXiv:1704.04928 [hep-ph]].

[106] Y. Huang, C. j. Xiao, Q. F. Lü, R. Wang, J. He and L. Geng, Phys. Rev. D **97**, no. 9, 094013 (2018) doi:10.1103/PhysRevD.97.094013 [arXiv:1801.03598 [hep-ph]].

[107] J. Nieves, R. Pavao and L. Tolos, Eur. Phys. J. C **78**, no. 2, 114 (2018) doi:10.1140/epjc/s10052-018-5597-3 [arXiv:1712.00327 [hep-ph]].

[108] V. R. Debastiani, J. M. Dias, W. H. Liang and E. Oset, Phys. Rev. D **97**, no. 9, 094035 (2018) doi:10.1103/PhysRevD.97.094035 [arXiv:1710.04231 [hep-ph]].

[109] N. Isgur and G. Karl, Phys. Rev. D **18**, 4187 (1978). doi:10.1103/PhysRevD.18.4187

[110] B. Chen and X. Liu, Phys. Rev. D **96**, no. 9, 094015 (2017) doi:10.1103/PhysRevD.96.094015 [arXiv:1704.02583 [hep-ph]].

[111] M. Tanabashi *et al.* [Particle Data Group], Phys. Rev. D **98**, no. 3, 030001 (2018). doi:10.1103/PhysRevD.98.030001

[112] S. Capstick and N. Isgur, Phys. Rev. D **34**, 2809 (1986) [AIP Conf. Proc. **132**, 267 (1985)]. doi:10.1103/PhysRevD.34.2809, 10.1063/1.35361

[113] D. Ebert, R. N. Faustov and V. O. Galkin, Phys. Lett. B **659**, 612 (2008) doi:10.1016/j.physletb.2007.11.037 [arXiv:0705.2957 [hep-ph]].

[114] L. Micu, Nucl. Phys. B **10**, 521 (1969). doi:10.1016/0550-3213(69)90039-X

[115] A. Le Yaouanc, L. Oliver, O. Pene and J. C. Raynal, Phys. Rev. D **8**, 2223 (1973). doi:10.1103/PhysRevD.8.2223

[116] A. Le Yaouanc, L. Oliver, O. Pene and J. C. Raynal, NEW YORK, USA: GORDON AND BREACH (1988) 311p

[117] W. Roberts and B. Silvestre-Brac, Phys. Rev. D **57**, 1694 (1998) doi:10.1103/PhysRevD.57.1694 [hep-ph/9708235].

[118] S. Capstick and W. Roberts, Phys. Rev. D **47**, 1994 (1993). doi:10.1103/PhysRevD.47.1994

[119] F. E. Close and E. S. Swanson, Phys. Rev. D **72**, 094004 (2005) doi:10.1103/PhysRevD.72.094004 [hep-ph/0505206].

[120] S. Capstick and W. Roberts, Prog. Part. Nucl. Phys. **45**, S241 (2000) doi:10.1016/S0146-6410(00)00109-5 [nucl-th/0008028].

[121] R. Bijker, J. Ferretti, G. Galatà, H. García-Tecocoatzi and E. Santopinto, Phys. Rev. D **94**, no. 7, 074040 (2016) doi:10.1103/PhysRevD.94.074040 [arXiv:1506.07469 [hep-ph]].

[122] C. Chen et al., Phys. Rev. D 75, 094017 (2007)

[123] R. Bijker et al. Phys. Rev. D 94, 074040 (2016)

[124] A. Le Yaouanc et al., Hadron Transition In The Quark Model, Gordon and Breach Science Publishers, 1988.

[125] V. Devanathan, Angular Momentum Techniques in Quantum Mechanics, Editor: ALWYN VAN DER MERWE, University of Denver, U.S.A.

[126] M. Tanabashi et al. (Particle Data Group), Phys. Rev. D 98, 030001 (2018) and 2019 update.